Charles University

Faculty of Science

Study programme: Molecular and Cellular Biology, Genetics and Virology

RNDr. Klára Frydrýšková

Noncanonical human eIF4Es in and out of the RNA granules

Nekanonické lidské translační iniciační faktory z rodiny 4E v RNA granulích i mimo ně

Doctoral thesis

Supervisor: RNDr. Martin Pospíšek, Ph.D.

Prague, 2019

Prohlášení:

Prohlašuji, že jsem závěrečnou práci zpracoval/a samostatně, a že jsem uvedl/a všechny použité informační zdroje a literaturu. Tato práce ani její podstatná část nebyla předložena k získání jiného nebo stejného akademického titulu

V Praze 31.10. 2019 Podpis:

Acknowledgements

At this place, I would like to thank my advisor, Dr. Martin Pospíšek for many happy years spent in his laboratory. I deeply enjoyed the work on a fascinating topic and above all the experimental freedom. Dr. Pospíšek is a very inspiring man and stays as a role model of moral principles to all of us. I value Dr. Pospíšek not only for his knowledge, out of the box way of thinking and exciting science that he pursue with stunning endurance, but also for the fact, that he has always supported me, even in situations completely unrelated to my Ph.D.

Another big "thank you" belongs to Dr. Dr. Tomáš Mašek, „a guardian angel of my Ph.D." Whenever I faced a difficult situation, Tomáš came to help me. Either it was cloning of the 4E3_A, treatment of the mycoplasma infection of stable cell lines or fixing the mutated clones of 4E2 and others. I also appreciate our frequent brainstorming on emerging questions.

My big thank you also belongs to Dr. Vopálenský, for his effective help and advice whenever possible. I would like to thank also to Dr. Leoš Valášek and his team, above all to Dr. Susan Wagner, for the help with GST pull-downs and a gift of several antibodies.

My gratitude also belongs to members of the RNA biology lab, especially those positively contributing to the nice working atmosphere and namely to Mgr. Natálie Moravcová, who has literally saved me several times in terms of the cell cultivation. For careful revision of this thesis, I would like to thank Dr. Michal Doležal and Mgr. Silvia Mrvová. For the help with statistical analysis, I would like to thank Dr. Vendula Novosadová.

My special "Thank You" belongs to Mgr. Ondřej Šebesta, the little I know about microscopy and data processing, I have learnt from him. I would also like to thank to my hard working students Mgr. Jana Kráčmarová and Mgr. Pavlína Hrbková.

Above all, I would like thank to my family, for the enormous patience they had with me, when I was working nights and weekends. Namely, without my mother´s and my husband´s help, my return to the laboratory would have been impossible. For the financial support, I would like to express my gratitude to Martina Roeselová memoriam fellowship, which enables me to write a review article, perform a substantial number of experiments and finish writing this thesis.

Contents

Abstract

Eukaryotic translation initiation factor eIF4E1 (eIF4E1) plays a pivotal role in the control of cap-dependent translation initiation, occurs in P- bodies and is important for the formation of stress granules (SG). Human cells encompass two other non-canonical translation initiation factors capable of cap binding although with a lower affinity for the cap: eIF4E2 and eIF4E3.

Here, I investigated the ability of individual eIF4E family members and their variants to localize to SGs and P-bodies in stress-free, arsenite and heat shock conditions. Under all tested conditions, both eIF4E1 and eIF4E2 proteins and all their variants localized to P-bodies unlike eIF4E3 protein variants. Under both arsenite and heat stress conditions all tested variants of eIF4E1 and the variant eIF4E3-A localized to SGs albeit with different abilities. Protein eIF4E2 and all its investigated variants localized specifically to a major part of heat stress-induced stress granules.

Further analysis showed that approximately 75% of heat stress-induced stress granules contain all three eIF4Es, while in 25% of them eIF4E2 is missing. Large ribosomal subunit protein L22 was found specifically enriched in arsenite induced SGs. Heat stress-induced re-localization of several proteins typical for P-bodies such as eIF4E2, DCP-1, AGO-2 and depending on the temperature also DDX6, to SGs. Thus, severe heat stress in mammalian cells induces SG fusion with P-bodies, as was published previously in yeast´s cells.

Last, I searched for eIF4E2 interaction partners using immunoprecipitation followed by mass spectrometry. I detected eIF3, eIF4E-T, eIF4E-BP2, PABP in a complex with eIF4E2. The possible implications for the eIF4E2 involvement in translation repression or initiation are discussed.

Keywords: eIF4E1, eIF4E2, eIF4E3, eIF3, stress granules, P-bodies, cap-dependent translation initiation, mass spectrometry, sodium arsenite stress, heat shock

Abstrakt

Eukaryontní translační iniciační faktor eIF4E1 řídí iniciaci translace závislou na čepičce, vyskytuje se v P-tělíscích a je důležitý pro vznik stresových granulí (SG). V lidských buňkách jsou obsaženy také dva další nekanonické translační iniciační faktory, eIF4E2 a eIF4E3. Oba váží čepičku, ačkoliv slaběji než eIF4E1.

V rámci této práce jsem se zabývala schopností jednotlivých členů z rodiny proteinů eIF4E a jejich variant lokalizovat do stresových granulí a P-tělísek za klidových podmínek a za podmínek tepelného a arsenitanového stresu. Za všech testovaných podmínek lokalizovaly proteiny eIF4E1 a eIF4E2 a všechny jejich testované varianty do P-tělísek na rozdíl od variant proteinu eIF4E3. Za obou stresových podmínek všechny varianty proteinu eIF4E1 a varianta eIF4E3-A lokalizovaly do SG, avšak schopnost jednotlivých proteinů lokalizovat do SG se lišila. Protein eIF4E2 lokalizoval ve zvýšené míře pouze do SG vyvolaných tepelným stresem.

Při detailnějším studiu jsme ukázali, že za tepelného stresu vznikají dva typy SG ve vztahu k eIF4E proteinům. Přibližně 75 % SG indukovaných tepelným stresem obsahuje všechny tři eIF4E proteiny, zatímco ve 25 % z nich protein eIF4E2 chybí. Dále jsme ukázali, že protein velké ribosomální podjednotky L22 je specificky nabohacen v SG vyvolaných arsenitanovým stresem. Tepelný stress vede k přechodu několika proteinů typických pro P-tělíska do SG. Jedná se o proteiny eIF4E2, DCP-1, AGO-2 a v závisloti na intenzitě teplotního stresu také o DDX6. Dlouhý stres způsobený extrémně vysokou teplotou vede k fúzi SG s P-tělísky, podobně jako je to publikováno u kvasinek.

V práci jsem se též zabývala hledáním interakčních partnerů faktoru eIF4E2. Pomocí imunoprecipitace následované identifikací vazebných partnerů pomocí hmotnostní spektrometrie jsem nalezla eIF3, eIF4E-T, eIF4E-BP2 a PABP v komplexu s eIF4E2. Možná role proteinu eIF4E2 v iniciaci translace nebo naopak v potlačení translace je v práci diskutována.

Klíčová slova: eIF4E1, eIF4E2, eIF4E3, eIF3, stresové granule, P-tělíska, iniciace translace závislá na čepičce, hmotnostní spektrometrie, stres arsenitanem sodným, tepelný stres

1 List of abbreviations

3´UTR untranslated region 3´
4E1 eukaryotic translation initiation factor eIF4E1
4E1/3 SG stress granules where 4E1 and 4E3 co-localized
4E2 eukaryotic translation initiation factor eIF4E2
4E2 SG stress granules where 4E1, 4E3 and 4E2 co-localized
4E3 eukaryotic translation initiation factor eIF4E3
4E-BP1,2,3 eukaryotic translation initiation factor eIF4E binding protein 1,2,3
4E-T eukaryotic translation initiation factor eIF4E transporter
4F eukaryotic translation initiation factor eIF4F, complex of 4A, 4G, 4E
5´UTR untranslated region 5´
ACTN4 actinin alpha 4
AGO-2/ EIF2C2 argonaute RISC catalytic component 2
ALS amyotrophic lateral sclerosis
AML acute myeloid leukemia
ARIH1/HHARI E3 ubiquitin-protein ligase ARIH1
ATXN2 ataxin-2
BB blocking beads
CASC3 exon-junction complex, CASC3
CCR4-NOT cytoplasmic deadenylase
CD circular dichroism spectroscopy
CDK2 cyclin dependent kinase 2
cDNA complementary DNA
CDX2 caudal type homeobox 2
CENPV centromere protein V
CIRBP cold inducible RNA binding protein
CPSF1,3,6 cleavage and polyadenylation specificity factor
CRISPR-CAS9 clustered regularly interspaced short palindr omic repeats
CUL7 cullin 7
CYFIP1 cytoplasmic fragile X interacting protein 1
DAP5 eukaryotic translation initiation factor 4G2
DAPI 4′,6-diamidino-2-phenylindole
DCP-1,2 decapping mRNA 1,2
DDX5,6 DEAD-box helicase 5,6
DIS3L DIS3 like exosome 3'-5' exoribonuclease
Dm4E *Drosophila melanogaster* 4E
EDC4 enhancer of mRNA decapping 4
eIF1A eukaryotic translation initiation factor 1A
eIF2C3 Isoform 2 of protein Argonaute-3
eIF2α eukaryotic translation initiation factor 2α
eIF3 eukaryotic translation initiation factor 3
eIF3B eukaryotic translation initiation factor 3, subunit B, marker of stress granules
eIF4A,B eukaryotic translation initiation factor 4A,B
eIF4G1,3 eukaryotic translation initiation factor 4G1,3
eIF4H eukaryotic translation initiation factor 4H
eIF5 eukaryotic translation initiation factor 5
eIF5A eukaryotic translation initiation factor 5, subunit A
ELAVL2/HUB ELAV like RNA binding protein
ER endoplasmic reticulum
ERK1/2 mitogen-activated protein kinase 3,1
EST expressed sequence tag
EXOSC2 exosome component 2
FMRP fragile X mental retardation protein 1
FRAP fluorescence recovery after photobleaching
FT flow through
FTLD-U fronto temporal lobar degeneration with ubiquitin inclusions
FUS fused in sarcoma
FXR 1,2 fragile X mental retardation syndrome-related protein 1,2
FXS fragile X syndrome
G3BP1,2 G3BP stress granule assembly factor 1,2
GCN2 general control nonderepressible 2
GFP green fluorescent protein
GIGYF1,2 GRB10 interacting GYF protein 1,2
GST glutathione S-transferase
GW182/TRNC6A trinucleotide repeat containing adaptor 6A
h4Es human 4E family of proteins
HA hemagglutinin
HDAC6 histone deacetylase 6
HHARI human homologue of ariadne
HIF 1,2 hypoxia induced factor 1,2
HIST2H3D histone cluster 2, H3D
HMGA1 high mobility group AT-hook 1
HNRNPA2B1 heterogeneous nuclear ribonucleoprotein A2/B1
HNRNPQ synaptotagmin binding cytoplasmic RNA interacting protein
HOAX A9 homeobox gene A9
HRE hypoxia response element
HRI heme regulated initiation factor 2 alpha kinase
HSP70-90 heat shock protein 70.90 kDa
HSPA2 heat shock-related 70 kDa protein 2
HUR ELAV like RNA binding protein 1
IDR intrinsically disordered region
IFE *C. elegans* eIF4E family member

IGF-BP1,2 insulin growth factor binding protein 1,2
IGF-IR insulin like growth factor 1 receptor
IN input sample
IP immunoprecipitation
IRS4 insulin receptor substrate 4
ISG15 ISG15 ubiquitin like modifier
KRT19 keratin 19
L22 ribosomal protein L22
LC liquid chromatography
LMV lettuce mosaic virus
LPS lipopolysaccharide
LSM3 U6 snRNA-associated Sm-like protein LSm3¨
MNK1,2 MAPK interacting serine/threonine kinase 1,2
MOV10 Mov10 RISC complex RNA helicase
mRNP messenger ribonucleoprotein particle
MS mass spectrometry
MT3 mRNA transporter protein 3
mTOR mammalian target of rapamycin
mTORC1 mammalian target of rapamycin complex 1
nCBP novel cap-binding protein
NES nuclear export signal
NMR nuclear magnetic resonance spectroscopy
N-MYC oncogene NMYC
NUFIP2 nuclear FMR1 interacting protein 2
O/N incubation over night
OD optical density
O-GlcNac O-linked N-acetylglucosamine
PABP polyA binding protein
PAR-CLIP photoactivatable ribonucleoside-enhanced crosslinking and immunoprecipitation
PATL1 protein PAT1 homolog 1
PB P-body
PCM1 pericentriolar material 1
PCNA proliferating cell nuclear antigen
PEI polyethyleneimine
PERK/PEK PRKR-like endoplasmic reticulum kinase
PIC pre-initiation complex
PKCα protein kinase C
PKR protein kinase R
PML protein promyelocytic leukemia
PRH proline- rich homeobox protein
PRPF8 pre-mRNA processing factor 8
PRRC2B proline rich coiled-coil 2B
PUM1 pumilio homolog 1
qPCR quantitative PCR
RANBP9 RAN binding protein 9
RBM4 RNA binding motif protein 4
RBMX RNA binding motif protein X-linked
RC3H1 isoform 2 of Roquin
RISC RNA induced silencing complex
RNF5 ring finger protein 5
RNP ribonucleoprotein particle
RPS14 ribosomal protein S14
RRP4, 40-46 exosome component 2,3,4,5,7,8,9,11
RT room temperature
S5 ribosomal protein S5
SART3 SART3 protein
SFPQ splicing factor proline and glutamine rich
SG stress granules
SHC src homology and collagen
SMG-1 serine/threonine protein kinase Smaug 1
SNAP23 synaptosome associated protein 23
snRNP small nuclear ribonucleoprotein particle
SR serine arginine proteins
SRPK1,2 SR protein kinase 1,2
SRSF7,9 serine and arginine rich splicing factor 7,9
SSBP1 single stranded DNA binding protein 1
SURF surfeit locus protein
TARS threonyl-tRNA synthetase
TEV tobacco etch virus
THRAP3 thyroid hormone receptor associated protein 3
TIA-1 T-cell-restricted intracellular antigen-1
TOP 5'terminal oligopyrimidine tract
TPRDII TPR repeat protein D
TRIM56 tripartite motif containing 56
TRNC6B/6B trinucleotide repeat containing adaptor 6A/6B
TTC3 tetratricopeptide repeat domain 3
TTP tristetraprolin
TuMV turnip mosaic virus
TWIST twist family BHLH transcription factor 1
UBE2S ubiquitin conjugating enzyme E2 S
UBCH7 ubiquitin conjugating enzyme E2 L3
UBR5 ubiquitin protein ligase E3
UPF1 UPF1 RNA helicase and ATPase
USP5,13 ubiquitin specific peptidase 5,13
XRN1,2 5'-3' Exoribonuclease 1,2
ZNF598 zinc finger protein 59

2 Introduction to the cap-dependent translation initiation

Translation initiation is an intensively studied topic and its detailed description is beyond the scope of this thesis, for review see (Jackson et al. 2010; Valasek 2012; Shirokikh and Preiss 2018). Cap-dependent initiation of translation is a step-wise assembly process of elongation competent 80S ribosome at the start codon of mRNA. In most of the cases, the translation initiation begins by eIF4F (4F) complex formation at the 5′ methyl-7-guanosine (m^7G) cap on the mRNA. The cytoplasmic cap-binding protein eIF4E binds the 5′cap and also binds to the scaffolding protein eIF4G. The helicase eIF4A with eIF4H and eIF4B additional helicase stimulatory factors interacts more transiently with eIF4G:eIF4E to form e4F complex (Fig. 1, step 1) Translation initiation factor eIF4G also recognizes polyA binding protein (PABP) bound at the poly A tail at 3′UTR of eukaryotic mRNAs, enabling its circularization and increasing the translation efficiency. Apart from the affinity to PABP, eukaryotic eIF4G protein displays affinity to eIF1, eIF5 and eIF3.

In the next step, 43S pre-initiation complex (PIC) is formed by 40S ribosomal subunit and several eukaryotic translation initiation factors eIF1, eIF1a, eIF3, eIF5 and a pre-formed ternary complex (eIF2-GTP-$_i$tRNA^{Met}). PIC joints the mRNA (Fig. 1, step 2). The joining of 43S PIC to the 4F complex is mediated by an interaction of eIF3 with eIF4G .

Successful translation initiation of the majority of eukaryotic mRNAs is thought to rely on the helicase activity of the eIF4A factor, which resolves the 5′UTR secondary structure at the expanse of ATP and prepares the landing pad for the 43S PIC. In the generally accepted ribosomal scanning model, the 43S PIC together with the components of the 4F complex scans through the 5′UTR mRNA in the 5′-3′direction (Fig. 1, step 3). This step also involves the eIF4A helicase activity to resolve weaker internal secondary structures, single stranded RNA is stabilized by eIF4B. More complex structures though, require helicase activity of additional associated proteins, such as DHX29, eIFF4H.

The 43S PIC scans until encountering an AUG in a strong Kozak context (A/GNNAUGG) (Fig. 1, step 4). At this point, base pairing between AUG and CAU of the anticodon loop on $_{i}tRNA^{Met}$, results in the ejection of eIF1. Translation initiation factors eIF1 and eIF1A are known to increase the stringency of AUG-start codon selection (Fig. 1, step 5). At this point, 40S subunit is bound to its selection of the start codon at the expense of eIF2:GTP hydrolysis and forms tighter interactions with the mRNA, known as 48S PIC. After each round of translation initiation, eIF2:GDP needs to be recycled by GDP/GTP exchange factor eIF2B.

In the final stage of translation initiation, 60S subunit joints the 48S at the expense of eIF5.GTP hydrolysis (Fig. 1, step 6). The majority of the remaining eIFs are ejected (Fig. 1, step 7) and translation proceeds into the elongation phase by the formation of elongation-competent 80S ribosome and the formation the first peptide bond (Green et al. 2016; Shirokikh and Preiss 2018)

Apart from the canonical cap-dependent translation initiation scanning model, there are also translation initiation mechanisms dependent on the cap, but avoiding scanning. The scanning-free mechanism is typical for the mRNAs with extremely short or highly complex UTRs and are advantageous in specific physiological settings, for review see (Haimov et al. 2015).

Among others, the repeat associated non AUG translation RAN, has been described. This mechanism relies on the instruction for translation coded in the secondary structure of the 5´UTR formed by expansion of repeats e.g. CAG, resulting in a production of toxic proteins involved in some neurodegenerative diseases, for review see (Green et al. 2016).

Fig. 1 Canonical scanning model of cap-dependent translation initiation, adapted from (Green et al. 2016)

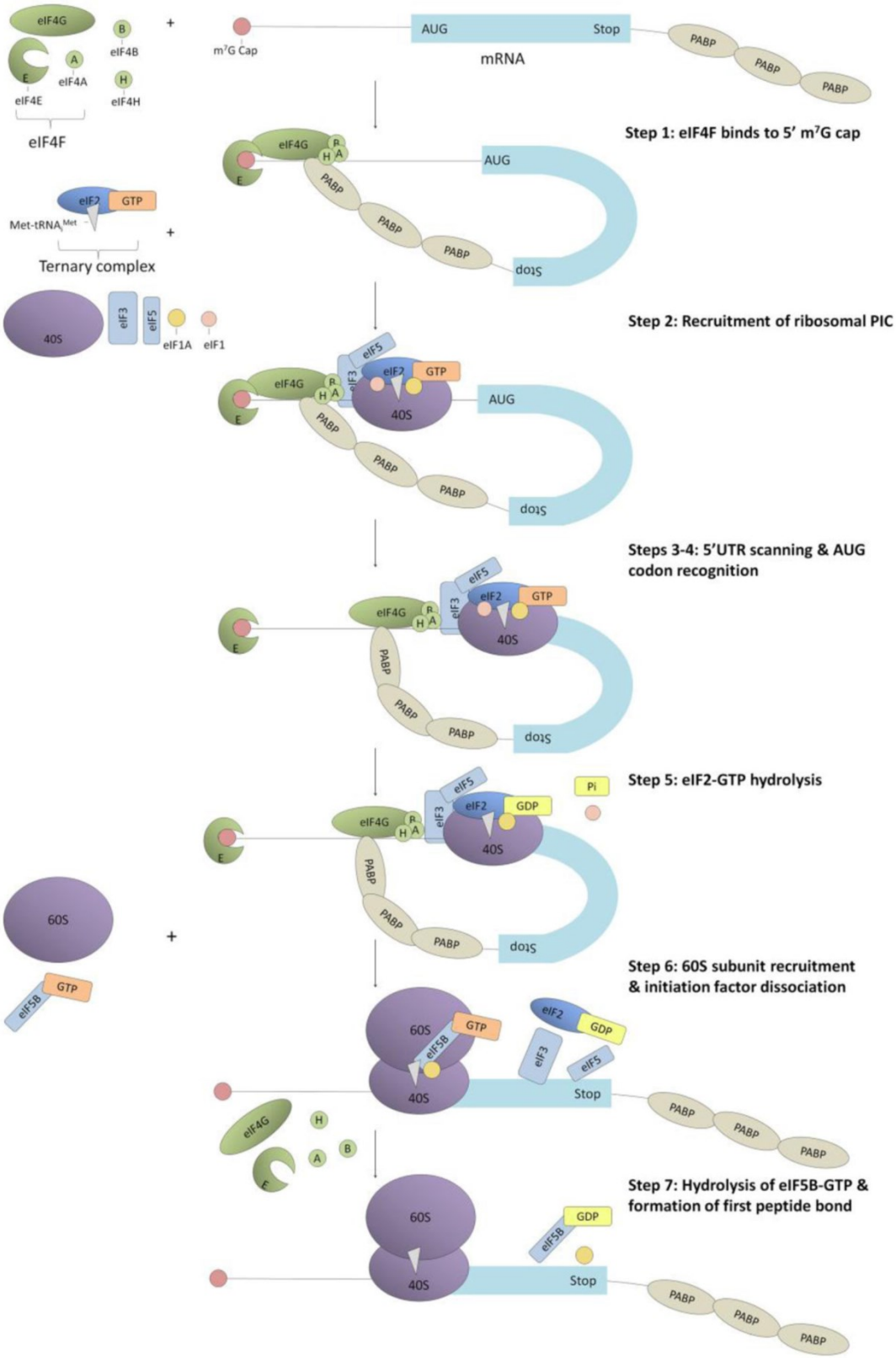

3 LITERATURE REVIEW

3.1 P-bodies and stress granules, the kissing relatives

Stress granules were first described by Nover et al. (1983) in tomato leaves and later on in mammals by Nancy Kedersha et al. (1999). The field of mRNP turnover has been intensively studied since with a number of excellent reviews published on the topic e.g. (Buchan 2014; Protter and Parker 2016; Ditlev et al. 2018).

Stress granules (SGs) and P-bodies (PBs) are cytoplasmic non-membrane bound cellular compartments termed as ribonucleoprotein particles (RNPs). RNP granules are dynamic and depend on RNA for their assembly. The formation of RNP in order to concentrate specific cellular components is considered to be a conserved strategy across multiple organisms and in different cellular compartments (Banani et al. 2017). Above all, stress-granules like RNP granules also exist in neurons and embryos where relevant pools of un-translating mRNPs are located (Martin and Ephrussi 2009)

SGs and PBs are two types of conserved cytoplasmic mRNP granules that are formed from pools of un-translating mRNAs. SGs form from mRNA stalled in translation initiation and contain various translation initiation factors, a variety of RNA binding proteins as well as non-RNA binding proteins. On the other hand, PBs contain mRNAs associated with translational repressors and mRNA decay machinery (Protter and Parker 2016). As evidenced by two recent proteomic studies, SGs and PBs are compositionally distinct, sharing only 10-25% of protein components. G3BP stress granule assembly factors (G3BP1, 2), PABP and eIF3 are restricted to SGs. The de-capping enzymes DCP1 and DCP2 and most components of the CCR4-NOT de-adenylase complex are only detected in PBs (Hubstenberger et al. 2017; Youn et al. 2018). The only members of 4F complex that occur in both the structures are 4E1 and 4E2 proteins (Frydryskova et al. 2016).

Nevertheless, the mRNA decay enzymes are likely inactive within PBs and the role of PBs in mRNA decay is being questioned (Luo et al. 2018; Standart and Weil 2018; Guzikowski et al. 2019).

PBs and SGs can dock and overlap in mammalian cells, suggesting a dynamic mRNA cycle wherein mRNPs can be remodelled and exchanged between polysomes, stress granules and P-bodies, Fig. 2.

During RNP disassembly, the mRNPs within PBs and SGs can be targeted to autophagy or returned for translation (Brengues et al. 2005; Bhattacharyya et al. 2006; Buchan et al. 2013).

SGs seem to be involved in the tumour progression and the failure of the cancer treatment (Anderson et al. 2015). Mutations that increase stress granule formation and/or limit clearance are causative agents in neurodegenerative diseases such as amyotrophic lateral sclerosis (ALS), frontotemporal lobar degeneration with ubiquitin-positive inclusions (FTLD-U) and others, for review see (Li et al. 2013; Ramaswami et al. 2013). Moreover, a reduction in the number of SGs in the cells has been already proposed as a new way to fight Alzheimer´s disease (Apicco et al. 2018). Evidence are that persistent and repetitive assembly of SGs is cytotoxic and is directly linked with the conversion of SGs into cytoplasmic inclusions that recapitulate the pathology of ALS-FTD (Ramaswami et al. 2013; Zhang et al. 2019).

Fig. 2 The turnover of mRNPs, adapted from (Protter and Parker 2016)

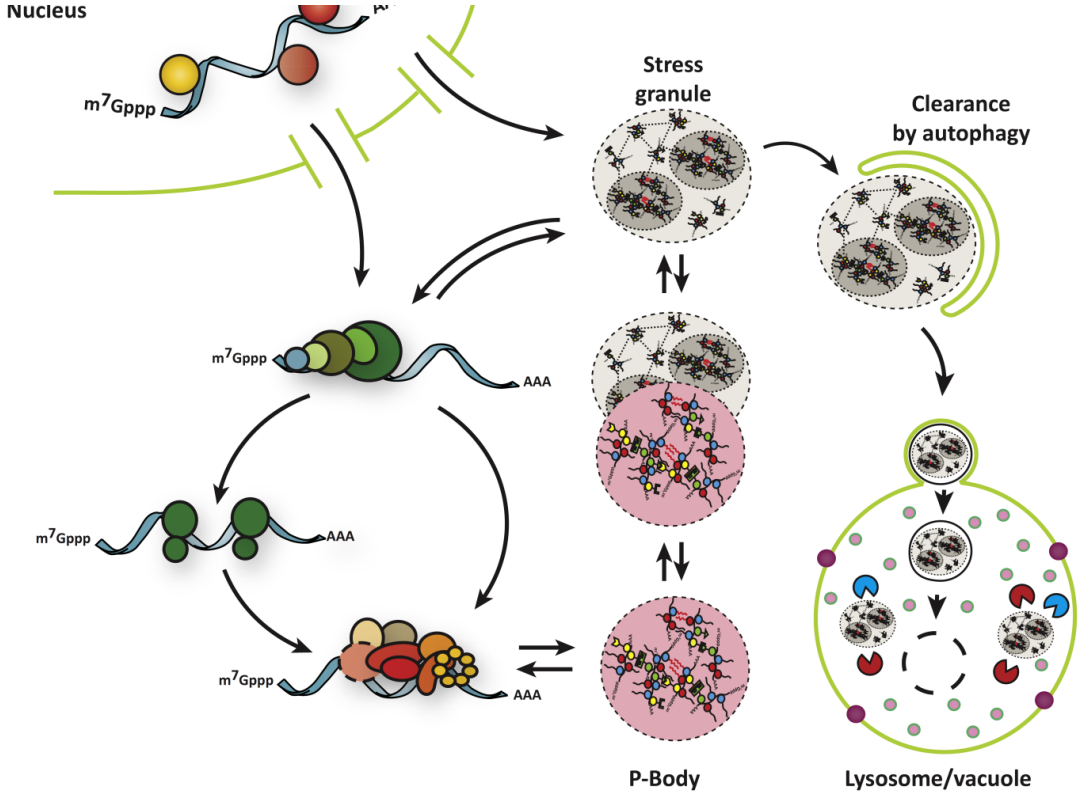

Nascent mRNP travels from the nucleus to the cytoplasm, where it can be translated or upon stress insult, targeted to stress granules that can fuse with P-bodies or be a subject of clearance by the autophagy.

3.2 How are stress granules and P-bodies formed?

SGs form when translation initiation is inhibited either by drugs or by a stress response (Anderson and Kedersha 2009). Usually, SG formation is provoked in an eIF2 α-phosphorylation-dependent manner, see herein below. Alternatively, disruption of the 4F complex leads to the assembly of SGs via eIF2 α-phosphorylation-independent manner e.g. inhibition of eIF4A helicase through following drugs: Pateamine A, hippuristanol and 15d-PGJ2 (Bordeleau et al. 2006; Dang et al. 2006; Kim et al. 2007). Further, 4E binding protein (4E-BP) mediated inhibition of 4E was observed following selenite treatment and hydrogen peroxide stress (Mokas et al. 2009; Emara et al. 2012; Fujimura et al. 2012).

The eIF2 α- phosphorylation -dependent manner of SG condensation is typically initiated when one of several stress-activated serine/threonine kinases phosphorylate eukaryotic initiation factor eIF2α at Ser51, a component of the eIF2/GTP/$tRNA_i^{Met}$ ternary complex, which loads the initiator tRNA onto the small ribosomal subunit to begin translation (Clemens 2001; Kedersha et al. 2002). Consequences of eIF2α phosphorylation are translational arrest, polysome disassembly and assembly of SGs (Anderson and Kedersha 2008). A family of stress-activated eIF2 α kinases appears to monitor different types of cellular stresses. For instance protein kinase R (PKR), a double stranded RNA-dependent kinase, is activated by a viral infection or selected environmental stresses (Williams 1997). PKR like endoplasmic reticulum (ER) kinase (PERK) is a resident ER protein, activated by changes in glycoprotein metabolism (Shi et al. 1998). General control nonderepressible 2 (GCN2) has been proposed to regulate the cellular response to amino acid starvation (Olsen et al. 1998). And finally heme – regulated eIF2 kinase (HRI) ensures the balanced synthesis of globin chains and heme during erythrocyte maturation and plays a role in translational control of non-erythroid tissues (Berlanga et al. 1998).

Many types of stresses can be used to provoke stress granules assembly, but among them, heat and arsenite stresses are the most studied (Aulas and Vande Velde 2015). Consequently, in my work I employed only these types of stresses to induce stress granules. Recent experimental work with near-haploid human cell lines lacking individual eIF2α kinases and a knock-in cell line containing a Ser51Ala phosphorylation-resistant substitution in the eIF2α gene proved that heat shock activates

all the four eIF2 kinase and an alternative eIF2α - phosphorylation-independent pathway (Lu et al. 2001; Taniuchi et al. 2016; Aulas et al. 2017). On the contrary, oxidative stress activates kinase HRI and to a minor extent GCN2 and is strictly eIF2 α phosphorylation-dependent (Taniuchi et al. 2016; Aulas et al. 2017).

There is a highly integrated, dense protein interaction network in unstressed cells that facilitates SG assembly in stress (Markmiller et al. 2018). Interactions that result into SG formation include protein-protein interactions, as well as interactions involving intrinsically disordered regions (IDRs). Assembly and disassembly are modulated by numerous ATP-dependent RNPs or protein remodelling complexes (Protter and Parker 2016). Further, the formation, composition and function of SGs is influenced by a number of post-translational modifications of proteins acting downstream of the translational arrest, such as O-linked N-acetylglucosamine (O-GlcNac) of ribosomal subunits, addition of poly (ADP- ribose), phosphorylation, acetylation, methylation, hypusination, ubiquitylation and neddylation (Li et al. 2010; Kedersha et al. 2013; Jayabalan et al. 2016; Protter and Parker 2016; Mahboubi and Stochaj 2017) .

Important trait of SGs is, that they fail to form when mRNAs are trapped on polysomes, suggesting that mRNAs associated with ribosomes are unable to enter SGs (Buchan and Parker 2009). This suggestion is further supported by an observation of specific mRNAs that occur in SGs and are stalled in a particular step of translation initiation such as transcripts with 5'terminal oligopyrimidine tract (TOP) mRNAs (Damgaard and Lykke-Andersen 2011).

SGs are highly dynamic in comparison with PBs. Fluorescence recovery after photobleaching (FRAP) studies showed that most components of SGs exchange rapidly with half-times for recovery of less than 30 seconds, reviewed in (Buchan and Parker 2009). These experiments also revealed an immobile pool of proteins that does not exchange on a similar timescale. Indeed, SGs are not uniform structures, instead they contain two regions with different components, functions and dynamics. A core, that can be biochemically purified, surrounded by a less concentrated and more dynamic shell (Jain et al. 2016; Wheeler et al. 2016). Based on proteomic studies cores, those are formed from roughly 50% by a subset of RNA-binding proteins (Jain et al. 2016). Non RNA-binding proteins are recruited to SGs via protein-protein interactions and include enzymes responsible for post-translational modification of SG member proteins, metabolic enzymes, RNA remodelling complexes, which can affect SGs assembly or

disassembly and some key components of signalling pathways (Buchan 2014; Jain et al. 2016).

Under some conditions, the oligomeric seeds of stress granules may form by the transitions in mRNP composition that occur at PBs. This is based on the observation of yeast cells stressed by glucose deprivation, where the SGs tend to form after and on PBs and that some SGs in mammalian cells appear to grow out of P bodies (Buchan et al. 2008). In mammalian cells, SGs are transported in a microtubule-dependent manner (Loschi et al. 2009).

SG formation might promote the interactions of mRNAs with translation initiation factors and thereby enhance the formation of translation initiation complexes (Buchan et al. 2008).

3.3 Stress granule´s composition varies among different stresses in mammals

There is a dense protein network, redundantly contributing for SGs formation in stress (Markmiller et al. 2018). The redundancy might be an underlying reason why SGs form under different conditions by different interactions. SG´s member proteins can be divided into scaffolds and clients. While scaffolds are required for the assembly of the granules, clients get localised in the granules via the interactions with scaffold components. The distinction between scaffolds and clients could be stress conditions dependent. Thus, the composition of SGs can vary under different conditions (Buchan and Parker 2009; Ditlev et al. 2018).

For example T-cell-restricted intracellular antigen-1 (TIA-1) and its yeast homologue Pub-1, facilitates SG assembly in response to arsenite and glucose deprivation. Unlike TIA-1, yeast Pub-1 does not localize to stress granules in heat shock (Gilks et al. 2004; Lopez de Silanes et al. 2005; Buchan et al. 2008; Grousl et al. 2009). Kedersha et al. (2016) reported that stress granule assembly factor 1,2 (G3BP 1,2) is essential for SG condensation initiated by both eIF2α-phosphorylation and eIF4A inhibition, but dispensable for SG induced by hyperosmolarity or severe heat shock. Both the G3BP1 and G3BP2, though, play important roles in SG formation in mammalian cells exposed to oxidative stress (Tourriere et al. 2003).

Selenite-induced stress granules are known to lack eIF3B, otherwise well established as a SG marker, eIF5A and ribosomal protein S14 (RPS14) (Fujimura et al.

2012). In the stress granules induced by hydrogen peroxide, eIF4E, eIF4G and eIF3B are missing and localization of PABP to those foci is severely compromised in comparison with sodium arsenite-induced stress granules (Emara et al. 2012). Cold inducible RNA binding protein (CIRBP) becomes a part of stress granules under distinct conditions such as hypoxia, UV irradiation or cold shock (De Leeuw et al. 2007; Zhu et al. 2016).

Two deubiquitylases, ubiquitin specific peptidase USP5 and USP13 are recruited specifically to heat, puromycin or VER (HSP70 inhibitor) stress-induced SGs and regulate assembly and disassembly of heat stress-induced SGs (Xie et al. 2018).

This suggests that SGs can assemble differently in response to specific stress conditions. Depletion of following proteins results in a severely altered SGs formation G3BPs, TIA-1, eIF4E1 and eIF3 (more specifically subunits i,e,g,d,c,b) (Tourriere et al. 2003; Ohn et al. 2008; Mokas et al. 2009; Emara et al. 2012; Fournier et al. 2013; Waris et al. 2014). Depletion of eIF4E leads to a minor decrease of SG number under arsenite stress, but to an important decrease of their number in hydrogen peroxide stress (Emara et al. 2012). Importantly, the ability of proteins to localize to SGs is not always tight up with a specific cellular role. SGs under the both arsenite and heat stresses encompass members of signalling pathways. Most of them become sequestered to SGs under both conditions, even though some of them are biochemically active under the condition of one stress only. For example, serine/threonine protein kinase Smaug-1 (SMG-1) is functionally important for SG assembly in cells induced by sodium arsenite and hydrogen peroxide but not by the heat (Brown et al. 2011). Protein kinase Cα (PKCα) localizes to SGs in heat stress and is important for their formation. Even though PKCα localizes to arsenite stress-induced SGs as well, its biochemical role is limited to heat stress (Kobayashi et al. 2012).

Heat and arsenite stress-induced SGs further differs in several post- translational modifications of their member proteins. For example while mono- ubiquitin localizes to the arsenite stress-induced stress granules, they are devoid of poly-ubiquitylated proteins (Markmiller et al. 2019). On the other hand, heat stress-induced SGs are enriched for poly-ubiquitin chains (Mateju et al. 2017; Xie et al. 2018). Detailed information about differences in SGs induced by the heat and arsenite stresses are summarized in “Changing faces of stress: Impact of heat and arsenite treatment on the composition of stress granules”.

3.4 A brief introduction to eIF4Es

eIF4E is found exclusively in eukaryotes, it possesses a unique alpha/beta fold, that is considered to have no homologues outside the eukaryotes, as determined by sequence comparison and structural analysis (Aravind and Koonin 2000). Evolutionary, it seems that a single eIF4E gene has undergone multiple duplications resulting in multiple structural classes (Joshi et al. 2005).

In mammals, three different members of eIF4E family exist: eIF4E-1 (4E1), eIF4E-2 (4E2) and eIF4E-3 (4E3). They differ in their structural features, functional characteristics, expression patterns and finally, binding partners.

The original description of human 4Es as described by Joshi and colleagues (2004) was as follows ”First, eIF4E-1 is found in all eukaryotes, eIF4E-2 though, is restricted to metazoans only and eIF4E-3 is specific to chordates.” The authors analysed various mouse tissues (heart, brain, spleen, lung, liver, skeletal muscles, kidney, testis) for expression of individual 4E. While eIF4E1 and 2 were found ubiquitously expressed, eIF4E2 levels were highest in the testes, eIF4E3 was detected only in heart, skeletal muscles, lung and spleen (Joshi et al. 2004). Human and *S. cerevisiae* eIF4E counterparts are 30% identical and therefore, mammalian 4E can rescue the lethality of *S. cerevisiae* 4E gene disruption (Altmann et al. 1989; Joshi et al. 2002). Unlike 4E1, neither 4E2 nor 4E3 can rescue growth of *S. cerevisiae* with 4E gene disruption. But all the three of them are capable of cap-binding *in vitro*. Whereas 4E2 cannot bind 4GI, it can bind 4E-BPs, conversely 4E3 fails to interact with 4E-BPs but interacts with 4GI.” With some limitations, which will be discussed further in the text, this description of h4Es has been valid till today. For the evolutionary relationship of 4E family members, see Fig. 3.

Fig. 3 Evolutionary relationship of eIF4E family members, adapted from (Hernandez and Vazquez-Pianzola 2005)

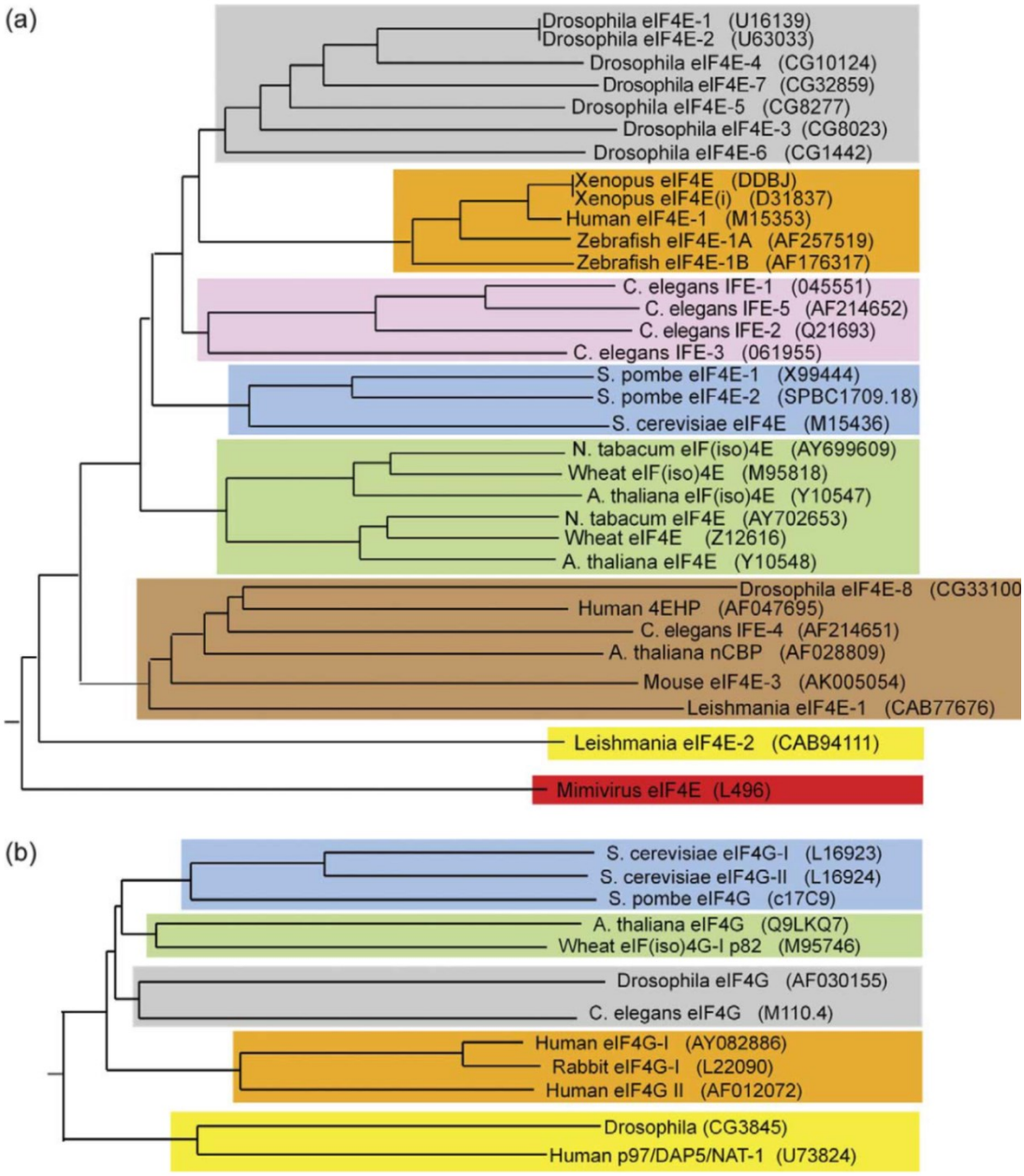

Cladograms were constructed using the CLUSTAL W algorithm in the Megaline program of the DNA Star software package. Since the carboxy-terminal moiety of eIF4E is highly conserved and contains all the functional residues, it was used to construct the eIF4Es tree. For a definition and comparison of the carboxy-terminal moiety of eIF4Es, see (Hernandez et al. 2005). The accession numbers are in parenthesis.

3.5 Diverse cellular roles of eIF4E1

eIF4E1 is a molecule essential for life of all eukaryotes from yeast to human as experimentally evidenced by the induction of cell death in Hela cells upon siRNA mediated depletion of 4E1 and studies with 4E gene disruption in yeast and mouse (De Benedetti and Rhoads 1990; Joshi et al. 2002; Truitt et al. 2015). Homozygous knockout of the *eif4e* gene is lethal in mice, the heterozygotes though exhibit normal growth and development and interestingly, they are resistant to oncogenic transformation (Truitt et al. 2015).

Concerning the sub-cellular distribution of 4E1, the substantial fraction is located in the cell nuclei (up to 68%) where it localizes to discrete sites, 4E nuclear bodies and PML bodies (Lejbkowicz et al. 1992; Cohen et al. 2001). In the nucleus, 4E1 promotes export of selected mRNAs, such as *cyclin D1* mRNA via an element in the 3′UTR, called 4E sensitivity element and thus regulates the abundance of mRNAs available for translation initiation (Culjkovic et al. 2005). Interestingly, although 4E mutant Trp73Ala preserves cap-binding properties, it cannot actively participate in translation due to inability to bind 4G. Nevertheless, it still functions in mRNA transport and transforms the cells (Ptushkina et al. 1998; Ptushkina et al. 1999; Cohen et al. 2001).

The activities of such a potent translation initiation regulator, as 4E is, must be tightly regulated. So far, 199 homeodomain proteins bearing potential 4E binding sites, has been identified, these could potentially be a tissue-specific regulators of eIF4E. One of them is a transcription factor, the proline- rich homeobox protein (PRH). PRH acts as a negative regulator of eIF4E in myeloid cells, inhibits eIF4E-depedent mRNA transport and subsequent transformation. eIF4E and PRH directly interact via phylogenetically conserved sequence of a consensus YXXXXLΦ in both the nucleus and cytoplasm. These activities are independent on PRH transcriptional functions (Topisirovic et al. 2003).

Consistent with the eIF4E function in translation, eIF4E level is a prognostic indicator of clinical outcome in a variety of human cancers including breast cancer, head and neck squamous carcinoma and several non-Hodgkin B-cell lymphoma and others, for review see (Bhat et al. 2015). The growth-promoting and transforming properties of 4E are thought to involve increased translation of mRNAs important to

growth control. eIF4E does not increase translation of all mRNAs uniformly, there is a subset of transcripts that are more sensitive to eIF4E levels than others (Sonenberg and Gingras 1998). The 5′UTR complexity is partially responsible for the transcript sensitivity to 4E-mediated translation. The complexity of 5′UTRs slows down the translation rates. The housekeeping genes tend to have rather short, unstructured UTRs and growth control mRNAs usually have more complex UTRs. As a result, the growth control mRNAs are not translated as efficiently as the housekeeping gene′s mRNAs. Consistently, eIF4E overexpression leads to increased translation of transcripts with highly structured 5′UTRs (Rousseau et al. 1996). The oncogenic potential of eIF4E1 has been characterized in many model systems and is an emerging therapeutic target for cancers, giving rise to the cap-binding inhibitors such as ISIS183750 and ribavirin in clinical trials (Assouline et al. 2009; Duffy et al. 2016).

The ability of 4E1 to bind the cap can be prevented via micro RNAs (miRNA). Namely, let-7 miRNA inhibit cap-dependent translation (Pillai et al. 2005). Both the functional cap structure and polyA tail are necessary for miRNA mediated mRNA repression (Humphreys et al. 2005; Mathonnet et al. 2007). Humphreys et al. (2005) showed, using constructs employing EMCV IRES capable of 4G but not 4E recruitment, that the molecular target of miRNA mediated repression is indeed eIF4E.

Recently, it was shown that expression of 4E is down-regulated by miRNA-496 in osteosarcoma cells from human patients and in this way osteosarcoma tumour progression could be efficiently down-regulated (Qi et al. 2019).

3.6 Comparison of eIF4E1 and eIF4E2 structures

In eIF4E1, amino acid alignment showed 170 aa long core, essential for cap-binding, conserved in all eukaryotes (Vasilescu et al. 1996). Most residues involved in binding of the m^7GTP is conserved across the species (Rosettani et al. 2007). eIF4E1 structure is formed of eight antiparallel β strands and three helices creating a cupped-hand shape (see Fig. 4). Two tryptophan residues Trp56 and Trp102, located in a cavity inside the concave surface, hold the guanine residue of the cap through $\pi - \pi$ stacking interactions. The interaction is further stabilized by a formation of hydrogen bonds between the nucelotide base and both the polypeptide backbone and a conserved Glu103. Trp166 recognizes the presence of the N^7-methyl group of the cap structure (Matsuo et al. 1997).

The overall structure of 4E2 is very similar to that of 4E1. 4E2 is formed by a central curved beta-sheet consisting of seven antiparallel β strands, surrounded on its convex site by three α-helices, see Fig. 4. The m^7GTP binding site is situated on the concave surface of the beta sheet, with the loop and helix between strands β1 and β2. The loop between strands β3 and β4 and the C-terminal α helix also contribute to formation of the cleft for the ligand. Strand β8 of 4E1 is completely missing in 4E2, due to the presence of Arg197 in 4E2 instead of glycine. C-terminal flexible loop starting at the position Ser207 of 4E1 is disordered in 4E2. The „cupped hand" structure of 4E1 therefore appears a little more closed in the case of 4E2.

Fig. 4 Comparison of eIF4E1 and eIF4E2 structures adapted from (Rosettani et al. 2007)

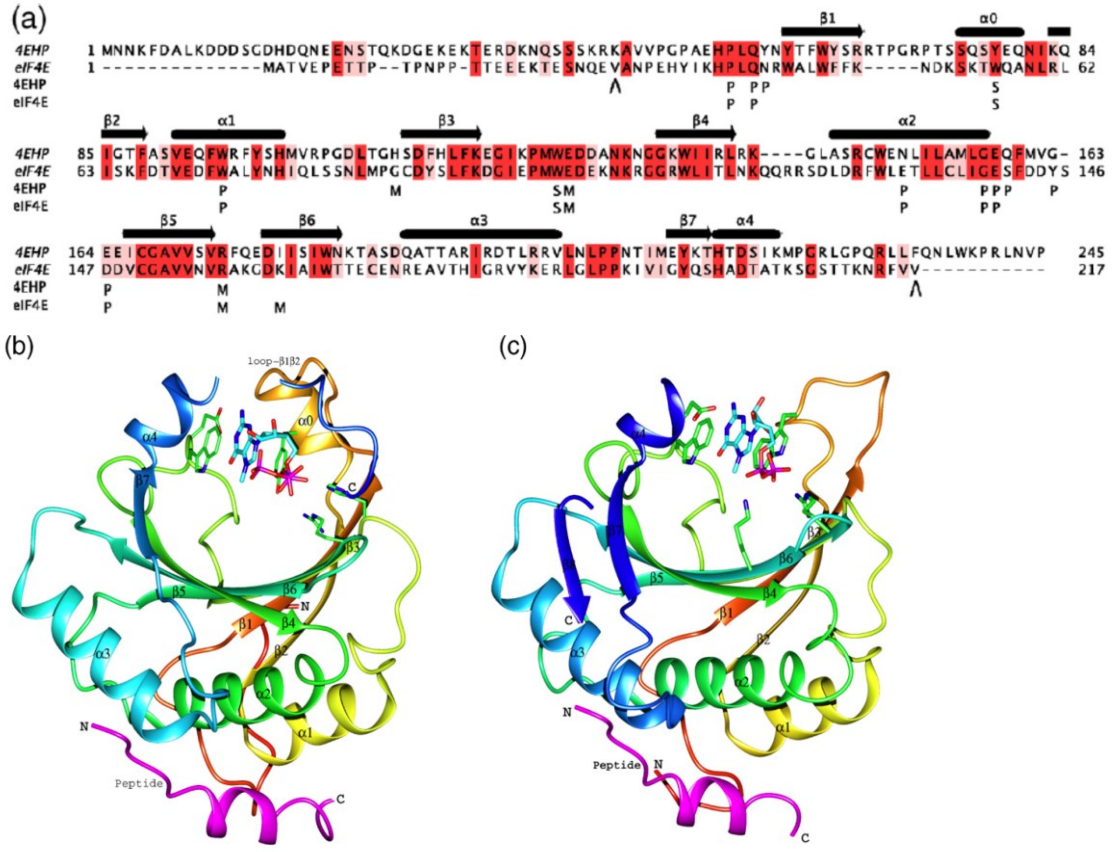

Alignment of human 4E1 and human 4E2 is shown in A) The alignment was prepared in Jalview version 2.1.1. The secondary structure elements have been named as for 4E with the additional helix in 4E2 labelled as α0. Identical residues are highlighted in red, 90% conservation is shown in pink. The annotations below the alignment show the residues that form a hydrogen bond with the peptide (P) or the M^7GTP (M) and the aromatic residues that sandwich the nucleotide (S). The limits of the protein used for the crystallization are marked with ^. B) Schematic representation of 4E2 (K45- P234). The protein has been colour ramped according to the residue number, starting with red on the N-terminus and finishing with blue at the C-terminus. The peptide has been coloured magenta. Tyr78 and Trp124 that sandwich the nucleotide and Glu125, His110 and Arg174 which are within hydrogen bonding distance of the ligand are shown in green carbon atoms C) The structure of mouse 4E bound to m^7GDP and 4E-BP1 (PDB accession number 1EJ4 shown in the same orientation and using the same colour scheme as in A.

Both 4E1 and 4E2 have disordered N-terminus, 4E3 on the other hand, has disordered C-terminus. The conformational differences of the aromatic residues involved in cap-binding of proteins 4E1, 4E2, 4E3 and 4Es from different organisms were studied using near UV circular dichroism spectroscopy (CD). The results showed that cap-binding of 4E1 is completely abolished upon substitution of both Trp56 and Trp102 to alanines. However, upon single tryptophan substitution, the residual cap-binding ability is preserved. Moreover, 4E3 binds the cap 12-fold weaker and 4E2 binds the cap 100-fold weaker than canonical h4E1 (Zuberek and Stelmachowska 2017).

3.7 eIF4E1 binding partners

Concerning binding partners, 4E-BP1 is a well-recognized translation regulator. 4E-BPs and 4G contain consensus 4E binding region YXXXXLΦ, where Φ stands for any hydrophobic amino acid. Consequently, 4E-BPs act as a competitive inhibitors of the eIF4E interaction with 4G, see Fig. 5 (Gingras et al. 1999; Marcotrigiano et al. 1999). The binding of 4E-BPs is controlled by phosphorylation at multiple sites under the control of phosphatidylinositol-3 kinase signal transduction pathway through protein kinase B (Gingras et al. 1998; Takata et al. 1999) and FK506 binding protein/rapamycin-associated protein or mammalian target of rapamycin (Gingras et al. 1999). 4E1 Trp73 is critical for 4E-BP1 binding to 4E1 (Ptushkina et al. 1998; Ptushkina et al. 1999). 4E1 binds all the three 4E-BPs to the same extent (Pause et al. 1994; Poulin et al. 1998; Joshi et al. 2004).

Another important structural feature of eIF4E1 is a phylogenetically conserved sequence containing Val69 and Trp73 of the consensus (S/T)V(e/d)(e/d)FW, where the lower case indicate acidic residues, that are not fully conserved. Substitution of Trp73 to a non-aromatic residue has been shown to disrupt the interaction of 4E with eIF4G or 4E-BPs (Ptushkina et al. 1999; Pyronnet et al. 1999). Similarly, a substitution of Val69 for a Gly residue results in a variant of 4E capable of binding 4E-BP1 but compromised in binding of eIF4G or 4E-BP2 (Ptushkina et al. 1999). Surprisingly enough, Trp73 is required for the ability of *Dm*4E1 to localize to SGs and PBs. On the other hand, the cap-binding residues Trp56 and Trp102 are dispensable. Therefore protein-protein rather than protein-mRNA interactions are essential for the recruitment of 4Es to the RNA granules. Strikingly, cycloheximide treatment prevents accumulation of both wt

and mutant (Trp56Ala and Trp102Ala) eIF4Es in PBs, suggesting at least a fraction of 4E1 is directed to PBs from the polysomes (Ferrero et al. 2012).

Other well-known binding partner of 4E1 is 4E transporter (4E-T), it competes with eIF4G for eIF4E1 binding, inhibits cap-dependent translation as well as regulates ARE (AU-rich element) mRNAs stability (Dostie et al. 2000). 4E-T localizes to PBs and is responsible for the translocation of 4E1 to the nuclei and PBs (Dostie et al. 2000; Andrei et al. 2005; Ferraiuolo et al. 2005; Lee et al. 2008).

Somewhat mysterious is a role of 4E Ser209 phosphorylation in the translation initiation process. Ser209 is phosphorylated via MAPK interacting serine/threonine kinase 1,2 (MNKs) and the phosphorylation does not alter the binding of 4E-BP or 4G to 4E (Duprat et al. 2002; Scheper et al. 2003). Nevertheless, 4E Ser209 is localized close to the channel where mRNA exits eIF4E, therefore phosphorylated 4E binds less tightly to the capped mRNA than does the non-phosphorylated protein (Song et al. 2010). It has been shown, that phosphorylation on 4E Ser209 is required for its pro-oncogenic properties (Lellis et al. 2002). Moreover, translation of specific mRNAs involved in the processes such as cell differentiation and migration (including cancer metastasis), synaptic plasticity and long term memory formation might be regulated via this phosphorylation. Cytoplasmic fragile X protein interacting protein 1 (CYFIP1) binds to 4E and blocks its interaction with 4G. Fragile X mental retardation protein (FMRP) binds directly the mRNAs and represses their translation at the elongation step via direct binding to the 60S ribosome, see Fig. 5. Diverse stimuli via MNK mediated phosphorylation of 4E Ser209 result in the CYFIP/FMRP release from 4E and subsequent 4E-4G complex formation (Bramham et al. 2016).

FMRP and CYFIP1 in coordination with 4E drive also synaptic maturation. Stimulation of neuron by neurotropic factors causes CYFIP to dissociate from eIF4E at synapsis and results in translation of previously repressed mRNAs (Napoli et al. 2008). Other 4E binding partners active in the development of nervous system in vertebrates via mRNA translational repression are Maskin and Neuroglinin (Richter and Sonenberg 2005; Jung et al. 2006).

Fig. 5 Mechanisms for regulation of 4E mediated translation initiation, adapted from (Bramham et al. 2016)

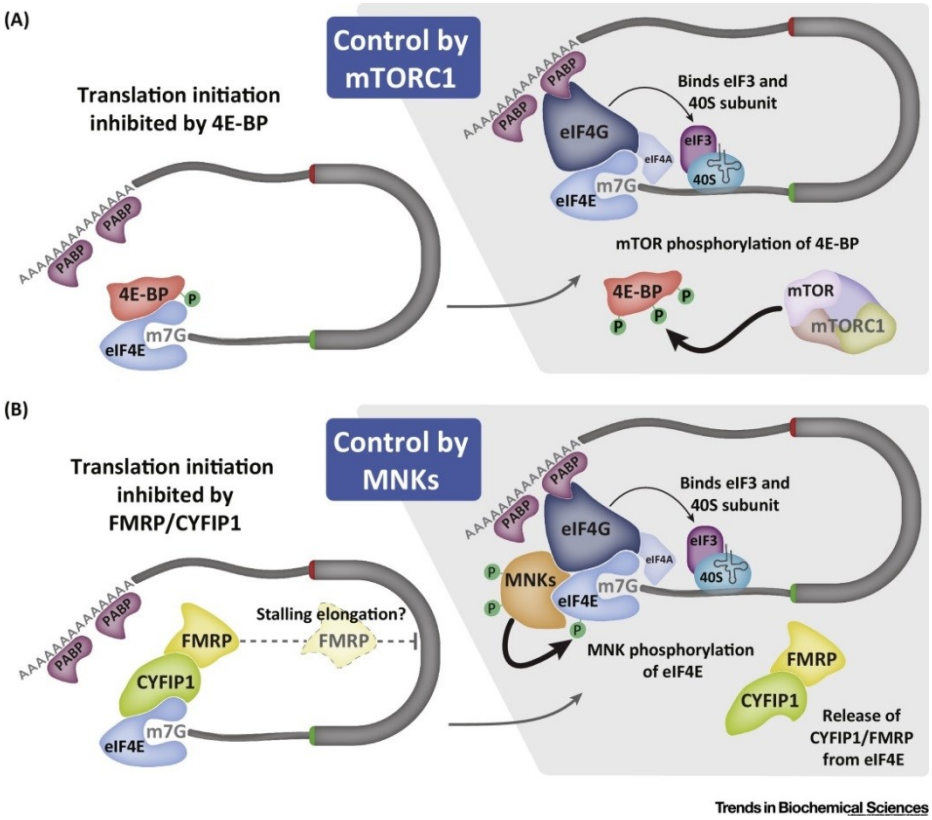

In the absence of mammalian target of rapamycin complex 1 (mTORC1) signalling (left), the 4E-BP is hypo-phosphorylated, which permit 4E sequestration away from the translation initiation machinery. When mTORC1 signalling is active (right), mTOR phosphorylates 4E-BPs, hyper-phosphorylated 4E-BP cannot bind 4E, thus permitting 4F complex formation. (B) Cytoplasmic FMRP-interacting protein 1 (CYFIP1) in a complex with fragile X mental retardation protein (FMRP) can bind 4E, thus inhibiting 4F complex formation (left). MNK signalling stimulates release of CYFIP1 from 4E (right), allowing 4F complex formation and recruitment of the translational machinery.

Beside their role in the nervous system development, eIF4E binding proteins are also involved in translation repression in embryogenesis. In *Drosophila* embryo, Nanos protein represses translation of *nanos* mRNA, permitting posterior body development. Spatial regulation of *nanos* translation requires Smaug protein bound to the 3´UTR of *nanos* mRNA. Smaug interacts with Cup, which is an eIF4E interaction partner (Nelson et al. 2004). *Oskar* mRNA is being repressed via Cup, an eIF4E binding protein, during its localization to the posterior of the oocyte (Nakamura et al. 2004; Zappavigna et al. 2004). In the anterior region of the embryo, 4E1 represses translation of ubiquitously expressed *caudal* mRNA via Bicoid protein partner (Niessing et al. 2002). In higher organisms, a variety of homeobox genes are regulated via eIF4E1 e.g., HOXA9, for review see (Topisirovic and Borden 2005).

3.8 eIF4E1 variants across kingdoms

Four transcript variants of 4E1, coding for four distinct proteins have been identified human to date (Mrvova et al. 2018). Eight variants of 4E1 were found in *Drosophila* (Lavoie et al. 1996; Reyes and Izquierdo 2008), five in *C. elegans* (Keiper et al. 2000) two in *S. pombe* (Ptushkina et al. 2001*)* and six in *Trypanosoma* (Dhalia et al. 2005; Freire E.R 2014; Freire et al. 2014). Class I family members can be identified in species from *Viridiplantae, Metazoa* and *Fungi* . The closest orthologues includes *H. sapiens* eIF4E1, *M. musculus* eIF4E1, *T. aestivum* eIF4E and eIFiso4E *S. cerevisiae* eIF4E. At the amino acid level they share 35-40% identity and 60-65% similarity with one another, for details see (Joshi et al. 2005). Human eIF4E-1 (Altmann et al. 1989), zebra fish eIF4E-1A (Robalino et al. 2004), *A. thaliana* eIF4E (Rodriguez et al. 1998) and *Drosophila* eIF4E-1, eIF4E-2, eIF4E-3, eIF4E-4, eIF4E-7 are capable of rescuing the yeast growth in the absence of endogenous eIF4E (Hernandez et al. 2005).

Usually organisms contain multiple genes encoding proteins that have sequence similarity to the prototypical eIF4E (Joshi et al. 2005; Mrvova et al. 2018). Nevertheless, for organisms with multiple 4E related genes, only one eIF4E protein is ubiquitously and constitutively expressed and therefore responsible for routine cap-dependent translation. For *Drosophila*, this is eIF4E1 (Hernandez et al. 2005), mammalian eIF4E1(Joshi et al. 2004), *C. elegans* IFE3 (Keiper et al. 2000), zebra fish eIF4E1A (Robalino et al. 2004) and plant eIF4E (Rodriguez et al. 1998). Other eIF4E – related proteins are active only in particular tissues or bind to a limited number of mRNAs, for review see (Hernandez and Vazquez-Pianzola 2005). The function of 4E related proteins is not yet understood. Some of them may act as a translation initiation factors or stimulate global or specific mRNA recruitment (Ruud et al. 1998; Dinkova et al. 2005).

3.8.1 Plants

Plants contain two different but related proteins termed plant eIF4E and eIFiso4E (Browning et al. 1987; Nicaise et al. 2003). In wheat germ, two forms of eIF4E exist, 26 and 28 kDa in molecular mass, but they share only 50% identity and are found in different cap-binding complexes (Browning et al. 1987; Allen et al. 1992; Metz et al. 1992). In lettuce, eIF4E is involved in the ability of potyviruses to infect and produce symptoms of lettuce mosaic virus. eIF4E has no role in plant´s response to the lettuce

mosaic virus (Nicaise et al. 2003). Nevertheless, disruption of eIFiso4E gene was associated with resistance to three different potyviruses (TEV, TuMV, LMV) and the gene is dispensable for growth (Duprat et al. 2002; Lellis et al. 2002). In tomato, there are three genes coding for 4E: eIF4E1, eIF4E2 and eIFiso4E. Whereas upon silencing eIFiso4E the plants developed no resistance to potyviruses, silencing for both eIF4E1 and eIF4E2 showed broad spectrum of resistances. (Mazier et al. 2011). Recently, the advent of CRISPR-CAS9 gene editing has enabled to introduce resistance to potyviruses to sensitive crops without adverse phenotype effect. Thus, trans-gene free genetic resistance in plants across species barriers is available (Bastet et al. 2019)

3.8.2 Zebrafish

Three eIF4E1 sub-family members can be identified from zebrafish (*Danio reio*), termed 4E1A, 4E1B and 4E1C. 4E1A and can bind the cap structure, eIF4G and 4E-BP *in vitro* and restore a growth of *S. cerevisiae* lacking a functional 4E gene. Conversely, 4E1B is expressed during early embryogenesis, limited to gonads and muscles and unable to sustain 4E1A functions (Robalino et al. 2004). Zebra fish eIF4E1B does not bind to the cap and eIF4G (Robalino et al. 2004).

3.8.3 Fruit fly

In *Drosophila*, seven genes code for 8 variants of eIF4E proteins. Therefore one of these genes, eIF4E1,2 gives rise to three mRNAs with different 5´UTRs. The alternative splicing is regulated by Half pint in the ovary and gives rise to the *eIF4E1a* and *eIF4E1b* mRNAs that encode eIF4E1 protein, while *eIF4E2* mRNA encodes eIF4E-II protein (not a homologue of human eIF4E2 but of a human eIF4E1). 5´UTR of *eIF4E1a* and *b* promotes important increase of translation efficiency of a luciferase encoding chimeric mRNA (Lavoie et al. 1996; Reyes and Izquierdo 2008)

All of the isoforms bind to the cap analogue and except for 4E6, all of them are able to interact with *Drosophila melanogaster* 4G or 4E-BPs. Their expression varies during fly´s life cycle. *eIF4E1* is the only isoform expressed throughout the life cycle. eIF4E6 displays lowered cap-binding activity due to C-terminal truncation and it does not interact with 4G at all. To support growth of yeast mutant lacking functional 4E was possible for following isoforms: eIF4E1, eIF4E3, eIF4E7, eIF4E2 and eIF4E4. Dm4E3 binds the cap structure, 4G and 4E-BPs (Hernandez et al. 2005). It is a testis-specific

protein that controls translation initiation exclusively during male germ line development. It is not only required for meiotic chromosome segregation and cytokinesis, but also for the later stages such as nuclear shaping and individualization. Consequently, 4E3 mutant flies fail to form mature, individual sperms (Hernandez et al. 2012).

3.8.4 Caenorhabditis elegans

C. elegans possesses five eIF4E family members IFEs. IFE3 binds only to mono-methylated cap structure. IFE1,2,5 interact with both mono-methylated and tri-methylated cap structure (Keiper et al. 2000). IFE1 is required for spermatogenesis (Amiri et al. 2001).

On the other hand, IFE2 is expressed in somatic tissues. Its knock out reduces global protein synthesis, protects from oxidative stress and extends life span (Syntichaki et al. 2007). IFE2 deletion leads to low brood size, severe embryonic lethality and high incidence of males in elevated temperature (25°C), suggesting a role in a conserved temperature-sensitive meiotic process (Song et al. 2010).

3.8.5 Schizosaccharomyces pombe

Class I family members in fission yeast *(Schizosaccharomyces pombe)* are named eIF4E1 and eIF4E2. Expression of eIF4E2 is not essential, both though, can bind the cap (Ptushkina et al. 2001). While eIF4E1 is required for general cap-dependent translation, eIF4E2 is involved in translation during stress response (Ptushkina et al. 2004).

3.8.6 Sea urchin

One eIF4E1 gene is present in the sea urchin genome (Morales et al. 2006).

3.8.7 Virus

4E gene was discovered in *Mimivirus* (Raoult et al. 2004)

3.8.8 Trypanosoma

There are six 4Es present in *Trypanosoma brucei*. All of them belong to the class I 4E protein family members and are constitutively expressed throughout the parasite life cycle. 4E3 is essential for the insect procyclic form and together with 4E1 and 4, they

are all essential for the mammalian bloodstream form. Meanwhile 4E1 and 2 are found in the nuclei and cytoplasm, 4E3 and 4E4 are cytoplasmic only. Nevertheless 4E1, 2 and 4 but not 3 are capable of cap-binding and only 4E3 and 4E4 are capable of binding 4G (Freire et al. 2011; Freire E.R 2014; Freire et al. 2014).Two distinct eIF4F complex has been confirmed in trypanosomatids. They consist of: eIF4E4/4G3/4AI and eIF4E3/4G4/4AI, respectively. The first complex has been implicated as performing a critical role in translation initiation (Pereira et al. 2013) and depletion of eIF4E3 by RNAi substantially inhibits protein synthesis in *T. brucei* (Freire et al. 2011). Both eIF4E3 and eIF4E4 are highly phosphorylated and the level of 4E4 phosphorylation strongly correlates with active growth and enhanced protheosynthesis (Pereira et al. 2013). Consistently, only 4E3 and 4E4 were found associated with the polysomes (Klein et al. 2015). *T. brucei* 4E1 and 4E2 aggregate into granules following heat shock(Kramer et al. 2008) and their double knock-down is lethal (Freire et al. 2011). *Tb*4E2 participates in association with a homolog of human histone mRNA stem-loop binding protein and in this way binds selective mRNA population and possibly influence their translation and stability by an unknown mechanism (Freire et al. 2017).

3.8.9 Giardia lamblia

eIF4E1 was also reported in *Giardia lamblia*, it binds to tri-methylated cap of sno-RNA-like molecules and is not involved in translation initiation of the protist. *Gardia lamblia* eIF4E is uncapable to rescue yeast mutant strain growth, bearing a 4E gene disruption (Li and Wang 2005)

3.8.10 Xenopus leavis

In *Xenopus*, two different eIF4E canvas have been isolated (Wakiyama et al. 1995). eIF4E1a is the canonical translation initiation protein. *eIF4E1b* gene arose in *Tetrapoda* via eIF4E ancestral locus duplication. It has an oocyte – restricted expression across all the classes of *Tetrapoda* and acts as a translational repressor of dormant maternal mRNA. This activity is surprising as all the residues critical for cap-binding and interaction with eIF4G and eIF4E-BP are absolutely conserved among eIF4E1b and eIF4E (Evsikov and Marin de Evsikova 2009). Assuming the functional identity among eIF4E1b proteins in vertebrates, the important characteristics is weak mRNA cap and 4G binding and strong affinity to 4E-T (Robalino et al. 2004; Minshall et al. 2007).

3.9 eIF4E2 – a molecule of two faces

3.10 History, structure, phylogenesis

Human eIF4E2 was first cloned in 1998 from a fetal brain library by Rom et al. (1998). The eIF4E2 variant referred to in this thesis as *eIF4E2_A* comprises of 989 base pairs in length and codes for 245 amino acid long open reading frame containing a protein with a calculated mass of 28 kDa. 4E2 is 28% identical and 60% similar to 4E1 and 25% identical to 4E3. The authors reported, there was 5-10x less 4E2 protein compared to endogenous 4E1 in Hela and HEK293 cell lysates (Rom et al. 1998; Joshi et al. 2004)

First structure was solved by Pamela Rosettani and colleagues (2007). They achieved better resolution than later on (Peter et al. 2017). X ray crystallography was the method of their choice with the achieved resolution of 1,7 Å see Fig. 4. Beside the structure, the authors show, that 4E2 is able to bind the cap and 4E-BP1, but with lower affinity compared to 4E1.

A sequence of eIF4E2 is very well conserved among wide variety of metazoans and plants (Joshi et al. 2004; Rosettani et al. 2007).

3.11 Zoom into the cap-binding

4E2 displays lower binding affinity for cap analogues in comparison with 4E1. 4E2 association constant for m^7GTP is about 100 times lower compared to that of 4E1. Whereas the dinucleotide triphosphate cap analogues (m^7GpppG, m^7GpppA and m^7GpppC) are bound by 4E2 approximately 30 fold weakly in comparison with 4E1 and finally the decrease for m^7GMP is only 10 fold. Interestingly, the underlying reason is not substitution 4E1 Trp56Tyr typical for Class II 4E, as shown by employing a 4E1 mutant with such a substitution, but it is the 4E2 Lys112Arg replacement analogous to 4E1 Arg112, which interacts with α-phosphate group of the cap by a water mediated hydrogen bond. Lysine, contrary to Arg possess a shorter side chain, which prevents the formation of water mediated hydrogen bond. This is partially the underlying reason for the lower cap-binding ability of 4E2 in comparison with 4E1 (Zuberek et al. 2007). On the contrary, mouse 4E2 binds the cap effectively (Morita et al. 2012). Recently, two

publications showed efficient human 4E2 cap-binding irrespective to the oxygen level (Chen and Gao 2017; Jeong et al. 2019).

3.12 eIF4E2 binding partners

Tee and colleagues (2004) together with Rossetani (2007) reported, that eIF4E2 is capable of binding 4E-BP1, unlike its Trp95Ala mutant lacking a residue corresponding to Trp73 in 4E1. The interaction of 4E2 with 4E-BP is not as strong as is that of 4E1. Using classical immunoprecipitation method with overexpressed 4E2, 4E2 did not co-purify with 4E-BP1. The authors hypothesize about 4E2 overexpression-induced basal and insulin stimulated phosphorylation of 4E-BP1 (Rom et al. 1998; Tee et al. 2004). Insulin stimulation causes dissociation of 4E-BP1 from 4E as a result of increased 4E-BP1 phosphorylation (Gingras et al. 2001; Wang et al. 2003) but does not cause the release of 4E-BP1 from 4E2 (Tee et al. 2004). Later on, it was shown that 4E2 binds more strongly 4E-BP2 and 3 than 4E-BP1 (Joshi et al. 2004). Kubacka and colleagues reported (2013) a new binding partner of eIF4E2, eIF4E-T. The authors reported that, the ratio of 4E1:4E-T range from 50:1 to 15:1 in Hela and HEK293 cells, meanwhile the ratio of 4E2:4E-T varies from 6:1 to 3:1. On the contrary to 4E1, 4E2 is trans-located to the nucleus in a Crm-1 dependent, but 4E-T independent manner (Kubacka et al. 2013).

3.13 eIF4E2 variants across kingdoms

Class II family members share 50 % identity and 70-80 % similarity with each other and share a structural core of 160-170 amino acids essential for cap-binding as well as 4E1 (Joshi et al. 2005). For the Class II of eIF4E2 protein family is typical, that Trp56 of eIF4E1 has been replaced with Tyr or other hydrophobic residue such as Phe, Leu. In mouse and human 4E2, both Trp43 and 56 of 4E1 have been replaced with Tyr. Members of this class from *Metazoa* and *Viridiplantae* also contain a substitution at the position equivalent to Trp43. This substitution does not disrupt stacking interaction essential for the cap-binding (Joshi et al. 2005). In human, seven transcript variants coding for four different variants of 4E2 protein exist. The most studied of them is the isoform 4E2_A (Mrvova et al. 2018). An equivalent of mammalian 4E2, IFE4 is found in *C. elegans* (Dinkova et al. 2005) and *Drosophila* eIF4E8 (Hernandez et al. 2005).

Plants possess novel cap-binding protein (nCBP) (Ruud et al. 1998). They all can bind to the cap. nCBP are special members of 4E2 family because they can both interact with the cap and with the plant isoform of 4G, eIFiso4G and thus take a part in the translation initiation (Ruud et al. 1998; Joshi et al. 2004).

On the contrary, mammalian 4E2 has been reported not to interact with eIF4G *in vitro* (Rom et al. 1998) similarly to *D. melanogaster* eIF4E2. Consistently, neither mouse 4E2, nor *Drosophila* eIF4E2 can substitute for the *S. cerevisiae* 4E in a strain lacking a functional gene (Joshi et al. 2004; Hernandez et al. 2005). *H. sapiens* and *M. musculus* eIF4E2 can interact with 4E-BPs, but to a lesser extent than mammalian eIF4E1 (Joshi et al. 2004; Tee et al. 2004). Knock-down of IFE4 suggests, that the protein is not required for normal development (Keiper et al. 2000). Class II family members can also be recognized in fungi from the sub-phylum *Pezizomycotina*, including *Coccidioides pasadasii* and *Sclerotina schleroiorum*, but are absent in the model ascomycetes *S. cerevisiae* and *S. pombe* (Joshi et al. 2005).

EIF4E2 was also reported in *Giardia lamblia*. It binds the mono-methylated cap and is involved in translation initiation, nevertheless, it is uncapable to rescue yeast mutant strain growth, bearing a 4E gene disruption. 4E1 Trp56 and Trp102 are replaced by Phe (Li and Wang 2005).

3.14 Regulatory role of eIF4E2

For 14 years, people have presumed *Metazoan* eIF4E2 to be unable to initiate protheosynthesis due to its inability to bind eIF4GI. A regulatory role has been assigned to it, instead.

3.15 Drosophila melanogaster

*Dme*IF4E8 may be either negative regulator of translation or simply non-functional protein because it is unable to bind 4G or 4E-BP or complement growth of yeast mutant lacking functional 4E and its ability to bind the cap is limited due to series of substitutions in the cap-binding residues. Nevertheless, its mRNA is produced in embryos and throughout the life cycle of the fly, even though to a lower level comparing to eIF4E1 (Hernandez et al. 2005). First example of a translational regulation mediated via eIF4E2 was shown by Cho and colleagues (2005), eIF4E8 is needed for

the translational inhibition of the *caudal* mRNA in the anterior part of the embryo. *Dme*IF4E8 is bound simultaneously to the cap structure and to the Bicoid protein bound in Bcd binding region located at the 3´UTR of *caudal* mRNA.

4E2 also inhibits *hunchback* mRNA by interacting with the cap and Brat, thus by inhibiting *hb* and *caudal* mRNAs, *Dm*4E2 plays a key role in establishing anterior-posterior body axis (Cho et al. 2006). Weidemann and Goldstrohm (2012) questioned the role eIF4E2 plays in the *hunchback* mRNA inhibition mediated via Pumilio. The authors uncover two modes of Pumilio mediated repression: a Nanos-dependent mode and a Nanos-independent mode. For both the modes 4E2 is dispensable. The authors depleted 4E2 using two independent siRNAs and measured the percentage of repression of NRE mRNA in a *Drosophila* cell lysate. Pumilio and Nanos co-operate to repress but 4E2 remained dispensable. How exactly Pumilio represses translation and why it possesses several repression domains remains an open question.

4E2 represses *bel* mRNA in the ovary. Bel protein is an 4E1 binding protein that represses *oskar* mRNA in cooperation with Bruno. Therefore *bel* participates in a series of translation inhibition events that leads to the correct expression of axis defining by the protein Osk in the developing oocyte (Yarunin et al. 2011).

A null mutation of 4E2 leads to delay in development, growth failure and eventually death as 4E2 is required to activate expression of several genes encoding enzymes responsible for ecdysone biosynthesis (Valzania et al. 2016). *Dm*4E2 binds both mono and tri-methylated caps approximately 3 times weaker than *Dm*4E1, yet still stronger than human 4E2. The highest affinity for the cap analogues was observed for *Dm*4E3 and the authors suggest, it binds the second nucleoside of the cap in an unusual manner via stacking interactions with histidine residues (Zuberek et al. 2016).

3.15.1 Sea urchin

There is an eIF4E2 protein present in the sea urchin proteome (Morales et al. 2006).

3.15.2 Mouse

Prep-1 is a homeodomain protein, during development it is essential for the embryonic patterning and cell fate determination. Prep1 and protein Pbx form stable complexes that regulate the transcription of some *homeobox* genes (Ferretti et al. 2006; Moens and Selleri 2006). Mouse *homeobox* gene´s 4 and 8 mRNAs can be effectively

immunoprecipitated by Prep-1. The authors also showed, neither Prep1 nor 4E2 were associated with polysomal fractions. Prep1 inhibited more than 95% of *in vitro* translation of a luciferase reporter mRNA fused to *hoxb4* 3´UTR via 4E2 mediated cap-binding. This is the first example of mammalian regulation of translation mediated by a transcription factor (Villaescusa et al. 2009).

Another translational repressor complex, essential for mammalian development, was described by Morita and colleagues (2012). It is composed of Grb10 interacting GYF protein 2 (GIGYF2) and the Zinc finger protein 598 (ZNF598) and mouse 4E2. It represses translation of a subset of mRNAs during embryonic development via cap-binding mediated by mouse 4E2. EIF4E2 bind effectively GIGYF1 and GIGYF2 *in vitro*, but GIGYF2 is bound preferentially, moreover it is not bound by mouse 4E1. Depletion of 4E2 causes an increase in translation measured by [^{35}S]-methionine incorporation normalized to total protein amount and 4E2 KO mice died in the hours following the natural birth.

Analysis of mouse microarray data revealed that, *4e2* is a subject of widespread, differential alternative polyadenylation events that are dependent on tissue, cell type or development state (Hu et al. 2014; Mrvova et al. 2018)

3.15.3 Human

Flag tagged eIF4E2, not the endogenous one, co-immunoprecipitates with human homologue of ariadne (HHARI), which is an E3 ubiquitin ligase from a Parkin family. HHARI potentially mediates 4E2 polyubiquitylation in coordination with ubiquitin conjugating enzyme E2 L3 (UBCH7) (Tan et al. 2003). HHARI, also known as ARIH1, protects stem and cancer cells against genotoxic compounds and gamma irradiation by promoting 4E2-mediated translational arrest. The 4E2 interaction with m^{7}GTP resin in the study is rather weak, but fortified upon genotoxic stress-induced poly-ubiquitylation. Upon silencing of 4E2, cells were subjected to the genotoxic stress and the viability of 4E2 silenced U2OS and ES cells was severely compromised. Thus the inhibition of 4E2 and ARIH1 might sensitise the cancer cells to different chemotherapeutics (von Stechow et al. 2015). Okumura and colleagues provided evidence that ARIH1 can ISGylate 4E2, therefore enhancing its affinity for the cap. The authors conclude, that 4E2 is able to replace 4E1 on the cap structure and behave like a translational inhibitor (Okumura et al. 2007; Kong and Lasko 2012). Contribution of

ISG15 and ISGgylation in tumour growth and resistance to chemotherapy is unclear and debated in (Sgorbissa and Brancolini 2012).

Besides post-translational modification of 4E2 by ISG15, the 4E2´s affinity for the cap can also be enhanced via binding of a protein partner such as tristetraprolin (TTP) and 4E-T. Which is an underlying mechanism of 4E-2 involvement in translational repression of either AU rich mRNAs or repression by direct binding to the components of RNA induced silencing complex (RISC) (Fu et al. 2016; Chapat et al. 2017; Chen and Gao 2017).

A translation of ARE-containing mRNAs is repressed via an indirect 4E2 interaction with TTP. Grb 10 interacting GYF protein 2 (GIGYF2) bridges 4E2 and TTP. TTP interacts with all five tested isoforms of human 4E2. For the repression of a reporter mRNA with 8 AREs, the cap-binding activity of 4E-2 is necessary as evidenced by an employment of 4E2 mutant Y78A with lowered cap-binding activity. Overexpression of all four isoforms of 4E2 (A, B, C, D) enhanced TTP mediated translation repression in a dose dependent manner, while the isoform eIF4E2-E failed to do so (Tao and Gao 2015; Fu et al. 2016). In this thesis, we worked with 4E2 isoforms A and C.

Later on, it was shown that additional member, RNA dependent ATPase DDX6, is necessary for an efficient TTP mediated translational repression of AU rich mRNAs. DDX6 is recruited to the complex via an interaction with GIGYF (Peter et al. 2019). The molecular basis for the selectivity of GIGYF1/2 proteins for 4E2 over 4E1 lies in two amino acid extension (YX) in the canonical 4E2 binding motif YXYX4LΦ (Peter et al. 2017).

Binding of another 4E2 interaction partner, 4E-T, potentially leads to the displacement of 4E1 by 4E2 on the cap (Chapat et al. 2017). 4E-T interacts directly with CNOT. The scaffolding unit CNOT recruits CCR4-NOT deadenylase to the 3´poly A tail of the mRNA and leads to the establishment of 4E-T-DDX6-CCR4-NOT complex, that is active in miRNA mediated silencing of mRNAs (Fabian et al. 2011; Rouya et al. 2014; Ozgur et al. 2015). 4E-T protein also interacts with 4E1 and facilitates decay of CCR4-NOT targeted mRNAs (Nishimura et al. 2015). Chapat et al. (2017) hypothesize, that while 4E2 binding of 4E-T potentiates translational repression, direct binding of 4E1 to 4E-T leads to mRNA decay. Indeed, upon transfection of mutant 4E2 W124A, with decreased ability to bind the cap to the mouse embryonic fibroblasts with KO of

eif4e2, the cap-binding role of 4E2 was found to be essential for the CCR4-NOT mediated translational repression see Fig. 6 (Chapat et al. 2017).

Similarly, another publication shows direct interaction of 4E2 with trinucleotide repeat containing protein 6 A and B (TRNC6A and TRNC6B), the components of RISC. The cap-binding activity of 4E2 was essential for miRNA-induced repression of target mRNA (Landthaler et al. 2008; Chen and Gao 2017).

Fig. 6 Model of miRNA mediated translational repression via 4E2-4E-T-CCR4-NOT axis, adapted from (Chapat et al. 2017)

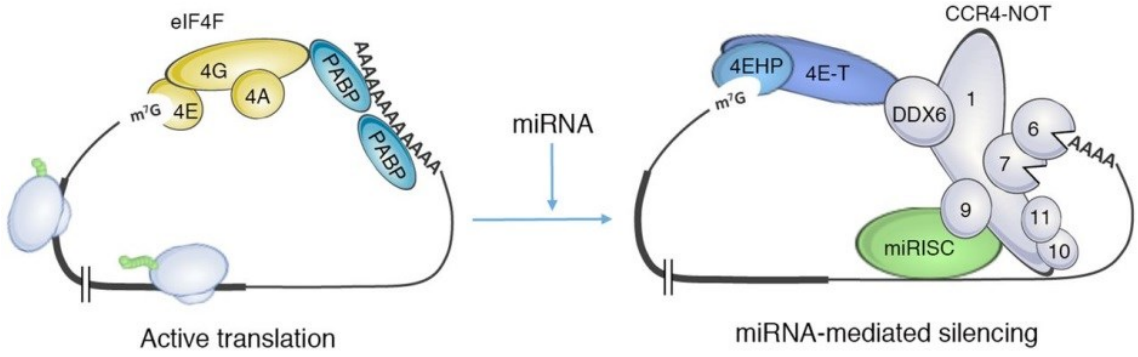

CCR4-NOT-DDX6-4E-T axis promotes 4E2 binding to the cap of miRNA target mRNAs (right). The assembly of the complex is likely to provoke formation of closed-loop structure similar to the one formed by 4E, PABP and 4G during translation initiation (left).

Recently, a way how 4E2 controls the extracellular regulated kinases (ERK) signalling cascade in mammalian cells has been discovered. *Dusp6* mRNA, which encodes ERK1/2 phosphatase, a key player in ERK regulatory feedback loops (Camps et al. 1998) is translationally repressed by 4E2 in cooperation with mir154. The mechanism of repression involves displacement of 4E1 by 4E2 on the cap via binding of 4E-T, followed by recruitment of CCR4-NOT, DDX6 and concomitant repression of 3´UTR of *Dusp6* mRNA by miRNA154. This promotes ERK1/2 phosphorylation, resulted in augmented cell growth and reduced apoptosis (Jafarnejad et al. 2018).

3.16 eIF4E2 as a translating protein

3.16.1 Caenorhabditis elegans

eIF4E2 homologue of *C. elegans*, IFE-4 is expressed preferentially in neurons, muscles and vulva. It is found in the translation initiation complexes. Nevertheless, its knockout affects the translational efficiency of only a subset of approximately thirty mRNAs and results in a phenotype that includes egg-laying defect and low brood size (Dinkova et al.

2005). Recently, the molecular mechanism of IFE-4 mediated effect on the worm´s fertility has been clarified. In somatic gonad precursor niche cells, a type of primordial germ cells, IFE-4 was shown to regulate p53-mediated UV-induced DNA damage response. The genome integrity of primordial germ cells is a pre-requisite for fertility in worms (Ou et al. 2019).

3.16.2 Human

A ground-breaking publication shed some light on the translating properties of human eIF4E2 in 2012 (Uniacke et al. 2012). The authors showed that low oxygen tension (hypoxia) represses cap-binding properties of eIF4E1 via sequestering it by 4E-BPs. Hypoxia also stimulates a formation of a complex, that includes oxygen-regulated hypoxia inducible factor 2 α (HIF2 α), the RNA binding motif protein 4 (RBM4) and the cap-binding eIF4E2. Photoactivatable ribonucleoside-enhanced crosslinking and immunoprecipitation (PAR-CLIP) analysis identified an RNA hypoxia response element (HRE) responsible for recruitment of such a complex to a wide array of mRNAs with critical function in cell proliferation, tissue development and cancer.

Once assembled, it targets mRNAs to polysomes for active translation. HIF2α but not HIF1α was observed in polysome fractions of hypoxic cells. Moreover, it was shown that 4E-BP1 has more affinity for eIF4E1 than for eIF4E2. Treatment with rapamycin, an inhibitor of mTOR, prevented the accumulation of eIF4E in normoxic polysomes but had no effect on eIF4E2. In line with that depletion of eIF4E2 severely limited global rate of hypoxic translation without affecting protein synthesis in normoxia measured by $_{35}$S-Met incorporation assay.

It is likely, that cancer cells hijack the eIF4E2 pathway for their proliferative advantage. A number of genetically diverse cancers converge at HIF2 α axis. that is obligatory for their growth (Franovic et al. 2009). Indeed,Kelly et al. (2018) showed that in hypoxic conditions, 4E2 drives translation of *Cad22* mRNA that codes for cadherin 22. This molecule is involved in cancer cell migration, invasion and adhesion. 4E2 is also a part of metastatic gene expression signature composed of 6 genes that distinguishes primary solid tumour from metastatic ones in multiple tumour types (Ramaswamy et al. 2003). Further details of 4E2 connections with cancers can be found in a recent review (Melanson et al. 2017).

Yi and colleagues (2013) presented a competing view on cap-dependent translation in hypoxic cells, that is promoted by HIF1α through up-regulation of eIF4E1 not eIF4E2 or eIF4E3 (4E3 being 1% of *4E1* expression level in normoxia and 0.3% in hypoxia). The authors showed that *eif4e3* expression is largely sequestered in the breast cancer cells at normoxia and hypoxia, meanwhile the expression of *eif4e1* and *eif4e2* is up-regulated in a HIF1α dependent manner. The promoter of *eif4e1* harbours multiple hypoxia response elements that are utilized by HIF1α to promote transcription of *4e1*. Up-regulated levels of eIF4E1 in hypoxic breast cancer cells contribute to tumour sphere growth via regulation of translation of subset of mRNAs, such as *c-Myc, cyclin-D1*, *eIF4G1*. Furthermore, hypoxic cancer cells are more sensitive to the inhibitor of eIF4G-I compared to the normoxic cells. Plus, the cellular level of eIF4E1 is increased 3 fold in hypoxia and that of eIF4E2 is increased 1.2 fold compared to that at normoxia.

A year later, James Uniacke responded by a study showing that tumorigenesis requires eIF4E2 directed translation to be able to overcome tumour size of 0.15 mm, which is the diffusion limit of oxygen. Cancer cells depleted of 4E2 are unable to proliferate under low oxygen conditions. And indeed, 4E-BP levels were induced in the majority of cells from hypoxic tumor core and eIF4E protein was observed mostly in the monosome fractions of hypoxic cells, which suggests 4E1 does not participate in active translation. Upon shRNA targeting 4E2, the glioblastoma cells were unable to produce tumours. Moreover, an established tumour of 50 mm^3 in nude mice decreased in size upon eight days of lentivirus-mediated depletion of 4E2. Those observations made 4E2 an attractive anti-cancer target (Uniacke et al. 2014).

Fig. 7 Comparison of hypoxic and normoxic 4F complexes, adapted from (Ho et al. 2016)

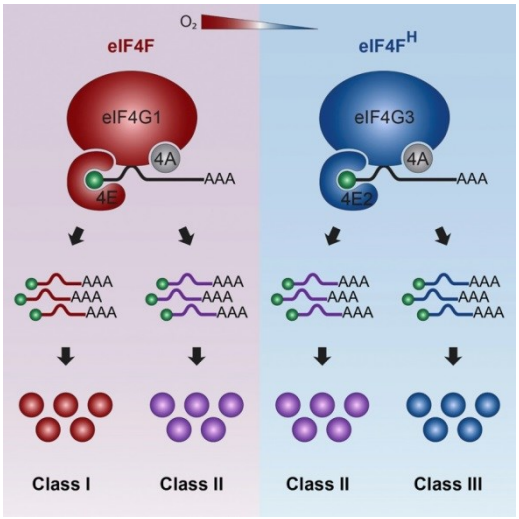

Cells rely on hypoxic switch in mRNA efficiency and not protein output on oxygen stimulus. The normoxic 4F complex consists of 4E1, 4G1, 4A and drives specifically translation of class I mRNAs, meanwhile the hypoxic 4F complex consists of 4E2, 4G3 and 4A and drives specifically translation of class III mRNAs. While class II mRNAs translation is driven by both the 4Es.

Translation efficiency is a superior predictor of steady-state protein levels compared to mRNA levels, mRNA stability and protein stability (Schwanhausser et al. 2011; Ho et al. 2016). Upon silencing of the normoxic translation initiation complex members such as eIF4E and eIF4GI, little effect on hypoxic global translation rate was observed. On the contrary, silencing hypoxic 4F complex members 4E2 and 4G3, abolished the global translation rate in hypoxic cells with little effect on normoxic cells.

The author classified cellular mRNAs into three classes with relation to the oxygen level, class I mRNAs are being effectively translated in normoxia but less in hypoxia, while class II mRNAs are efficiently translated independently on the oxygen level and class III mRNAs maintain or increase their translation efficiency in hypoxic conditions (Ho et al. 2016).

In his latest publication, Dr. Uniacke revealed that physiooxia in human tissue ranges from 1-11%, disproving anticipitated 21%. He showed that two distinct modes of cap-dependent translation are active on separate pools of mRNAs. While 4E1 is a dominant cap-binding protein at 21% of oxygen (standard cell culture conditions), 4E2 is the dominant cap-binding protein in 1% of oxygen (cancerous tumours or ischemic disease) and both cap-binding proteins act simultaneously to initiate the translation of

mRNAs in the 1-11% range of oxygen (during development and stem cell differentiation), see Fig. 7 (Timpano and Uniacke 2016).

Recently, a non-canonical translation initiation complex irrespective to the oxygen level was found in human HEK293T cells. It was shown to be responsible for vertebrate specific translation initiation of mRNAs responsible for vascular development such as *Vascular endothelial growth factor*. Threonyl t-RNA synthetase (TARS) represents both scaffold for assembly and selector of target mRNAs and binds both eIF3 and eIF4A. TARS specifically interacts with eIF4E2 but not eIF4E1 or eIF4E3. eIF4E2 in the author's hands binds the cap under normoxia (Jeong et al. 2019).

3.17 eIF4E1 and eIF4E3, what makes the difference?

In human, five different transcript variants code for two protein variants of eIF4E3: 224 amino acid long variant 4E3_A and 118 amino acid long variant 4E3_B. Besides us, nobody ever studied protein eIF3_B (Frydryskova et al. 2016; Mrvova et al. 2018) EIF4E3 was first described by Joshi and colleagues in (2004). For the class III family members it is typical, that 4E1 Trp56 is substituted with a Cysteine, meanwhile 4E1 Trp43 and 102 remain unaltered in 4E3.

Due to its Trp to Cys substitution, 4E3 is unique in its cap-binding properties as contacts between 4E3 and the cap are more extensive than in any other 4E-family members. The binding affinity of 4E3 is 10 to 40 fold lower than that of 4E1.The importance of the cysteine residue for the cap-binding was assessed by Cys to Ala substitution which severely impaired m^7G cap-binding and a backward mutation of Cys to Trp that led to 3-5 fold reduction in binding relative to wild type 4E3. Although, Cys52 in 4E3 makes less intensive contact with purine ring and m^7GDP, than is observed for Trp56 of 4E1, additional contacts are provided by the C- terminus of 4E3, which is disorder from residues His197, see Fig. 8.

Therefore, 4E3 binds m^7GTP with an equal affinity to that reported for eIF4E2. Mouse 4E3 was reported not to be able to associate with either 4G or 4E-BP1 and the central residue for phosphorylation –mediated regulation of 4E1(Ser209) is absent in 4E3 (Osborne et al. 2013; Volpon et al. 2013).

Fig. 8 NMR solution structure of the eIF4E3 bound to m^7GDP, adapted from (Osborne et al. 2013)

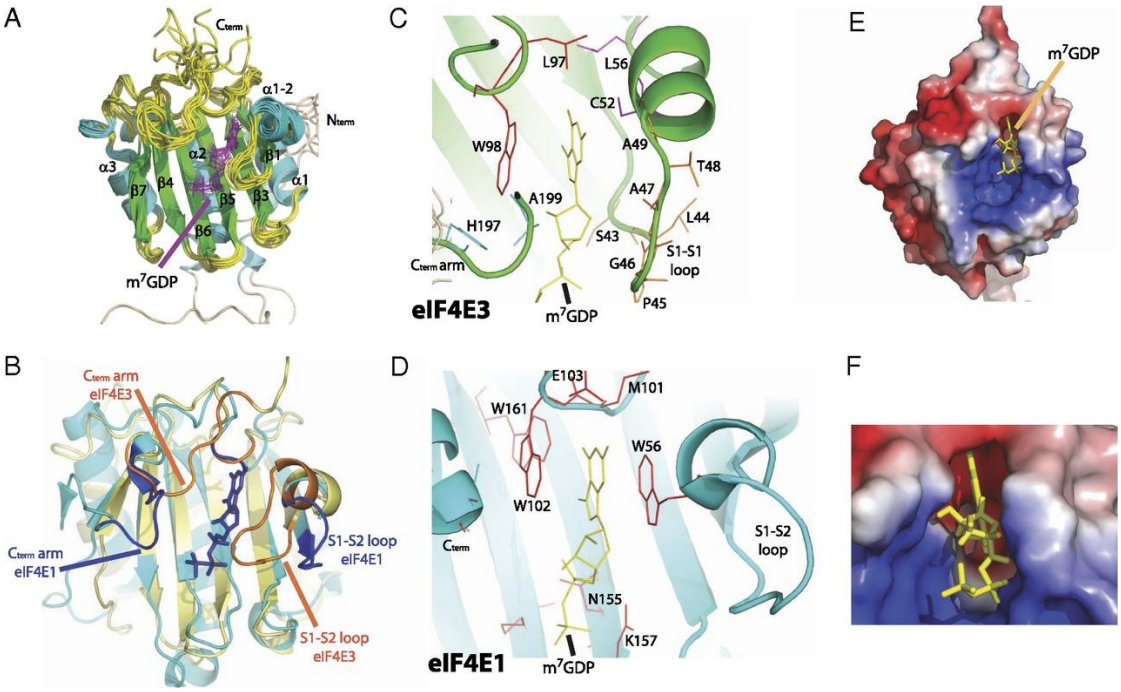

Superposition of the 10 lowest-energy NMR structures (A). (B) Overlay of m7G cap structures of 4E3 (yellow) and 4E1 (blue). Mobile residues and cap- binding regions were excluded from the superposition (residues 1-35, 42-56, 92-105, 195-207). Regions involved in cap-binding are highlighted orange (4E3) and dark blue (4E1). The m^7G cap-binding pocket of eIF4E3 (C) and eIF4E1 (D). E,F surface electrostatic potential of 4E3 in the m^7G cap complex. The strength of the potential is coloured, red for negative, blue for positive. m^7GTP is shown as yellow sticks, a magnified view can be found in F.

A study conducted using mouse 4E3 suggested, that 4E3 acts as an inhibitor of translation and oncogenic transformations and this ability is dependent on its cap-binding properties. 4E3 overexpression decreased expression of 4E1 target mRNAs including *vascular endothelial growth factor, c-Myc, cyclin D1* and others.

Furthermore, it does not associate with 4G in the cells. Therefore the authors assumed 4E3 to be unable to form translation initiation complexes but rather to form inactive complexes and sequester the mRNA away from the active translation machinery. Consistently, the level of *4E3* mRNA is found to be reduced 3- to 10- fold in M4/M5 AML patients relative to healthy volunteers (Osborne et al. 2013). Moreover, eIF4E3 gene deletion was found among other six frequent deletions of the genes in the cancerous tissue of oral squamous carcinoma, the most common malignancy of the oral cavity (Cha et al. 2011). Consistently, in breast cancer cells, eIF4E3 is largely sequestered at normoxia and hypoxia, the mRNA level of 4E3 are only about 2% of 4E1 mRNA level and in hypoxia, it is about 1%. The protein level is almost undetectable under both conditions (Yi et al. 2013). Deletion of *eif4e3* gene is viable in humans

(Pariani et al. 2009; Thevenon et al. 2014), but as it is only published together with associated deletion of *foxp1* gene, it makes it hard to assess the phenotype.

On the other hand, in a B-cell malignancy called multiple myeloma, eIF4E3 was found among the underlying mechanisms for treatment failure via translation-mediated enrichment of a transcription factor nuclear factor erythroid 2 like (Nrf2). In the cell line that do not responded to the treatment, the *eIF4E3* mRNA and protein levels were elevated, whereas the responsive cell line had corresponding levels of *eIF4E1* (Riz et al. 2016). Moreover, the abundance of un-phosphorylated 4E1 is found to be a trigger for eIF4E3 protein level up-regulation. This up-regulation is mediated via translation process not via the mRNA enrichment. The authors also showed that the overexpression of 4E3 not only reduces 4E1 cap-binding capacity, but also exhibited enhanced binding of 4E3 to the cap, potentially by the competition for the substrate mechanism. 4E3 was further found to be able to bind 4G and to be specifically enriched in light polysomes fractions, similarly to 4E1, affirming its role in translation initiation in DLBL cell line. The knockdown of both the proteins caused cell death and the microarray analysis revealed, that both 4E1 and 4E3 commonly regulate the translation of high percentage of genes and displayed mostly overlapping translatomes with a few exceptions. 4E1 regulates translation of *Map-interacting serine threonine kinase 2* (*MNK2),* 4E3 the one of *Proliferating cell nuclear antigen (PCNA)* and *Cycline dependent kinase 2 (CDK2). NF-κB* complex was enriched in 4E1 translatome, assigning a prominent role in the oncogenic transformation via an NF-κB-dependent transcriptional up-regulation. On the other hand, 4E3 was found to modulate miRNA maturation via up-regulation of *Dicer*. 4E3 also affects *Adar*, which is known to regulate RNA editing and transcript stability and a number of transcription factors such as protocogene *n-Myc, high mobility group AT-hook 1 (HMGA1), caudal type homeobox 2 (CDX2), Twist family BHLH transcription factor 1 (TWIST). MAPK interacting serine/threonine interacting kinase 1,2 (MNK1 and MNK2) kinases* therefore act as a switch that modulates 4E1- and 4E3-driven translation (Landon et al. 2014).

In the human muscle tissue specific miRNAs: miRNA-206 and miRNA-21 are involved in the regulation of *eIF4E3* and transcription factor *YYI* expression, which is sufficient to start the muscle- atrophy program (Soares et al. 2014). The expression of eIF4E3 protein in human trabecular meshwork cells, is regulated by miRNA 1298,

which protects them from the development of glaucoma caused by chronic oxidative stress (Wu et al. 2018).

Recently, it was shown that pro-growth and tumour promoting function of eIF4E3 can be efficiently supressed by MIR-584-5p via regulation of the cell cycle progression in cooperation with histone deacetylase 6 (HDAC6) and in this way, the progression of meduloblastoma tumour in model mice can be efficiently inhibited. eIF4E3 was also shown to be an important regulator of microtubule dynamics and inductor of c-myc expression. Importantly, depletion or overexpression of eIF4E3 did not alter the mRNA levels of *eIF4E1*. MIR-584-5p was proposed as chemotherapeutic adjuvants for treatment of high risk meduloblastoma tumour patients (Abdelfattah et al. 2018).

3.17.1 eIF4E-3 class family members in non-human chordates

Class III members share 25-30% identity and 45-55% similarity with members from Class I and II. Tyr56 of eIF4E-1 has been replaced for Cys in *Vertebrata.* Class III members have been identified in *Metazoa* only and are well represented in chordates and higher vertebrates. Nevertheless, they can be sporadically found in *Cnidaria*, molluscs, insect and arachnids (Joshi et al. 2005).

Mouse eIF4E3 is capable of cap-binding *in vitro* (Joshi et al. 2004). Joshi et al. (2005) reported, that mouse eIF4E3 is able to interact with 4G, but not with 4E-BPs. Yet it is unable to rescue the growth of *S. cerevisiae* lacking a functional 4E gene. Later, however Osborne et al. (2013) found mouse 4E3 unable to interact neither with 4G nor with 4E-BPs.

In the sea urchin, there is eIF4E3 protein present with a unique substitution of Val residue instead of typical Cys/Tyr substitution at the position of Trp56 in eIF4E-. Authors reported other two echinoderms with such a substitution (Morales et al. 2006). In an unfertilized egg of sea urchin, there is an alternative translation initiation complex that localizes to polysomes and is translated upon fertilization. It is composed of mRNAs coding for eIF4E2, eIF4E3, DAP5 (a truncated homolog of eIF4G, unable to interact with PABP) and hnRNP Q (a corresponding protein is able to interact with PABP). In the amount exceeding their canonical counterparts, these mRNAs were also detected in the maternal transcriptome (Chasse et al. 2019).

4 Aims of this work

I. To investigate localization of individual human eIF4Es and their variants into P-bodies and stress granules during heat and arsenite stresses.

II. To search for proteins differentially localized into stress granules induced by either heat shock or arsenite stress

III. To search for the eIF4E2 interaction partners

5 Material and methods

5.1 Material

5.1.1 Bacterial strains

E. coli XL-1 Blue: *recA1 endA1 gyrA96 thi-1 hsdR17 supE44 relA1 lac* [*F′ proAB lacIqZ_M15 Tn10* (*Tetr*)] (Stratagene)

Escherichia coli BL21(DE3): F^{-} *ompT hsdSB* (rB^{-} mB^{-}) *gal dcm* (DE3)(Hinnebusch)

5.1.2 Cultivation of the bacterial strains

Bacterial strains were cultivated at 37°C, 2xTY liquid medium or LB liquid medium supplemented with antibiotics were used for the protein production and plasmid isolation (ampicillin 100 μg/ml or kanamycin 50 μg/ml). For the selection of individual clones, 2xTY plates were used. For the long term storage, fresh bacterial clones were grown in a selective 2xTY media and mixed with glycerol to a final concentration 50% (v/v) and stored at minus 80°C.
LB medium: 1% (w/v) tryptone, 0.5% (w/v) yeast extract, 1% (w/v) NaCl, pH=7.0
2xTY: 1.6% (w/v) peptone; 1% (w/v) yeast extract; 0.5% (w/v) NaCl; pH 7.0
Agar plates 2xTY: 2xTY medium, 2% (w/v) agar; antibiotics (ampicillin 100 μg/ml or kanamycin 50μg/ml)

5.1.3 Mammalian cell lines

Mrc-5 (human lung fibroblasts, non-transformed, diploid in 70% of cells) (ATCC number CCL-171)
U2OS (human osteosarcoma, ATCC number HTB-96)
HEK293 (human embryonic kidney, transformed by Adenovirus 5 DNA, ATCC number CRL-1573)
HEK293T (human embryonic kidney, transformed by Adenovirus 5 and SV40-T antigen, ATCC number CRL-3216)
HELA (human adenocarcinoma cells, contain human papilloma virus, ATCC number CCL-2)
U2OS.FLIP IN (gift from Dr. David Staněk)
HEK293 T-REX FLIP IN (Invitrogen)

5.1.4 Cultivation of mammalian cell lines

Cell lines were maintained in DMEM (Gibco) supplemented with 10% FBS, 2 mM glutamine at 37 °C in 5% CO_2.

5.1.5 Recombinant plasmids used in the thesis

For the expression of human 4Es in both the mammalian cell lines and bacterial strains, as well as for the development of stable cell lines, I used a variety of recombinant

plasmids, listed in Table 1. Some of them were purchased, others were created by other lab members or cloned by myself and my undergraduate student Jana Kráčmarová and finally, donated by other researchers.

Table 1 Summary of expression vectors prepared or used in this work

Name	Purpose	Origin
pEGFP C1	Protein production in mammalian cells	Clontech
pEGFP 4E1_1	Protein production in mammalian cells	K. Borčin
pEGFP 4E1_3	Protein production in mammalian cells	K. Borčin
pEGFP 4E2_A	Protein production in mammalian cells	T. Mašek
pEGFP 4E2_C	Protein production in mammalian cells	K. Borčin
pEGFP 4E2_CRA_A	Protein production in mammalian cells	T. Mašek
pEGFP 4E3_B	Protein production in mammalian cells	K. Borčin
pEGFP 4E3_A	Protein production in mammalian cells	T. Mašek
mCherry C1	Protein production in mammalian cells	R. Janoštiak
mCherry 4E1_1	Protein production in mammalian cells	J. Kráčmarová
mCherry 4E2_A	Protein production in mammalian cells	J. Kráčmarová
mCherry 4E3_A	Protein production in mammalian cells	J. Kráčmarová
pCDNA3.1 HA	Protein production in mammalian cells	Nahum Sonenberg
pCDNA3.1 HA 4E-T	Protein production in mammalian cells	Nahum Sonenberg
pCDNA3.1 3HA 4EBP2	Protein production in mammalian cells	Nahum Sonenberg
POG44	Stable cell line generation	ThermoFisher Scientific
pFRT.TO	Stable cell line generation	ThermoFisher Scientific
pFRT.TO 4E2_A	Stable cell line generation	T. Mašek
pGEX.TEV	Protein production in bacteria	Joint Centre for Structural Genomics, Genomics Institute of the Novartis Research Foundation
pGEX.TEV 4E2_A	Protein production in bacteria	K. Frydrýšková
pGEX.TEV 4E3_A	Protein production in bacteria	K. Frydrýšková
pGEX.TEV 4E3_B	Protein production in bacteria	K. Frydrýšková
pTEV	TEV protease production in bacteria	Ladislav Bumba

5.1.6 Antibodies

Table 2 and Table 3 summarize primary and secondary antibodies used in the thesis.

Table 2 The list of primary antibodies used in the study

Protein	Host	Cat. No	Manufacturer	Dilution for WB	Dilution for IF
β-actin	Mouse	A2228	Sigma	1:500	-
DDX6	Rabbit	A300-461A	Bethyl laboratories	-	1:500
eIF3B	Mouse	SC-137214	Santa Cruz	1:500	1:500
eIF3B	Rabbit	pA5-23278	Pierce		1:1000
eIF3B	Goat	SC-16377	Santa cruz	Used for IP	
eIF4E1	Mouse	AM1852a	Abgent	1:500	1:500
eIF4E1	Rabbit	E5906	Sigma	1:200	-
eIF4E2	Rabbit	ARP40555_T100	Aviva	1:50	-
eIF4E2	Rabbit	GTX82524	Genetex	1:50	1:200
eIF4E3	Rabbit	SC-133542	Santa Cruz	-	1:50
eIF4E3	Rabbit	AV41168	Sigma	-	1:50
eIF4EBP1	Rabbit	A300-501A	Bethyl laboratories	1:500	-
eIF4E-T	Rabbit	A300-706A	Bethyl laboratories	1:200	1:1000
eIF4GI	Mouse	SC-373892	Santa Cruz	1:200	-

eIF4GII/III	Rabbit	A301-768A	Bethyl laboratories	1:50	-
GFP	Mouse	SC-9996	Santa Cruz	1:1000	-
HA	Mouse	H9658	Sigma	1:500	1:500
PABP	Mouse	ab6125	Abcam	1:1000	-
TIA-1	Goat	SC1751	Santa Cruz	-	1:50

Table 3 List of secondary antibodies used in the study

Target	Conjugated with	Host	Manufacturer	Cat. No	Dilution
Anti-rabbit	Alexa Fluor 488	Goat	Invitrogen	A11001	1:1000
Anti-mouse	Alexa Fluor 647	Donkey	Jackson Immunoresearch	715-605-150	1:1000
Anti-goat	Cy3	Donkey	Jackson Immunoresearch	705-165-147	1:1000
Anti-rabbit	Cy5	Donkey	Jackson Immunoresearch	711-175-152	1:500
Anti-mouse	Cy3	Donkey	Jackson Immunoresearch	715-165-151	1:500
Anti-mouse	HRP	Goat	Santa Cruz	SC-2005	1:5000
Anti-rabbit	HRP	Goat	Santa Cruz	SC-2004	1:5000

5.2 Protocols

5.2.1 PCR

To clone 4E3_A into GST fusion, primers had to be ordered (Generi Biotech):
37 mer 4E3-long-R-xhoI
5′-CCC TCG AGT TAG TGT TTT CCA CGT CCA CCT TCA AAA G′-3′
25 mer 4E3_long-F-BamHI
5′-AAG GAT TGG CGC TGC CCC CGG C-3′

Primers were diluted to 10 µM. Template DNA pFRT.TO_4E3_A was diluted to 30 ng/µl.
PCR total volume…25 µl
…….
Template DNA…1 µl
Forward primer…1.25 µl
Reverse primer….1.25 µl
dNTPs ….0.5 µl
Taq with 5% (v/v) Pfu polymerase mixture…1 µl
Buffer with $MgCl_2$…….2.5 µl
Nuclease free water…..17.5 µl

Using the eppendorf cycler Gradient S, 25 cycles long PCR was run:
105°C…….10 min (pre-heating of the lid)
95°C……..3 min (initial denaturation)

95°C…….30s (denaturation)
Temperature gradient of 50. 55, 60. 65 °C……..30 s (primers annealing)
72°C……1 min (synthesis app. 1kb per min.)¨

72°C……10 min (final extension)
10°C……hold

dNTPs: 10 mM dATP; 10 mM dGTP; 10 mM dCTP; 10 mM dTTP (Roche / Fermentas)
Primers (Generi Biotech)
Taq with 5% Pfu (v/v) (Fermentas)

5.2.2 Agarose gel electrophoresis of DNA

Appropriate amount of agarose was weighted to reach the final concentration of 0.5 % (w/v) to 1.5 % (w/v), depending on the character of the sample, and dissolved in 1xTAE buffer. The mixture was quickly boiled 3 times in a microwave oven. Then the flask was cooled down using cold water until it was possible to hold it by hands and poured to the casting tray, the ethidium bromide solution was added to a final concentration of 0.175 µg/ml. A comb was placed and the gel was allowed to solidify. For the sample loading, 6x sample loading buffer was used, together with appropriate set of markers. The electrophoresis was run from 1 V/cm^2- 8 V/cm^2. Gel was pictured using Gel Logic 112 Imaging System (Kodak) and Carestream software.
6xLB: 10mM TRIS.HCl pH=7.6, 0.03% (w/v) bromophenol blue, 0.03 % (w/v) xylene blue, 60% glycerol (v/v), 60mM EDTA -NaOH
EZ Load™ 1 kb Molecular Ruler (BIO-RAD)
GeneRuler™ 100 bp Plus DNA Ladder (Fermentas)
Lambda DNA/Eco91I (BstEII) Marker, 15 (Fermentas)
Lambda DNA/Eco130I (StyI) Marker, 16 (Fermentas)
50x TAE: 200 mM Tris-HCl; 5.7 % (v/v) Acetic acid ;5 mM EDTA pH 8.0

5.2.3 Restriction cleavage

All the restriction enzymes and the corresponding buffers used were bought from Fermentas and restriction cleavage was performed according to the manufacturer´s instructions.

5.2.4 Isolation of the bands from the agarose gel

The bands of cleaved plasmids and PCR insertions were cut out from the gel and cleaned using PCR/Gel purification kit (Favorgen).

5.2.5 Vector dephosphorylation

A vector dephosphorylation was performed only when the target vector was cut with one restriction enzyme. In the total volume of 20 µl, 10 µl of the vector DNA was mixed with 2 µl Shrimp alkaline phosphatase buffer, 1.6 µl Shrimp alkaline phosphatase enzyme (Fermentas), 6.4 nuclease free water. Incubated at 37 °C for 30 min, than inactivated by heat for 15 min, 65 °C.

5.2.6 Ligation

The vector and the insert was ligated using T4 DNA ligase (Fermentas) and a corresponding buffer. The ligation mix was prepared following manufacturer´s instructions and incubated overnight at 16°C. 3 µl of the ligation mixture was used for transformation of *E. coli* by electroporation.

5.2.7 Transformation of E. coli by electroporation

For the electroporation, the competent *E. coli* cells were used. In a 2-mm electroporation cuvette, 40 µl of a cell suspension was mixed with DNA (a ligation mixture or a plasmid) and incubated for 1 min on ice, an electric pulse was applied using Gene Pulse X Cell (Biorad) with appropriate settings: capacitance 25 µF; 2.5 kV; 200 Ω). 1 ml of 2xTY non-selective growth medium was added immediately to the cell suspension and the tube was incubated for 1 h in 37 °C in a shaker. Cells were plated on an appropriate selective plates in at least three different densities: 10 µl, 100 µl and the rest of the suspension. The following day, individual clones were inoculated on another selective plate, so that they grow on a marked area of approximately 1 cm^2.

5.2.8 Plasmid minipreparation

Transformed bacterial cells grown on an area of approximately 1 cm^2 of a selective agar plate were scarped using a sterile toothpick and transferred into an eppendorf tube containing 400 µl of STET buffer and 5 µl of 5 % (w/v) lysozyme. The tubes were incubated at 95 °C for 2 minutes using thermoblock. Samples were spun for 10 minutes at 13 000 g and the pellet was carefully removed using a sterile toothpick. 0.4 volume of isopropanol was added to the supernatant and the tubes were incubated at -20 °C for 1 h. Precipitated DNA was spun for 15 minutes at 13 000 g, washed by 1 ml of 70% ethanol and spun again for 15 minutes at 13 000 g. The pellets were allowed to dry at 37°C and resolved in 30 µl of water or TE buffer. Samples were analysed by the agarose electrophoresis.
STET buffer: 10 % sucrose; 50 mM Tris-HCl pH 8; 50 mM EDTA-NaOH pH 8; 1% Triton X-100
TE buffer: 10 mM Tris-HCl pH 8; 1 mM EDTA-NaOH, pH 8

5.2.9 RNAse treatment of the DNA minipreparations coupled with restriction cleavage

In the total volume of 20 µl, 6 µl of the minipreparation´s DNA and 1 µl of restriction enzyme one, 1 µl of restriction enzyme two and a corresponding buffer were mixed with 2 µl of TRN and left for 2 hours in 37°C. Afterwards, half of the reaction was loaded on 1,5% agarose electrophoresis gel and run until samples reaches 2/3 of the gel length.

TRN: Ribonuclease A 110 mg/ml; 0.1 mM Tris-HCl pH 7.5; 0.045 mM NaCl

5.2.10 Sequencing of recombinant genes

Sequencing of individual recombinant gene´s clones was done at the Faculty sequencing facility, according to the instructions on its web page.

5.2.11 Plasmids midipreparation

For transfections of the mammalian cells, Qiagen Midi or Maxi kit was used and I proceeded according to the manufacturer´s instructions.
For storage of the plasmids, Plasmid Flex Spin Kit (Genebond) was used and I proceeded according to the manufacturer´s instructions.

5.2.12 Transient transfection of mammalian cells

Turbofect (Fermentas): For 35 mm dish, 4 µg of the plasmid was diluted in 400 µl of Optimem media (Gibco), 12 µl TBF was added to the solution and the mixture was vortex-mixed shortly and incubated for 20 min at RT, then dropwise added to the cells. The average efficiency was about 37%.
Universal transfection reagent (Sigma): For 35 mm dish, in the tube A, 3 µg of plasmid DNA were diluted in the 100 µl of Optimem media (Gibco) and in the tube B, 6 µl of Sigma Universal transfection reagent were diluted in 100 µl of the Optimem media and vortex-mixed quickly. B was then added to A, vortex-mixed quickly and incubated for 20 minutes at RT, then dropwise added to the cells. The average efficiency is higher than with Turbofect. The reagent performs better when used with Optimem than with serum-free DMEM. Nevertheless, the reagent is more toxic and not suitable for transfection of U2OS based stable cell lines followed by the stress treatments.
Lipofectamine 2000 (Thermo Fisher Scientific): For 35 mm dish, in a tube A, 7,5 µl of Lipofectamine were mixed with 150 µl of Optimem medium (Gibco), in the tube B, 2,5 µg of plasmid DNA was mixed with 150 µl of Optimem medium (Gibco). Then tube A was added to the tube B, shortly vortex-mixed, incubated at RT for 5 minutes and dropwise added to the cells. The average efficiency is higher than with Turbofect. It performs better with Optimem than with serum-free DMEM. Nevertheless, the reagent is more toxic and not suitable for transfection of U2OS based stable cell lines followed by the stress treatments.
Polyethyleneimine (PEI; Sigma): Due to its low prize, PEI was preferentially used for the transfection of 100 mm dishes. In the tube A 30 µl of PEI was mixed with 225 µl of Optimem medium (Gibco), in the tube B 10 µg of plasmid DNA was mixed with 225 µl of Optimem medium, then tube A was added to the tube B, shortly vortex-mixed, incubated at RT for 25 min and then dropwise added to the cells.

5.2.13 Generation of stable cell lines

HEK based stable cell lines:
Antibiotic concentrations:
Zeocin 100 µg/ml - to assay the FRT site
Hygromycin 200 µg/ml - to select the transformants
Tetracyclin 1 µg/ml – to induce the expression
Blasticidin 15 µg/ml - to keep tetracycline repressor in its position

Plasmids:
pOG44 – carries the recombinase that enables site-specific recombination. The site is carried in the maternal cell line HEK.FLIP IN.
pCDNA5.FRT.TO - carries the gene of interest under the control of inducible tetracycline promotor. The goal was to co-transfect both plasmids in a cell.

Day 0:
For the stable cell line generation, as low passage of HEK FLIP IN cells as possible was used. The cells were split 1:5 and seeded to a 6 well plate, transfected 5 hours later by Lipofectamine 2000.

- Ratio of pOG44 : pCDNA5.FRT.TO plasmids 9:1 worked way much better than 15:1
- The ratio DNA:transfection reagents 1:2 (transfection mixture: 4,5 ug pOG44 + 0.5 µg Gene + 10 µl Lipofectamine 2000 per well) was used. *(We tried also DNA:Lipofectamine 1:4 as suggested in the protocol but were not successful at all.)*
- 6 well plate included: not transfected cells- control of growth, control of plasmid expression-cells transfected with pEGFP using the same ratio as was used above, FRT site control under zeocin selection (to see the FRT site was preserved while passaged without antibiotics)

Day 1:
The medium was changed (still without hygromycin).
Day 2-40

- The cells were passaged to another 6 well plate with the selective media (hygromycin)
- The medium was changed every 3-4 day, on the day 15, the first colonies became visible by eye while changing the media.
- The colonies were let to grow for the next 14 day and then 24 of them were picked one by one and transferred to a 96 well plate either by scraping them by a tip of or trypsinize them by 2 µl of trypsin.
- Half of the colonies died on a 96 well plate, the rest was transferred (when fully grown) to a 24 well plate
- The fastest growing colonies were transferred to scale-up
- After every transfer to a new dish, the selective medium was added to the old dish to create a backup.

Altogether, 6 clones of GFP-4E2_A expressing cells and 6 clones of GFP-4E3-A expressing cells were obtained.

U2OS based stable cell lines
Antibiotic concentration
Zeocin 200 µg/ml- to assay FRT site
Hygromycin 200 µg/ml- to select the transformants
Tetracyclin 1 µg/ml – to induce the expression
Blasticidin 15 µg/ml- to keep tetracyclin repressor in its position

For the transfection, Turbofect was used as the transfection with Lipofectamine 2000 had been unsuccessful twice, before. Transfection mixture consisted of 0.3 µl plasmid of interest, 2.7 µl of POG44 and 6 µl of Turbofect in 400 µl of the Optimem media. The rest of the protocol followed the protocol of HEK based stable cell line generation.

Altogether 4 clones expressing GFP-4E2_A, 4 clones expressing GFP-4E3_A and 4 clones expressing GFP-4E1_1 were obtained. For the clone analysis, see the Result´s section.

5.2.14 SDS -PAGE electrophoresis

If not stated otherwise, usually 10% polyacrylamide gel was used for SDS-PAGE. In a dispensable falcon tube, 5 ml of 30% acrylamide/0.8% bis-acrylamide was mixed with 3.75 ml 4x Tris-HCl/SDS pH 8.8; 6.25 ml ddH2O; 50 µl ammonium per-sulphate and 10 µl TEMED for 4 gels.

The solution was poured between the glasses and overlaid with 0.375M Tris pH=8.8. When the polymerization was finished, the overlay was removed using filter paper, and the stacking gel was poured: 650 µl of acrylamide/bis-acrylamide; 1.25 ml 4x Tris-HCl/SDS pH 6.8; 3.05 ml ddH2O; 25 µl ammonium per sulphate and 5 µl TEMED for 2 gels. The combs was placed and the polymerization had been running for at least 20 minutes. Afterwards, the gel was either used immediately or stored sealed in a plastic box with a wet tissue paper at 4°C up to a week.

If not stated otherwise bellow the figure, cells were washed in pre-warmed PBS and lysed directly in the 2xLaemli loading buffer. For the lysis of a fully grown 100 mm dish, 300 µl of the loading buffer was used. The lysate was sonicated, boiled for 2 minutes and as much of it as possible was loaded on the gel. After sample loading the electrophoresis was run for 1h and 15 minutes at 160 V in a 1xSDS-PAGE buffer.
4x Tris-HCl/SDS pH 8.8: 1,5 M Tris-HCl; 0.4 % (w/v) SDS
4x Tris-HCl/SDS pH 6.8: 0.5 M Tris-HCl; 0.4 % (w/v) SDS
5x SDS-PAGE buffer: 25 mM Tris; 192 mM glycine; 0.1 % (w/v) SDS
5x Laemli loading buffer: 145 mM Bis-Tris, pH 6,8, 10% glycerol, 0.02% bromophenol blue, 10% SDS, 5% β-mercaptoethanol, 1mM TCEP
Acrylamide + N,N′-methylenebisacrylamide: 30 % (w/v) acrylamide; 0.8 % (w/v) N,N′-methylenebisacrylamide; filtrated
PageRuler™ Unstained Protein Ladder (Fermentas)

5.2.15 Coomassie blue staining

Gels were fixed for 30 minutes in the fixing solution and then incubated in the Coomassie staining solution on the rocking machine O/N. Following day, gels were de-stained in double distilled water and scanned wrapped in a plastic foil.
Coomassie staining solution: 10 % (v/v) acetic acid; 0.006 % (w/v) Coomassie Brilliant Blue G250
Fixing solution: 25 %(v/v) isopropyl alcohol; 10 % acetic acid (v/v)

5.2.16 Western blotting

After the electrophoresis, the gel were incubated in a blotting buffer for 15 minutes. In a meantime, the PVDF membrane (Biorad), if not stated otherwise below the figure, was cut, wetted sequentially in water, methanol and finally incubated in the blotting buffer as well and the filter papers were prepared (6 pieces per gel).

Next I prepared the sandwich composed of 3 pieces of 3mm Whatman filter paper, the gel, the membrane, followed by a 3 pieces of 3mm Whatman filter paper and I got rid of all the bubbles in the process.

The western blot was run on a Mini Trans-Blot Electrophoretic transfer cell (Biorad) for 1h, 100V. Next, the membrane was blocked in the blocking solution for 35 – 60 minutes at RT, followed by an incubation with a primary antibody diluted appropriately in the blocking solution as well, for 1h in RT or O/N at 4°C.

The following day, the membrane was washed 2x5 minutes in TBST solution and 1x10 minutes in the blocking solution and incubated with a secondary antibody of appropriate dilution in the blocking solution for 1h at RT. Afterwards; the membranes was washed 3x5 minutes in TBST and 1x5 minutes in TBS.

Blotting buffer: 20 % (v/v) methanol; 0.29 % (w/v) glycine; 0.58 % (w/v) Tris; 0.037 % (w/v) SDS

TBS/Tween: 50 mM Tris; 150 mM NaCl; 0.05% Tween-20

Blocking solution: 5% (w/v) Sunar baby (Heinz) in 1x TBS/Tween

PageRuler™ Prestained Protein Ladder (Fermentas)

5.2.17 Chemiluminescence detection

In this step, the signal of the horseradish peroxidase conjugated to a secondary antibody was detected. In the laboratory, two falcon tubes were prepared each with 18 ml of water and 2 ml of 1 M Tris.HCl pH=8.5, one was provided with 200 µl of 0.25 M luminol and 88 µl of 0.1 M p-coumaric acid. To the other one, 12 µl of 30% hydrogen peroxide solution was added. The falcon tubes were carried together with the membrane to another building, where a camera ImageQuantTM LAS 4000 was located**.** The tubes were mixed and the mixture was quickly pipetted to a membrane. The membrane was exposed for 2 minutes standard exposition followed by other exposition times and modes as needed.

Luminol : 250 mM luminol in DMSO

p-coumaric acid: 93.5 mM p-coumaric acid in DMSO

5.2.18 GFP Trap (Chromotek)

Seeding

2x100 mm dishes of stable cell line were seeded, in the case of GFP-4E2_A expressing cells, the cell dilution was 1:1,5. The cells were induced with tetracycline to a final concentration of 1 µg/ml for 24 h.

OR transfection

Cells were transfected 5 h after seeding. For transfection the PEI protocol was used.

Harvesting

The cells were washed gently with a pre-heated PBS at 37 °C. For 2x100 mm dishes, 300 µl of the lysis buffer (provided in the kit) was added, enriched with 1mM PMSF and 1 protease inhibitor cocktail with EDTA and the dishes were rocked. The dishes were placed on ice and the cells were scraped off using the scraper. The lysate was collected in the 1.5 ml pre - cooled (4 °C) low binding eppendorf tube and re-used for the second dish. Next, the cells from both the dishes were lysed together in one tube for 15 minutes on ice, pipetted through several times.

The lysate was sonicated in an ice bath at 50 % amplitude, 5 s on, 15 s off, 1 min in total using Q 700 sonicator (Qsonica). The sample were spun in the pre-cooled table

centrifuge for 10 min, 4 °C at maximum speed. The supernatant was transferred(leaving approximately 1 mm above the pellet) to a new, pre-cooled eppendorf tube and spun again. This step was repeated one more time and the volume was adjusted to 1000 µl with the dilution buffer (provided with the kit).

For an immunoblot analysis, 50 µl of the lysate was transferred to another tube and mixed with 50 µl of 2x SDS sample buffer (input).

A GFP trap A beads slurry was resuspended, 25 µl of it was spun for 2500 g, 2min. The supernatant was discarded and the beads were washed 3 more time with 500 µl of an ice cold dilution buffer.

The lysate was added to the equilibrated GFP-Trap A beads and incubated 30 min-1h at 4°C under constant mixing (beads have to move in the tube and do not settle while rotating).

The lysate with the beads was spun for 2 min, 2500 g, 4°C than 50 µl of the lysate was transferred to a new tube and mixed with 50 µl of 2x SDS sample buffer (flow through). The rest of the supernatant was discarded or freezed and the beads were washed three times with 500 µl of an ice cold wash buffer (provided with the kit). With the last wash, the beads were transferred to a new eppendorf tube. (If you run it for the first time, you may want to analyze all the washes so that you see how the clearing process is efficient).

25 µl of 2x SDS page buffer was added to the washed beads and spun at the maximum speed for 5 min (sample IP).

Analysis

The samples were boiled for 2 minutes in a water bath, 8 µl of each was loaded to a 10% SDS page gel, input and IP samples next to each other to see the enrichment.

Lysis buffer: 10 mM Tris/Cl pH 7.5; 150 mM NaCl; 0.5 mM EDTA; 0.5 % NP-40

Dilution buffer and washing buffer: 10 mM Tris/Cl pH 7.5; 150 mM NaCl; 0.5 mM EDTA

5.2.19 Benzonase cleavage

1 µl of the benzonase enzyme (Novagen) was added to the 25 µl of GFP trap beads after Wash 3 and incubated on ice O/N. The following day, beads were washed 3x again and analysed.

5.2.20 m^7GTP-agarose pull-down

The experiment consisted of two 100 mm fully confluent dishes of HEK293 cells, that were transfected with pEGFP-C1-eIF4E1_1 vector using PEI and two 100 mm fully confluent dishes of. GFP-4E2_A expressing HEK-based stable cell line. 24 hours post transfection or induction, the cells were lysed in 300 µl of the GFP-Trap® lysis buffer, enriched with 1mM PMSF and complete, EDTA-free® protease inhibitor cocktail, spun, sonicated and 8 µl of the lysate was directly loaded to the gel as input. Remaining part of the lysate was incubated with 40 µl of m^7GTP agarose resin from Jenna Bioscience (AC-142L) on the rotating wheel in 4 °C for 1hour. The resin was washed with 3x1ml of GFP-Trap® washing buffer and subsequently boiled with 24 µl of 2x PAGE loading buffer; 8 µl of the sample was loaded on the gel.

5.2.21 Polysome profile analysis

HEK293 cell line stably expressing GFP-4E2_A was grown to 60-70% confluence at 150 mm diameter dishes. Cells were washed by an ice-cold PBS and lysed in a lysis buffer.

Lysates were cleared by centrifugation at 10 000 g for 5 min at 4°C and then casted on 5-20% sucrose gradients in a gradient solution. Ultracentrifugation was done in SW41.Ti rotors (Beckman) for 3h, 35 000 rpm, 4°C. Profiles were fractionated using Density Gradient Fractionation Systems ISCO to a final number of equal fractions; proteins were purified by TCA – isopropanol procedure and dissolved in a loading buffer (see SDS page protocol).

Lysis buffer: 10 mM Hepes, pH 7.5; 62.5 mM KCl; 5 mM $MgCl_2$; 2 mM DTT; 1% Triton X-100; 100 µg/ml cycloheximide; Complete EDTA-free (Roche, 1 tablet/10 ml); and 40 U/ml Ribolock (Fermentas)

Gradient solution: 10 mM Hepes, pH 7.5; 100 mM KCl; 5 mM $MgCl_2$; 2 mM DTT; 100 µg/ml cycloheximide; Complete EDTA-free (1 tablet/100 ml); and 5 U/ml Ribolock (Fermentas)

5.2.22 Trichloroacetic acid - isopropanol procedure

To the individual fractions of the polysomal profile, 50 % trichloroacetic acid was added to a final concentration of 10 %. Samples were shortly vortex-mixed and allowed to be precipitated in the fridge O/N.

The following day, the samples were spun for the 20 minutes at the maximum speed, 4 °C in a pre-cooled centrifuge. The supernatant was carefully removed and 200 µl of ice-cold acetone was added to the pellet. Samples were vortex-mixed for next 15 minutes and spun at a maximum speed, 4 °C, 10 minutes.

The supernatant was carefully removed and the samples were left to get dry at 37 °C, followed by resolution in the loading buffer heated to 80 °C proportionally to the size of the pellet, vortex-mixed and incubated at 80 °C for an additional 10 minutes and then loaded on the gel to run SDS page followed by a western blot.

5.2.23 Immunoprecipitation via eIF3B

- 2x 150 mm dishes of fully grown GFP-4E2_A stably expressing cell line, were induced for 72 hours, lysed in 500 µl of buffer GA on ice for 15 minutes, pipetted through several times, sonicated and spun according the GFP trap protocol, altogether 1600 µl of the total cell lysate was produced.
- 210 µl of Protein G agarose (Exalpha) were equilibrated in buffer GA (spun for 2 minutes, 100 g, 4 °C, supernatant was removed and 1 ml of buffer GA was added, repeated 3x)
- In the last wash, the beads were split: 80 µl of the beads were mixed with 12 µl of the goat eIF3B antibody- IP +; 80 µl of the beads with no antibody- IP-; 50 µl of the beads were used for the pre-clearing of the lysate (1h, 4°C on the rotating wheel).
- After the lysate pre-clearing, the resin was removed and 200 µl of the cell lysate was mixed with 200 µl of 2x loading buffer- INPUT, boiled and 40 µl was loaded on the gel.

- Remaining cell lysate was split into two parts 600 µl was added into IP+ and 600 µl was added into IP-, binding was allowed on the rotating wheel O/N, 4°C.
- The other day, the lysate was spun and 100 µl of the lysate was mixed with 100 µl of the 2x loading buffer- Flow through sample.
- IPs were washed 3x by 1 ml of GA buffer, 100 µl of the last wash were mixed with 100 µl of 2x loading buffer- Wash 3.
- Beads were mixed with 120 µl of 2x loading buffer.
- INPUT, IP+, IP-, Flow through and Wash3 samples were boiled for 5 minutes, spin and 40 µl of each was loaded on the gel.

Lysis buffer GA: 10 mM HEPES pH7.5, 62,5 mM KCl, 2,5 mM $MgCl_2$, 1% Triton-X-100. 1x Mini Complete EDTA-free protease inhibitor (Roche), 1 mM DTT, 10 mM PMSF
GA buffer: 10 mM HEPES pH7.5, 62,5 mM KCl, 2,5 mM $MgCl_2$
Loading buffer (see SDS page protocol, diluted with water)

5.2.24 Bradford assay

For the determination of protein concentration I used Bradford reagent (Sigma) and I proceeded according to the manufacturer´s instructions.

5.2.25 Protein production and purification via GST tag

Optical density was measured on the Spectronic Helios Beta (Thermo Spectronic) spectrophotometer.

Day 1

- *E. coli* BL21DE3 transformed by individual GST-h4E were inoculated into 50 ml of LB media enriched with ampicillin, grown O/N, 28 °C, 180 rpm (GFL 1086)
- 2x 2 l bottles with 400 ml of LBA were left O/N in 28°C to equilibrate

Day 2

- The cells were innoculated into the 2 l bottles OD_{660nm}=0.05, 180 rpm, 28 °C and cultivated for approximately 1.5 h
- When the OD reached 0.2, the rocking machine (Schoeller) was ventilated properly and adjusted to the temperature of 15 °C¨
- The cell cultures were propagated for another 4 h in 15 °C and OD was checked frequently
- When the OD reached 0.4-0.6, 1 ml of the cell suspension was transferred to an eppendorf tube, spun and the pellet was freezed (cells before expression)
- The expression of the gene of interested was induced by 0.1 mM IPTG, and the culture was propagated at 15 °C, 180 rpm, O/N

Day 3

- 1 ml of the cell suspension was transferred to an eppendorf tube, spun and the pellet was freezed (cells after production of the protein)
- The whole cell culture was spun at 5000 g, 10 min, the pellet was resuspended in water, spun, the supernatant was removed and the whole step was repeated with TRIS¨
- The pellet was freezed at -80 °C.

Cell lysis

All the work was done on ice.

- The cell culture was melted by hands and placed on ice
- Lysed in 25 ml of B-per (ThermoFisher Scientific) enriched with 1mM PMSF, 0.5 ml of lysozyme and 1 tablet of complete (Roche) for 1 h on ice, sonicated every 15 minutes (30 s on and 1 min off using the sonicator Bandelin Sono Plus HD 2070)
- In the meantime, 2 ml of Gluthation Sepharose 4 Fast Flow (GE Healthcare) was equilibrated in the TRIS
- The cells were lysed enough to be pipetted without problems, spun for 20 min, 4°C, 15 000 g
- The supernatant was transferred to a new cuvette and the previous step was repeated with 10 min-long spinning
- A bit of the pellet was taken to a new tube and lysed in 50 µl of 2x loading buffer (pellet)
- 50 µl of the supernatant was taken to a new tube and mixed with 50 µl of the 2x loading buffer
- The pellet was freezed

Purification via GST tag

- The supernatant was transferred to a 15 ml falcon tube, GST resin was added and the binding was allowed at 4°C O/N
- Following day, the resin was spun at 500 g, 2 min and 50 µl of the supernatant was mixed with 50 µl of 2x loading buffer (flow through sample)
- The resin was washed 3x by 1 ml of TRIS, from the last wash, 50 µl of the supernatant was mix with 50 µl of 2x loading buffer (Wash 3)
- The proteins were eluted with 3x1ml of elution buffer (elution 1, 2, 3)
- SDS page was run, the protein was aliquotted and stored at -80°C

Tris: 10mM Tris, pH=8. 5% (w/v) glycerol
Elution buffer: 20 mM reduced glutathione, 50 mM NaCl, 50 mM Tris-HCl, pH 8.0
Loading buffer (see SDS page protocol, diluted with water)

5.2.26 TEV cleavage

Purified TEV protease at the concentration 1 µg/µl was capable of cutting the GST tag off the h4Es-GST proteins in the ratios 1:20-1:30. 4°C, O/N.

5.2.27 GST pull-down

1) Radiolabelling

The radiolabelling was done by Promega TNT Quick coupled Transcription/Translation Kit according to the manufacturer instructions, 10 µl of TNT reaction per a GST protein

2) GST pull-down experiment

- In a 250 µl of buffer B a GST fusion protein was dilluted (1-5 µg, stored aliquot at -80°C prior elution, TRIS buffer was replaced by PBS) and 10 µl of the TNT mixture was added
- A set of controls with GST only was included
- Samples were gently vortex-mixed at low rpm
- Incubated on a rocking machine at 4°C for 2h
- Spun down at 100 g for 2 min, the supernatant was carefully removed (20-30 µl of the liquid was left at the bottom of the eppendorf tube)

- The beads were washed 3 times with 1ml of an ice cold PBS, after the last washing step, as much supernatant as possible was removed, 20 µl at the most should remain in the tube

3) SDS-PAGE

- the reaction was mixed with the loading buffer, vortex-mixed, heated for 3-4 min at 95°C and vortex-mixed again
- the entire reaction and 20% of the input sample (2µl of the TNT mixture) was loaded on the gel and the gel was run
- Washed 3 times with water
- Incubated O/N in a Coomassie Brilliant blue staining solution
- De-stained with water O/N
- Dried and put it into a cassette

Buffer B: 20 mM HEPES (pH 7.5), 75 mM KCl, 0.1 mM EDTA, 2.5 mM MgCl2, 0.05% IPEGAL, 1 mM DTT, 1 % fat free powder milk

5.2.28 RNA isolation from the GFP trap

- 1 ml of TRIZOL was added (Thermo Fisher Scientific) to 7 µl of the GFP trap beads (1/12 of the beads from a GFP Trap immunoprecipitation of 6x100 mm dishes)
- Samples were vortexed-mixed for 3 minutes. Spun for 16 000 g, 20 minutes, 4°C
- The supernatant was carefully removed and 1.5 µl of linear polyacrylamide (Sigma) was added to the sample.
- The same volume of isopropanol was added, sample was vortex-mixed and precipitated O/N, -20 °C
- Spun for 16 000 g, 4°C and the supernatant was carefully removed
- 1 ml of 75% ethanol was added and the sample was spun for additional 10 minutes
- The previous step was repeated
- The pellet got dried in RT and was dissolved in 10 µl of pre-heated water (65°C)
- The concentration was measured using Nano Drop® ND-1000 Spectrophotometer (Thermo Fisher Scientific)

5.2.29 Preparation of cDNA by reverse transcription

Mix following:
Nuclease free water.....5 µl
RNA .....4 µl
Oligo dT (0.5 µg/µl).....1 µl

The reaction was incubated on ice for 5 minutes and then shortly spun in a pre-cooled centrifuge, following step were done on ice. The following ingredients were added to the mixture:

Nuclease free water.....2.5 µl
5x buffer.....4 µl
dNTP (10 mM).....2 µl
Ribolock (40 U/µl) (ThermoFisher Scientific).....0.5 µl
RevertAid reverse transcriptase (ThermoFisher Scientific)...1 µl

The reaction was placed into the Mastercycler gradient (Eppendrof) and the reverse transcription programme was run:
37°C.....5 min
42°C.....1h15 min
70°C.....10 min
4°C.....hold
Samples were stored at minus 80°C.

5.2.30 Quantitative real time PCR

Specific set of primers for the detection of H3 clustered histone 13 (HIST2H3D), ring finger protein 5 (RNF5) and SURF cytochrome c oxidase assembly factor (SURF) were diluted to 10 µM by mixing 10 µl of forward primer with 10 µl of reverse primer in 80 µl of water. Each of the three samples: IP0. IP+ and IP- (Benzonase treatment) was diluted 10x, 100x and 1000x. The experiment was run in a triplicate.
SURF forward
5′CTCAGAGTGGGGCCTATGTG 3′
SURF reverse
5′CCTGGGAACGAACCCTCTAT 3′
HIST2H3D forward
5′GAAGCAGCTGGCTACCAAAG 3′
HIST2H3D reverse
5′CTTAAAGTCCTGCGCGATCT 3′
RNF5 forward
5′TGGAGACACGGCCAGAAC 3′
RNF5 reverse
5′CTCTCCGGAGCTGGTCTCT 3′

Per one reaction:
Total volume.....10 µl
LC 480 Sybr Green Master (Roche).....5 µl
Water.....2 µl
Primer mix (10 µM, Generi Biotech).....0.5 µl
Template cDNA.....2.5 µl

Samples were loaded on the 96 well plate according to the scheme prepared in advance. The reaction was run at the Faculty qPCR facility, LC 480 machine

Pre-incubation:
5 min…….95 °C
Amplification 45x:
15 s……94 °C
20 s……58 °C (HIST2H3D, RNF5), 60 °C (SURF)
30s……72 °C
Cool down to 4° C

5.2.31 Fixed preparations of U2OS cells

In a hood on a day 0:

- The fully grown 100 mm dish of U2OS cells was trypsinized with 1ml of trypsin and diluted in media to a total volume of 10 ml
- The coverslips (Microscope cover glasses, diameter of 24 mm, Assistent™, 41001124) stored in ethanol were fire-sterilized and placed in a 35 mm dish, one coverslip per dish
- 250 µl of the cell suspension was added to the coverslip in a dish, the medium was added and the cells were resuspended
- Cells grew O/N or were transfected 5 h later

On the table, Day 1:

- The cells were washed with 2 ml of the pre-heated PBS (37 °C) for 5 min on a rocking machine
- Fixed in 1 ml of the fixation solution for 18 min on a rocking machine
- Permeability of the cell membranes was increased by the incubation in 1 ml of the solution for membrane permeabilization for 5 minutes on a rocking machine
- Preparations were washed 3x 2 ml in PBST for 10 min on a rocking machine
- Incubated for 40 minutes in 1 ml of the blocking solution on a rocking machine
- Primary antibodies were diluted in a 60-80 µl of blocking solution per sample
- The diluted antibodies were pipetted on a parafilm creating a drop and coverslips with cells were placed the coverslip on it and incubated O/N at 4 °C
- The preparations were washed 3x 2 ml for 10 min in PBST,
- Probed with secondary antibodies diluted in the blocking solution for 1h, RT
- Washed 3x 10 minutes by 2 ml of PBST (to the second PBST wash, DAPI staining solution was added 1:500), washed in PBS, washed in water and mounted in ProLong Gold Antifade mounting medium (Invitrogen).
- Images were captured using one of the following instruments: an inverted confocal microscope Leica TCS SP2 with an Acousto-Optical Beam Splitter (AOBS), Zeiss LSM 880 or Cell-R system on an inverted Olympus IX81 microscope and if not stated otherwise in the legend, UPLSAPO 60x objective. The particular machine type is stated in the legend bellow each figure Images were then compiled using ImageJ (Fiji 1,48b) and a graphics editor.

Fixation solution: 4% (w/v) paraformaldehyde, pH= 7.5, 4 °C
Solution for membrane permeabilization: 0.5 % (w/v) Triton X 100 in PBS, 4 °C
Blocking solution: 0.25 % (w/v) porcine gelatine and 0.25 % (w/v) bovine serum albumin in PBST, 4 °C
DAPI staining solution: 40 µg/ml DAPI, in 50% (v/v) ethanol and water, freezer temperature
PBST: 0.05 % (w/v) Tween 20 in PBS, 4 °C

5.2.32 Live cell imaging

For the life cell imaging, cells were seeded on the glass-bottomed dishes, the following day prior microscopy, dead cells were washed out by a pre-warmed PBS (37°C) and DMEM medium was replaced by a DMEM medium without phenol red (Gibco).

Hoechst stain (Invitrogen) was added to the media to a final concentration of 2.5 µg/ml to stain cells nuclei (takes approximately 10 minutes to be well visible) and cells were microscoped.

5.2.33 Heat stress in U2OS

Pre-warmed medium (49°C) was added to a cell culture and the cultivation dish was immediately placed on a pre-heated thermoblock for 30 minutes. Temperature was measured directly on the coverslip, inside the dish, using a submersible probe and a digital thermometer (Testo 735-2).

5.2.34 Arsenite stress in U2OS

A stock solution of sodium arsenite (Sigma-Aldrich, 35000-1L-R) was diluted to 1 mM in a medium preheated to 37 °C shortly before use; cells were treated for 40 min in an incubator.

5.2.35 Fixed preparations of stable cell lines

U2OS cell based stable cell lines were maintained in a selective medium (200 µg/ml of hygromycin) till the moment of the experiment, otherwise the gene of interest became silenced. After trypsinization, higher amount of the cells was used for one 35 mm dish (upon trypsinization of the fully grown 100 mm dish, a suspension of 10 ml was made. Out of this suspension, 400 µl of the cells were seeded on a 35 mm dish provided with a fire-sterilized glass coverslip and induced by tetracycline to a final concentration of 1 µg/ml). Fixation was done after two days, otherwise the protocol was the same as for the U2OS cells.

5.2.36 Heat stress in U2OS based stable cell lines

Pre-warmed medium was added to a cell culture and the cultivation dish immediately placed on a pre-heated thermoblock (47°C, 1h). Temperature was measured directly on the coverslip, inside the dish, using a submersible probe and a digital thermometer (Testo 735-2).

5.2.37 Arsenite stress in U2OS based stable cell lines

A stock solution of sodium arsenite (Sigma-Aldrich, 35000-1L-R) was diluted to 0.5 mM concentration in a DMEM medium preheated to 37 °C shortly before use; cells were treated for 1h.

5.2.38 Resazurin growth assay

Resazurin was purchased from Sigma and diluted in water to 50 µg/ml. Cells from 2x60 mm dishes were trypsinized and seeded on a 96 well plate in a dilution 1:3, 1:7, 1:11, 1:17, each in 8 technical replications to a final volume of 135 µl od DMEM media. Every day, 15 µl of resazurin was added to the cells and the cells had been incubated for 4h in an incubator, afterwards the optical density was measured using Varioscan (Scanlab).

6 RESULTS

6.1 Localization of h4Es and their variants to stress granules and P-bodies in heat, arsenite and stress-free conditions

The aim of this part was to visualize human eIF4Es listed in Fig. 11 in mammalian cells subjected to heat and arsenite stresses, to examine their co-localisation with the markers of P-bodies and stress granules and to compare those results with stress-free conditions.

The initial experiments were done in HEK cell line (Fig. 9), but these cells are not well suited for microscopy due to their growth in several layers and frequent formation of clusters. Next, I have been trying to employ human diploid MRC-5 cell line (Fig. 10), a cell line that is not continuous but has a limited number of divisions instead. I soon encountered growth problems and difficulties with transfection efficiency. Moreover, I found MRC-5 cell line to be almost impossible to become stressed. When I applied various concentrations of sodium arsenite for 30 minutes (0.5 mM, 1 mM, 2.5 mM, 10 mM), these cells did not form any SGs under any tested conditions. Interestingly enough, working concentration of sodium arsenite for U2OS cell line is 1mM and stress granules readily assembles from 0.25 mM applied for the same time (Fig. 17). I experienced similar problems with heat - shocked cells, so I switched to a much nicer, flat, growing in a monolayer and therefore for microscopy more suitable U2OS cell line. I haven´t experienced any major differences in the h4E´s subcellular distribution among cell lines or between live cell imaging and fixed preparations approaches, compare Fig. 9, Fig. 10, Fig. 20.

Fig. 9 Live cell imaging of h4Es and empty pEGFP vector in HEK293T cells

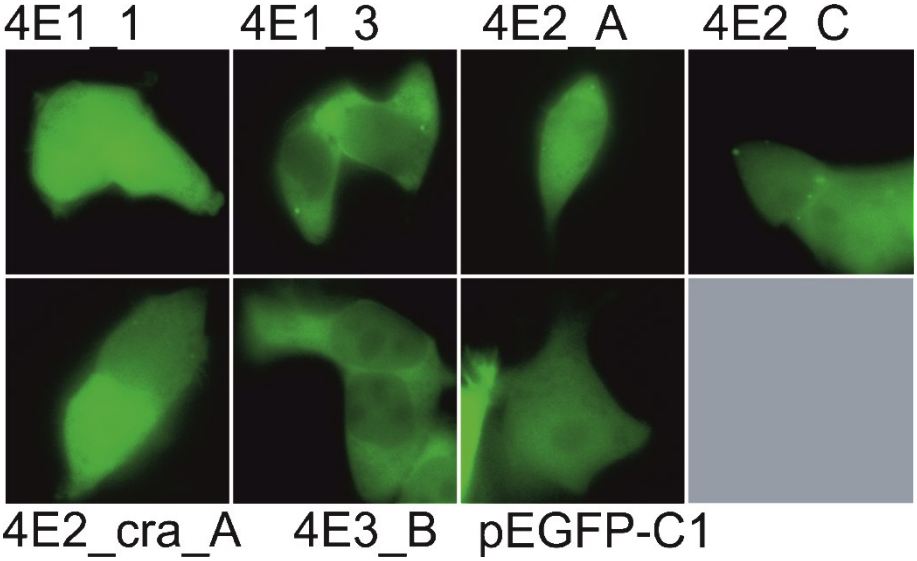

HEK293T cells were seeded in a dish with glass bottom and transfected with 1,5 µg of DNA per dish, observed 24h later using CellR microscope. 4E2-C and 4E1-3 shows PB-like structures.

Fig. 10 Stress-free distribution of h4Es in MRC-5 cell line

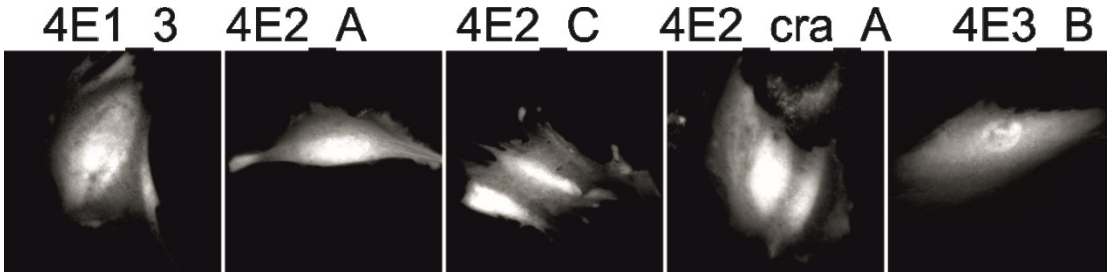

MRC-5 cells were transfected using turbofect and 4 µg of GFP-h4Es, fixed and visualised with using CellR microscope 48h later.

6.1.1 Insertion of h4Es into GFP fusion

Originally, I got an array of cloned h4Es into both the GFP and ds RED fusion by my colleague Kateřina Borčin. Unfortunately, when I sequenced them, I found mutations in some of them that were subsequently repaired in cooperation with Dr. Tomáš Mašek. For details, see Table 4. For the complete list of protein isoforms that we used in this study, please refer to Fig. 11.

Table 4 List of h4Es cloned into pEGFP plasmid

Gene	Plasmid	Mutation	Conclusion
4E1_1	pEGFP-C1	L300 (TTA-TTG)	Silent
4E1_1	pEGFP-C1	P351 (CCG-CCT)	Silent
4E1_3	pEGFP-C1	-	OK
4E2_A	pEGFP-C1	K222R (AAG)-(AGA)	Fixed by Dr. Tomáš Mašek
4E2_C	pEGFP-C1	-	OK
4E2_G	pEGFP-C1	Y216H	Not fixed, not used
4E2_CRA_a	pEGFP-C1	S660P (TCA)- (CCA)	Fixed by Dr. Tomáš Mašek
4E3_A	pEGFP-C1	-	Cloned later by Dr. Tomáš Mašek
4E3_B	pEGFP-C1	-	OK

Fig. 11 List of h4Es and their variants with the emphasis on N-, C- termini variations

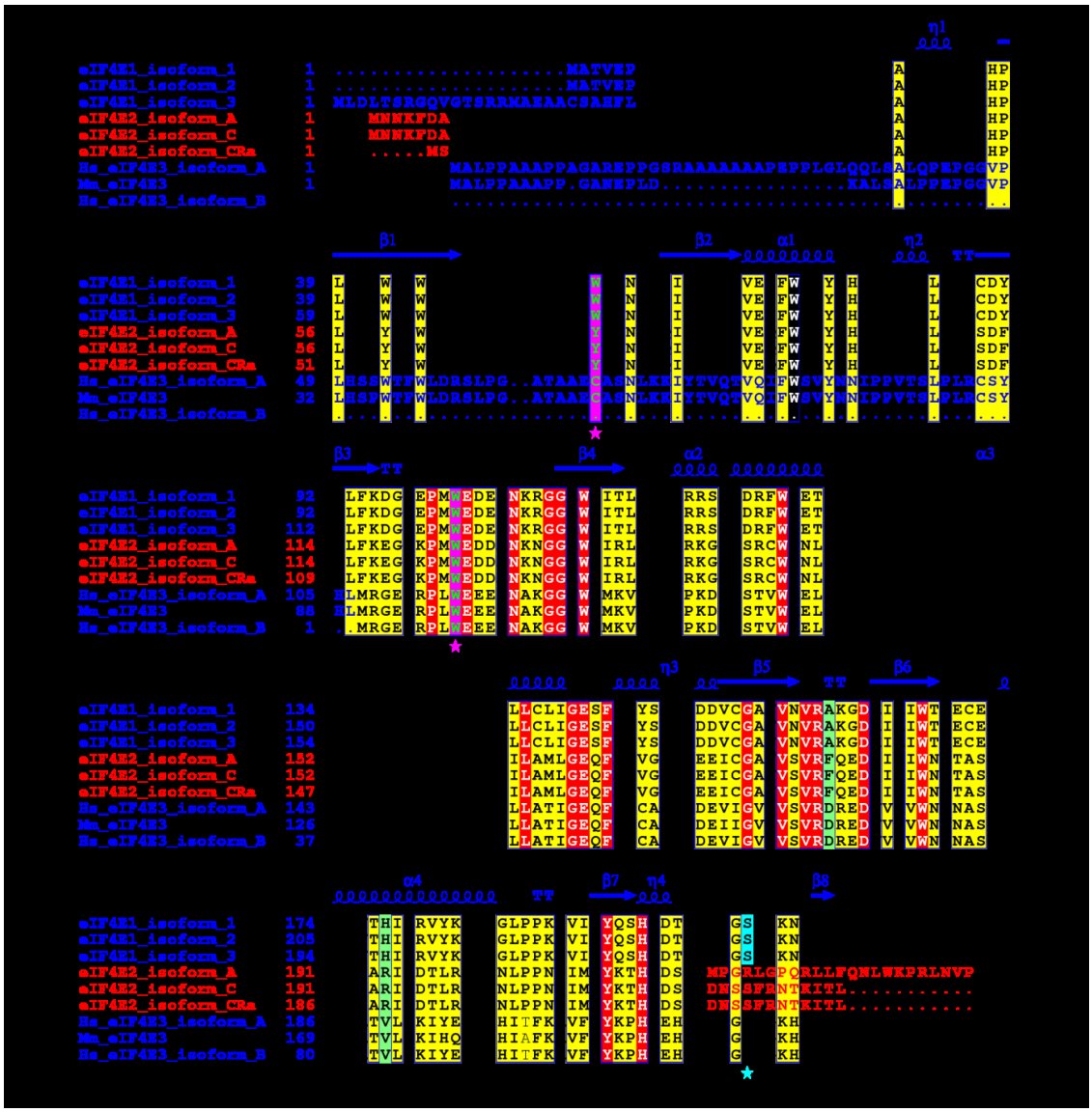

Yellow and red boxes denote amino acids' high similarity and identity, respectively. Utilization of alternative exons coding for different N- and C- protein termini is marked with blue and red letters. Cap-binding residues W56 and W102 in eIF4E1 and corresponding amino acids in eIF4E2 and eIF4E3 are highlighted as green letters in purple boxes and marked with purple asterisks. The conserved Trp73Ala (on the basis of eIF4E1_1) is marked with black box and black asterisk. Ser209 in eIF4E1 (numbering as of eIF4E1_1) is shaded in turquoise blue. Mouse eIF4E3 was added to highlight differences in primary structure between mouse and human orthologs. PDB file 3AM7 was used to depict eIF4E1 secondary structure (Fukuyo et al. 2011).

6.1.2 Labelling

Next part of this project was the labelling optimization to minimize fluorescence cross talk. With the ambitious aim in our minds to visualize cell nuclei, enhanced GFP tagged eIF4Es, cy3 conjugated secondary antibody recognizing marker for stress granules and cy5 conjugated secondary antibody recognizing marker of P-bodies, we were literally touching the limits of fluorescence microscopy. To prove we did our best, please see Fig. 12 for excitation settings and Fig. 13 for emission settings. Naturally, I also checked for the secondary antibody background (Fig. 14), non-transfected cells background and all the channels labelled individually.

Fig. 12 Graph of excitation spectra of all the four channels used for microscopy

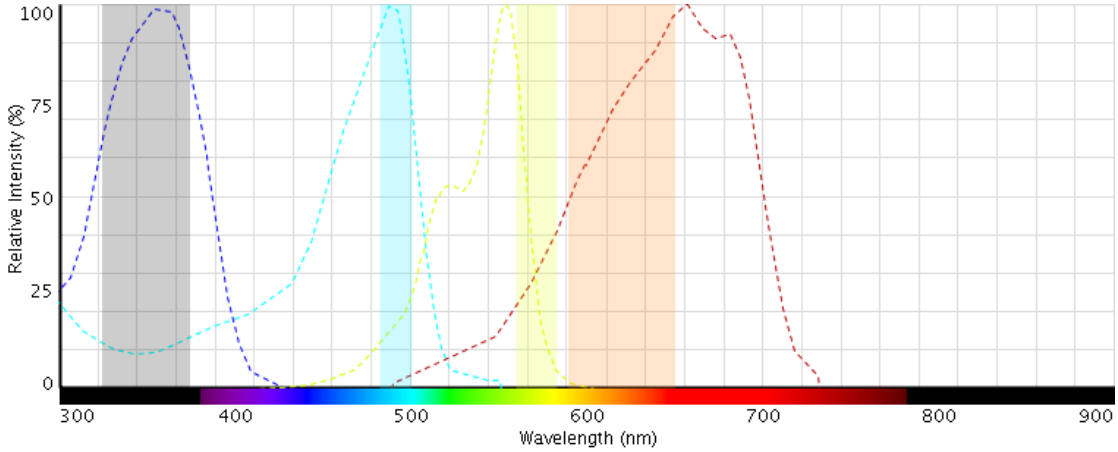

The graph is showing excitation spectra of the individual fluorophores in dashed lines, DAPI is visualized in dark blue, eGFP in blue, Cy3 in yellow and Cy5 in red. The settings of filters are depicted in the boxed area.
https://www.thermofisher.com/cz/en/home/life-science/cell-analysis/labeling-chemistry/fluorescence-spectraviewer.html

Fig. 13 Graph of emission spectra of all the four channels used for microscopy

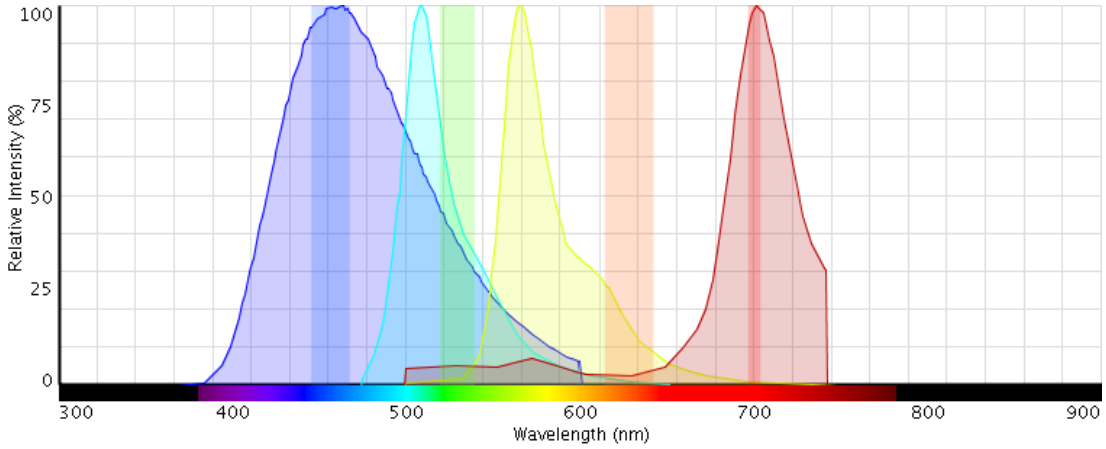

The graph is showing excitation spectra of the individual fluorophores in coloured lines, DAPI is visualized in dark blue, eGFP in blue, Cy3 in yellow and cy5 in red. The filters settings are shown in the boxed area.
https://www.thermofisher.com/cz/en/home/life-science/cell-analysis/labeling-chemistry/fluorescence-spectraviewer.html

Fig. 14 Secondary antibodies: donkey anti mouse, cy3 conjugated and donkey anti rabbit, cy 5 conjugated create mild background that can be easily distinguished from a signal of primary antibodies

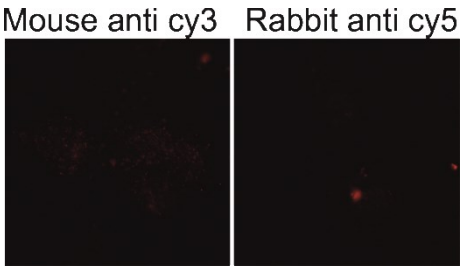

U2OS cells were seeded on a glass coverslip, fixed and incubated with secondary antibody only in the absence of primary antibody. Pictured using Cell R microscope and the same exposure time, intensity that I use usually for preparations with primary antibody.

6.1.3 Heat stress optimization

Originally, our attempts to provoke SGs following published protocols failed, therefore we set out to find optimal temperature for reproducible SG induction using pre-heated thermoblock and a submersible probe connected with a thermometer that measured temperature directly on the coverslips with cells. Fig. 15 shows that SGs rise in a quite narrow high fever- like temperature of 39,5-42,7 °C, as measured in the media. Neither in lower nor in higher temperatures SGs are detected.

Fig. 15 Precise optimization and accurate calibration of temperature measurement were key pre-conditions for efficient and reproducible SGs formation

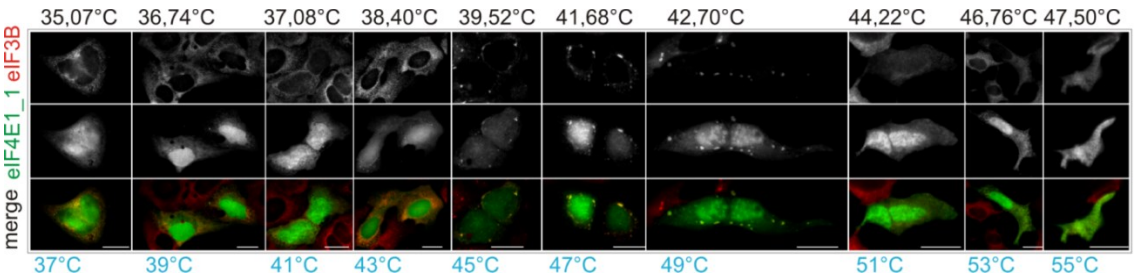

U2OS cells were grown on a glass coverslip and transfected with an expression vector coding for the GFP-eIF4E1_1 fusion protein. Twenty-four hours post-transfection, the cultivation dish was placed on a pre-heated thermoblock and a temperature-calibrated submersible probe was placed into the medium in a direct contact with the coverslip. The medium was then exchanged with another one, pre-warmed to the required temperature. The dish containing the coverslip was closed, covered with a plastic box and incubated on the thermoblock for 30 min. Temperatures of the pre-warmed medium and the thermoblock were set experimentally in order to reach the required temperature on the coverslip. Temperature was read at the beginning and at the end of the treatment. Calculated mean temperature values are displayed above each panel. Corresponding temperature values which were set on the thermoblock are shown below each panel in blue. Following heat shock, cells were fixed and assessed for eIF3B-stained SGs. The temperature gradient clearly shows that only a narrow range of high-fevered temperatures was suitable for efficient induction of SGs formation. The images were acquired using CellR system. Scale bar, 20 µm.

Following a 30-min long heat exposure, all the isoforms of the ectopically-expressed eIF4E2 co-localized with PBs and intriguingly also with SGs (Fig. 16 C, D, E) similarly as both isoforms of eIF4E1 (Fig. 16 A, B). On the other hand, eIF4E3_A was found within SGs only, whereas never observed in PBs (Fig. 16 F); eIF4E3_B isoform was not detected in either SGs or PBs (Fig. 16 G).

Fig. 16 Co-localization of the eIF4E proteins and their protein isoforms with PBs and SGs during heat shock

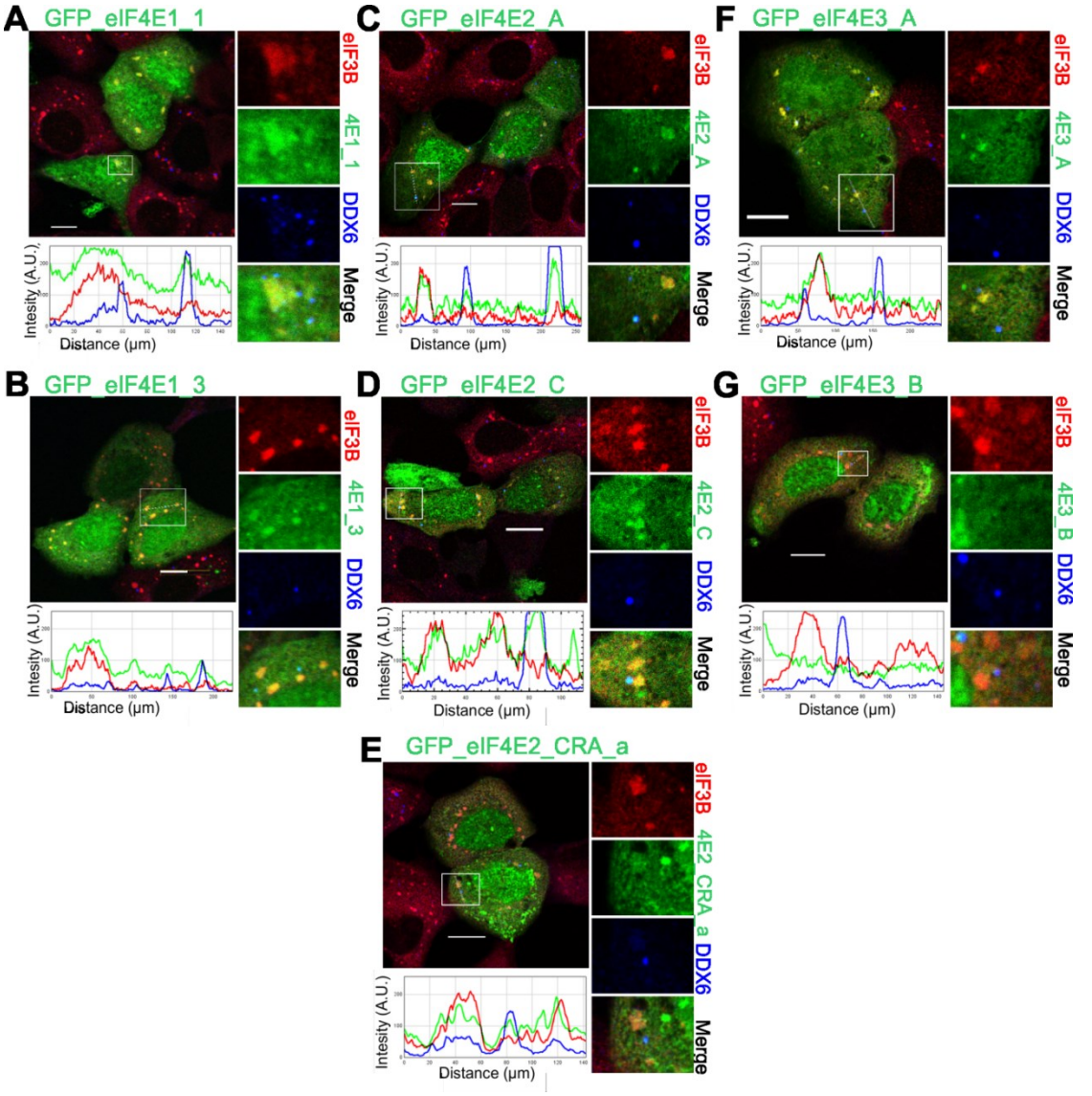

The eIF4E1,2,3 proteins (green) were ectopically produced in fusion with GFP in U2OS cells. Nineteen hours after transfection the cells were exposed to 41.7 °C for 30 min, fixed and assessed for eIF3B-stained SGs and DDX6-stained PBs (blue). Co-localization of the particular eIF4E with SGs and PBs is demonstrated by merge (on the right of each panel) and the intensity profile along the dashed white line in the boxed area (shown again in 4x magnification on the right of the corresponding intensity profile). Both eIF4E1 (A,B) and all three eIF4E2 (C, D, E) variants co-localized with SGs and PBs. The eIF4E3_A (F) was recruited to SGs only and eIF4E3_B (G) co-localized neither with SGs nor PBs. The images were acquired using Leica TCS SP2 with an Acousto-Optical Beam Splitter (AOBS) system. Scale bar, 20 µm.

6.1.4 Arsenite stress optimization and quantification of SGs and PBs that were formed

Originally, we chose to use arsenite stress as a control to heat shock. Heat shock is harder to reproduce than arsenite stress, the use of a different thermoblock or a six-well plate instead of single 35 mm diameter dish, this all influence outcome of the heat shock. Working concentration of sodium arsenite for SG induction in U2OS cell line had to be found experimentally. U2OS cell line was subjected for 30 minutes to various concentrations of sodium arsenite diluted in the media and TIA-1 specific antibody was used as a marker for stress granules (Fig. 17). Using 0.25mM concentration, the SGs are just about to be formed, 0.5mM concentration resulted in an unequal distribution of SGs among cells and therefore, I chose 1mM concentration of sodium arsenite for further experimentation.

Fig. 17 Optimization of the sodium arsenite working concentration for reproducible stress granules formation

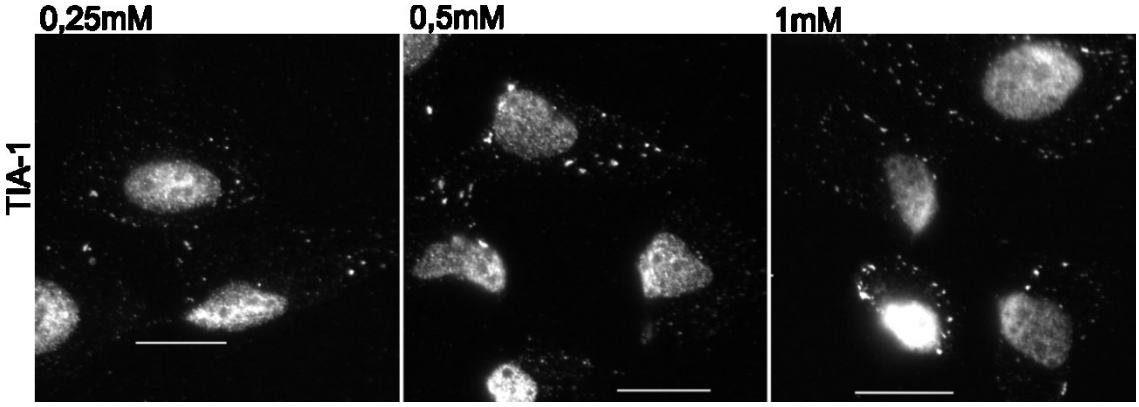

U2OS cells were grown on the glass coverslip. 19h later, the medium was changed for the medium with defined concentration of sodium arsenite and the cells were placed back to the incubator for additional 30 minutes, than fixed, probed with anti TIA-1 antibody and observed using Cell R system. 1mM concentration of sodium arsenite was chosen for further experimentation. Scale bar, 20 μm.

Following a 40-min-long exposure to 1mM sodium arsenite of the U2OS cell line, ectopically-expressed eIF4E2 co-localized with PBs and in vivid contrast with heat stress, it did not localize to SGs (Fig. 18 C, D, E). On the contrary, eIF4E1 (Fig. 18 A, B) was found in both SGs and PBs. eIF4E3_A was found within SGs only, whereas never observed in PBs (Fig. 18 F); eIF4E3_B isoform was not detected in either structure (Fig. 18 G).

Fig. 18 Co-localization of h4Es and their isoforms with SGs and PBs in cells subjected to oxidative stress

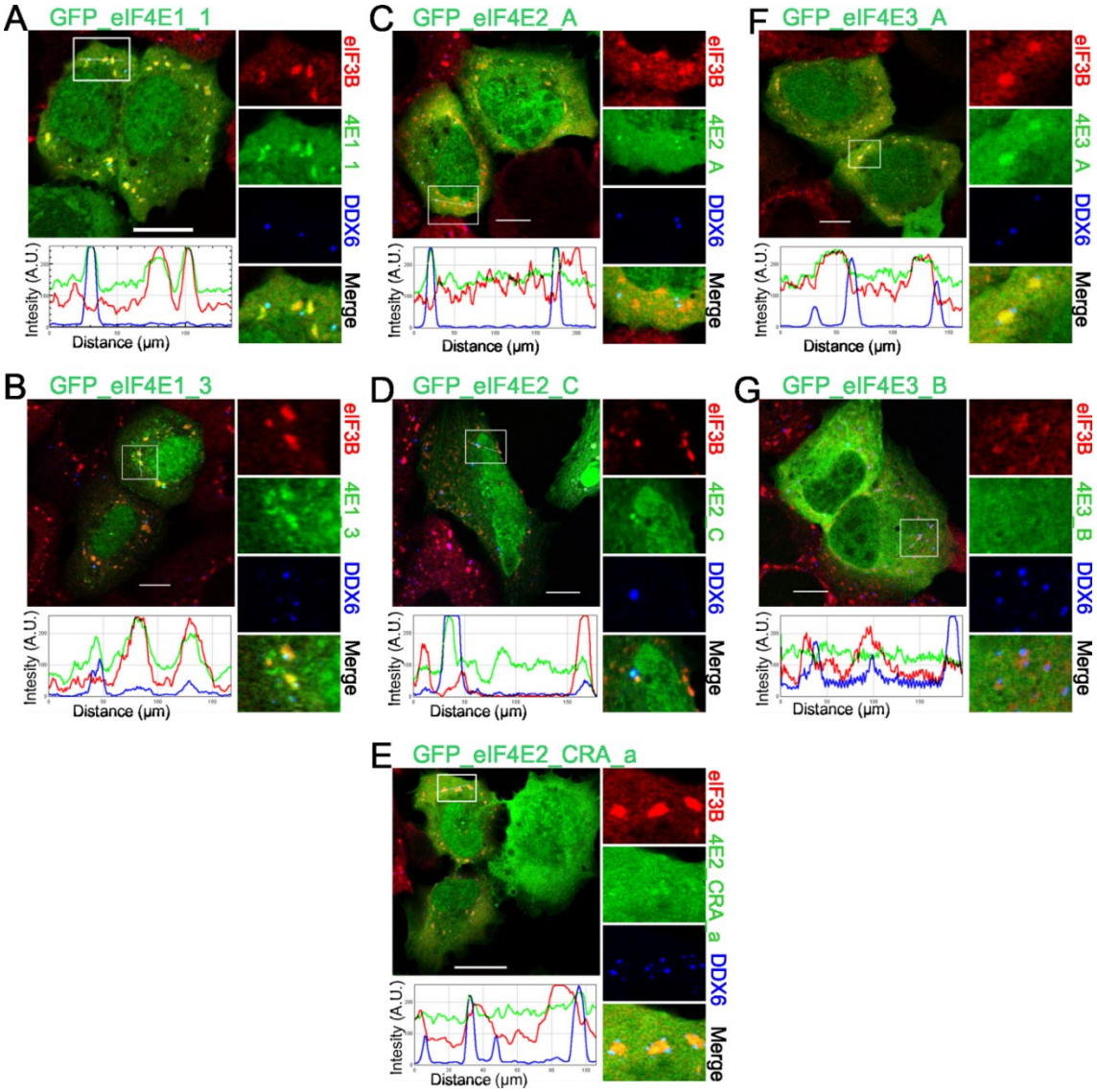

The eIF4E1,2,3 proteins (green) were ectopically produced in fusion with GFP in U2OS cells. Twenty-four hours after transfection the cells were treated with 1mM sodium arsenite for 40 min., fixed and assessed for eIF3B-stained SGs and DDX6-stained PBs (blue). Co-localization of the particular eIF4E with SGs and PBs is demonstrated by merge (on the right of each panel) and the intensity profile along the dashed white line in the boxed area (shown again in 4x magnification on the right of the corresponding intensity profile). Contrary to heat shock, only the eIF4E1 variants were able to co-localize with both SGs and PBs (A,B). The eIF4E2 protein variants (C, D, E) co-localized with PBs only. The eIF4E3_A (F) was present in SGs only and eIF4E3_B (G) co-localized neither with SGs nor PBs. Pictures were taken using Leica TCS SP2 with an Acousto-Optical Beam Splitter (AOBS) system. Scale bar, 20 μm.

When microscoping the stressed cells, I noticed differences in the number of stress granules among particular protein isoforms and decided to quantify them. Using three biological replication, each of approximately 100 cells, stressed by sodium arsenite, I counted manually number of cells with stress granules formed by individual eIF4Es that

co-localized with eIF3B marker (Fig. 19). This analysis revealed that 75 % of cells ectopically producing the prototypical GFP-eIF4E1_1 formed eIE4E1-1-positive SGs, whereas the number of cells forming SGs dropped to 52 and 49 % for those ectopically producing GFP-eIF4E1_3 and GFPeIF4E3_A, respectively. Statistical analysis was run by Vendula Novosadová.

Fig. 19 eIF4E1_3 and eIF4E3_A isoforms are less prone to form SGs

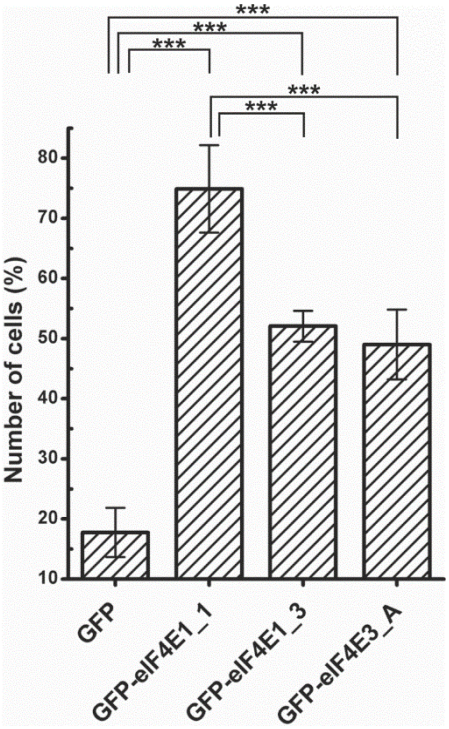

eIF4E1_1, eIF4E1_3, and eIF4E3_A proteins were ectopically produced in fusion with GFP from the same vector in U2OS cells. Nineteen hours post-transfection, the cells were treated with 1 mM sodium arsenite for 40 min, and those forming SGs were counted and plotted as a fraction of all transfected cells. Error bars indicate differences among three independent experiments in which approximately 100 of the transfected cells were assessed. We applied Chi square test to analyse differences between number of cells forming stress granules among all transfected cells expressing individual eIF4E proteins or a GFP control. GFP-eIF4E1_1, GFP-eIF4E1_3, GFP-eIF4E3_A were compared to control pEGFP and to each other by post hoc Chi square test with Bonferroni correction for multiple testing. Except for the GFP-eIF4E1_3 x GFP-eIF4E3_A pair, all other differences were statistically significant (p values <0.0001, marked with asterisk).

I also looked at the number of cells with PBs co-localizing with the ectopically expressed eIF4E1 and eIF4E2. I measured approximately 50 cells in three independent biological replications, see Table 5. Linear regression model was applied when analysing data of stress-free conditions and stress conditions together, confirming there is no significant difference among individual proteins tested at $\alpha=0.05$. Nevertheless if you split the data and analyze arsenite-stressed cells and cells in stress-free conditions separately using Chi-square test with Bonferroni correction for multiple testing,

significant differences at α=0.05 were found for the following pairs in stress-free conditions: 4E1_1 vs. 4E2_A (Bonferroni = 0.0119), 4E1_3 vs. 4E2_A (Bonferroni = 0.0024), 4E2_A vs. 4E2_C (0.0304).

Table 5 h4E positive P-bodies' quantification did not reveal any major differences between individual h4Es

Construct	Percentage of cells with PBs	
	Stress-free	Arsenite stress
GFP-4E1_1	28,3	54,5
GFP-4E1_3	39,5	51,5
GFP-4E2_A	37,7	60
GFP-4E2_C	35,3	53,2
GFP-4E2_CRA_a	34,5	61,2

6.1.5 Stress- free conditions and other control experiments

When applying stress-free conditions on the U2OS cell line transfected with GFP-h4Es, both the eIF4E1 and eIF4E2 co-localized with PB´s marker DDX6 (Fig. 20 A-E), while both the eIF4E3 isoforms did not localize to PBs. To make sure, the subcellular distribution of GFP tagged h4Es is not an artefact caused by fixation, please refer to Fig. 9 showing live cell imaging of GFP tagged h4Es in Hek cell line.

Fig. 20 Co-localization of h4Es and their isoforms with PBs in stress- free conditions

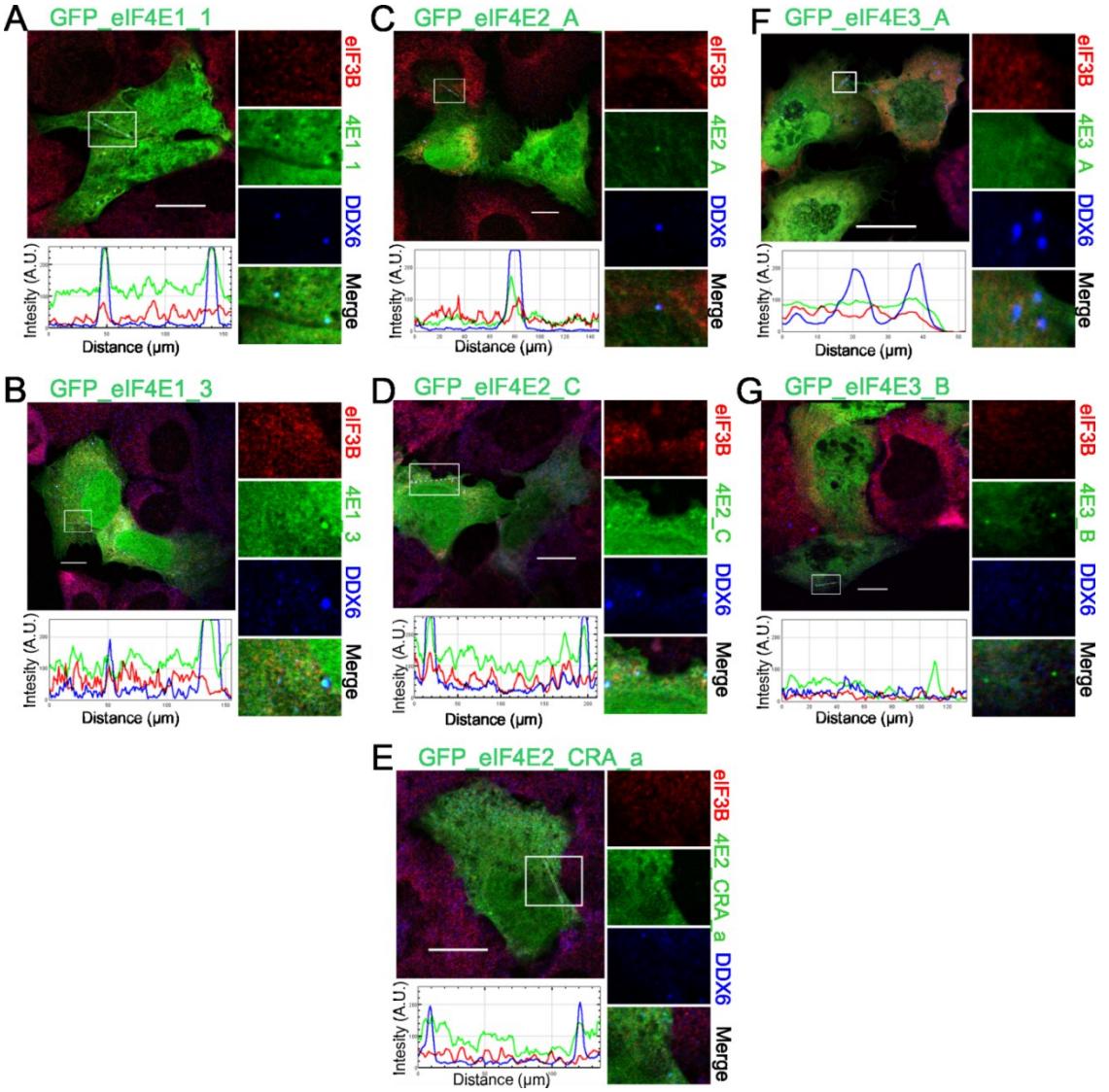

The eIF4E1, 2, 3 proteins (green) were ectopically produced in fusion with GFP in U2OS cells. Nineteen hours after transfection, the cells were fixed and assessed for eIF3B-stained SGs and DDX6-stained PBs (blue). No development of stress granules was observed. Co-localization of the particular eIF4E with PBs is demonstrated in the boxed area replicated in a higher magnification on the right side of each panel and by the intensity profile measured along the dashed white line within the boxed area. Both eIF4E1 (A, B) and all three eIF4E2 (C, D, E) variants co-localized with PBs. No co-localization with PBs was detected for eIF4E3_A (F) or eIF4E3_B (G). Approximately fifty cells transfected with each plasmid were investigated in two independent biological replicates. Pictures were taken Leica TCS SP2 with an Acousto-Optical Beam Splitter (AOBS) system. Scale bar, 20 µm.

To ensure that the phenomenon we were observing is not an artefact caused by GFP overexpression, we decided to check for endogenous eIF4E´s localization.

Unfortunately, I was unable to find working eIF4E3 antibody. Altogether, we tested three antibodies against eIF4E3 (AB136091, sc-133542, AV41168). I performed seven independent western blots using different cell lines and out of those, only two

were successful, once with AB136091 and once with sc-133542. Therefore, I did not trust the antibodies enough to publish immunofluorescence pictures using them. Nevertheless, two of them were tested for immunofluorescence and the signal was quite good (see Fig. 21).

Fig. 21 Visualization of endogenous eIF4E3

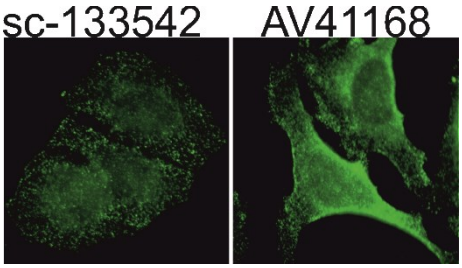

Endogenous eIF4E3 was visualized using U2OS cell line, two distinct primary rabbit antibody were diluted 1:50 and incubated O/N, secondary antibody Alexa Fluor 488 goat anti-rabbit was diluted 1:1000 and incubated for 1h. Observed using Cell R system.

Thus, I had to probe for eIF4E2 and eIF4E1 only. As both the eIF4E´s antibodies were produced in a rabbit, I could not use our PB marker DDX6, produced in a rabbit as well, together with 4E specific antibodies in one preparation. I was limited to analyse only stress granules only.

U2Os cell line was analysed in heat, arsenite and stress-free conditions and probed either against eIF4E1 and eIF3B, or eIF4E2 and eIF3B. In agreement with what we had observed for the overexpressed proteins, eIF4E1 formed SGs under both treatment (Fig. 22 B,C) and eIF4E2 formed SGs in heat stress only (Fig. 22 F,E). Using endogenous protein approach it became more obvious, that unlike 4E1, 4E2 is not present in all the eIF3B foci in heat stress. This became a beginning of another promising story (see results Part II).

Fig. 22 Co-localization of endogenous eIF4E1 and eIF4E2 with SGs

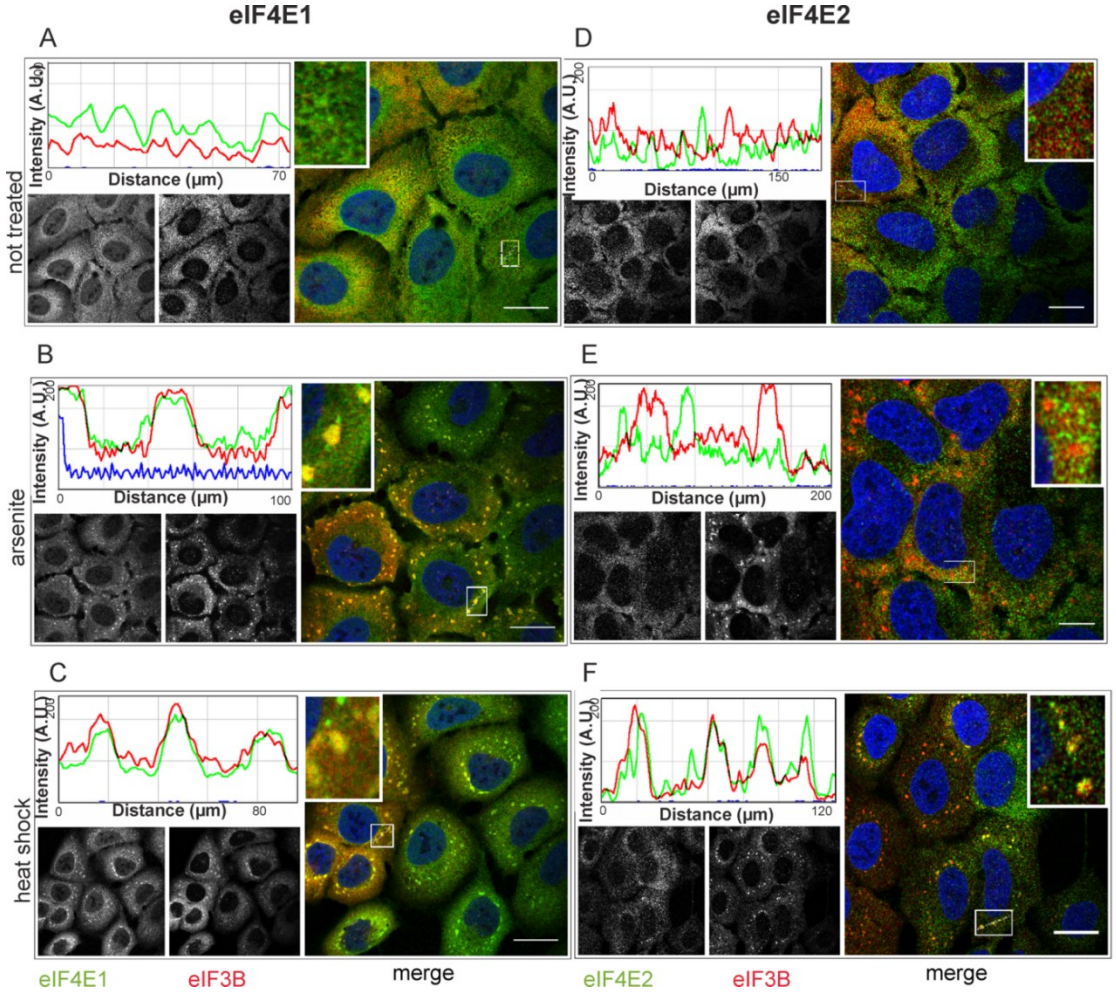

U2OS cells were grown in stress-free conditions (A, D), treated with sodium arsenite (B, E) or exposed to heat (C, F), then stained with antibodies against eIF4E1 (A, B, C, green), eIF4E2 (D, E,F, green) and eIF3B (SG marker, red). Co-localization of the particular eIF4E with SGs is demonstrated by merge (on the right of each panel) and the intensity profile along the dashed white line in the boxed area (shown again in 3x magnification on the right of the corresponding intensity profile). In agreement with experiments based on GFP-tagged proteins, immunostaining of endogenous eIF4E1 and aIF4E2 shows their nuclear-cytoplasmic distribution and a specific recruitment of eIF4E2 to SGs during heat stress (F). Nuclei were stained with DAPI (blue). Picture were taken using Leica TCS SP2 with an Acousto-Optical Beam Splitter (AOBS) system. Scale bar, 20 µm.

Because we struggled with publishing the data, I ran two more control experiments. First, it was the cap-binding assay to prove that GFP tagged 4E1 binds the cap similarly to the endogenous protein (Fig. 53 in Part III). Second, it was the GFP-IP. In the publication, we are showing that members of translation initiation machinery e.g. eIF4G and PABP bind specifically to eIF4E1, eIF4E3_A but not eIF4E3_B (data are not shown here as I did not perform this particular experiment). Therefore we had to be sure

that, the interaction is not mediated via any sort of non-specificity caused by GFP itself (Fig. 23).

Fig. 23 Control immunoprecipitation does not reveal any non-specific interaction between GFP and PABP or eIF4G

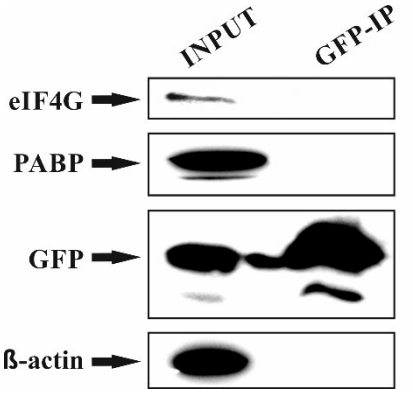

HEK293 cells transiently transfected with a control expression vector pEGFP-C1 were lysed 24 h post-transfection and the lysate was subjected to immunoprecipitation using GFP-Trap approach. Western blots were developed with anti-eIF4G, anti-PABP, anti-GFP and anti β-actin antibodies. The results clearly show that while all the proteins tested were present in the lysate, only GFP remained bound to the resin upon GFP-Trap immunoprecipitation.

6.2 Visualization of two 4Es in a cell

The aim of this part is to visualize pairs of h4Es in a cell under both arsenite and heat stresses, to characterize the differences in the protein composition of SGs induced by the two stresses and to compare SGs containing 4E2 with SGs lacking 4E2. As multiple antibodies are rather difficult to combine in one preparation and we are initially interested not only in fixed preparation, but also in kinetic properties of SG assembly, we chose settings with one 4E being expressed by stable cell line in fusion with GFP and the other being fused with mCherry.

6.2.1 Characterization of U2OS Flip In stable cell lines

First, it was necessary to prepare stable cell lines expressing GFP- 4E1_1, GFP-4E2_A and GFP-4E3_A. Those we prepared in co-operation with my bachelor student Jana Kráčmarová. We used commercially available U2OS Flip IN system and followed manufacturer´s protocol. Individual cell lines were named and their clones were numbered due to space restrictions on a freezing tubes. GFP-4E1 expressing cells were named ELA (name of Jana´s choice), GFP-4E2_A expressing cell line BAL (to honour my best friend MUDr. Barbora Lomnická) and finally GFP-4E3_A expressing cell line was named MAP to pay tribute to our mentor. The functionality of the cell lines was checked by both western blot (Fig. 24) and microscopy (Fig. 25).

Fig. 24 Detection of GFP-h4Es of accurate size upon tetracycline induction of U2OS Flip In based stable cell lines

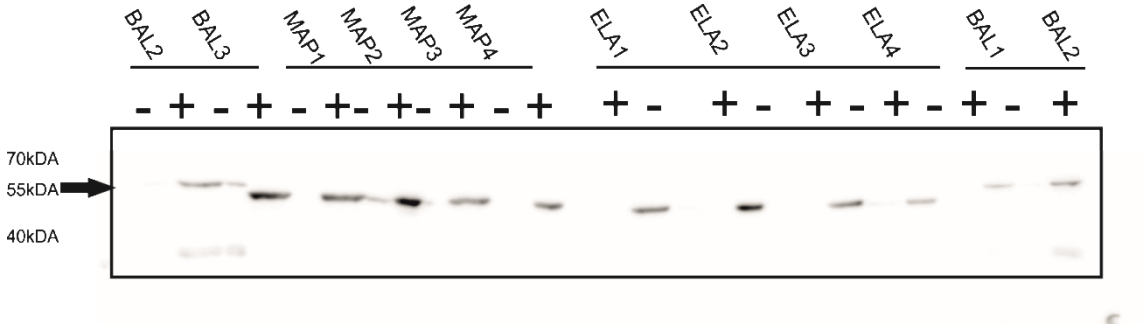

U2OS cell lines stably expressing h4Es were grown in six well plates, induced with 1mM tetracycline (+), or un-induced (-) and lysed 24h later. Western blot was developed with anti-GFP antibody. Bands of supposed sizes were successfully detected: GFP-4E1_1 (ELA 52 kDa), GFP-4E2_A (BAL 54 kDa), GFP-4E3_A (50 kDa).

Fig. 25 Live cell microscopy of all U2OS stable cell line´s clones

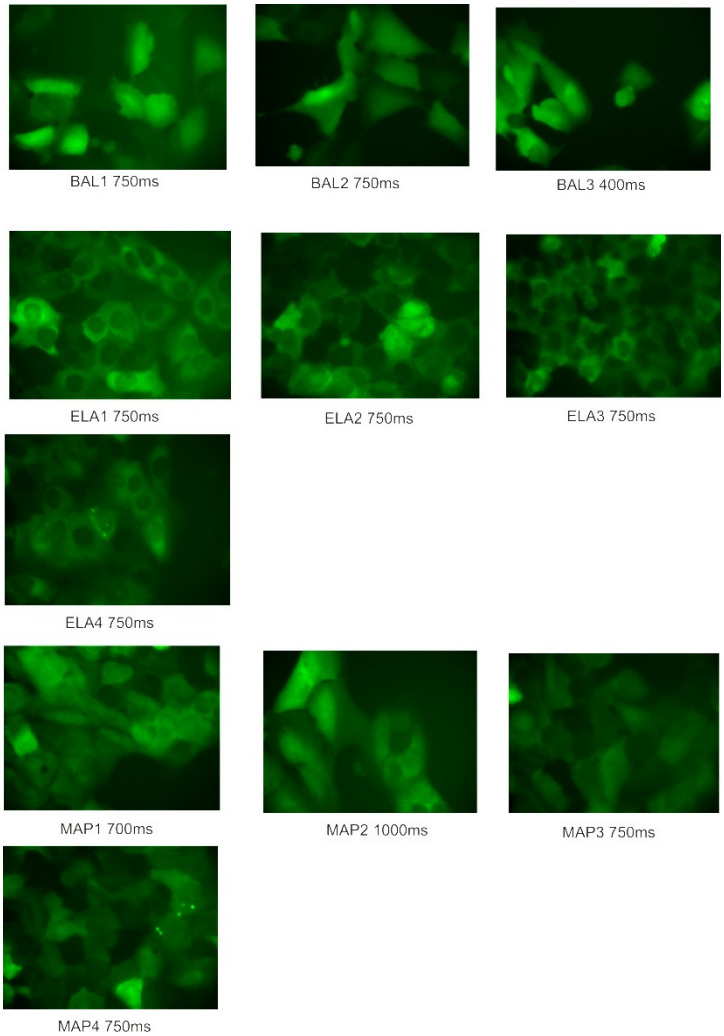

U2OS Flip In cell lines stably expressing h4Es were seeded in a dish with glass bottom, induced and observed using CellR system 24h later. Although all the clones are expressing 4Es under the control of the same promoter, not all the clones express 4Es at the same cell to cell level, compare ELA1 and ELA2 and MAP1 and MAP4.

These cell lines were supposed to be used mainly for microscopy, we were interested preferentially in those having lowest cell to cell variations at the expression level and those having undetectable expression level prior induction. Therefore following stable cell line´s clones were chosen for further experimentation: MAP 1, BAL 2 and ELA 3.

6.2.2 Insertion of h4Es into N-terminal mCherry fusion

mCherry C-1 plasmid was kindly provided to me by Radoslav Janoštiak from the Department of Cellular Biology, faculty of Science. I preferred mCherry over the dsRED plasmid, that was available in our laboratory with some h4Es already cloned in this fusion, because mCherry has superior photo stability and brightness over dsRed (Shaner et al. 2005). The constructs were prepared by Jana Kráčmarová under my

supervision. We took pEGFP-4E1_1 and cut it with Acc65I and BglII, pEGFP-4E2_A and pEGFP-4E3_A were cut with SalI, KpnI. The target plasmid mCherry-C1 was cut with the same set of restriction enzymes and the final products mCherry-4E1_1, mCherry-4E2_A, mCherry-4E3_A were ligated (Fig. 26), control cleaved with Acc65I and BglII or PstI in the case of the last two constructions and sequenced.

Fig. 26 Maps of constructs expressing mCherry-4E1_1, mCherry-4E2_A and mCherry-4E3_A

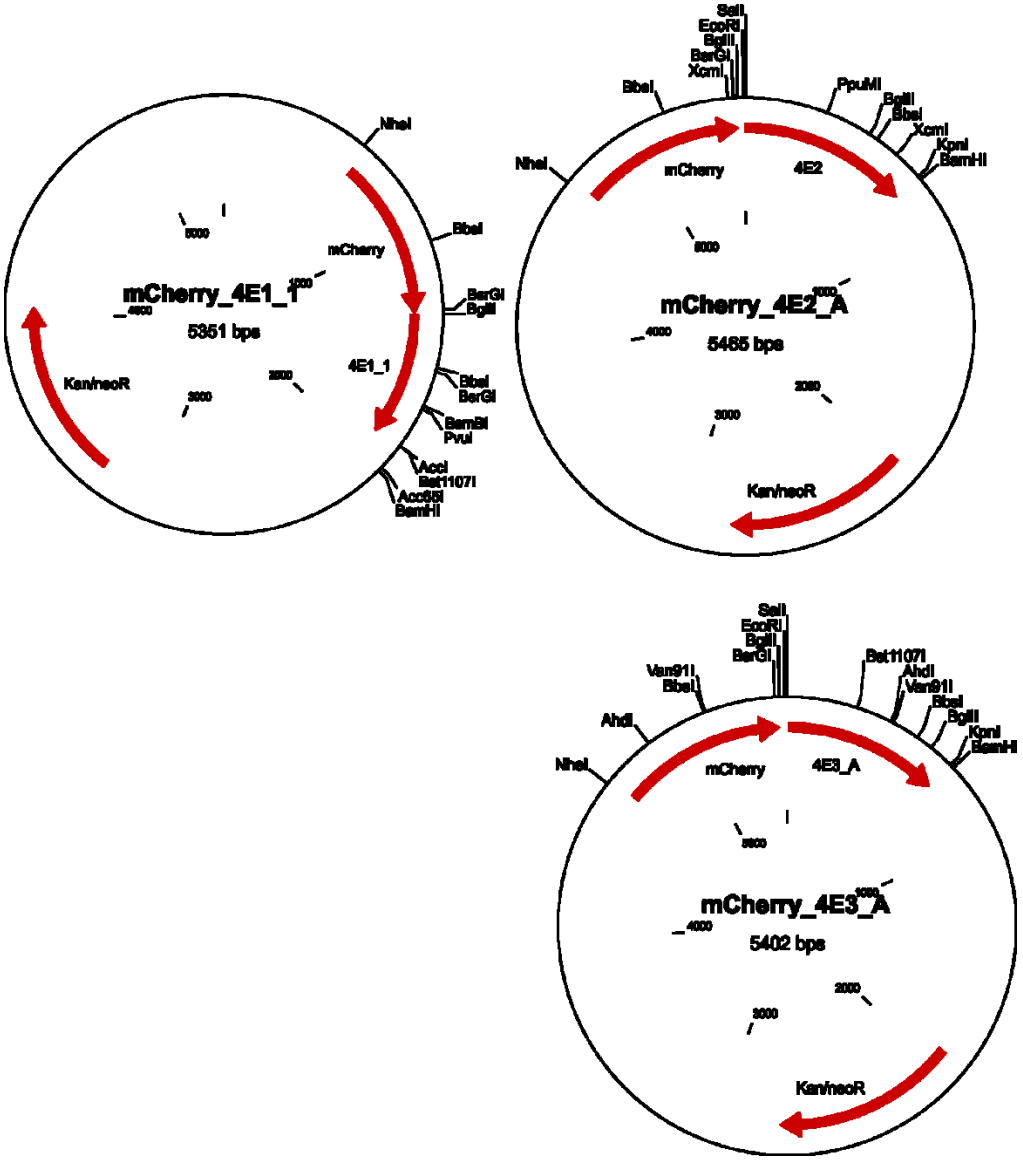

We also checked new construct´s functionality using the microscope. Fig. 27 shows two 4Es in mCherry and GFP fusion in stress-free conditions in a cell. Unfortunately, the list of possible combinations is not complete. Nevertheless it demonstrates, that there are no major difference between distributions of GFP-tagged and mCherry-tagged h4Es.

Fig. 27 Comparison of GFP tagged and mCherry tagged 4Es does not reveal any major differences in their distributions

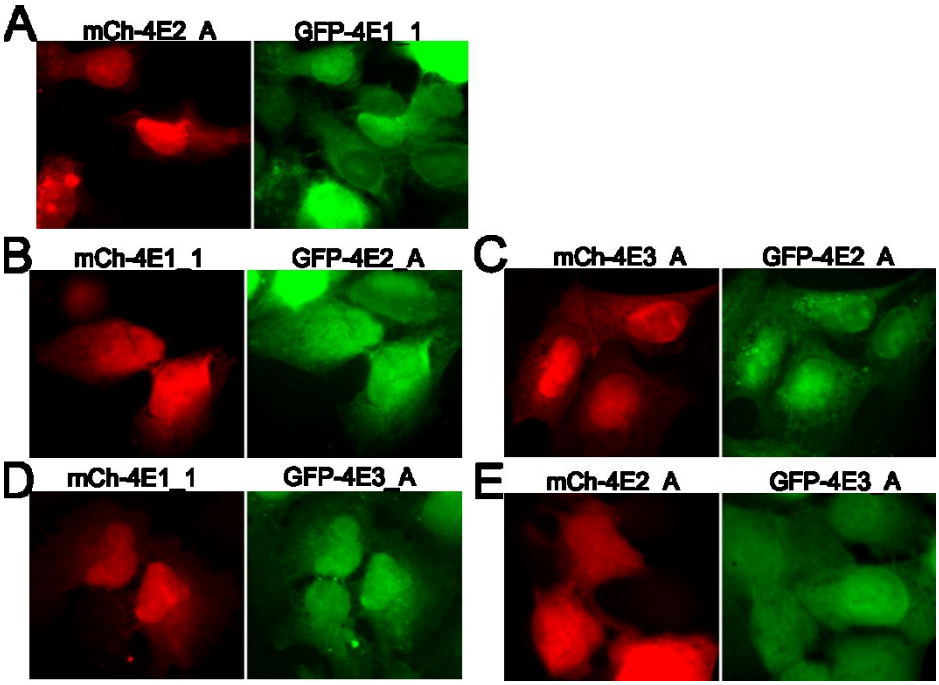

Stable cell lines expressing 4Es in GFP fusion were seeded on a glass coverslip, induced with tetracycline and transfected 5 hour later with Sigma Universal transfection reagent and Optimem media for the transfection mix. Cells were fixed 24h later and observed using CellR system.

As a result, we could not wait to see if mCherry tagged h4Es would be able to form SGs and finally unravel whether those SGs are going to be a mixture of 4Es or rather 4E specific.

Unfortunately, the approach we chose was not without problems. For instance, stable cell lines were losing expression when not cultivated under hygromycin-selective pressure. Upon transfection a lot of cells died so the preparation then looked like an abandoned battle field and we were having hard time finding at least two healthy, transfected and stressed cells in the same spot to picture. That is why the following figure is also incomplete. Conclusions from the figure Fig. 28 has to be drawn extremely carefully as those data has never been repeated so far. Sadly, I could not add the stress granule´s marker eIF3B to the preparations as we only had cy3 labelled secondary antibody against the mice at that time and cy3 signal would overlap with the mCherry signal.

Fig. 28 Visualization of two h4Es under the heat stress unravelled two types of SG-like structures: h4E specific and mixture of two h4Es

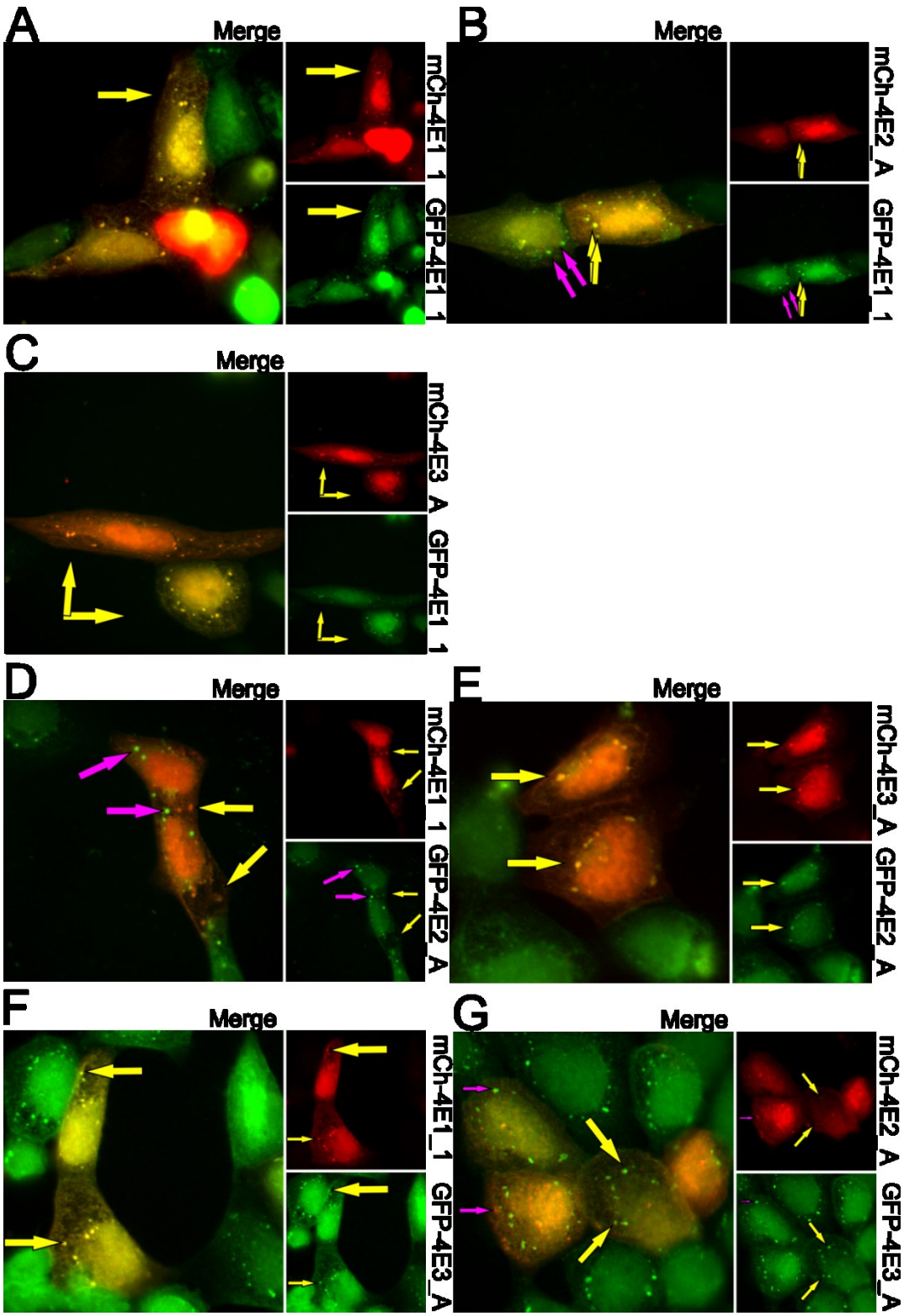

Stable cell lines expressing h4Es in GFP fusion were seeded on a glass coverslip, induced with tetracycline and transfected 5 hour later with Sigma Universal transfection reagent and Optimem media for the transfection mix. Cells were stressed with heat and fixed 24h later. Yellow arrows point to the SG-like structures where two h4Es co-localize and magenta arrows are showing h4E specific SG-like structures. Preparations were observed using CellR system.

Fig. 28 A shows almost 100% overlap of GFP-4E1 and mCherry-4E1, proving that the tag has no influence on the 4E1 ability to localize to SG-like structures and also, that the type of the tag makes probably no major difference in terms of kinetics. C and F are showing almost 100% overlap between the SG-like structures formed by 4E1 and 4E3. On the contrary, whenever 4E2 is involved, with one exception of E, there are always two types of SG-like structures present (compare B and C, F and G). Although it is likely, that not all the SG-like structures are indeed SGs, especially in the case of D, where 4E1 is supposed to be an essential part of stress granules and yet, 4E2 specific granules are present (could as well be PBs or else). Fig. 28 B and G are important hints for us to think, there might be something special on the 4E2 stress granules.

6.2.3 Optimization of transfection versus induction of stable cell lines

Time went by and I got a new master student Pavlína Hrbková. With the new blood in the lab, the courage to get back to this project has returned. First, we found out, that it is necessary to cultivate stable cell lines under hygromycin pressure up to the moment of starting the experiment. When taking this under consideration we were able to effectively prevent the loss of expression. Another improvement was to seed twice more cells per dish than while using U2OS, this gave us enough material for further dying on transfection and stress. For the SG visualization, we got a new secondary antibody anti-mouse Alexa 647, that worked well in one preparation with mCherry and GFP. The stress treatment was prolonged to 1 hour, resulting into more SGs present after the stress and we played around with the order of transfection and induction see Table 6. Unfortunately, Sigma transfection reagent that we were using with Jana was no longer available in the lab, so we switched to Lipofectamine 2000. Data in the Table 6 are showing, that transfection of the stable cell lines works better when cells are transfected 48 hours prior microscopy than when they are transfected 24 h prior microscopy (compare A, C and B). On the other hand, in terms of transfection efficiency, it makes no major difference, if the cells are induced for 24h or for 48h hours (compare B and C). We could not wait for more than 48 h with the transfection as the other steps involved in creating fixed preparation take two more days and we tried to fit in a week with one experiment to make things easier in a long term. Similarly, we tried to avoid using antibiotics directly in the experiment. First, I am not a big fan of antibiotic usage for cell cultivation when not necessary. I prefer to see the contamination immediately to

passage it along for several experiments before realizing it. Second, we study translation, common antibiotic´s target and this could potentially be misleading. Anyway, preparation E was the one with the least cells left alive, so beside numbers, we used common sense and the overall fitness of preparations to pick our favourite conditions-B.

Table 6 Preparation B was opted as a best way to obtain reliably transfected and induced cell line at the same time

Preparation	Seeding	Transfection	Induction	Microscopy	Percentage of transfected cells
A -Hygro	Day 1	Day 1 7h p.i.	Day 1	Day 2	13
B -Hygro	Day 1	Day 1 7h p.i.	Day 1	Day 3	36
C- Hygro	Day 1	Day 1 7h p.s.	Day 2	Day 3	35
D -Hygro	Day 1	Day 2	Day 1	Day 3	13
E + Hygro	Day 1	Day 1 7h p.s.	Day 1	Day 2	45

U2OS cells stably expressing GFP-4E2_A were seeded on the glass coverslip, treated as written in the table: p.s. stands for post seeding, p.i. stands for post induction, transfected by 2,5 µg of mCherry-4E1_1 in 150µl of Optimem and mixed with 7,5 µl of Lipofectamine 2000 as previously tested (data not shown), fixed, DAPI stained and observed using Cell R system with 20x magnification. 10 independent field using DAPI filter were imaged and combined the same fields imaged using Texas Red filter (mCherry signal), this gave us from 400 to 1000 of cells in each preparation to analyse. In the merged images all the transfected cells were counted manually using Image J Cell Counter plug in and divided by the number of all the nuclei for each image, average percentage of transfection efficiency is written in the table. Upon using Lipofectamine 2000 for the cell transfection, approximately 30% of transfected cells died within a day post transfection.

Even though we tried really hard to make the experimental settings with the other 4E transfected work, we failed. First, Lipofetamine is certainly not a good transfection reagent to work with in terms of these rather sensitive stable cell lines. I ran a control transfection with the last bit of Turbofect and it became obvious that Turbofect is much less toxic for our cells. Second, when we stressed the transfected cells, they died out in a greater extent than what we observed with Jana and Sigma transfection reagent. And last, Pavlína was in a hurry for some results due to personal reasons, so we decided to switch the Cherry tagged h4Es for antibody against the endogenous h4Es.

6.2.4 Simultaneous localization of two h4Es in one cell

After switching from transfection to endogenous protein detection in stable cell lines, things have improved fundamentally. Although we were aware of the fact, this approach would limit us with kinetic studies. For SG visualization, we used two separate antibodies. A rabbit eIF3B antibody was used together with the detection of endogenous

4E1, because working 4E1 antibody was raised in a mouse. The original mouse eIF3B antibody was used for simultaneous detection of 4E2, because working 4E2 antibody was raised in a rabbit.

We started with simultaneous visualization of endogenous 4E1 and 4E2 in the U2OS cell line. Unfortunately, we found out that confocal is more demanding on the fluorescence signal than Cell R fluorescence microscope. The affinity of eIF4E2 antibody was at the detection limit of the microscope, compare Fig. 29 stress-free panel (Zeiss) and Arsenite stressed panel (CellR) not to mention super resolution microscope, which was also scheduled. That is why the other Figures from this section were mostly imaged using Cell R. The ultimate inability of endogenous 4E2 to localize to SG-like structures in arsenite stress was nicely visible in Fig. 29 arsenite stress panel (compare endogenous 4E1 and 4E2).

Fig. 29 Simultaneous visualization of endogenous eIF4E1 and eIF4E2 in the U2OS cell line in stress- free and arsenite stress conditions

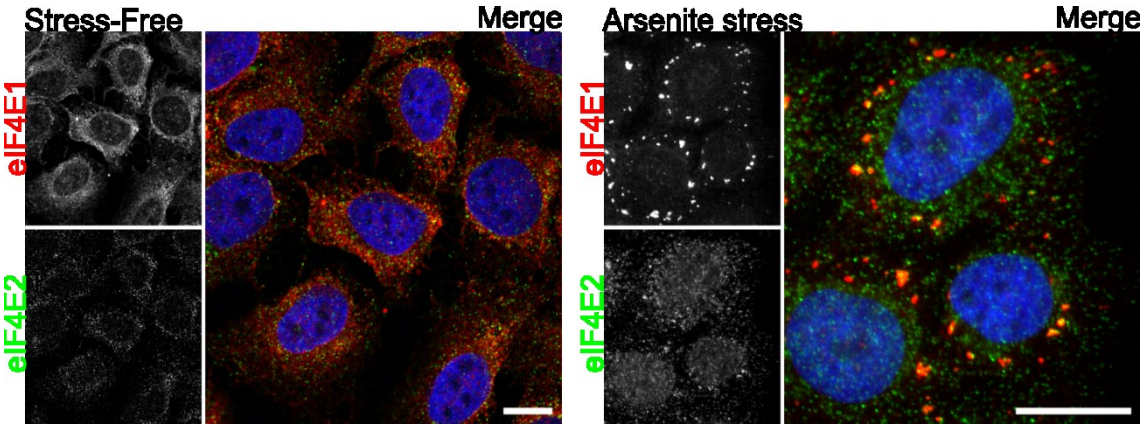

U2OS cells were grown on a glass coverslip, fixed and simultaneously probed for endogenous eIF4E1 and eIF4E2. Stress-free panel was observed using Zeiss confocal microscope, panel with arsenite stress was observed using CellR system. Scale bar is 20 μm.

Next, we visualized 4Es in arsenite stressed stable cell lines (Fig. 30). Again, neither endogenous nor overexpressed 4E2 localized to SGs upon arsenite stress (Fig. 30 A,D). And similar to Fig. 28 C and F, we observed 100% co-localization of 4E3 and 4E1 in the SGs (Fig. 30 C).

Fig. 30 Arsenite stress renders both overexpressed and endogenous 4E2 unable to localize to SGs, whereas 4E3 and 4E1 co-localize in SGs

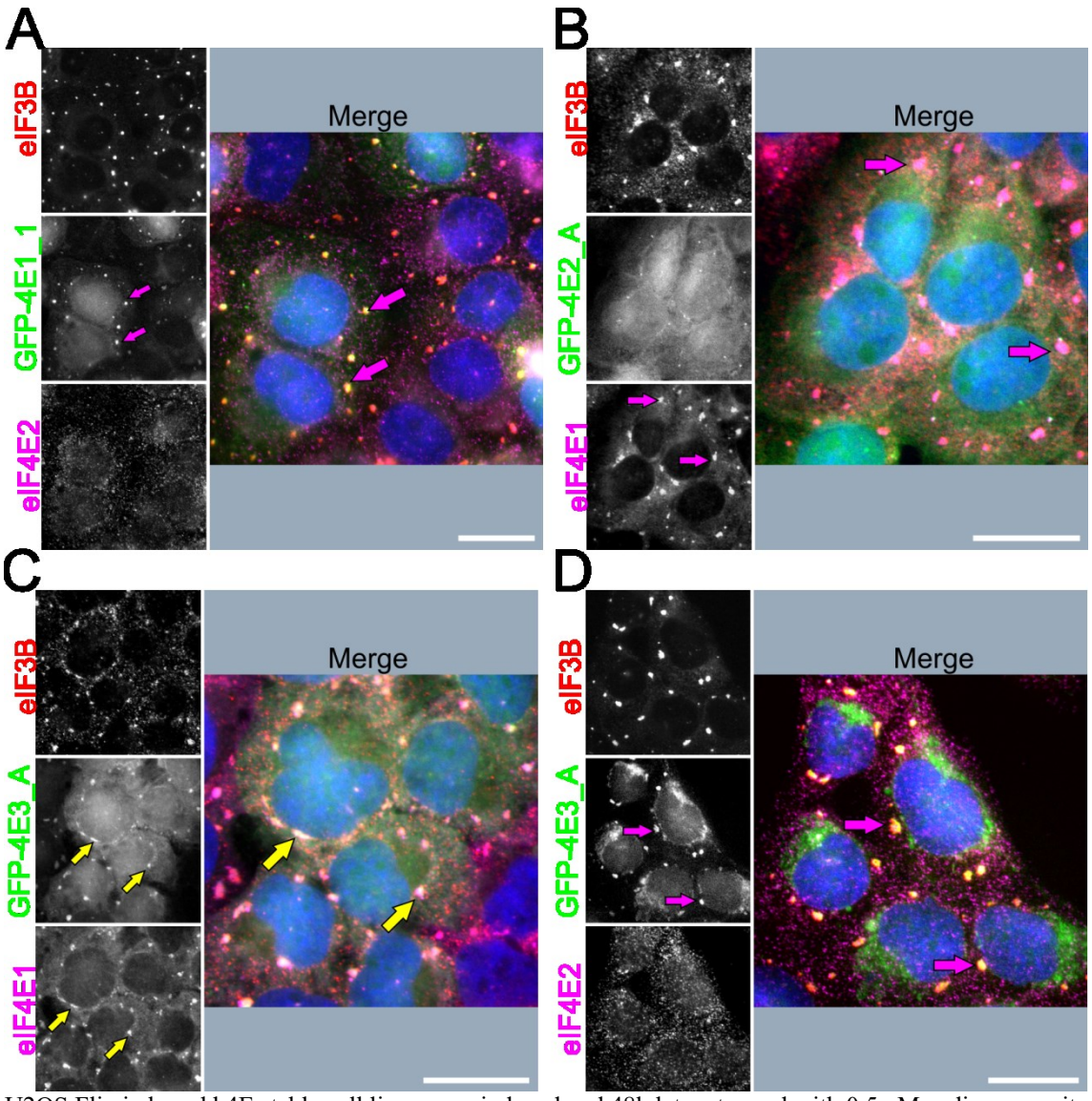

U2OS Flip in based h4E stable cell lines were induced and 48h later stressed with 0.5mM sodium arsenite for 1h, fixed and probed for the other h4E using antibodies (rabbit anti 4E2 or mouse anti 4E1 and therefore rabbit or mouse eIF3B). Preparations were observed using CellR system, magnification 60x, scale bar, 20 µm. SGs where two 4Es co-localize together are pointed with yellow arrows and those where 4E1 is on its own are highlighted with magenta arrows.

Fig. 31 clearly showed, that 4E3 co-localized in virtually all the 4E1 SGs. We called this stress granules "4E1/3 SGs". On the other hand, both endogenous and overexpressed eIF4E2 formed a sub-population of stress granules in the total population of 4E1/3 SGs (compare Fig. 31 A and B with C and D). This subpopulation of so called "4E2 SGs" contained all the three 4Es.

Fig. 31 Two types of stress granules in heat stress can be observed, 4E1/3 and 4E2 SGs

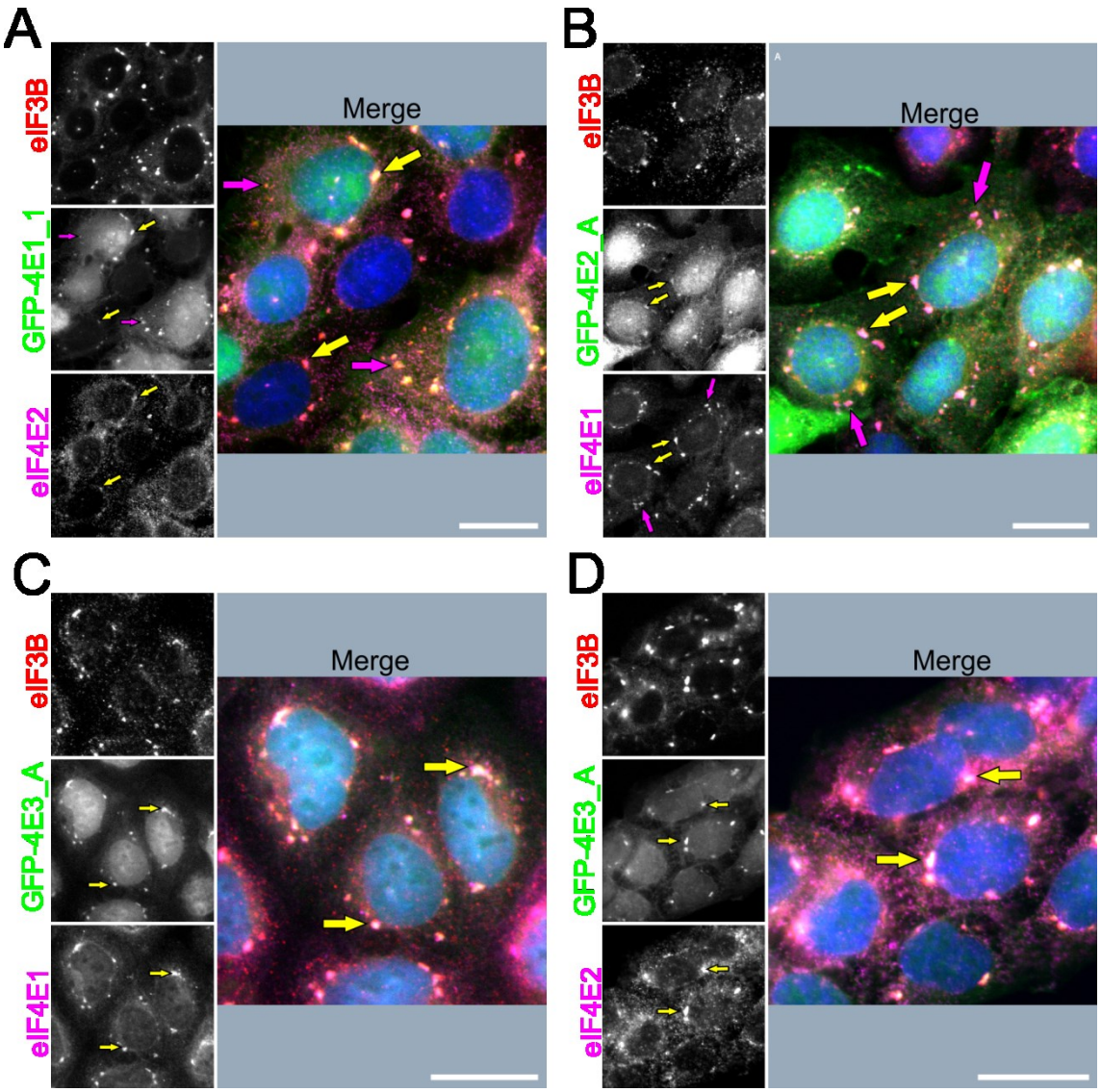

U2OS Flip in based h4E stable cell lines were induced and 24h later stressed with heat for 1h, fixed and probed for the other h4E using antibodies (rabbit anti 4E2 or mouse anti 4E1 and therefore rabbit or mouse eIF3B). Preparations were observed using CellR system, magnification 60x, scale bar, 20 µm. SGs where two h4E co-localize together are pointed with yellow arrows and those where 4E1 is on its own are highlighted with magenta arrows.

Using three independent biological replication of approximately 50 cells under both stress conditions, Pavlína counted manually stress granules, that co-localized with a particular 4E see Fig. 32 and Fig. 33 and I perform a statistical analysis with the data see Statistical analysis.

Fig. 32 eIF4E2 localizes to 75% of SGs while eIF4E3 and eIF4E1 localize to 99% of heat stress-induced SGs

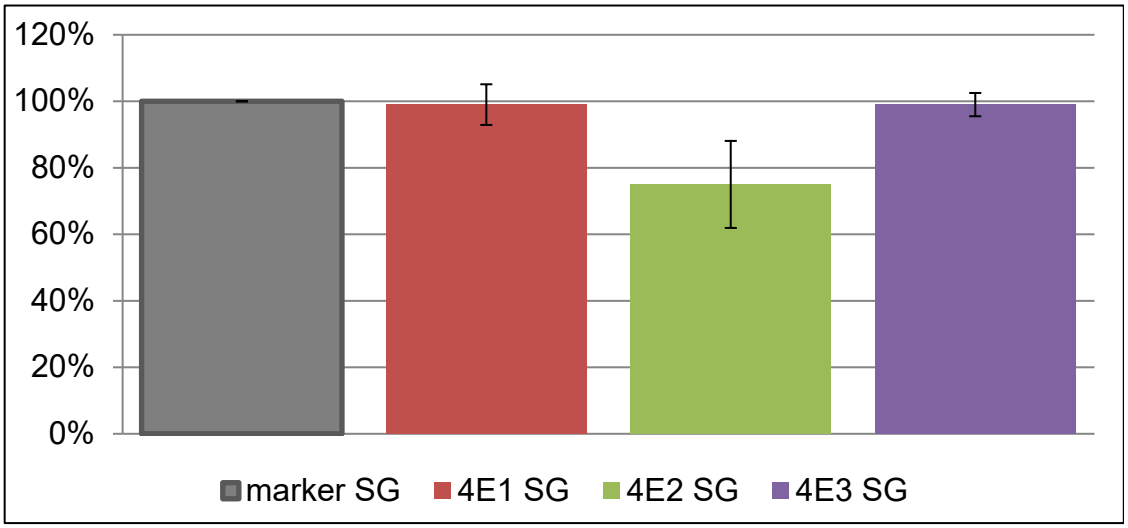

U2OS Flip in based h4E stable cell lines expressing individual h4Es were induced and 24h later stressed with heat for 1h, fixed and probed for the other h4E using antibodies (rabbit anti 4E2 or mouse anti 4E1) and a marker for stress granules. Using three independent biological replications of approximately 50 cells, SGs were quantified. Graph shows medians, error bars stand for standard deviations.

Fig. 33 Only 2% of sodium arsenite induced SGs contain 4E2 while 99% contain 4E3 and 4E1

U2OS Flip in based h4E stable cell lines expressing individual 4Es were induced and 24h later stressed with sodium arsenite for 1h, fixed and probed for the other 4E using antibodies (rabbit anti 4E2 or mouse anti 4E1) and a marker for stress granules. Using three independent biological replications of approximately 50 cells, SGs were quantified. Graph shows medians, error bars stand for standard deviations.

6.2.4.1 Statistical analysis

Using three biological replications of approximately 50 cells, Pavlína counted all the stress granules stained by eIF3B antibody (marker of stress granules) and assessed how many of them contained 4Ex and 4Ey within the same cell (4Ex,y stands for 4E1,2,3) see Table 7. Next, I formulated several statistical hypothesis. Because the data were collected in the same cells, I used two tailed paired Student´s t-test and computed it using online calculator.

https://www.graphpad.com/quickcalcs/ttest1.cfm

1) There are two group of stress granules within a cell in heat stress. 4E1SG and 4E1/2SG. The difference of their numbers is statistically significant at α=1% H_0:

   $\mu_{4E1SG} = \mu_{4E2SG}$

   H_A: $\mu_{4E1SG} \neq \mu_{4E2SG}$

   P<0.0001

   α=1%

   P< α, thus we dismiss the null hypothesis and accept H_A

2) There is no statistically significant difference between the numbers of SGs in cells upon HS, containing 4E3 and those containing 4E1 at α=5%

   H_0: $\mu_{4E1SG} = \mu_{4E3SG}$

   H_A: $\mu_{4E1SG} \neq \mu_{4E3SG}$

   P=0.461

   α=5%

   P>α

   Thus we fail to reject H_0 .

3) There are two group of stress granules within a cell in heat stress. 4E3SG and 4E3/2SG. The difference of their numbers is statistically significant at α=1%

   H_0: $\mu_{4E3SG} = \mu_{4E2SG}$

   H_A: $\mu_{4E3SG} \neq \mu_{4E2SG}$

   P<0.0001

   α=1%

   P< α, thus we dismiss the null hypothesis and accept H_A

4) There is no statistically significant difference between the number of SGs containing 4E3 and those containing 4E1 in arsenite stress at α=5%

   H_0: $\mu_{4E1SG} = \mu_{4E3SG}$

H_A: $\mu_{4E1SG} \neq \mu_{4E3SG}$

P= 0.566

α=5%

P> α, thus we fail to dismiss the null hypothesis.

Next, I was considering the possibility that the GFP tag itself could influence the number of SGs that are formed. Due to its size (27 kDa) which is bigger that the size of 4E1 itself (24 kDa) and due to all sorts of protein-protein interactions that takes place in the stress granules, I assumed the number of SGs, where the exogenous protein localize could be both higher (due to protein-protein interactions) or lower (due to slower kinetics caused by higher protein size) than the number of SGs containing its endogenous counterpart. Thus we tested 4E1 protein in both heat stress and arsenite stress conditions and 4E2 protein in heat stress conditions. Since the data were not acquired from the same cells, I used two tailed, two sample student t- test. Indeed, there is statistically significant difference in the number of stress granules co-localizing with endogenous and those co-localizing with transiently expressed 4E1 in both the stress conditions and strangely, there is not in the case of 4E2.

Heat stress:

$H_{0:}$ $\mu_{4E1SG\ exo} = \mu_{4E1Sgendo}$

H_A: $\mu_{4E1SGexo} \neq \mu_{4E1SGendo}$

P=0.04754

α=5%

P< α, thus we dismiss the null hypothesis and accept H_A.

$H_{0:}$ $\mu_{4E2SGexo} = \mu_{4E2Sgendo}$

H_A: $\mu_{4E2SGexo} \neq \mu_{4E2SGendo}$

P=0.22

α=5%

P>α Thus we fail to reject H_0

Arsenite stress:

$H_{0:}$ $\mu_{4E1SGexo} = \mu_{4E1Sgendo}$

H_A: $\mu_{4E1SGexo} \neq \mu_{4E1SGendo}$

P=0.0006

α=1%

P< α, thus we thus we dismiss the null hypothesis and accept H_A

It seemed to me, that mouse eIF3B antibody was performing better than the rabbit one and I was afraid it might detect more stress granules and influence the analysis. Thus, I set off to test it. As for the fact, that the data was not acquired in a single cell, I choose two-tailed two sample t-test. The difference between the numbers of SGs detected via mouse eIF3B and those detected via rabbit eIF3B is not statistically significant.

https://www.socscistatistics.com/tests/studentttest/Default2.aspx

5) H_0: $\mu_{3BMSG} = \mu_{3BRbSG}$

H_A: $\mu_{3BMSG} \neq \mu_{3BRbSG}$

P=0.41

α=5%

P>α Thus we fail dismiss H_0.

Table 7 Total numbers of stress granules related to the statistical analysis

	No. SGs Heat stress	No. SGs Arsenite stress
eIF4E1 eIF4E2	3080	-
	2302	-
eIF4E1 eIF4E3	1022	1857
	1036	1803
eIF4E2 eIF4E3	727	-
	1090	-
Mouse 3B	2896	-
Rabbit 3B	2498	-
GFP-4E1	1687	1267
4E1 endo	1455	1655
GFP-4E2	1060	-
4E2 endo	1191	-

Table four summarizes numbers of stress granules per protein in all the three biological replicates. Data, which are paired in the analysis share a column. The total of 11 884 SGs in 1391 cells in both the stresses were analysed.

To conclude, in arsenite stress virtually all the SGs contain both 4E1 and 4E3 proteins while only 2% of them co-localize with 4E2. Under the condition of heat stress, there are two types of granules in a cell. One type that contains 4E1 and 4E3, I call them 4E1/3 SGs (25%) and the majority that contains all the three 4Es, so called 4E2 SGs (75%). This result is statistically significant at the probability level greater than 99% in comparison with both 4E1 and 4E3. Next, I have found out that the GFP tag itself influences the localization of 4E1 to the stress granules in both the stress conditions but we cannot conclude the same about 4E2 and the quick look into Table 7 reveals that there is indeed bigger difference in the 4E1 SG numbers than is in the case of 4E2. I can

conclude that there is no significant difference in the numbers of SGs detected by rabbit and mouse antibody against eIF3B in heat stress.

6.2.5 Differences in protein composition between stress granules induced by arsenite and heat stresses

eIF4E transporter (4E-T) is a published interaction partner of both eIF4E1 and eIF4E2. Via an interaction with 4E-T, 4E2 is transported to PBs (Kubacka et al. 2013). I was therefore naturally curious about 4E-T´s ability to potentially transport 4E2 to SGs as well. I therefore tested, whether 4E2 immunoprecipitates 4E-T in my hands. Fig. 34 clearly shows robust interaction between GFP-4E2 and HA-4E-T (gift from Nahum Sonenberg).

Fig. 34 eIF4E transporter interacts with 4E2 in my hands

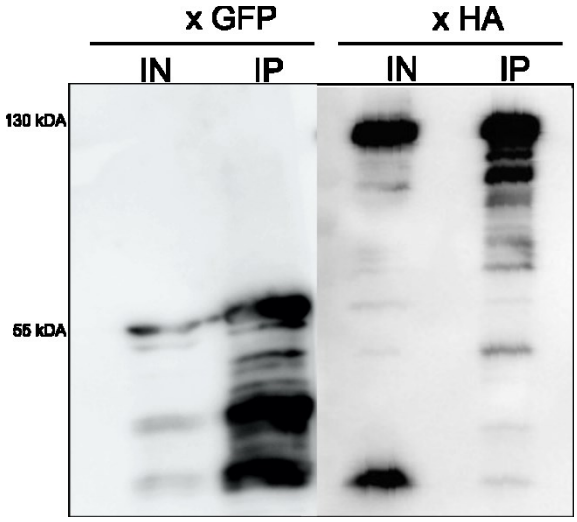

A GFP trap immunoprecipitation was performed in HEK based cell line stably expressing GFP-4E2 (54kDA), transfected by HA-4E-T (110kDA). IN stands for input, IP for immunoprecipitation.

Next, I wondered, whether eIF4E2 co-localize with 4E-T in the stress granules. U2OS.FRT cell line was transfected with HA-4E-T, stressed with heat and probed for endogenous eIF4E1 and eIF4E2. Interestingly, 4E-T was detected in stress granules co-localizing with both the assayed proteins see Fig. 35.

Fig. 35 In heat stressed cells both eIF4E1 and eIF4E2 co-localize in SGs with eIF4E-T

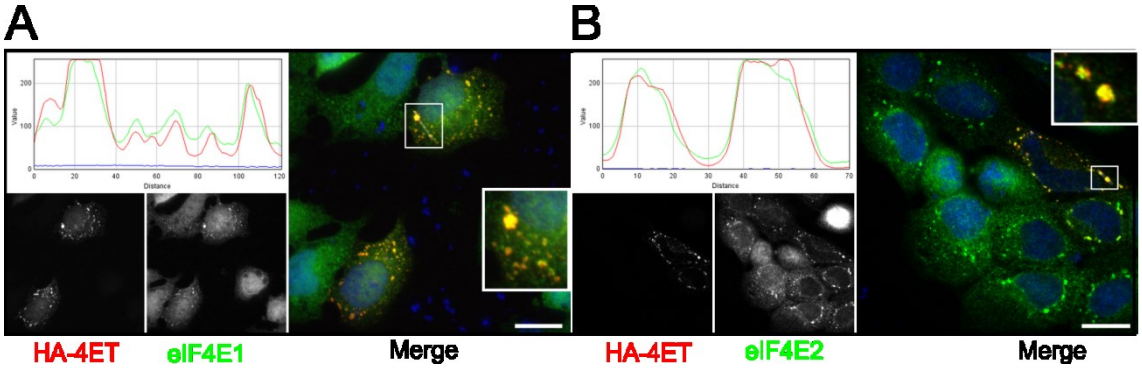

U2OS.FRT cells were transfected with HA-4E-T, heat stressed, fixed and probed with anti HA and 4E1 (A) and anti HA and 4E2 (B). Preparation were observed using Cell R system, scale bar represents 20 µm.

Last, I wanted to know, whether 4E-T becomes a part of SGs in arsenite stress as well. U2OS cell line transfected with GFP-4E1 was therefore probed with antibody against 4E-T (gift from Nahum Sonenberg). Fig. 36 showed that, 4E-T does not localize to SGs induced by arsenite stress.

Fig. 36 Upon arsenite stress eIF4E transporter does not localize to SGs

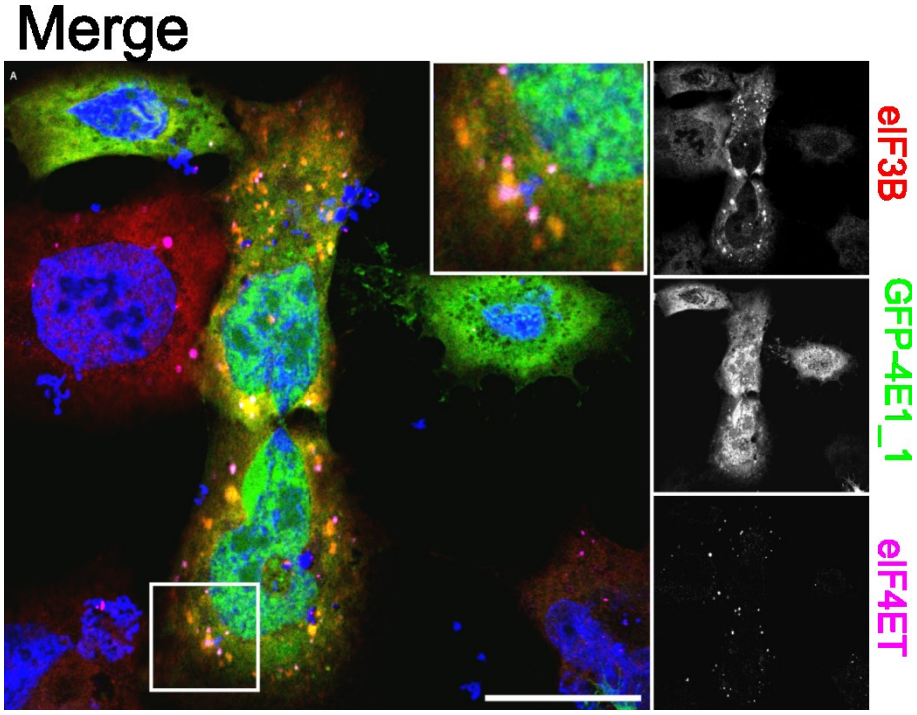

U2OS cells were transfected with GFP-4E1_1, stressed with sodium arsenite, fixed and probed with mouse eIF3B antibody (SG marker) and rabbit eIF4E-T antibody. Observed using Leica SP6 confocal microscope, scale bar stands for 20 µm.

Another SG member specific for heat stress was found by coincidence by Jana Kráčmarová who first noticed that in U2OS.FRT stable cell line, DDX6 becomes a part of SG in heat but not arsenite stressed cells, see Fig. 37.

Fig. 37 In U2OS.FRT based stable cell lines DDX6 becomes a part of SGs upon heat stress only

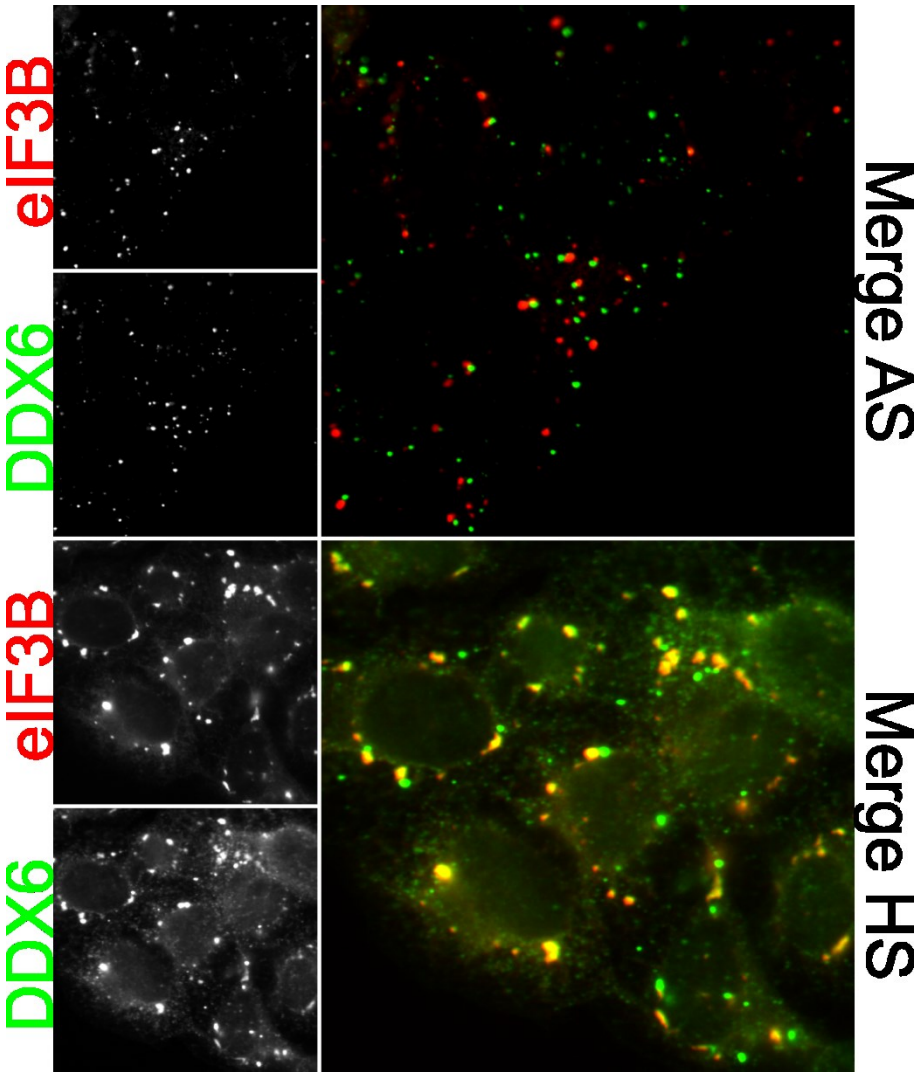

U2OS.FRT stably expressing GFP-4E1_1 were arsenite or heat stressed and simultaneously probed with antibodies detecting DDX6 (PB marker) and mouse eIF3B (SGs marker). Images were captured using CellR system. Strikingly enough, in heat stressed cells DDX6 became a part of stress granules.

We wanted to make sure, this phenomenon is not limited to the U2OS.FRT cell line. We have found out that in severely stressed U2OS cell line , DDX6 localized to SGs as well, see Fig. 38.

Fig. 38 In U2OS DDX6 becomes a part of SGs after a severe heat stress

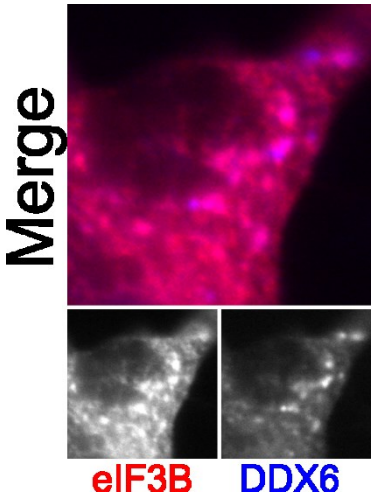

U2OS cell line was heat stressed for 49 °C (thermoblock temperature) for 1 hour and probed with antibodies detecting DDX6 (PB marker) and mouse eIF3B (SGs marker). Images were captured using CellR system.

Next we looked for the triggering temperature of DDX6 localization to SGs in GFP-4E2 stably expressing cell line. Indeed, when I heated the cells to 46 °C for 1 hour, I was able to observe distinct PBs and SGs but upon higher temperatures, DDX6 readily localized to SGs, see Fig. 39.

Fig. 39 In GFP-4E2 stable expressing cell line, DDX6 engages to SGs under the temperatures above 47 °C

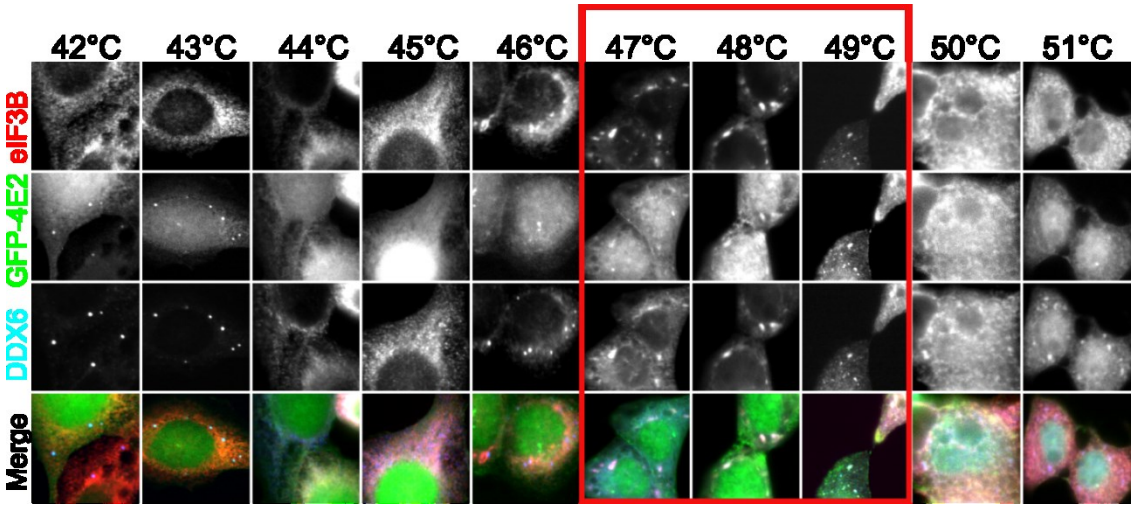

GFP-4E2 stably expressing cell line was heated on the pre-heated thermoblock for 1h, the corresponding temperatures are indicated above each panel. Cells were fixed, probed with antibodies and observed using CellR system.

Recently, Dr. Václav Vopálenský prepared HEK cells lacking 4E2 gene (clone J9-24, chromosome 1 deletion 16780-17099, chromosome 2 16780-16817) using CRISPR-CAS9 technology as a first man in our laboratory. I was curious whether the deletion will have deleterious effect on the formation of SGs and PBs. Fig. 40 nicely showed

that PBs and SGs form normally in these cells. Thus we can conclude, 4E2 is not functionally important for assembly of SGs and PBs.

Fig. 40 Cells with deletion of 4E2 gene assembles both SGs and PBs

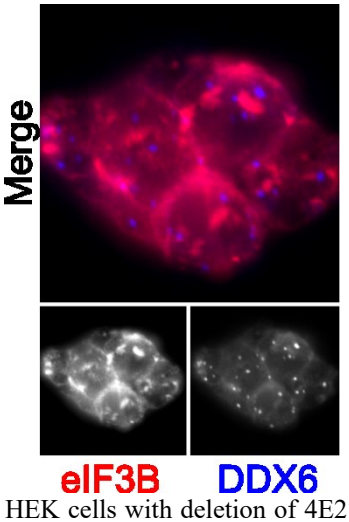

HEK cells with deletion of 4E2 gene, prepared by Dr. Václav Vopálenský, were heat stressed for 47 °C, 1h, fixed, stained with antibodies and observed using CellR system.

To evaluate kinetics of heat and arsenite stress-induced SGs, I applied cycloheximide on the stressed cells and compared its effect with the effect of recovery phase of the same length.

Fig. **41** panel B shows that heat stress-induced SGs disassembly rate is slower than the disassembly rate of arsenite stress-induced SGs. Precise quantification would be necessary for drawing any conclusions from this experiment.

Fig. 41 Upon cycloheximide treatment SGs provoked by HS and AS display different kinetics

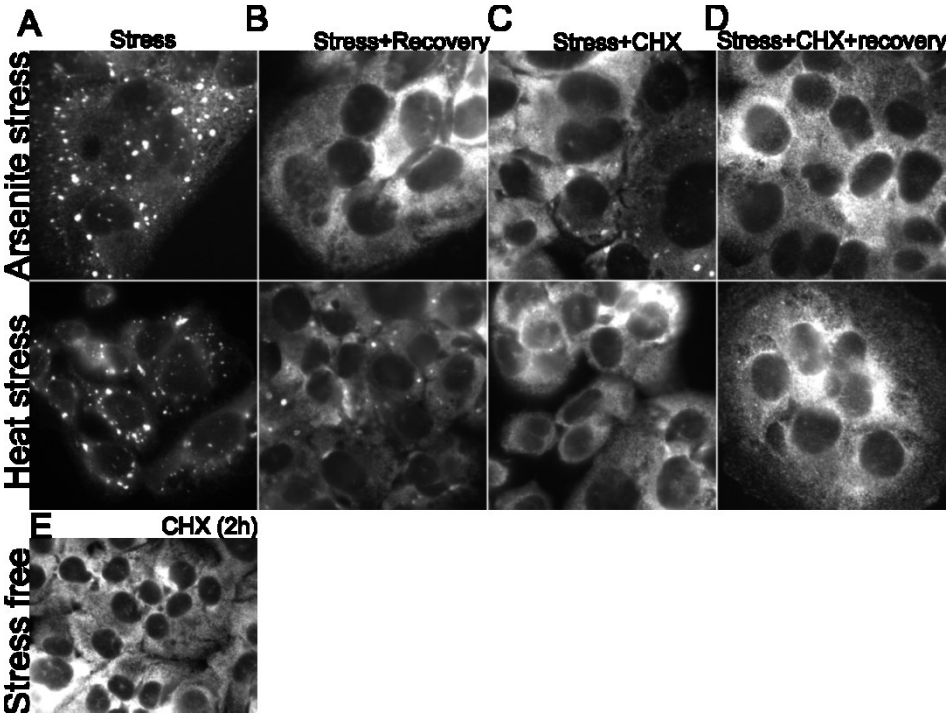

U2OS.FRT stably expressing GFP-4E1_1 were arsenite or heat stressed for 1hour (A), then either the medium was changed and a recovery phase of 1h was applied (B) or the medium was changed for the cycloheximide (10 μg/ml) containing medium for 1 hour (C, D). Next the cells were fixed (B,C) or an additional recovery phase was applied to the cells (D). E is a control that cycloheximide itself does not provoke SG assembly. In the end of each treatment, cells were fixed a probed with anti eIF3B antibody raised in mouse (SG marker) and captured using CellR system.

Compare

Fig. 41B arsenite and heat stress conditions. In heat stress, there are some SGs left after the stress followed by the recovery not in arsenite stress conditions. Thus, the kinetic of disassembly of arsenite stress provoked SGs is likely to be faster.

Next, I wanted to analyze the protein composition of AS and HS SGs. And possibly, I wanted to see if a particular protein is specifically recruited to 4E2 SGs. So I selected 11 antibodies and a construct (GFP-AGO-2) that might be of interest in relation with stress granules. Among this selection, there were proteins active in translation such as members of 4F complex eIF3E, eIF3H, 4GI, 4GIII, PABP and ribosomal proteins S5 and L22 and those active rather in the inhibition of translation, such as active player in ARE-mediated decay ELAV like RNA binding protein (HUR), de-capping mRNA 1a (DCP-1a), PB-specific DEAD-box helicase (DDX6), 4E-T, competitive inhibitor of 4G binding to 4E1, 4E-BP1 and a member of the RNA induced silencing complex argonaute RISC catalytic component 2 (AGO-2). Pavlína took GFP-4E1 and GFP-4E2 expressing stable cell lines, stressed them by both heat and arsenite stress and stained them for eIF3B (SG marker) and all the selected antibodies one by one, see Fig. 42 and Fig. 43 . Largely accepted fact by the scientific community is that the large ribosomal subunit is not present in the stress granules. Thus we found it interesting that large ribosomal protein subunit L22 localized specifically to arsenite but not heat stress-induced SGs. On the contrary, heat stress-induced stress granules in Pavlína´s hands became enriched with several P-bodies' member proteins such as DDX6, DCP-1a and AGO-2, see Fig. 42.

Fig. 42 Different composition of arsenite and heat stress-induced 4E1 SGs

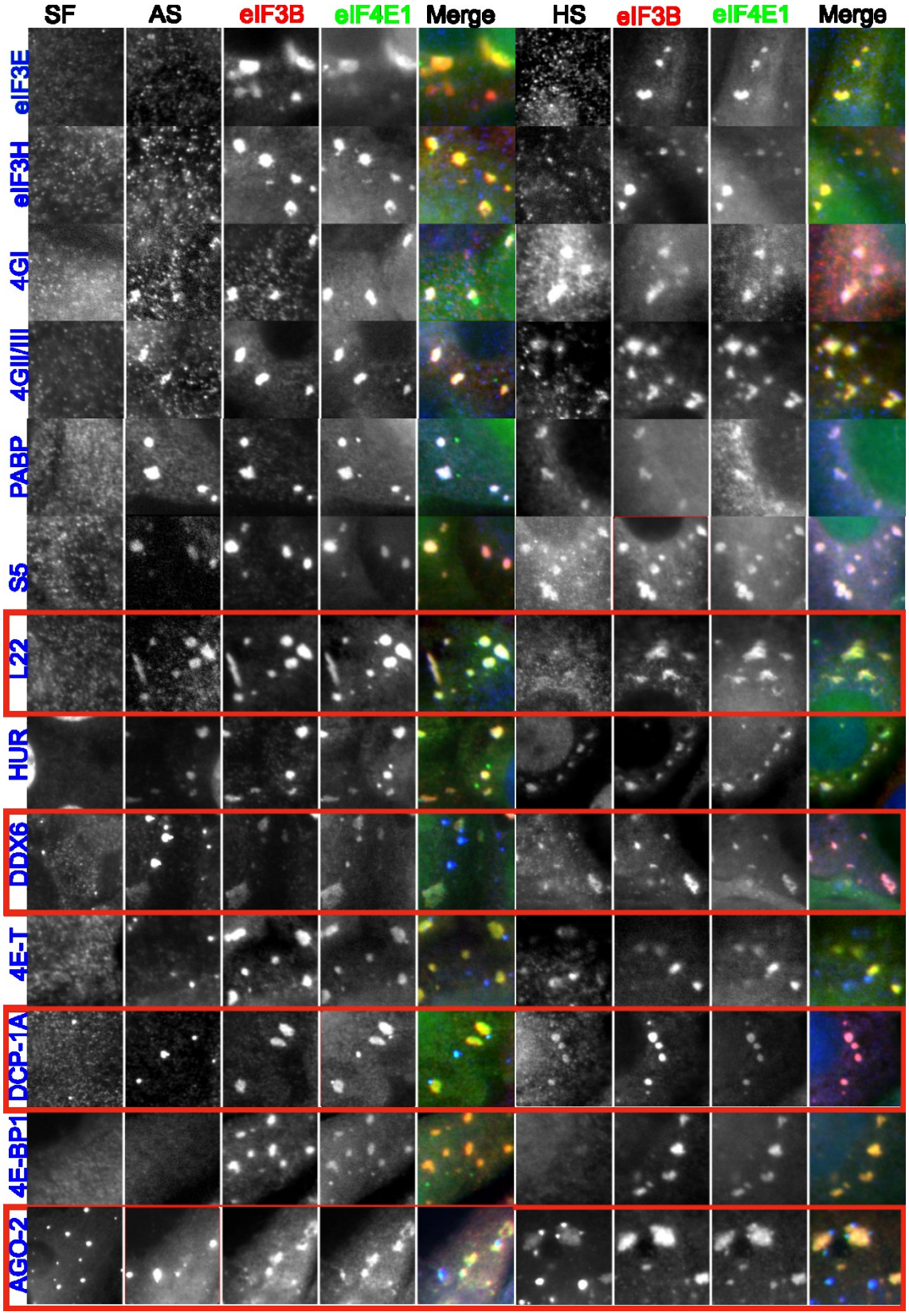

U2OS.FRT stably expressing GFP-4E1_1 were arsenite or heat stressed for 1hour. Cells were fixed and probed with anti eIF3B antibody raised in a mouse or a rabbit (SG marker) and individual proteins and captured using CellR system. Proteins that localized differentially in heat and arsenite stresses are highlighted in red rectangle. Following proteins localized to SGs under both arsenite and heat stress

conditions: 4GI, 4GIII, PABP, S5, HUR. L22 is recruited to SGs arsenite stress specifically. On the contrary, in heat stress, L22 no longer forms SGs, while DDX6, DCP1A, AGO-2 readily localize to SGs.

Fig. 43 Different composition of arsenite and heat stress-induced 4E2 SGs

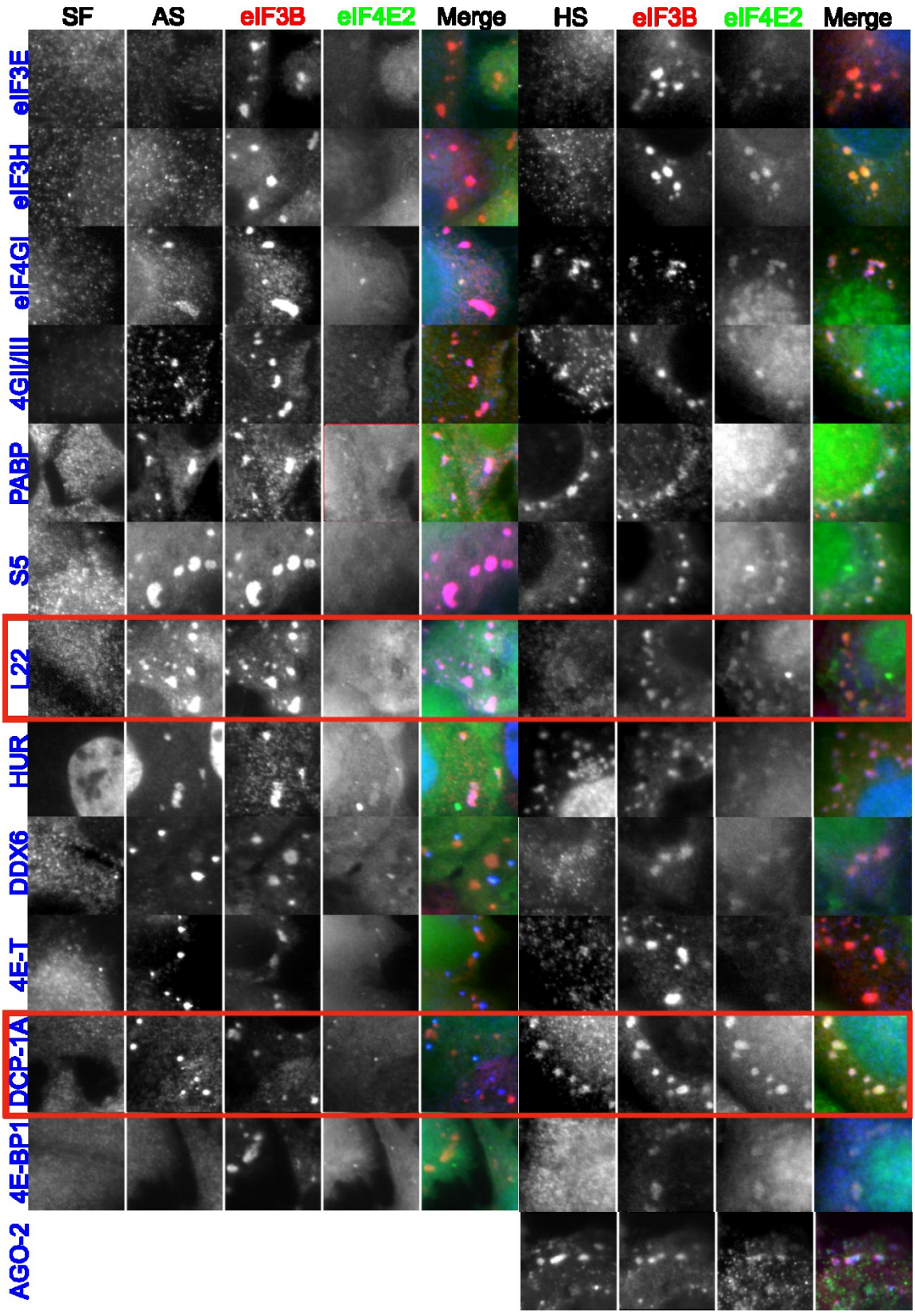

U2OS.FRT stably expressing GFP-4E2 were arsenite or heat stressed for 1hour. Cells were fixed and probed with anti eIF3B antibody raised in a mouse or a rabbit (SG marker) and individual proteins and captured using CellR system. Proteins that localized differentially in heat and arsenite stresses are highlighted in red rectangle. Following proteins localized to SGs in both arsenite and heat stress conditions: 4GI, 4GIII, PABP, S5, HUR. L22 was recruited to SGs induced by arsenite stress. On the contrary, in heat stress, L22 no longer forms SGs, DCP1A, AGO-2 readily localized to SGs.

6.3 The cellular role of 4E2

During my post gradual studies a number of publications emerged unravelling the cellular role of eIF4E2 as a translating cap-binding protein mainly in hypoxic conditions (Uniacke et al. 2012; Ho et al. 2016) and as an inhibitor of translation in normal conditions in mouse and human (Morita et al. 2012; Tao and Gao 2015). Human translation initiation factor that had been rather neglected for almost a decade suddenly became a rock star of the translation initiation research. Nevertheless, we aimed to look at the cellular role of 4E2 in general, above all in stress-free conditions. This very ambitious goal splits the data of this section into two main lineages. First lineage deals with preparation of stable cell lines and experiments with both overexpressed and endogenous protein in human cells. And the second is focused on cloning eIF42 into glutathione S-transferase (GST) fusion and its production in bacteria followed by experiments with a recombinant protein.

6.3.1 Stable cell line generation and characterization

For the development of stable cell lines, we used HEK293 base T-Rex Flip In system. pFRT.TO plasmid carrying GFP-4E1_1, GFP-4E2_A and GFP-4E3_A were kindly prepared by Dr. Tomáš Mašek. I optimized the transfection by Lipofectamine 2000 (LPF). Upon tested combination see Table 8, the best results were given by the combination I.

Table 8 Tested combinations for effective transfection for stable cell lines generation

Combination	R: I	I: LPF	Transfection mix	Outcome
I.	9:1	1:1	4,5µg R+0.5µg I+10µl LPF	Colonies
II.	9:1	1:4	2,25µg R+0.25µg I+10µl LPF	No colonies
III.	15:1	1:1	4,7µg R+0.3µg I+10µl LPF	Colonies
IV.	15:1	1:4	2,3µg R+0.15µg I+10µl LPF	No colonies

The experiment was performed on a six well plate, insert DNA was diluted to 300 ng/µl. First colonies appeared on a day 12 post transfection. R stands for recombinase plasmid (pOG44), I strands for insert carrying plasmid pFRT.TO::GFP-4E2_A and LPF is an abbreviation of Lipofectamine 2000. Controls included not transfected cells (growth control) and mock transfection with pEGFP in the same LPF:pEGFP ratio.

I performed the transfection of all the three cell lines (GFP-4E1_1, GFP_4E2_A and GFP-4E3_A) and then we alter with Dr. Veronica Venturi and Mgr. Silvia Mrvová with change of the media an each of us took care of clones of her particular cell line. Two months later, I ended up having 6 individual clones expressing GFP-4E2_A and due to the space restrictions on the freezing tubes, I named them HAF (to honour my husband Honza Frydrýšek) and 6 individual clones expressing GFP-4E3_A, were named TAK to pay tribute to my sister, Tereza Kazdová. I verified their functionality by western blot and microscopy, see Fig. 44 and Fig. 45. HAF5 and TAK4 were chosen for further experimentations .

Fig. 44 Production of GFP tagged 4E2 and 4E3_A in HEK T-Rex Flip in based stable cell lines

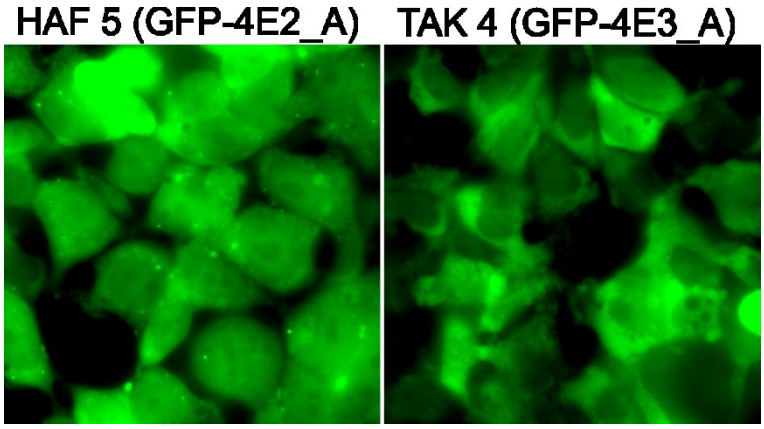

Clones HAF5 and TAK4 were seeded on a dish with glass bottom, induced with 1µg/ml of tetracycline and observed 48h later using CellR system with 60x magnification objective.

Fig. 45 Functionality of HEK based stable cell lines producing eIF4Es was verified via western blot

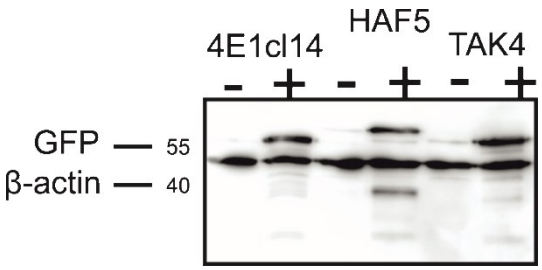

Clones producing GFP-4E1_1 (4E1 clone14), GFP-4E2_A (HAF5), GFP-4E3_A (TAK4) were cultivated on a six well plate, induced (+) with 1µg/ml of tetracycline or uninduced (-) and lysed 48h later using the loading buffer only. Western blot was simultaneously probed with two mouse antibodies anti GFP and anti β-actin. Minor slippage-through the promoter can be observed in uninduced lanes.

6.3.2 Immunoprecipitation using GFP trap system followed by mass spectrometry

Initially, I was focusing on immunoprecipitation using 4E2 antibodies. Upon 7 tested antibodies, only two were found to be of the immunoprecipitation quality (Aviva and GTX82524). I also performed several qPCRs and optimized several primer sets for detection of some homeobox gene´s mRNAs and some housekeeping genes mRNAs. The goal was to understand what kind of mRNAs are being pulled down by 4E2.

Using GTX82524 for IP, I run my first LC-MS/MS analysis at the faculty service. This analysis has not ended up well, sample was full of keratins and tubulins, the only potential hit was Ras-related protein Raichu. Next, I switched to GFP trap system, brought to the laboratory by Dr. Martin Pospíšek. It had been optimized before by my colleague Dr. Veronica Venturi and I tried Faculty MS service for the second time, again I got Raichu and a few bacterial proteins.

Nevertheless, thanks to my mentor´s acquaintances and substantial financial support, we were able to finally run LC-MS analysis at the EMBL core facility (Fig. 46). And the results we got, were excitingly different. The analysis was run on two immunoprecipitations, one was performed in empty HEK293 cells (control IP) and the other in Hek based GFP-4E2 expressing stable cell line (experiment). The total of 1466 hits returned, out of which 205 protein were specific for the experiment and 671 hits were overlapping with the control, but the enrichment was greater than 2x. The rest was omitted. First step of data analysis was a search for already published hits, see **Table 9** Next, in the attempt to distinguish more relevant hits from the least relevant, I counted Score X with all the hits. For the summary of top ten hits using service ranking and score X ranking, see Table 10 and Table 11.

$$\text{Score X} = \frac{No.peptides\ in\ the\ experiment}{MW\ of\ the\ hit} \times \frac{1}{No.peptides\ in\ the\ control}$$

Then, I applied several bioinformatics tools to link genes active in the particular pathway together e.g. Gorilla, Vanderbilt, David and Kegg mapping tools. Last, I tried to dig more into the individual complex´s members using Genecards and Pubmed.

Fig. 46 GFP-4E2 immunoprecipitation that was sent for LC/MS Orbitrap analysis in EMBL

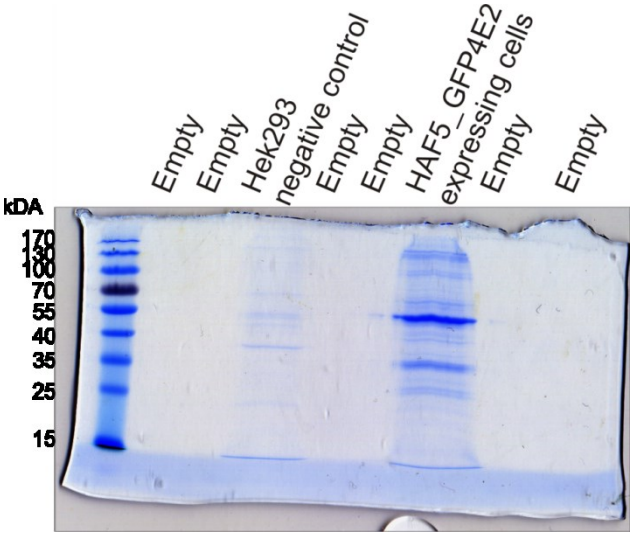

2x 100mm dish of fully confluent HEK293 and HAF5 (GFP-4E2 expressing cell line, 54 kDa), were induced for 48h by 1 µg/ml of tetracycline and GFP trap was performed according to protocol (Methods).

Table 9 List of published 4E2 interaction partners found or not in the mass spectrometry analysis

Protein	Exp	Ctr	Process	Organism	Publication
eIF4GI	18	10	Translation	Mouse	(Rom et al. 1998)
eIF4GIII	9	0	Translation hypoxia	Human	(Ho et al. 2016)
eIF4E-BP1	0	3	Inhibition of translation	Mouse	(Joshi et al. 2004)
eIF4E-BP2	4	0	Inhibition of translation	Mouse	(Joshi et al. 2004)
HHARI	5	0	Ub mediated degradation of 4E2	Human	(Tan et al. 2003)
PREP-1	0	0	Inhibition of translation	Mouse	(Villaescusa et al. 2009)
GIGYF-1	62	0	Unknown	Mouse♣	(Morita et al. 2012)
GIGYF-2	152	3	Inhibition of translation	Mouse♣	(Morita et al. 2012)
ZNF598	44	2	Inhibition of translation	Mouse♣	(Morita et al. 2012)
RBM4	5	2	Translation	Human	(Uniacke et al. 2012)
HIF2 α	0	0	Translation	Human	(Uniacke et al. 2012)
eIF4E-T	52	0	Transport to PBs	Human	(Morita et al. 2012; Kubacka et al. 2013)
eIF4G3	9	0	Translation	Human	(Ho et al. 2016)

Table shows all the known interaction partners of eIF4E2 at the time of the analysis, column headings „Exp.“ stands for the number of peptides in the experiment, „Ctr“. stands for number of peptides in the control IP. ♣ The interaction was found in human cell line, but the mechanism was studied in the mouse.

Table 10 List of top ten hits using service ranking

	Gene	Exp.	Ctrl.	Cellular process
1	eIF4E2	288	10	Translation inhibition and initiation
2	GIGYF1	62	0	Insulin-like growth factor signalling
3	eIF4E-T	52	0	Transport to PBs
4	IRS4	51	0	Insulin-like growth factor signalling
5	HSPA2	21	0	Insulin-like growth factor signalling
6	TARS	19	0	Calmodulin binding
7	PRRC2B	18	0	Poly(A)RNA binding
8	CUL7	17	0	Ubiquitin pathway
9	ACTN4	15	0	Actin binding
10	PATL1	15	0	Nucleic acid binding, PBs

Table shows top ten MS hits using EMBL service ranking. The abbreviations „Exp.“ stands for the number of peptides in the GFP-4E2 immunoprecipitation, „Ctr“. stands for number of peptides in the control IP from empty HEK293 cells.

Table 11 List of top ten hits using Score X ranking

	Gene	Exp.	Ctrl.	Cellular process
1	GIGYF1	62	0	Insulin-like growth factor signalling
2	eIF4E2	288	10	Translation inhibition and initiation
3	eIF4E-T	52	0	Transport to PBs
4	IRS4	51	0	Insulin-like growth factor signalling
5	GIGYF2	152	3	Translation inhibition
6	eIF4E-BP2	4	0	Translation inhibition
7	HSPA2	21	0	Insulin-like growth factor signalling
8	KRT19	13	0	Keratin
9	SNAP23	4	0	Vesicle transport-Insulin-like growth factor signalling
10	SSBP1	4	0	Nucleic acid binding

Table shows top ten MS hits using Score X ranking. The abbreviations „Exp.“ stands for the number of peptides in the GFP-4E2 immunoprecipitation, „Ctr“. stands for number of peptides in the control IP from empty HEK293 cells.

6.3.3 Mass spectrometry data analysis

6.3.3.1 The insulin-like growth factor signalling pathway

The IGF signalling plays a key role in the growth and development of many tissues. The insulin like growth factor I receptor (IGF-IR) is a receptor tyrosine kinase that serves as a positive regulator of the system. The level of IGF-I in serum plays important role in neurodevelopment during childhood and puberty and in neuronal survival throughout the whole life. Stimulatory ligands IGF-I and IGF-II results in IGF-IR signalling with proliferative and anti-apoptotic effect. Deregulation of the system is involved in the development of resistance to various anticancer therapies.

Altogether, there are three ligands: IGF-I, II and insulin. These ligands interact with four receptors: IGF-IR, IGF-IIR, insulin receptor and a hybrid receptor of IGF and

insulin. The IGF system also consists of six binding proteins (**IGF-BPs**) that regulate ligand bioavailability. They can prolong the half-lives of IGFs and also compete with receptor for the free IGFs. Binding of the ligands induce conformational changes of the IGF-IR and activation of intrinsic tyrosine kinase activity. Once phosphorylated, the intracellular portion of IGF-IR serve as docking site for substrates such as insulin receptor substrate **IRS**1-**4** and src homology and collagen (SHC). These substrates initiates phosphorylation cascade that transmit the IGF-IR signal. Phosphorylated IRS-I activate phosphatidylinositol 3´kinase leading to activation of kinase B/Akt among others. Kinase B/Act enhances protein synthesis via mammalian target of rapamycin (mTOR) (Ryan and Goss 2008). For the mass spectrometry (MS) hits related to this pathway see Table 12.

Table 12 Summary of all the hits that were successfully mapped back to the insulin-like growth factor pathway

Gene	**Full name**	**Exp.**	**Ctr.**	**Role in the pathway**	Citation
IRS4	Insulin receptor substrate 4	51	0	Located on the plasma membrane-signal transduction.	(Ryan and Goss 2008)
IGF2BP3	Insulin-like growth factor 2 mRNA-binding protein 3	31	9	Regulates ligand bioavailability.	(Ryan and Goss 2008)
IGF2BP1	Insulin-like growth factor 2 mRNA-binding protein 1	35	17	Regulates ligand bioavailability.	(Ryan and Goss 2008)
IGF2BP2	Insulin-like growth factor 2 mRNA-binding protein 2	24	12	Regulates ligand bioavailability.	(Ryan and Goss 2008)
HSPA2	Heat shock-related 70.00 protein 2	21	0	High level protect cell from development of the insulin resistance.	(Chichester et al. 2015)
SNAP23	Synaptosome associated protein 23	4	0	Transport of GLUT4 containing vesicles upon insulin stimulus.	(Widberg et al. 2003)
GIGYF1	GRB10 Interacting GYF Protein 1	62	0	Binds to GRB10 and to IGF-1 receptor.	(Giovannone et al. 2003)
CUL7	Cullin-7	17	1	E3 ligase-degradation of IRS.	(Mieulet and Lamb 2008)
ACTN4	Actinin alpha 4	15	1	Control of localization of IRS4 on a cell surface.	(Talior-Volodarsky et al. 2008)
GIGYF2	GRB10 Interacting GYF Protein 2	150	3	Binds to GRB10 and to IGF-1 receptor.	(Giovannone et al. 2009)

6.3.3.2 The eIF3 complex

The eIF3 complex is a highly complex, multi-protein assembly with multiple functions in translation initiation. First of all, it orchestrates formation of the 43S-48S pre-initiation complexes by aiding the Met-tRNAi ^{Met} and mRNA loading on the 40S ribosomal subunit, next, it re-initiates protein synthesis on polycystronic mRNAs and acts as a receptor of protein synthesis kinases. It is also involved in scanning for AUG recognition. The eIF3 also acts as a docking site for mTOR (Hinnebusch 2006). The eIF3 was demonstrated to link translation initiation to transcription (Harel-Sharvit et al. 2010), mRNA export (Bolger et al. 2008) and nonsense mediated decay (Isken et al. 2008). Last but not least, the eIF3 is involved in translation termination and ribosome recycling (Pisarev et al. 2007).

De-regulation of expression of several subunits has been implicated in oncogenesis and maintenance of the cancerous state (Spilka et al. 2013). Structure of the human eIF3 displays anthropomorphic features with subunit C in a head position, A resembles left arm, F,H,M form left leg, K and L form right leg and finally E, D form right arm (Querol-Audi et al. 2013). Masutani et al. (2007) showed that the functional core of the eIF3 complex, capable to recruit 40S subunit to the mRNA, comprises of A,B,C,E,F,H . eIF3 complex consists of three stable modules: i) A,B,G,I ii) C,D,E,K,L and iii) F,H,M. C subunit is proposed to link modules i and iii by simultaneous binding of B,H (Zhou et al. 2008). All 13 subunits of eIF3 have been found in the MS Table 13.

Table 13 All 13 members of the human eIF3 complex have been successfully detected in a mass spectrometry analysis

Gene	Exp	Ctrl	Role in the complex	Citation
eIF3A	51	6	Interacts with eIF1 and eIF1a; Thought to dictate assembly of the complex; Part of the minimal sub complex essential for translation initiation in cells.	(Querol-Audi et al. 2013; Wagner et al. 2014; Smith et al. 2016)
eIF3C	42	9	Interact with eIF1 and eIF1a; Interacts with eIF4GI; Thought to dictate assembly of the complex; Part of the minimal sub complex essential for translation initiation in cells.	(Querol-Audi et al. 2013; Villa et al. 2013; Wagner et al. 2014; Smith et al. 2016)
eIF3B	33	6	Part of the minimal sub complex essential for translation initiation in cells.	(Smith et al. 2016)
eIF3I	28	7	Part of the minimal sub complex essential for translation initiation in cells.	(Smith et al. 2016)
eIF3E	20	5	Might recruit specific subset of mRNA in stress conditions; Interacts with eIF4GI; Thought to be dispensable for assembly of the complex.	(Hinnebusch 2006; Villa et al. 2013; Smith et al. 2016)

eIF3L	20	4	Requires K and H for the self-assembly to the complex.	(Smith et al. 2016)
eIF3D	16	4	Might recruit specific subset of mRNA in stress conditions; Interacts with eIF4GI; deletion is lethal in *N. crassa.*	(Hinnebusch 2006; Villa et al. 2013; Smith et al. 2016)
eIF3H	10	0	In *N. crassa* enhances translation initiation, contingent on H, K and L assembles to the complex.	(Smith et al. 2016)
eIF3F	9	4	Minimal sub complex essential for translation initiation in cells.	(Smith et al. 2016)
eIF3M	7	0	Minimal sub complex essential for translation initiation in cells.	(Smith et al. 2016)
eIF3G	7	0	Minimal sub complex essential for translation initiation in cells.	(Smith et al. 2016)
eIF3K	3	0	Requires L and H for the self-assembly to the complex.	(Smith et al. 2016)
eIF3J	2	0	40S ribosome biogenesis, promotes binding of eIF3 to 40S; Promotes ribosome recycling; Mediates mRNA interactions; Loosely associated with the rest of the complex.	(Hinnebusch 2006; Pisarev et al. 2007; Querol-Audi et al. 2013; Wagner et al. 2014)

6.3.3.3 The FMR complex

Fragile X mental retardation protein (FMRP) is a RNA binding protein, known to bind 4% of total mRNA in the brain. The identities of the targets are largely unknown, though. FMRP is associated with a subset of mRNAs and control their dendritic localization and local translation. In the case of ***fmr1*** gene, the aberration of the tri-nucleotide repeat CGG in the 5′untranslated region can result in two discrete pathologies. More than 200 CGGG repeats, so called "full mutation" leads to transcriptional silencing and loss of FMRP expression, resulting in fragile X syndrome (FXS). FXS is characterized by mental retardation, autistic-like behaviour and anxiety.

On the other hand, the fragile X-associated tremor/ataxia syndrome, characterized by progressive cerebellar gait ataxia (inability to maintain certain positions and coordinate movements) and intention tremor (tremor that occurs upon intentional movement, for example while touching some object). It appears to be a gain of function phenotype, which occurs when CGG expansions is within the range of 55-200 copies, so called "pre-mutation", the likely cause is the toxicity of the aberrant levels of mRNA. Biochemically, FMRP co-sediments with both the polysomes and the mRNPs. It possibly represses translation at multiple steps. For review on FMRP control of neuronal mRNA metabolism see (De Rubeis and Bagni 2010). FMR is known to associate with Fragile X mental retardation syndrome-related protein 1 and 2 (**FXR1, FXR2**). All the three of them are known to form homomers on their own and

heteromers with the others, both are likely to play important role in the pathogenesis of Fragile X syndrome (Zhang et al. 1995).

For eIF4E1, FMRP-CYFIP1-4E complex that inhibits translation of several FMRP target mRNAs, has been described (Napoli et al. 2008). I dare to hypothesize similar parallel for 4E2 and GIGYFs might exist, with the MS results of 152/3 for GIGYF-2 and 62/0 for GIGYF-1. List of all the hits that are known to interact with FMRP is shown in the Table 14.

Table 14 Summary of all the hits that were successfully mapped back to the FMR complex

Gene	Full Name	Exp.	Ctrl.	Role in the complex	Citation
FMRP1	Fragile X mental retardation protein 1	3	0	Control of mRNA localization and local translation, above all in the brain. Interacts with FXR1 and FXR2 and RANBP9.	(Zhang et al. 1995; De Rubeis and Bagni 2010)
FXR1	Fragile X mental retardation syndrome-related protein 1	9	0	Export of specific mRNAs from the cell nuclei; Plays a role in the brain and testes development.	(Tamanini et al. 1997; Tamanini et al. 1999)
FXR2	Fragile X mental retardation syndrome-related protein 2	13	2	Export of specific mRNAs from the cell nuclei; Plays a role in the brain and testes development.	(Tamanini et al. 1997; Tamanini et al. 1999)
ATXN2	Ataxin-2	6	0	Associates with FMR in neurons and functions in a long term olfactory habituation and neuronal translation control.	(Zhang et al. 1995; Sudhakaran et al. 2014)
AGO2	Isoform 2 of Protein argonaute-2	7	0	Mammalian FMRP interacts with miR pathway, Ago-2 and Dicer. FMRP and FRX2 containing complexes have dicing activities against dsRNA.	(Nakamoto 2005; Maurin et al. 2014)
DICER-1	Isoform 2 of Endoribonuclease Dicer	6	0	Mammalian FMRP interacts with miR pathway, Ago-2 and Dicer. FMRP and FRX2 containing complexes have dicing activities against dsRNA.	(Nakamoto 2005; Maurin et al. 2014)
NUFIP2	Nuclear FMR1 interacting protein 2	4	0	Regulates nuclear function of FMRP.	(Bardoni et al. 1999)
RANBP9	Ran-binding protein 9	2	0	C-terminal part interacts with FMRP, regulates nucleation of microtubules and affinity of FMRP for its target.	(Menon et al. 2004)

6.3.3.4 The spliceosomal complexes

The spliceosome is a multi-megadalton-big complex that consists of 5 small nuclear ribonucleoprotein particle (snRNP) and a large number of proteins. It catalyses pre-mRNA splicing. In eukaryotes, two types of spliceosome exist: U2 and U12. The U2 spliceosome is assembled from U1, U2, U5 and U4/U6 **snRNP** and a number of **non-snRNP** proteins. Each snRNP consists of snRNA (two in case of U4/U6), **seven Sm proteins** and a number of particle specific proteins. While active in splicing of short introns, not spanning more than 250 nt, spliceosome forms subsequently **E complex-A complex-precatalytic B complex-B activated complex and finally C complex**. When intron exceeds 250 nt, which is the case for most introns of higher eukaryotes, splicing complexes first form across the exon in a process called exon definition. Defined exon is further stabilized by a number of serine arginine proteins **(SR)** proteins. Over 20 proteins involved in splicing were identified in the MS (see Table 15), more than 170 proteins were found associated with the spliceosome. Some of the spliceosome-associated proteins play a critical role in the recognition and pairing of splice sites and structural re-arrangement of the spliceosome ensuring that the reactive sites are properly positioned for catalysis. The kinetic challenge of splicing is met in part by pre-packaging of many spliceosomal proteins in the form of snRNPs (Will and Luhrmann 2011). Using bioinformatics tool Gorilla, supra-spliceosomal complexes (usually 4 spliceosomes connected via pre-mRNA) have been highlighted among hits. Dr. David Staněk, Czech spliceosomal scientist suggested that those hits might more likely point towards mRNA transport than towards splicing itself.

Table 15 Summary of all the MS hits that were linked with the spliceosome

Gene	Full name	Exp.	Ctrl.	Role in the complex	Citation
SRSF7	Serine/arginine-rich splicing factor 7	4	0	SR protein	(Will and Luhrmann 2011)
SRSF9	Serine/arginine-rich splicing factor 9	2	0	SR protein	(Will and Luhrmann 2011)
SRPK1	SR protein kinase 1	4	2	Phosphorylation of SR splicing factor and regulation of splicing.	(Nikolakaki et al. 2001)
SRPK2	SR protein kinase 2	2	0	Phosphorylates hPrp28 thus enabling B-complex formation.	(Will and Luhrmann 2011)
RBMX	RNA binding motif protein X-linked	17	3	Part of hnRNP G, controls alternative splicing of several mRNAs.	(Kanhoush et al. 2010)

HNRNPA2B1	Heterogeneous nuclear ribonucleoproteins A2/B1	36	10	One of the most abundant RNA binding proteins, hnRNP, transport of mRNAs.	(He and Smith 2009)
SFPQ	Splicing factor, proline- and glutamine-rich	3	0	Binds mRNA in a spliceosome C complex.	(Will and Luhrmann 2011)
DDX5	DEAD box helicase 5	18	8	Pre-mRNA binding protein.	(Zonta et al. 2013)
THRAP3	Thyroid hormone receptor-associated protein 3	2	0	Recruited at A complex.	http://spliceosomedb.ucsc.edu/
PRPF8	Pre-mRNA processing factor 8	2	0	Sm protein U5 snRNP, regulates Brr2 (integral spliceosomal helicase) activity to prevent premature unwinding U4/U6.	(Will and Luhrmann 2011)
CPSF6	Cleavage and polyadenylation-specificity factor subunit 6	2	0	CPSF	http://spliceosomedb.ucsc.edu/
CPSF3	Cleavage and polyadenylation specificity factor subunit 3	2	0	CPSF	http://spliceosomedb.ucsc.edu/
CPSF1	Cleavage and polyadenylation specificity factor subunit 1	2	0	CPSF	http://spliceosomedb.ucsc.edu/
HNRNPA0	Heterogeneous nuclear ribonucleoprotein A0	5	2	hnRNP, transport of mRNAs.	(He and Smith 2009)
SART3	SART3 protein	5	0	U4/U6 recycling	(Bell et al. 2002)
LSM3	U6 snRNA-associated Sm-like protein LSm3	2	0	Associates with B complex, tri snRNP.	(Will and Luhrmann 2011)
RBM4	RNA-binding protein 4	5	2	Modulates alternative 5'-splice site and exon selection.	(Lai et al. 2003)

6.3.3.5 The 3´UTR processing and connection to the exosome

The exosome, complex of 3´-5´exonucleases, functions in the accurate processing of nuclear RNA precursors and degradation of RNAs in both the nucleus and the cytoplasm. Therefore exosome has a dual role in total RNA degradation (pre-mRNAs, pre-tRNAs, pre-rRNAs, mRNAs with structural defects and control of expression level of some mRNAs) and the accurate RNA processing (ribosomal RNAs, snoRNAs, snRNAs).

In human cells, the exosome is also recruited to the mRNAs that contains AU rich signals-AREs, those are present in many mRNAs that encode proteins for transient expression such as proto-oncogenes and growth factors. The RNA degradation machinery is ubiquitous, degradation of RNAs in human cells occurs from both the 5′and 3′end. In the nucleus, 3′end exosome mediated degradation seems to be more effective, while in the cytoplasm 5′end has the predominant role.

The eukaryotic exosome comprise of a ring of six proteins with PH domains (phoshorolytic exonucleases), each domain being present in a distinct exosome components: RRP41, RRP46, mRNA transporter protein 3 (MTR3), RRP42, RRP43, RRP45. The eukaryotic exosome also contains Cls4 homologues of two archebacterial proteins **RRP4** and RRP40. together they are referred to as RRP44. **RRP4** displays *in vitro* exonuclease activity. To access the active site of the exosome, the substrate must pass the PH ring, that excludes dsRNA and helicases are very likely to contribute to this action. Exosome on its own has very little RNAse activity, it must be therefore activated either by a specific RNA sequence in the target RNA or it is likely to recognize specific protein-RNA complexes based on specific structural features (Houseley et al. 2006).

It was no surprise for us that in the MS analysis, no component of 5′end RNA degradation pathway was found e.g. 5'-3' Exoribonuclease 1, 2 (XRN1 or XRN2) as we supposed, 4E2 was bound to the cap. Interestingly, a number of 3′UTR RNA binding proteins were found. Table 16, lists all the MS hits related either directly to the exosome complex, or acting as 3′UTR binding proteins.

Table 16 List of MS hits related to the exosome complex or acting as 3′UTR binding partners

Gene	Full name	Exp.	Ctr	Role in the complex	Citation
EXOSC2	Exosome Component 2	2	0	Part of S1 pore structure with S1 and KH RNA binding domains.	(Houseley et al. 2006)
ELAVL2 /HUB	ELAV Like RNA Binding Protein	9	0	GAAA motif, binds its own 3′UTR, FOS and ID mRNA, interacts with IGF2-BP1; binds ARE elements and acts as translational repressor, neuron and germ cell specific.	Genecards and Uniprot, (Chalupnikova et al. 2014)
CIRBP	Cold-inducible RNA-binding protein	3	0	Binds 3′UTR and stabilizes transcripts and increases their translation via 4G interaction.	(Yang et al. 2006)
FXR1	Fragile X mental retardation syndrome-related protein 1	9	0	3′UTR binding, regulates intercellular transport and local translation of mRNA in neurons.	(Mientjes et al. 2004)

RBM4	RNA-binding protein 4	5	2	Binds CU-rich responsive elements in 3´UTR, exerts suppressive activity on cap-dependent translation but enhances IRES, interacts with Ago-2.	(Lin and Tarn 2009)
RC3H1	Isoform 2 of Roquin	2	0	Post-transcriptional repressor of mRNAs containing a conserved stem loop motif, called constitutive decay element (CDE), which is often located in the AU rich 3'-UTR.	(Leppek et al. 2013)
PUM1	Pumilio homolog 1	13	2	Binds to an RNA consensus sequence, the Pumilio Response Element (PRE), 5'-UGUANAUA-3'; Mediates post-transcriptional repression of transcripts via recruitment of the CCR4-POP2-NOT de-adenylase; Or via facilitating miRNA mediated translation inhibition.	(Dong et al. 2011; Miles et al. 2012; Van Etten et al. 2012)
AGO-2	Argonaute RISC Catalytic Component 2	7	0	It is recruited via AU rich region to TNF mRNA and together with FXR1, activates translation; Translational repression via siRNA with complete match with 3´UTRs of mRNAs.	(Vasudevan et al. 2007; Wu et al. 2008)
DIS3L	DIS3 Like Exosome 3'-5' Exoribonuclease	5	0	Cytoplasmic catalytic component of the exosome, with 3´-5´exoribonucelase activity, degrades mRNAs with ARE elements.	(Tomecki et al. 2010)
UPF1	UPF1 RNA helicase and ATPase	15	3	Part of the activating complex for NMD decay (premature termination codon).	(Houseley et al. 2006)

6.3.3.6 The RISC complex

The RNA induced silencing complex (RISC) is a term for a family of heterogeneous molecular complexes that can be programmed to target almost any gene for silencing. RISC programming is turned on by the appearance of dsRNA in the cytoplasm of a eukaryotic cell. dsRNA is subsequently processed into small regulatory RNAs (20-30 nt in length), that guide RISC to complementary RNA targets through base-pairing interactions. RISC can silence target genes via several distinct mechanisms: a) through repression of translation, b) at the transcript level through mRNA degradation, c) on the genome level through formation of heterochromatin and DNA elimination.

Every RISC contains a member of Argonaut protein family to bind to the regulatory RNAs and positioned it in a conformation that facilitates target recognition. Argonauts can either cleave target directly or via other proteins, that Argonaut recruits to the target. Human contains four copies of *ago* genes. For review see (Pratt and MacRae 2009).

The minimal RISC complex requires AGO protein, ribonuclease DICER, dsRNA binding protein (e.g. Mov10 RISC complex RNA helicase, MOV10) and heat shock protein 70.90 kDa (HSP70-90) system (to keep Ago protein in an open conformation while loading si/miRNA) (Meister 2013). In this MS, all the components of the minimal RISC are present, with Heat shock-related 70 kDa protein 2 (**HSPA2**) being among top hits (see Table 17). Moreover, it has been proposed, that so called Lim domain proteins help to stabilize the silenced complex by simultaneously interacting with 5′cap-binding complex, namely eIF4E and AGO proteins. eIF4E co-localize with Lim domain proteins in PBs (James et al. 2010). The results of this analysis let us hypothesize, eIF4E2 might be another protein to connect the cap with this silencing machinery. Moreover, human Ago-1 and Ago-2 have been shown to interact with chromatin modifiers and splicing factors. They affect RNA polymerase II elongation rate via H3K9 methylation, allowing spliceosome assembly (Ameyar-Zazoua et al. 2012).

Table 17 List of MS hits related to the RISC complex

Gene	Full Name	Exp	Ctrl	Role in the complex	Citation
DICER 1	Isoform 2 of endoribonuclease Dicer	6	0	Generates miRNAs from a pre-mRNAs, to be incorporated into RISC.	(Meister 2013)
AGO-2	Argonaute RISC Catalytic Component 2	7	0	AGO protein specific to humans capable of target slicing (mRNA hydrolysis).	(Pratt and MacRae 2009)
RBM4	RNA-binding protein 4	5	2	Co-localizes with Ago-2 in SGs, interacts directly with Ago-2 to supress translation of target mRNAs.	(Lin and Tarn 2009)
TNRC6 A/ GW182	Trinucleotide Repeat Containing Adaptor 6A	4	0	Direct mRNAs to the PBs. Directly interacts with Ago proteins, binds PABPC to prevent mRNA from circularization and binds to NOT to recruit CCR4-NOT de-adenylase.	(Pratt and MacRae 2009; Meister 2013)
TNRC6B	Trinucleotide Repeat Containing Adaptor 6B	6	0	Directly interacts with Ago proteins, binds PABPC to prevent mRNA from circularization and binds to NOT to recruit CCR4-NOT de-adenylase.	(Meister 2013)
EIF2C3	Isoform 2 of protein Argonaute-3	3	0	All 4 human AGO proteins bind miRNA, distinct miRNA subpopulations might preferentially be bound by a particular Ago protein.	(Meister 2013)

MOV10	Mov10 RISC complex RNA helicase	14	7	miRNA or siRNA duplex unwinding to produce catalytically active Ago protein.	(Meister 2013)
FXR1	Fragile X mental retardation syndrome-related protein 1	9	0	Together with FMR1, interacts with RISC to ensure eye and neural crest development of *Xenopus laevis.*	(Gessert et al. 2010)
UPF1	UPF1 RNA helicase and ATPase	15	3	Supports Ago-2 complexes with target association.	(Jin et al. 2009)
PABPC4	Poly(A) binding protein, cytoplasmic 4	27	10	Might recruit miRNA RISC to the mRNA. Is bound by GW and prevent mRNA from circularization.	(Meister 2013)

6.3.3.7 The others

Apart from already mentioned hits, other interesting complexes were found. I list here the most important ones with peptides in experiment slash peptides in control in the bracket. Centromeric proteins such as Centromere protein V (CENPV) (4/0), Pericentriolar material 1 protein (PCM1) (5/0) were found.

Some parts of the ubiquitin-proteasome pathway, such as Ubiquitin-conjugating enzyme E2 S (UBE2S) (2/0), ubiquitin-protein E3 ligase HECTD3 (8/0), E3 ubiquitin-protein ligase ARIH1 (5/0), E3 ubiquitin-protein ligase HERC2 (4/0), Isoform TPRDII of E3 ubiquitin-protein ligase tetratricopeptide repeat domain 3 (TTC3) (3/0), E3 ubiquitin-protein ligase UBR5 (3/0), Tripartite motif containing 56 (TRIM56) (2/0), 26S protease regulatory subunit 10B (6/3).

Furthermore proteins known to localize to stress granules: Cold-inducible RNA-binding protein (CIRBP) (3/0), RNA-binding protein 4 (RBM4) (5/2), La-related protein 4B (LARP4B) (5/0), Ataxin-2 (6/0), Pumilio homolog 2 (5/0), Poly(A) binding protein, cytoplasmic 4 (27/10), Insulin-like growth factor 2 mRNA-binding protein 1 (35/17), and to both stress granules and P-bodies: DEAD box helicase (DDX6) (10/3), Isoform 2 of Protein LSM14 homolog A (LSM14A)(3/0), Isoform 2 of Roquin (2/0), Fragile X mental retardation protein 1 (3/0). And also a number of proteins localizing to PBs: Protein PAT1 homolog 1 (15/0), CCR4-NOT transcription complex subunit 3 (3/0), Isoform 2 of protein argonaute-2 (7/0), Isoform 2 of protein argonaute-3 (3/0), RNA helicase and ATPase (UPF-1) (15/3), Trinucleotide repeat-containing adaptor protein 6A (TRNC6A) (4/0), Trinucleotide repeat-containing gene 6B

(TRNC6B) (6/0), Isoform 2 of Enhancer of mRNA-de-capping protein 4 (EDC4) (8/3), Mov10 RISC complex RNA helicase (MOV10) (14/7).

5 transcription factors and 17 proteins linked to mitochondria and apoptosis. And finally, some parts of different signalling pathways. For complete list of MS hits see Table 20.

6.3.4 Characterization of the GFP trap assay

First, it was necessary to optimize the GFP trap protocol, this optimization was done by my colleague Veronica Venturi. I used the optimized protocol to run GFP-trap IPs with all available HEK-based stable cell lines expressing GFP-4E1_1, GFP-4E2_A, GFP-4E3_A, GFP-4E3_B and empty HEK cells. We included empty IP in HEK cells to make sure, there is no detectable unspecific binding of cell lysate to the beads.

For coomassie blue stained immunoprecipitations see Fig. 47. For the western blot, we include the detection of beta-actin, common cellular protein, not supposed to be enriched in the immunoprecipitation, see Fig. 49 and finally, for the western blot with blocking beads, both first and last washes and the flow through sample, see Fig. 48.

Fig. 47 SDS page of GFP-4Es immunoprecipitations showed high specificity, good washing and undetectable non-specific binding to the blocking beads

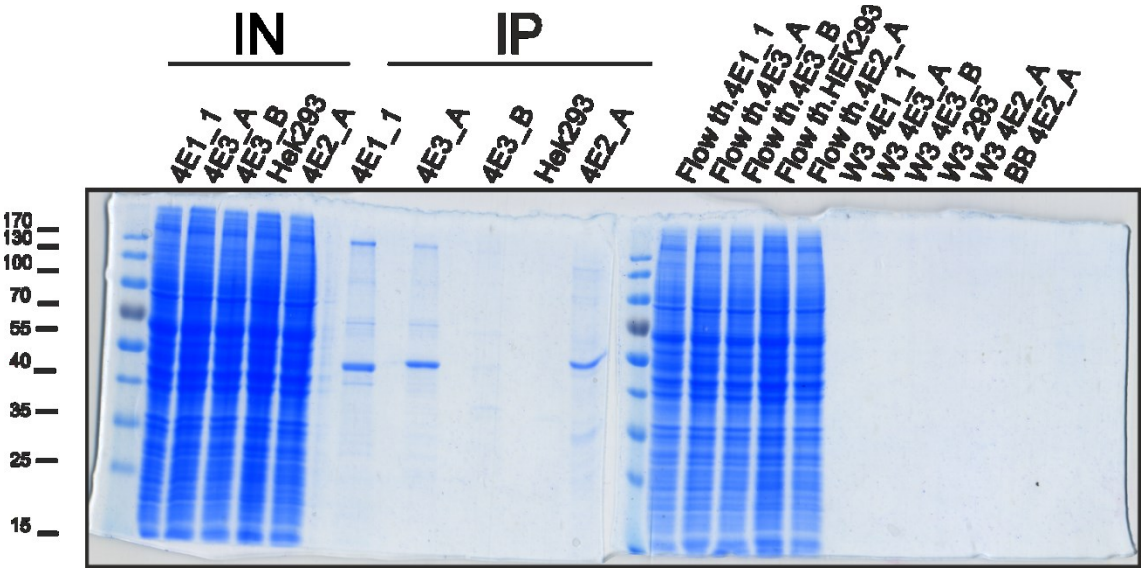

2x 100mm of fully grown stable cell lines were lysed and GFP trap was performed according to the protocol (Methods), 8 µl of the lysate per well was loaded on the 10% gel, SDS page electrophoresis was run and the gel was stained by Coomassie Brilliant blue. IN stands for input, IP stands for immunoprecipitation, Flow th. Represents flow through, W3 is the last wash and BB are blocking beads, applied prior immunoprecipitation with no antibody bound to them. One major band can be found in the IP lane, with minor co-purified products, no band can be detected in empty HEK cells IP lane since there

was no GFP. This is in agreement with no band being present on the blocking beads. No signal can be detected in the lanes of the final washes, proving that the washing step was efficient enough.

Samples from the previous figure were probed with anti GFP, eIF4G and beta-actin antibodies using Western blot see Fig. 48. The low detected amount of the immunoprecipitated GFP-eIF4E3_B corresponds with the low level of the protein stained by Coomassie blue, see Fig. 47.

Fig. 48 WB shows specific binding of eIF4GI in the case of eIF4E3_A and eIF4E1_1 but not in the case of eIF4E2_A or eIF4E3_B

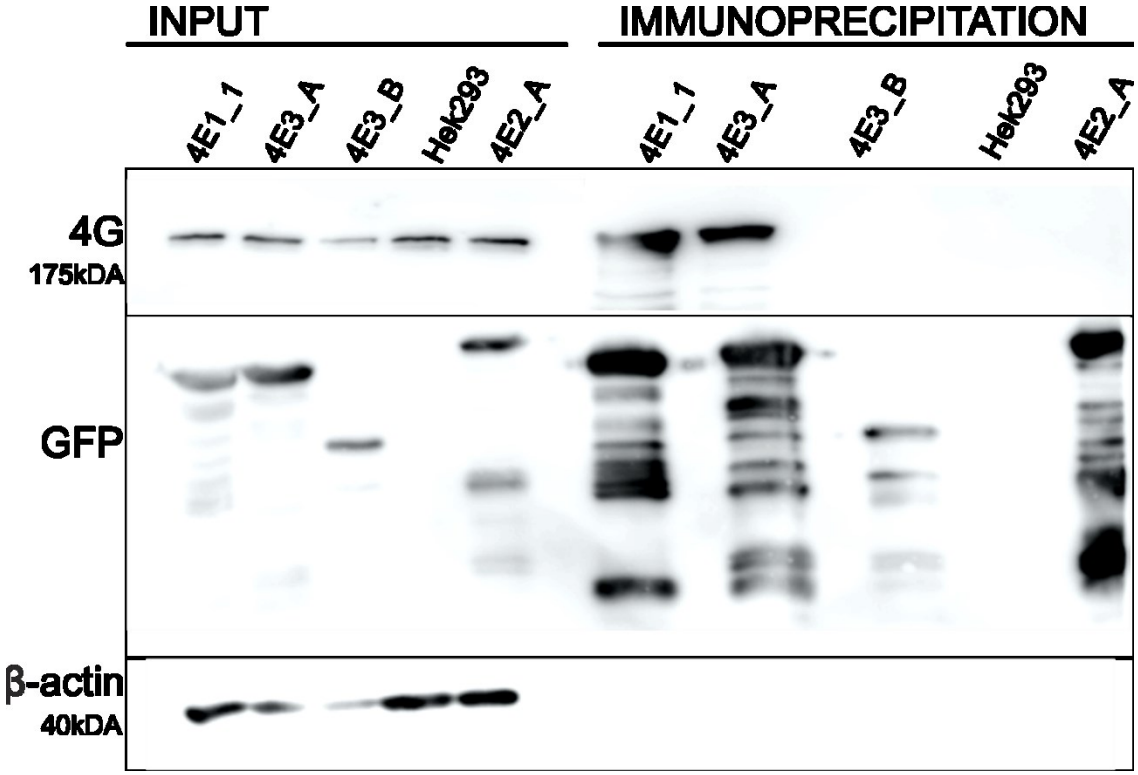

2x 100mm of fully grown stable cell lines were lysed and GFP trap was performed according to the protocol (Methods). 8 µl of the lysate per well was loaded on the 10% gel and SDS page electrophoresis was run and probed with eIF4GI, GFP and beta-actin. Expected size of individual GFP fusions are 4E2 (54 kDa), 4E1 (51 kDa), 4E3_B (39 kDa) and 4E3_A (50 kDa). IN stands for input, IP stands for immunoprecipitation. No band can be detected in empty HEK cells IP lane since there was no GFP present. No signal was detected in the IP lanes probed with beta-actin antibody and we therefore assumed that the washing was sufficient enough.

Fig. 49 Controls of GFP-4E2_A IP showed no unspecific binding to the blocking beads and sufficient washing

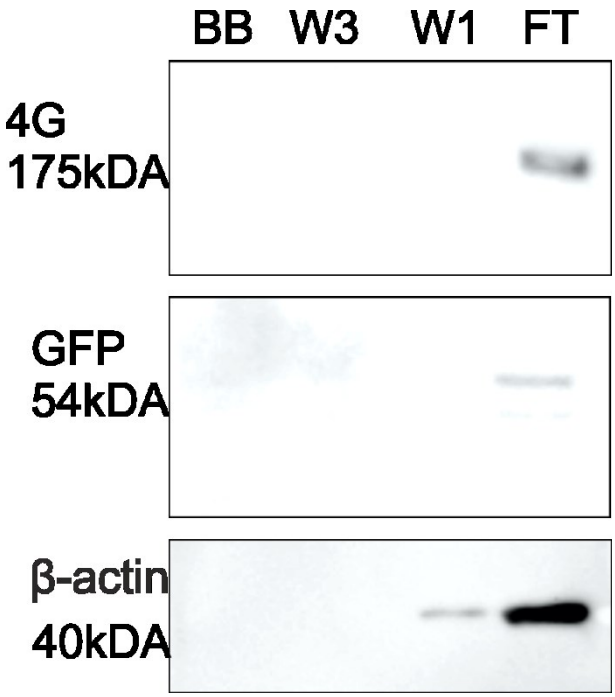

2x 100mm of fully grown stable cell lines expressing GFP-4E2_A were lysed and GFP trap was performed according to the protocol (Methods), 8 µl of the lysate per well was loaded on the 10% gel, SDS page electrophoresis was run, western blotted and probed with antibodies against eIF4GI, GFP and beta-actin. Expected size of the GFP-4E2 fusion was 54 kDa. No band could be detected in the blocking beads lane, proving specificity of the system. No detectable impurities were found in the last washing step (Wash 3), proving three washes to be sufficient.

6.3.4.1 Other 4E2 interaction partners confirmed by the GFP trap

I set out to test more MS hits using GFP trap approach. Fig. 50 summarizes the effort. The ultimate 4E2 inability to bind eIF4GI was tested independently six times with the same result. Poly A binding protein (PABP), eIF3 subunit B (eIF3B) and eIF4E transporter (4E-T) were successfully confirmed as 4E2 interaction partners. Those observations were repeated two times or three times for the last two.

I was also able to show in two independent experiments that eIF4E binding protein 2 (4E-BP2) but not eIF4E binding protein 1 (4E-BP1), interacts with 4E2. All those observations are in complete agreement with the MS results.

Fig. 50 eIF4E transporter, eIF3B, PABP, 4EBP-2 but not 4EBP-1 and 4GI were confirmed as interaction partners of eIF4E-2

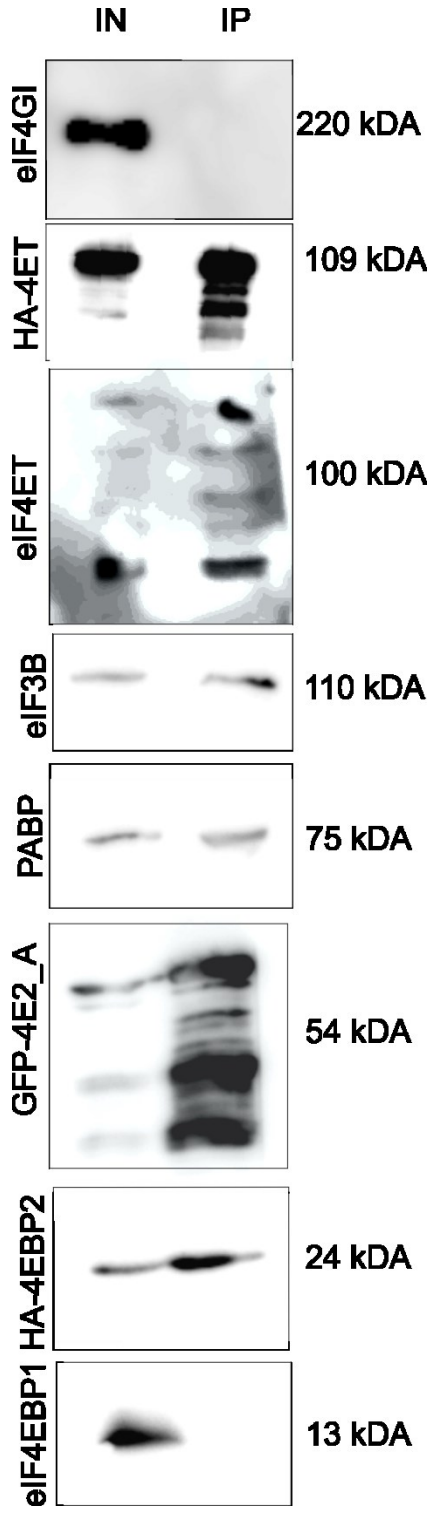

This figure is a summary of several independent GFP traps performed in GFP-4E2_A stably expressing cell line. pCDNA-3HA-4EBP2 and pCDNA-3HA-4E-T were transfected using Sigma universal transfection reagent. Approximate sizes of detected bands are listed on the right side of the image.

With the idea of 4E2 being present in stress granules in heat stress in mind, we tried to apply heat stress to the cells and run GFP trap analysis from the stressed cells and compare those results with unstressed control. Sadly, no detectable increase in the binding of eIF4E binding protein 2 or eIF4E transporter was observed (data not shown). Last but not least, we also checked for the potential non-specific binding of GFP itself, luckily enough, we didn´t observed any see Fig. 23 part I.

6.3.5 Characterization of the 4E2 interaction with eIF3

Among numerous MS hits, we chose eIF3 complex for further characterization. Our attention to this complex was drawn by two aspects. First, we were amazed that all the 13 eIF3 subunits were detected in the 4E2 immunoprecipitation and second, we are in good terms with Leoš Valášek´s lab, which has been studying eIF3 ever since and therefore we could co-operate.

First, we were naturally curious whether eIF4E2 interacts with eIF3 via mRNA. To test this we chose benzonase (enzyme known to cut both NAs) and compare aliquots of GFP trap without benzonase with those treated by benzonase over-night (see Fig. 51). This experiment was done in two independent biological replications and the cleavage properties of the benzonase were tested via cleavage of RNA isolated from potatoes by students in a practical course (Fig. 52) and qPCR (Table 18). Consequently, we are sure, that this interaction is protein-protein mediated. Both the control experiments were done in co-operation with Dr. Tomáš Mašek.

Fig. 51 eIF4E2 binding of eIF3B is not mRNA mediated

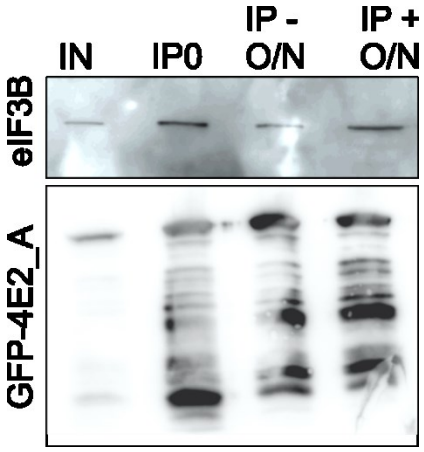

6x 100 mm dish of fully grown GFP-4E2 expressing cells were lysed 24 h after induction, 80 µl of GFP trap beads were added and in the last wash, IP was divided into 12 parts. 4 of them were processed immediately and the time=0: 1 for RNA isolation, 3 for eIF3B, GFP and β-actin detection. The other four were treated over-night with 1 µl of benzonase on ice: RNA isolation, 3B, GFP and β-actin detection (highlighted on the WB with +) and the last four was left over-night on ice without benzonase (as a

control of RNA degradation), later on they were split into RNA isolation, 3B, GFP and β-actin detection (highlighted on the WB with -). Prior WB, IPs were washed three more times. Then loaded on the SDS page gel, western blotted and probed against eIF3B and GFP. β-actin detection failed at this experiment, but the repetition showed no non-specificity.

Fig. 52 Potato RNA was effectively cleaved by the benzonase on ice

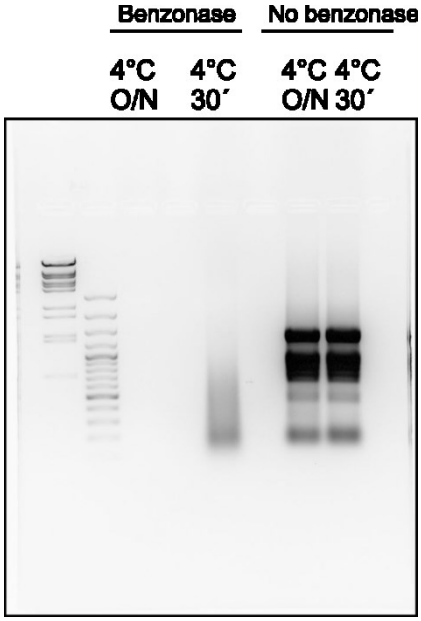

Total RNA from potatoes was isolated by the students at the practical course and stored at -80 °C. 6 µg of RNA was mixed with 1 µl of benzonase and left on ice for 30 minutes or over-night. Simultaneously, control amounts were incubated on ice without benzonase.

RNA samples from Fig. 51were reverse transcribed to cDNA, diluted 10x, 100x and 1000x and qPCR was performed with following primer sets: *Histone cluster 2, H3D* (*hist2h3d*), *Ring finger protein 5* (*rnf5*) and *Surfeit locus protein* (*surf*) see Table 18. Meanwhile *surf* is a conserved gene expressed in a variety of tissues and was therefore widely used as a reference gene for quantification, *rnf5* and *hist2h3d* were chosen to confirm hits from the 4E2 RNA-IP sequencing previously done by my colleague Dr. Veronica Venturi.

Table 18 qPCR from IP isolated RNA showed important decrease in copy numbers after benzonase treatment

Gene	IP 0 copy no.	IP without benzonase	IP with benzonase	Total decrease
hist2h3d	1,14 x10^4	4,98x10^5	3,86x10^3	129x
rnf5	9,64x10^5	2,03x10^5	5,03x10^2	403x
surf	1x10^6	2,88x10^5	1,65x10^3	174,5x

Next, we set out to explore whether eIF4E2 is capable of cap-binding under studied conditions. Published literature on the matter was really confusing with some authors

showing data about 4E2 being able to bind the cap in hypoxic conditions only (Ho et al. 2016) and others showing strong cap-binding of 4E2 under normal conditions as well (Rom et al. 1998; Tao and Gao 2015).

To find out how 4E2 behaves in my hands, I designed the experiment with 4E1 as a control and performed it twice with the same result see Fig. 53. Although m^7 – GTP IP was free of contaminations (see β-actin panel), both endogenous and overexpressed 4E1 effectively bound the cap, while 4E2, expressed in a higher level than 4E1 (see GFP panel) was unable of cap-binding. Next, I tried to treat cells with heat stress and lipopolysaccharide, neither of those treatments provoked cap-binding (panel B). I also tested cap-binding potential of 4E2 fused with C-terminal Flag tag (cloned by an undergraduate student Vendula Čečmanová), but no cap-binding was observed neither in 4E1 nor in 4E2. The underlying reason for this would likely be the insufficient amount of plasmids available for transfections (data not shown). Along with cap-binding potential of our GFP tagged 4Es we also proved GFP-tag fusion does not disrupt functionality of 4E1.

Fig. 53 Under normal conditions, 4E2 is unable of cap-binding. Neither heat stress (A) nor lipopolysaccharide treatment (B) induced cap-binding

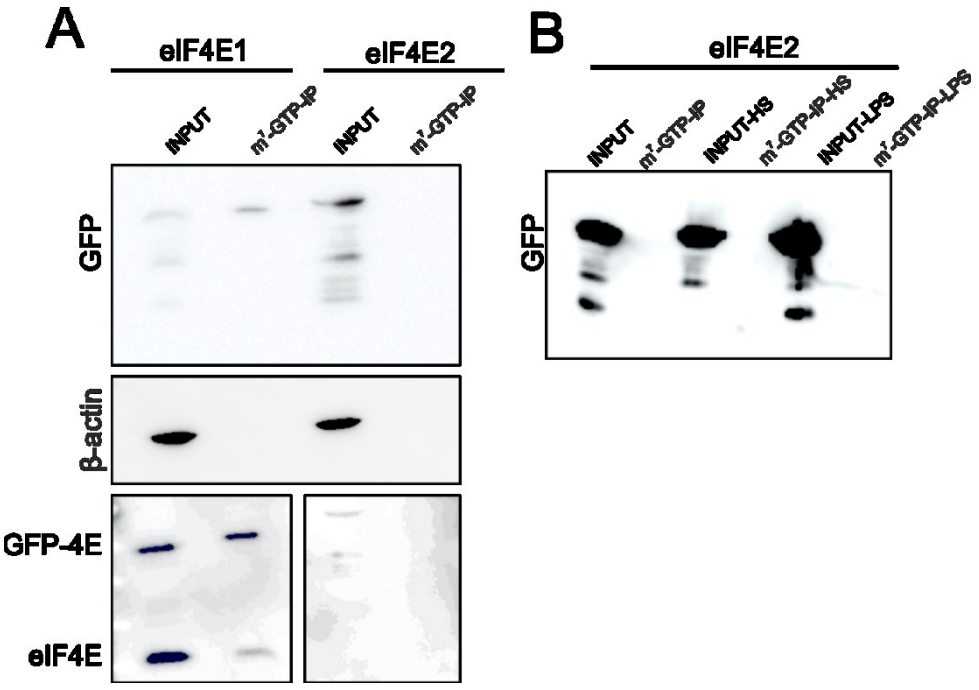

Panel A. 2x100 mm of T-rex cells were transfected with 12 μg of GFP-4E1_1 per dish using PEI. 2x100 mm of GFP-4E2_A stably expressing cell line was induced and lysed 24h later, cap-binding immunoprecipitation was performed (Methods). Wb was probed with mouse anti-GFP (1:1000) and β-actin (1:1000) rabbit anti 4E1 (Sigma 1:200) and rabbit anti 4E2 GTX82524 (1:50).

Panel B. Heat stress treatment: 2x 100 mm of 4E1 and 4E2 expressing Hek-based stable cell lines were treated with heat stress. As the heat stress conditions were developed and tested for U2OS cell line and 35 mm dish only, I was scared the cell might detach. Therefore one dish was heated by 45°C 30 minutes and the other with 47°C 30 minutes and the temperature in the medium was measured by the probe, for the first dish, measured temperature was (37,2 °C-40.8°C) and for the second one (39,7°C-42,7°C). After the stress, cells were checked under microscope and no detachment was observed. **Lipopolysaccharide treatment:** LPS conditions were optimized by my colleague Josef Novák, so I used 100 ng/ml of LPS diluted in the media and treated one dish for 4 h and the other for 16 h. After the treatment, cells were lysed and cap-binding immunoprecipitation was performed (Methods).

Next, we set out to investigate whether the interaction would be strong enough for the reverse immunoprecipitation to be performed (Fig. 54). The experiment has been performed twice with the same result, eIF3B is capable of GFP-4E2 binding but to a lesser extent then while performed the other way around. Moreover, the credibility of the result is lowered by β-actin contamination of both beads with 3B antibody (IP+) and beads itself without any antibody (IP-). This observation is in the sharp contrast with superior contamination- free agarose beads of GFP trap.

Fig. 54 Endogenous eIF3B immunoprecipitates GFP-4E2 but to a lesser extent than when performed the other way around

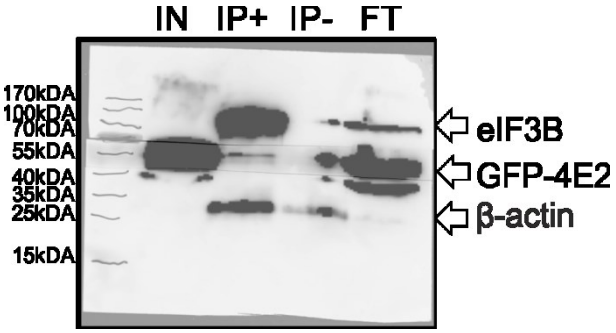

2x150 mm dishes of HEK based stable cell line expressing GFP-4E2_A for 72 hours were lysed. The lysate was pre-cleared by the beads for 2 hour and incubated with 80 µl protein G agarose beads with 12 µl of goat anti 3B antibody overnight. In the case of immunoprecipitation + and with the same amount of the beads without antibody in the case of immunoprecipitation -. Western blot was probed with mouse anti eIF3B (1:500. 110kDa) and GFP (1:1000. 54kDa) and β-actin (1:1000. 40kDa).

To assay the potential involvement of 4E2 in the translation initiation, we performed polysome profile analysis with detection of 4E2 and eIF3 proteins, see (Fig. 55). The profiles itself were done by Dr. Tomáš Mašek with the aim to better differentiate the beginning of the profile. Tomáš hoped to see some pre-assembled complexes, containing both translation initiation factors prior 40S formation. My part of the work was to isolate proteins from the profile and run the western blot. Between protein isolation and the western blot, samples were kept on minus 80 °C for a month. Surprisingly enough, while eIF3B signals peaks at the beginning of 40S, where the 43S translation pre-initiation complex forms, 4E2 signal peaks unexpectedly in the

monosome fractions 10-13 and the attempts to detect endogenous 4E1 and 2 failed. In my opinion, this experiment would be worth repeating as the result is inconclusive. But if one shall be forced to draw conclusions out of one experiment, the two proteins are unlikely to co-operate in the event of translation initiation.

Fig. 55 The maxima of individual eIF signals do not overlap in the same fractions of the polysome profile

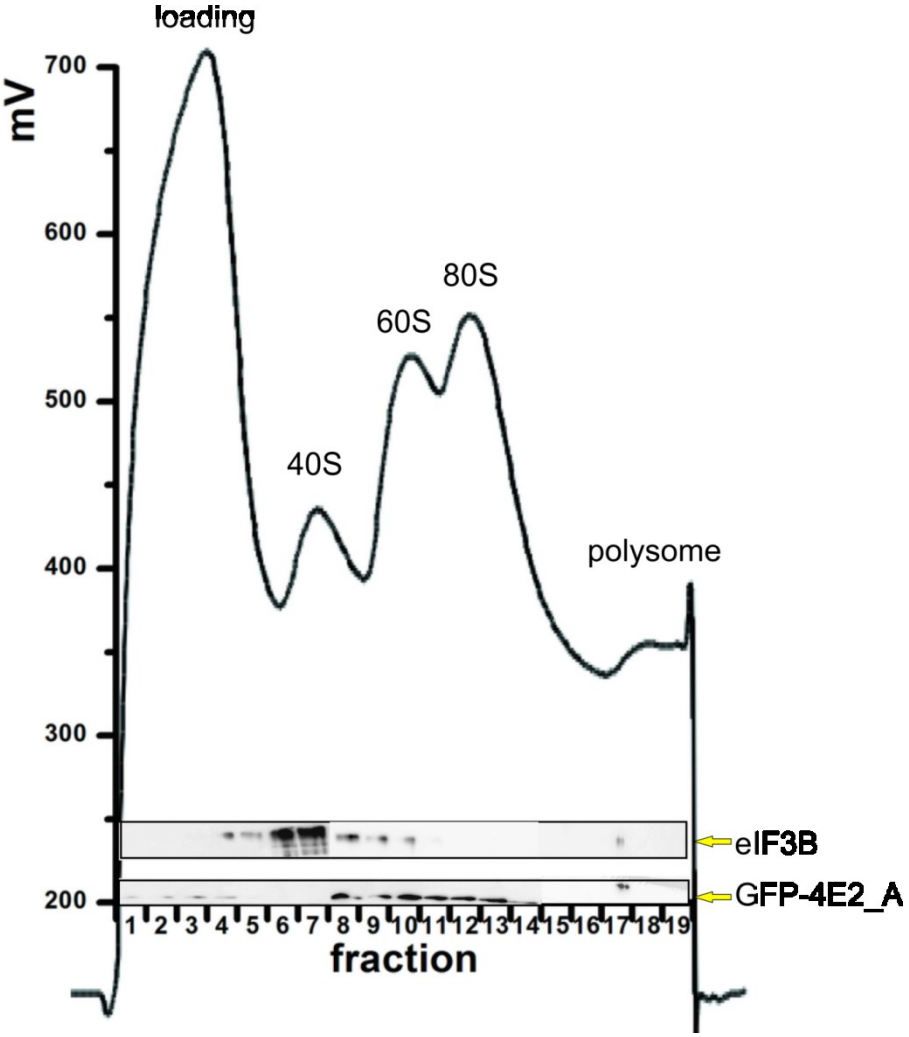

HEK based cell line stably expressing GFP-4E2 was induced for 24 hours and separated using 5-20% sucrose gradient containing 100 mM KCl. Fractions 1-19 were collected and analysed.

It is worth mentioning here that prior development of stable cell lines, we used to run polysome profiles with GFP-4Es transfected HEK293 cells. We were happily collecting results in arsenite stressed and stress-free conditions of cells transfected by 4E3 and 4E1 fused with GFP until the day we ran pEGFP transfected cells and found eGFP to be present from the fraction 1-27 all over the profile (26.10.2012). At that time, we were

using 62,5 mM KCl in the gradient (for details, see the Methods). Optimization of salt concentration to get rid of the eGFP itself from the profile was done by Dr. Tomáš Mašek.

Next question, that we have addressed, related to the interaction of 4E2 with eIF3, was whether 4E2 overexpression increases the growth properties of the cell line. In other words, whether this protein displays any pro-growth and pro-translational properties. To address this question, the resazurin growth assay was designed by Dr. Tomáš Mašek, kindly performed by our technician Natálie Moravcová and assessed by me. In agreement with all the results of this section, 4E2 does not promote growth at all. In comparison with 4E1, cells grow much slower, very much alike empty HEK T-Rex cells or cells expressing 4E3_B, known by its inability to bind the cap, please refer to Fig. 56. I personally think dilution of the cells higher than 1:7 is not physiologically relevant, as the ATCC recommends for the HEK293 cells to be sub-cultivated 1:6-1:10 weekly. And indeed using the dilution 1:17 GFP-4E3_B growths similarly to GFP-4E1, see the last graph. Linear regression GLM model was applied to all the cell dilution together, yet no significance was found at the α=0.05 among individual cell lines, the only significant parameter were individual dilutions in time.

Fig. 56 GFP-4E2_A displays no pro-growth properties of GFP-4E1, instead, it grows similarly to GFP-4E3_B and HekT-Rex cells

A

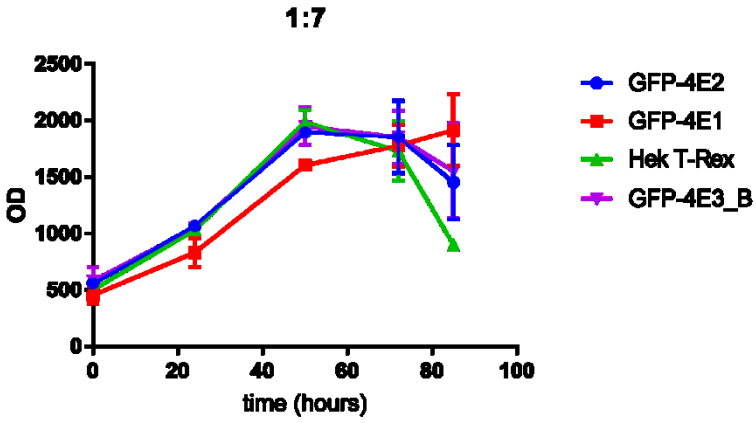

B

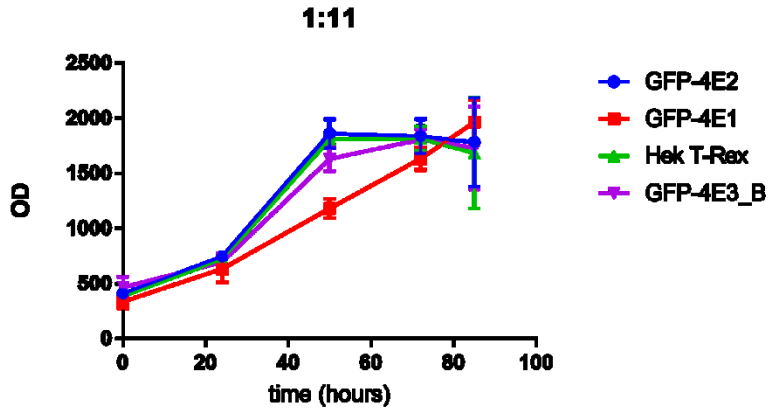

C

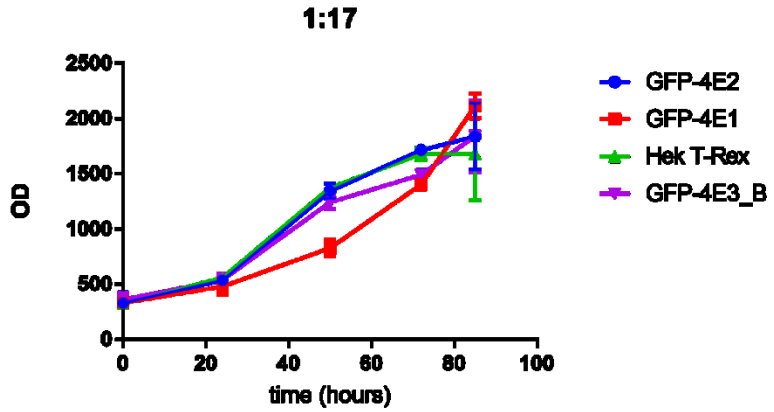

Hek T-Rex cells and stable cell lines expressing 4Es were diluted 1:7 **(A),** 1:11 **(B**) and 1:17 **(C)** and seeded on a 96 well plate in 8 technical replications for each cell line. Optical density was measured after 24h, 50h, 72h and 85h. The whole experiment was repeated the other week. Altogether 16 technical replicates in two biological replications were analysed. Means were counted from each BR, followed by standard errors of the mean, graphs were created in trial version of Graph pad Prism version 7.

Last idea to mention here would be following. Since the interaction between 4E2 and eIF3 is rather weak (see results from the recombinant protein herein bellow) and reverse immunoprecipitation fairly gives any signal at all, it could be potentially indirect, possibly mediated by eIF4G3, another MS hit and later on a published interaction partner (Ho et al. 2016).

Therefore we bought an antibody specific to eIF4G3 (260 kDa) and I did my best to make the western blot against this huge protein work, but I failed permanently. I tried to lower the gel percentage as low as possible (6%), I prolonged the wet blotting to up to 2h 100V, I lowered the methanol concentration in the blotting buffer from 20 to 12%, I tested variety of loading buffers and performed western blot with both HEK and

HELA cells as shown on the company web page, but all I managed to do was efficiently blotted protein ladder of 260kDa in size and eIF4GI (220 kDa) signal, but no sight of eIF4G3 (data not shown). To make sure it is not me, it is the antibody, I took it to the microscope, where I could observe beautiful, bright signal, see Fig. 42 and Fig. 43 from the second part of the Result section.

6.3.6 Cloning, expression and experiments with the recombinant eIF4E2

The idea of cloning eIF4E2 to GST fusion arose from the hard struggle we have experienced while looking for a working antibody on the market. I tested nine antibodies out of those only two were working, but upon 1:50 dilution and over- night binding only. From mouse antibodies, it was Abgent (AT1877a), Santa Cruz (SC100731) and ABD Sérotec (MCA4287Z). Rabbit antibodies comprise of Genetex (GTX103977), Sigma (HPA019253), Cell Signalling (D540C2) and Protein Tech (122227-1-AP). Out of those we found Aviva (ARP40555_T100) and Genetex (GTX82524) to be working, but none of them was of immunoprecipitation-grade quality. So we decided to clone eIF4E2 into GST fusion and produce both the recombinant protein for further studies and our own antibody.

During my first attempt to clone 4E2 into GST fusion, I accidentally used a mutated version of 4E2. While repairing the construction though, I cloned eIF4E3_A and B into GST fusion as well. For 4E2 and 4E3_B cloning, the topo clones were cut with EcoRI and the target vector pGEX_TEV was also cut with EcoRI and the final constructs were ligated, transformed to *E.coli* XL1 Blue cells via electroporation and subsequent miniprepreparations of GST-4E2_A were control cleaved with XhoI, BamHI and minipreparations of GST-4E3_B were control cleaved with StyI and PstI, purified and sequenced. For the cloning of 4E3_A, primers had to be ordered. Forward primer carried XhoI restriction site and reverse primer carried BamHI restriction site. The template vector pFRT.TO_4E3_A was diluted to 30 ng/µl and subjected to PCR. Final product was cleaved by XhoI, BamHI as well as the target vector and the final product was ligated, transformed to *E.coli* XL1 Blue cells via electroporation and subsequent miniprepreparations of GST-4E3_A were control cleaved with BamHI, XhoI and sequenced, please refer to Fig. 57.

Fig. 57 pGEX-TEV-4E3_A, B and pGEX-TEV-4E2_A maps

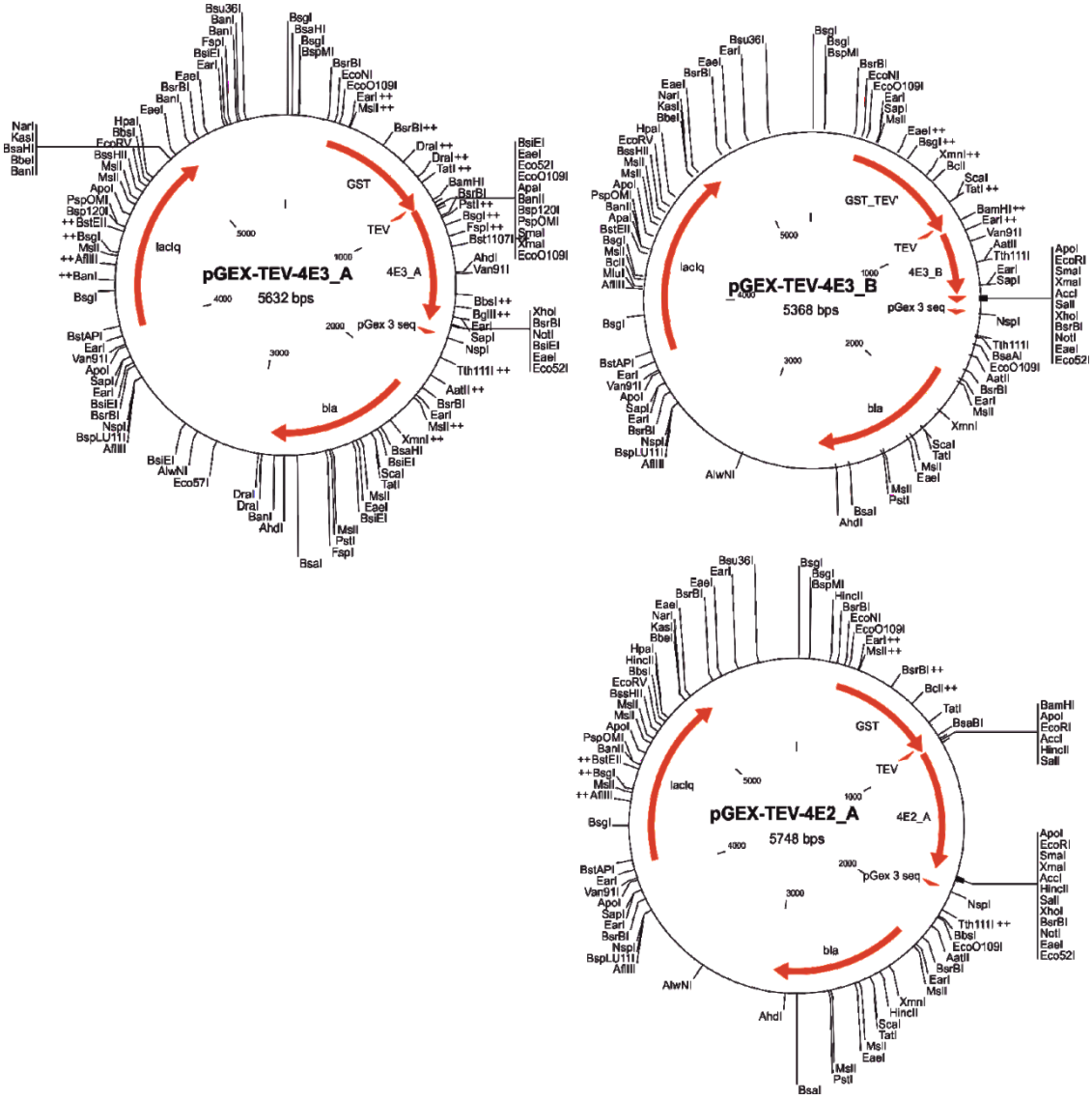

After successful cloning, the extensive optimization of the production of proteins has begun. For the final protocol, please refer to the Methods. In the end, I was able to produce interesting amount of all the proteins: 11 mg/ml of GST-4E2_A, 11 mg/ml of GST-4E3_A and 5 mg/ml of GST-4E3_B (Fig. 58) measured by the Bradford assay, which were stored aliquotted in minus 80 and cleaned by my supervisor using HPLC chromatography and finally used for the antibody production in mice.

Fig. 58 Production of the recombinant GST-h4Es, later used for an antibody development

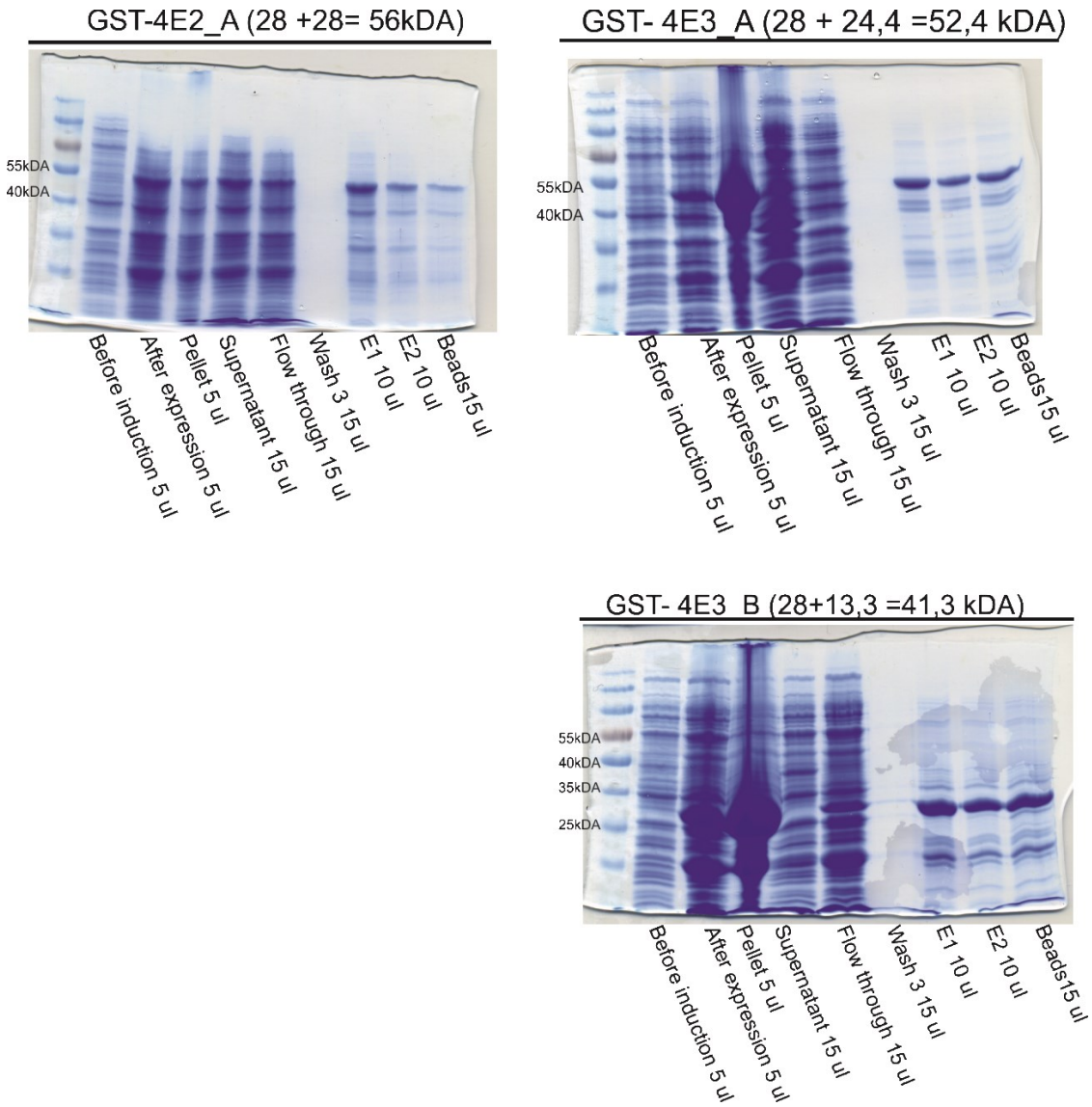

GST-h4Es were produce in the media according the protocol (Methods), E1 and E2 stands for elution step 1 and 2. Apparently one more elution step would be beneficial as there is still a lot of protein left on the beads.

Along with the protocol for GST-4Es expression, I also tested TEV protease used previously in our laboratory for GST tag removal. This protease was found not to be efficient enough and new TEV protease was generously provided to our lab by Dr. Ladislav Bumba. Its cleavage properties were verified, see Fig. 59 and protocol in Methods.

Fig. 59 Efficient tag removal by the TEV protease cleavage

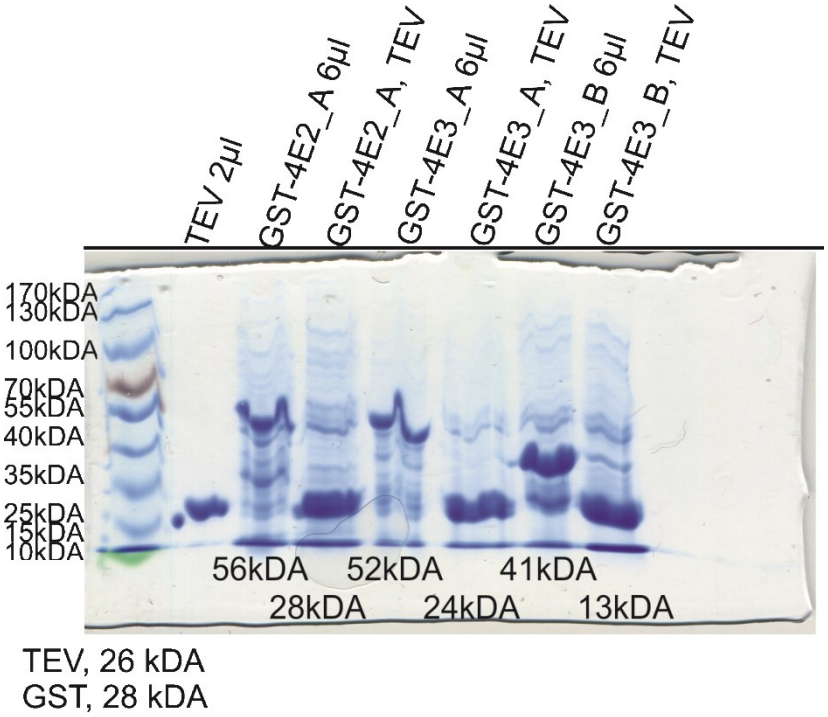

Recombinant proteins fused with GST were loaded on the gel along with the TEV protease itself before and after the cleavage. Stained with Coomassie Brilliant blue.

Along with the cleavage, the stability test of GST-4E3_A and GST-4E3_B was performed. The same amount (10 µl) of the protein elution was left at 4°C, -20°C and room temperature O/N, samples were run on SDS page and stained by coomassie blue, no detectable changes in the protein size were observed (data not shown).

With the recombinant protein in our hands, the idea of finding out which eIF3 subunit binds 4E2 was born and we set out to perform GST pull down in co-operation with Dr. Susan Wagner and Dr. Leoš Valášek. For the experiment, a fresh stocks of GST-4E2 and GST itself bound to the GST sepharose, were prepared see Fig. 60.

Fig. 60 Protein preparation for the GST pull down experiment

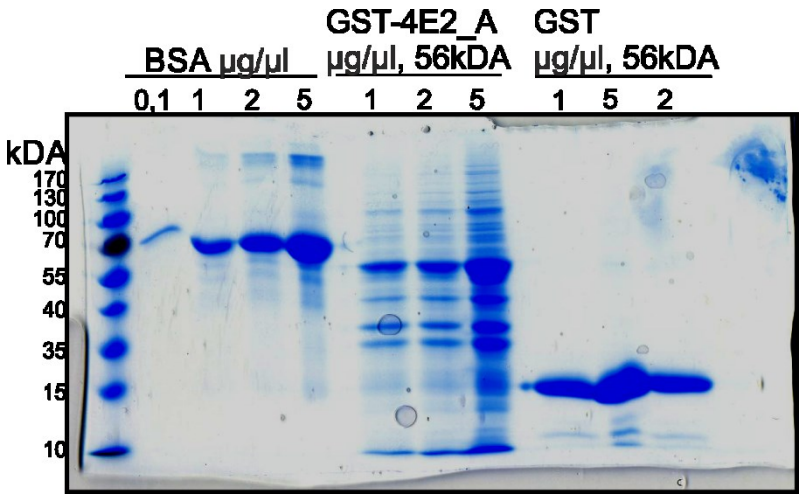

0.1, 1, 2, 5 µg of BSA and 1,2,5 µg of GST-4E2 and GST itself were loaded on the gel and stained by Coomassie blue. Based on this gel, we figure out ratio of GST itself and fused 4E2 for the pull-down experiment.

The experiment was performed twice in Dr. Leoš Valášek´s lab by myself with the same results, dr. Valášek kindly provided plasmids coding for all the eIF3 subunits that were translated using *in vitro* translation system with rabbit reticulocyte lysate. Data were kindly evaluated by Susan Wagner (Fig. 61). When comparing 4E2 interaction with the positive control, we clearly see, there is no major strong interaction between 4E2 and eIF3 as there is between eIF3C and eIF5, a positive control. We rather observe weak interactions of 4E2 with C,D,E,H,L. We also tried to reconstitute eIF3 *in vitro* by mixing all the subunits together, but it didn´t lead to any strong interaction anyway. We could only hypothesize about the underlying reasons, which could varied from a missing post-translational modification of either partner, interaction mediated via multiple subunits or an indirect interaction mediated via a third partner.

Fig. 61 GST pull down does not reveal any strong interaction partner of eIF4E2, minor enrichment could be repeatedly observed for eIF subunits C, D,E,H,L

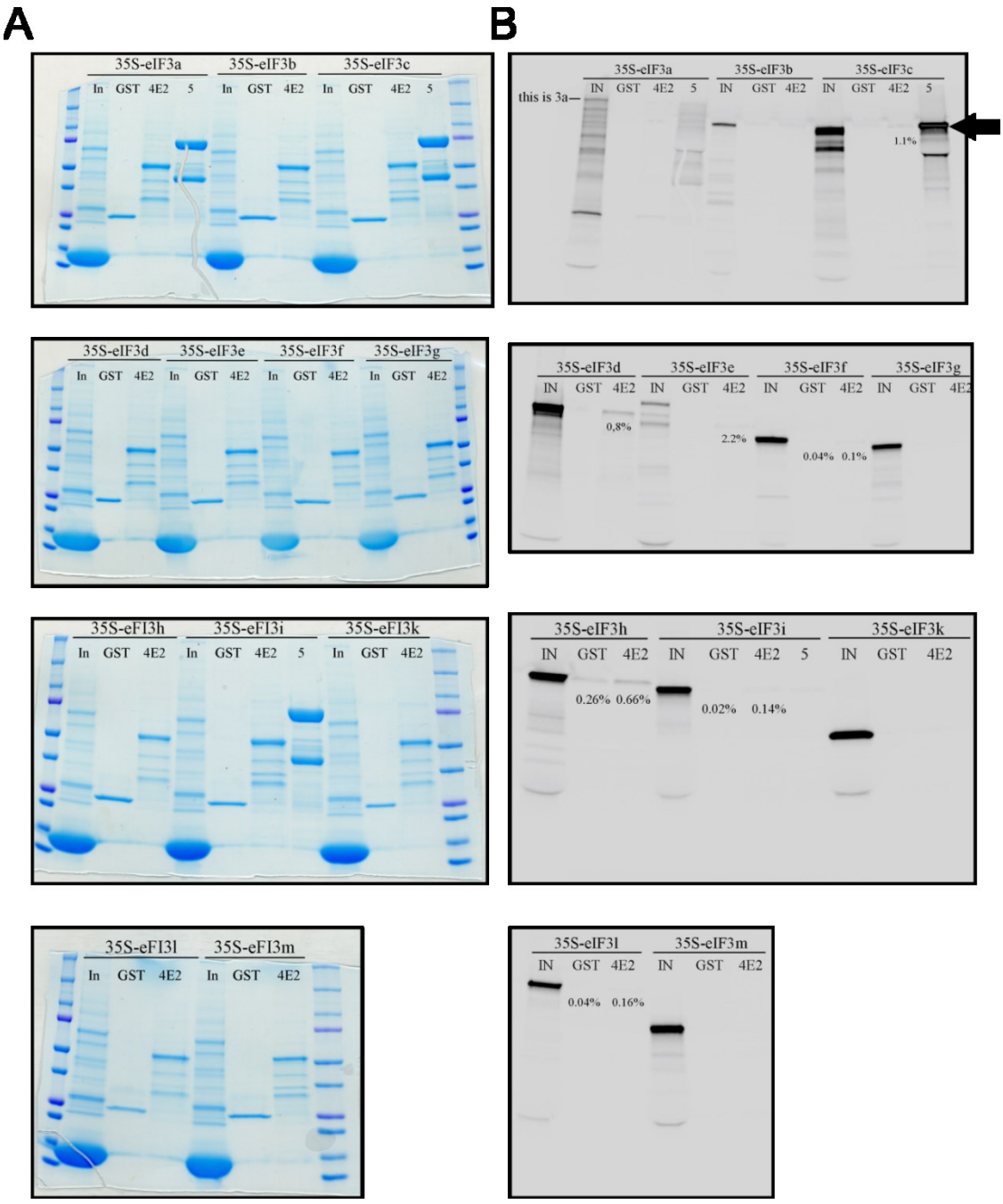

Section A displays coomassie-blue stained gels, the same gels after development of radioactive signal are shown in section B. Positive control eIF5-eIF3C interaction is highlighted with the black arrow. In stands for 2% of input, GST stands for 100% GST elution and 4E2 stands for 100% 4E2 elution. Per reaction, 4µl of GST-4E2_A and 1,5 µl of GST was used.

7 DISCUSSION

7.1 Co-localization of eIF4Es and their variants with stress granules and P-bodies in heat, arsenite and stress-free conditions

7.1.1 Why we used the tagged protein for our study

Ectopic production of proteins in fusion with a fluorescent tag has several undeniable benefits over endogenous protein visualization. First, it makes labelling easier. Major part of commercially available antibodies is produced either in a rabbit or in a mouse, one protein of interest visualized by a fluorescence tag, will open a possibility to combine it with both the mouse and rabbit antibodies and visualize all the three proteins at once.

Second, it enables us to study kinetics and to shoot videos. Last and major advantage for us is that it allows us to study a variety of alternatively spliced eIF4E variants and by the process of cloning itself, we confirmed their existence in the cell. Namely, we cloned a used eIF4E2_CRA_A variant prior its publication in RefSeq database (Mrvova et al. 2018). All those reasons were strengthen by the fact, that we found it hard to find a working eIF4E2 or eIF4E3 specific antibody (for details about 4E2 antibody testing, see Immunoprecipitation using GFP trap system followed by mass spectrometry, for details about 4E3 antibody testing, see stress Stress- free conditions and other control experiments*)*.

7.1.2 On the optimization of heat stress

Initially, I tried to provoke stress granule´s assembly using life cell imaging microscopy on Cell R system. Altogether, there were four attempts to shoot videos similar to (Wheeler et al. 2016; Hamada et al. 2018). I used several cell lines: HEK 293, U2OS, Mrc-5 and Hela transfected with pEGFP-4E1_3. Even though I was able to reach 37-55°C temperatures of the stage and up to 45°C temperature of the chamber´s air and took pictures every two minutes, all the experiments were unsuccessful. The cells either

died (HEK293) or did not form any granules at all (Mrc-5). We also struggled a lot with focusing. With the rising temperatures, the microscope went out of focus. At that time, CellR system did not have a full-microscope chamber, it had only a stage chamber coupled with objective heating, and naturally, this settings resulted in the empty non heated space surrounding the specimen and I think this space partially accounted for the problem, along with short time in the appropriate temperature and wrong plasmid for optimization. Nowadays, with the new equipment and with our knowledge advancement, we shall be able to overcome this problem and shoot the videos of stress granule´s assembly and I am very much looking forward to try it.

After switching from life cell to fixed preparation, we decided to follow published protocol and to incubate living cells seeded in the dish in a water bath preheated at 44 °C for 30 min (Sukarieh et al. 2009). Possibly due to a range of physical and biological factors such as different cell line and thickness of the dish and coverslips, we did not succeed in SGs induction.

Fortunately enough, my supervisor invented and I developed a new approach of stress granule´s assembly using pre-heated thermoblock, pre-warmed medium and thermometer with submersible detector. Using this approach we discovered, that stress granules in U2OS cell line assembles only in the narrow temperature range of 39,5 °C-42,7 °C, upon which the middle value of 41,7 °C (measured in the medium) was opted for further experimentation. Interestingly enough, upon higher temperatures cells did not die, but SGs assembly was no longer observed (Fig. 15).

7.1.3 Alternative transcription initiation, post-transcriptional events and eIF4E variants

Several chemical and physical insults are known to have an important effect on cellular translation. Exposure to heat and oxidative stress inducers provokes a multiplicity of cell responses, including the re-localization and sequestering of initiation factor eIF4E1 to messenger ribonucleoprotein particle (mRNP) foci. In the present study, we investigated the effect of heat shock and arsenite treatment on the changes of the subcellular localization of canonical human eIF4E1 and its less investigated isoforms. The subcellular localization of the majority of the h4E isoforms were assessed in the following cell lines: HEK293T, MRC-5, and U2OS (Fig. 9, Fig. 10, Fig. 20). Although the expression level of the endogenous proteins corresponding to the GFP tagged

constructs varies among individual cells, we observe no major difference among the cell lines in terms of the nucleo-cytoplasmic distribution of the assessed isoforms.

Alternative transcription initiation and post-transcriptional maturation events generate multiple distinct transcripts from a single gene. It is estimated that 95-100% of human multi-exon genes undergo alternative splicing (Pan et al. 2008; Wang et al. 2008), which (i) increases the amount of protein isoforms, leading to changes in enzymatic properties and the spectrum of interacting partners, and (ii) may influence protein localization in the cell, along with other protein features (Scheper et al. 2003). Our study is thoroughly focused on seven human eIF4E protein isoforms belonging to all three eIF4E protein classes, which further differed in their N- and C-termini Fig. 11. Six out of seven corresponding transcript variants were cloned from one cDNA derived from B-cell precursor leukemic cell line REH, underscoring the coexistence of distinct splice variants of one gene in human cells. The present study assessed the ability of distinct eIF4E variants to localize into RNA granules, i.e., SGs and PBs. Proteins eIF4E1_1 and eIF4E1_3 served for comparison with protein variants from less studied eIF4E2 and eIF4E3 classes. Notably, upon arsenite treatment, cells transfected with the eIF4E1_1 construct formed eIF4E1-positive SGs more readily than those producing eIF4E1_3 proteins Fig. 19. As a result of alternative splicing, transcript variant eIF4E1_3 possesses a longer N-terminal part than the prototypical isoform 1. It remains, however, challenging to explain how distinct N-termini might influence the localization of both eIF4E1 isoforms to SG. Changes in protein stability and folding, modified affinity to their binding partners and different post-translational modifications might account for the reasons. This result emphasizes the importance of carefully differentiating even highly related protein variants generated from alternatively spliced mRNA transcripts when pursuing functional studies.

In this study, the eIF4E2 protein family was represented with eIF4E2_A, eIF4E2_C and eIF4E2_CRA_a variants. All of them were recruited to PBs and were absent in SGs in cells undergoing arsenite-driven oxidative stress Fig. 18. This distinct localization pattern clearly distinguishes eIF4E2 from eIF4E1 and eIF4E3, although all these proteins are related at the sequence and structural levels. Moreover, it suggests that eIF4E2, unlike prototypical eIF4E1, is functionally unimportant for SG assembly (Fournier et al. 2013). This finding enriches the intriguing spectrum of roles attributed to eukaryotic translation factor 4E2, which is also known to act as a translational

repressor of specific mRNAs (Cho et al. 2005; Cho et al. 2006; Villaescusa et al. 2009; Tao and Gao 2015; Chapat et al. 2017; Peter et al. 2019). It is understandable that the exclusive recruitment of eIF4E2 to PBs may reflect its role in processes as translation repression and mRNA storage or decay. Indeed, a year after our results were published, 4E2 was shown to directly interact with components of RISC and repress target mRNAs in human cells (Chapat et al. 2017; Chen and Gao 2017). Noteworthy is that Morita and colleagues described in 2012 a translation repression complex, composed of GIGYF2, ZNF598 and eIF4E2 in mouse. Four years later, the same complex was confirmed in human cells as well (Morita et al. 2012; Fu et al. 2016). Beside us, the only publication dealt with spliced variants of 4E2 (Tao and Gao 2015), all others are limited to the isoform 4E2_A.

Notably, we observed eIF4E2 co-localizing with a number of SGs in heat-shocked U2OS cells containing both ectopically expressed GFP-tagged eIF4E2 and/or expressing entirely its endogenous levels Fig. 16 and Fig. 22. We detected the co-localization of eIF4E2 with a substantial portion—but not all—of eIF3B-specific foci in the same cell. This result provides clear evidence that the protein composition of SGs can vary over different types of stresses. Some other examples of variations in SG protein content, depending on the stress type and/or its severity, have been reported in the literature and are discussed in the chapter “Changes in the composition of mammalian stress granules induced by heat and arsenite stresses” .

The eIF4E2_A protein isoform contains five C-terminal leucines, the spacing of which might fulfil the criteria of a nuclear export sequence (NES). The corresponding sequence is, however, missing in the eIF4E2 protein isoforms C and CRA_a because these utilize different C-terminal exon composition Fig. 11. Using naturally occurring protein variants, we showed that eIF4E2_C and eIF4E2_CRA_a did not demonstrate increased accumulation in cell nuclei in comparison to prototypical isoform eIF4E2_A Fig. 16, Fig. 18, Fig. 20, thus confirming that the C-terminal extension of eIF4E2_A does not contain a NES (Kubacka et al. 2013).

Surprisingly, the eIF4E3_A isoform exhibits a unique stress response, being recruited to SGs in both heat-shocked and arsenite-treated cells but never localizing to PBs (Fig. 18F and Fig. 16F). The localization of human eIF4E3_A to SGs led us to hypothesize that this isoform may complement the roles of eIF4E1 in the process of translation initiation. This assumption is additionally advocated by a study reporting on

neural trans membrane receptor DCC in a complex with many components of the active translational apparatus, including eIF4E3 (Tcherkezian et al. 2010) and by the study showing that 4E3 drives translation of a transcription factor nuclear factor erythroid 2 like (Nrf2) and the elevated expression of *4E3* is therefore a prognostic of poor survival in multiple myeloma B-cell malignancy (Riz et al. 2016). There is also a study, showing that 4E3 acts as an inhibitor of translation and is unable to interact with 4GI, but it is based on the work with mouse protein (Osborne et al. 2013). Mouse and human eIF4E3 proteins are not identical: Mouse eIF4E3—similarly to its rat homologue—is only 207 amino acids long, whereas its human counterpart spans 224 amino acid residues. It appears that rodent eIF4E3 proteins are more derived and lack the N-terminal extension, which is present in other known eIF4E3 sequences. Human eIF4E3 further differs from the mouse homologue in six amino acid residues with substitutions of uncharged or neutral amino acids residues to polar or charged ones, respectively Fig. 11. An explanation of the possible differences in the binding properties of both proteins remains, however, an open matter.

In mice, the expression of eIF4E3 is fairly limited; in fact, eIF4E3 mRNA was reported only in skeletal and heart muscles, lungs and the spleen (Joshi et al. 2004). In humans, the eIF4E3_A protein was detected in several hematopoietic cell types (Osborne et al. 2013). A systematic human proteome study summarized in The Human Protein Atlas detected eIF4E3 at high or medium expression levels in 11 out of 79 analysed normal tissue cell types (Uhlen et al. 2015). Moreover, *eif4e3* is sparsely covered by deposited full-length cDNA or expressed sequence tag (EST) sequences. There are 156 ESTs available in the UniGene Database, supporting the existence of eIF4E3 in human cells; however, only one of them evidences the eIF4E3_A protein isoform (DR159502.1). The clone originates from human embryonic stem cells differentiated to an early endodermal cell type; this could explain our finding of eIF4E3_A in HEK293 cells, which are derived from an embryonic kidney. In addition to cancerous cell lines, human *eif4e3* is expressed in brain and placenta (Mrvova et al. 2018).

The truncated isoform of human eIF4E3, eIF4E3_B, lacks an important part of the eIF4G-binding consensus, including the Trp73Ala residue. In this study, we demonstrated that eIF4E3_B neither localized to SGs or PBs nor bound scaffold protein eIF4G (Fig. 16G, Fig. 18G and data shown in the enclosed publication only). This

outcome is in agreement with the reported importance of the conserved motif containing a Trp73Ala residue, which is critical for eIF4E1 interaction with both eIF4G and 4E-BPs and, consequently, for eIF4E1 localization to both SGs and PBs (Marcotrigiano et al. 1999; Joshi et al. 2005; Ferrero et al. 2012). To elucidate the possible function of eIF4E3 in humans, determination of protein abundance and tissue/developmental specificity for each eIF4E3 protein isoform is needed.

Our results presented in this thesis, current knowledge about links between translation and PB or SG formation and known data about the eukaryotic translation initiation factors belonging to the eIF4E family allow us to suggest a speculative model of distinct function of different eIF4Es in human cells (Fig. 62). PBs contain non-poly-adenylated mRNAs, components of mRNA repression pathways, mRNA decay machinery and numerous RNA-binding proteins (Stoecklin and Kedersha 2013; Ayache et al. 2015). Although, recently a direct role of P-bodies in mRNA decay is being questioned, they are still viewed as sites of mRNA repression (Luo et al. 2018; Standart and Weil 2018; Guzikowski et al. 2019). SGs on the other hand contain poly-adenylated mRNA, small ribosomal subunits, most translation initiation factors, cytoplasmic poly(A)-binding protein and varying set of RNA-binding proteins and thus are considered as sites of accumulated stalled translation initiation complexes, which are formed in response to various stress conditions (Stoecklin and Kedersha 2013).

Several studies evidenced that mRNAs within SGs are in a continuous flux and remain in a highly dynamic equilibrium with polysomal mRNA (Kedersha et al. 2005; Mollet et al. 2008; Stoecklin and Kedersha 2013). In our model a tightly regulated eIF4E1 (Kong and Lasko 2012) shuttles between sites of active translation, PBs and as a response to stress insult also SGs (Stoecklin and Kedersha 2013). eIF4E2 is generally considered as a protein mainly involved in translation repression (Cho et al. 2005; Cho et al. 2006; Villaescusa et al. 2009; Tao and Gao 2015; Chen and Gao 2017; Peter et al. 2019) which however can associate with translating ribosomes in human cells during hypoxia (Uniacke et al. 2012; Ho et al. 2016). This is in good agreement with our observation that all three eIF4E2 variants tested (eIF4E2_A, eIF4E2_C and eIF4E2_CRA_a) localize to PBs both in normal conditions and in arsenite-induced stress. Intriguingly, eIF4E2 appears in some, but not all, stress granules as a result of heat shock. One of the possible explanation might be, that translation of small subset of mRNAs could be facilitated by eIF4E2 even in normal conditions in human cells,

similarly as in nematodes (Dinkova et al. 2005) and their translation initiation might be sensitive to elevated temperature but not to arsenite treatment. We prefer another possible explanation, that human SG composition is different in heat shock and arsenite treated cells and thus the dynamic flux and protein and mRNP exchange between PBs and SGs allow trapping of eIF4E2 (or mRNPs containing eIF4E2) in heat shock-specific SGs, but not arsenite-specific SGs, due to possible protein-protein interactions.

Fig. 62 Possible roles of eIF4E1, eIF4E2 and eIF4E3 in translation initiation and mRNA repression

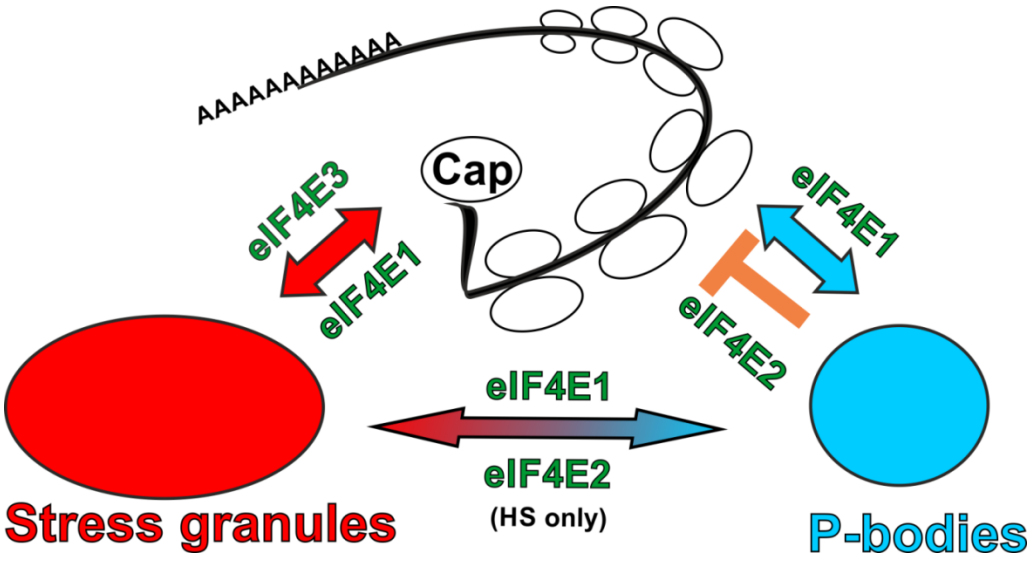

Abundant and tightly regulated eIF4E1 plays important role both in translation initiation and translation repression and thus localizes to sites of active translation, PBs and SGs. The major role of eIF4E2 is in translation repression and thus localizes mainly to PBs. Different composition of SGs as a consequence of different stresses and dynamic flux of molecules between PBs and SGs is suggested by presence of eIF4E2 in SGs after heat shock but not sodium arsenite treatment. Low abundant eIF4E3_A may serve as a keeper of basal translation initiation which is not regulated by 4E-BP pathway and is not involved in mRNA repression and decay pathways. eIF4E3_A thus localizes to SGs but never to PBs upon stresses. Colour coding is the same as in other figures: eIF4Es are in green, PBs are blue and SGs are red. For simplification, we do not include other eIF4E1 regulatory pathways and shuttling of all three eIF4Es between cytoplasm and nucleus.

The mRNP exchange between PBs and SGs is facilitated by docking PBs with SGs, which has been reported in cells treated with sodium arsenite or the mitochondrial poison FCCP but never in cells subjected to heat shock (Kedersha et al. 2005; Souquere et al. 2009; Stoecklin and Kedersha 2013). In contrast, we observed association of SGs and PBs in U2OS cells after heat shock frequently, regardless if they overexpressed any of the eIF4E proteins tested or not Fig. 16 and Fig. 22. The reason might be that we optimized heat shock conditions to maximize SG formation and well controlled each

experiment by measuring temperature with a microprobe directly attached to coverslips with growing cells.

eIF4E3_A does not bind 4E-BP proteins (Joshi et al. 2004) and thus is probably less tightly regulated than eIF4E1. eIF4E3_A is also much less abundant in cells than eIF4E1 and eIF4E2 as can be inferred from northern blot analyses, low occurrence of ESTs corresponding to eIF4E3_A in databases (this text) and apparent difficulties to detect endogenous eIF4E3_A by western blot (Joshi et al. 2004; Landon et al. 2014; Soares et al. 2014; Mrvova et al. 2018) and our unpublished results. In our experiments, eIF4E3_A did not localize to PBs but readily moved to SGs upon arsenite stress and heat shock.

eIF4E1 is abundant and dominant cap-binding translation initiation factor, which is responsible for most of the cellular translation initiation. eIF4E1 is tightly regulated and acts also as an important regulator in itself (Kong and Lasko 2012; Osborne et al. 2013). We can speculate that eIF4E3_A carries out basal translation initiation when eIF4E1 is repressed and/or eIF4E3_A secures translation of specific subset of mRNAs which should not respond to changes directed by cellular pathways controlling eIF4E1 function.

This would explain low abundance of eIF4E3_A in most tissues because, as we show here, human eIF4E3_A can readily associate with translation initiation complexes (data shown in the publication only), but its inability to bind 4E-BPs might allow eIF4E3 to escape from the overall cellular translation control and thus ruin the whole eIF4E1 regulatory network. Besides eIF4E1 and eIF4E3, eIF4E2, which is quite abundant in all tissues (Joshi et al. 2004), presumably mainly functions in repressing specific cellular mRNAs, which corresponds with its localization to PBs both in normal and stressed cells.

7.2 Visualization of two 4Es simultaneously in a cell

The idea to visualize multiple h4Es in a cell arose from Dr. Catherine Borden´s note to my talk at the RNA club that “it might be interesting to see what the other 4E does.” From the Fig. 22 it was evident, that not all the eIF3B foci in heat stress are occupied by eIF4E2, nevertheless eIF4E1 seemed to be always there. Although the literature (Tourriere et al. 2003; Buchan and Parker 2009; Mokas et al. 2009) has not agreed on one single protein essential for the SGs formation. Rather multiple proteins were

described to severely impair assembly of SGs upon their siRNA- mediated depletion e.g. TIA-1, G3BP-1,2, eIF3, histone deacetylase 6 (HDAC6), we and others believe that another member of the compendium of proteins required for SG formation is 4E1 (Kwon et al. 2007; Ohn et al. 2008; Fournier et al. 2013; Kedersha et al. 2016). Under the studied conditions, I have never seen in my life a stress granule lacking 4E1 (Fig. 16, Fig. 18, Fig. 22, Fig. 29, Fig. 30). We supported this further with statistical analysis, using three independent biological replications of approximately 50 cells, eIF4E1 protein was found co-localized with almost 100% of eIF3B-labelled SGs under both heat and arsenite stresses, see Fig. 32 and Fig. 33, altogether 11 884 SGs in 1 391 cells were analysed, summarized in Table 7.

To visualize pairs of h4Es together in a cell, we first decided to clone h4Es in the mCherry fusion and visualize pairs of 4Es fused one with GFP and the other with mCherry. Luckily enough, we did not observe any influence of the tag over the localization of the GFP-4E1, 2, 3 and their mCherry tagged counterpart proteins whatsoever see Fig. 27 A-E, even though mCherry exists as a monomer while pEGFP forms weak dimers (Shaner et al. 2005). In terms of the molecular mass they are comparable, both migrate around 28 kDa. Moreover we did not observe any differences between the numbers of SGs formed by mCherry-4E1 in comparison with GFP-4E1, judged by eye, see Fig. 28 A. Additional green granules observed in GFP-4E2 not co-localizing with mCherry-4E1 in Fig. 28 D could well be P-bodies or others, since the experiment is missing the eIF3B marker of SGs. Though Fig. 28 G is nicely showing that apart from GFP-4E2 and endogenous 4E2, also mCherry-4E2 localizes to the SG-like structures provoked by the heat.

Two types of SGs can be observed on Fig. 28, highlighted by yellow arrows are SG-like structures, where two assayed 4Es co-localize together, on the contrary violet arrows point to those that are SG-like structures where only one 4E is present. In heat stressed cells, 4E1 and 4E3 co-localized together in SG-like structures see Fig. 28 C, F regardless the fusion type while 4E2 co-localized with the other 4E in a certain part of SG- like structures and formed also SG-like structures on its own, see Fig. 28 G, D but not Fig. 28 E. Concerning 4E3-A in heat shock, our possibilities to visualize it have been limited to the overexpressed protein in either GFP or mCherry fusion because we had not have a working antibody detecting 4E3_A in both western blot and immunofluorescence till today. Nevertheless, Dr. Pospíšek himself is working hard to

produce one, using the protein I cloned into GST fusion Fig. 57, so the situation might soon get better.

Unfortunately, other problems related to transfection efficiency and toxicity arose, therefore in order to gain at least some data, we switched to the detection of endogenous 4E in a stable cell line expressing the other 4E in GFP fusion. Under the condition of arsenite stress, both endogenous and overexpressed 4E2 were unable to localize to SGs, see Fig. 30 A,D,B. When we quantified the data using three independent biological replications of approximately 50 cells, only 4E2 localized to only 2% of SGs in arsenite stress, see Fig. 33 and 4E1 and 4E3 on the other hand, co-localized in almost 100% of SGs, see Fig. 33 and Fig. 30 C. Indeed, the total numbers of SGs with 4E1 and 4E3 in arsenite stress are comparable, see Table 7 and Fig. 31, Fig. 32.

Since SGs are known to be stalled aberrant 48S complexes (Kedersha et al. 2002), the ability of 4E3-A to co-localize in virtually all the SGs with 4E1 could suggest an important pool of actively translating mRNAs in the cell might be driven by 4E3-A. We have previously shown that 4E3-A interacts with 4GI and associates with translation initiation complexes and light polysome fractions (Frydryskova et al. 2016). Further work is needed to shed some light on the question of how 4E3-A gets localized to SGs? Are amino acids residues important for cap-binding needed also for its localization to SGs or is it rather via protein-protein interactions, as suggested previously in *Dm*4E3 (Ferrero et al. 2012)? Upon cycloheximide treatment, would there be a difference in the number of SGs between 4E1 and 4E3 stable expressing cell lines?

The initial observation of 4E2 not being present in all the eIF3B foci in heat stress, proved to be right as evidenced by both the pairs GFP-4E1 and 4E2 endogenous Fig. 31 A and GFP-4E2 and 4E1 endogenous Fig. 31 B. Both the situations are clearly showing the existence of two types of stress granules in heat stress: 4E1/3 specific granules and 4E2 SGs containing all the three 4Es. Although Fig. 31D shows complete overlap of 4E2 and 4E3 SGs in heat stress, SG-quantification and analysis related Table 7 clearly shows, there were significantly less 4E2 SGs in comparison with 4E1 and 4E3. Indeed, statistical analysis proved that two classes of SGs can be observed in heat stress: 4E2 SGs and 4E1/3 SGs. Approximately 75% of SGs in heat stress are 4E2 SGs, see Fig. 32. There is statistically significant difference in numbers of both 4E2 SGs and those where 4E3 and 4E1 localized.

Last, I attempted to evaluate the influence of the GFP tag. I took the total of 167 cells that were analysed in arsenite stress-induced three independent biological replications and 176 cells that were analysed from heat stress –induced three independent biological replications and compared the total number of SGs where endogenous 4E1 localized with those co-localizing with GFPtagged 4E1. I tested whether there is significant difference between the total counts of stress granules containing endogenous or overexpressed 4E1 and indeed, there is. Nevertheless, I failed to show the same for endogenous and overexpressed 4E2, see Table 7. This data discrepancy is likely caused by a use of different eIF3B SG markers. In the preparations with endogenous 4E1 detections, eIF3B antibody raised in the rabbit was used, while in the preparations with endogenous 4E2 detection, eIF3B antibody raised in the mouse was used. Even though any statistically significant difference was found between the counts of eIF3B positive SGs using the mouse and rabbit antibodies, Table 7 shows that counts of SGs detected by mouse antibody were actually higher than those of rabbit: 2896 versus 2498. This assumption is further strengthen by unusually high P value in the comparison of heat-stressed 4E1 exogenous and endogenous counts of SGs.

To my knowledge, this is the first attempt to visualize multiple h4Es in a cell. Although the project suffers from the lack of human power, the pre-eliminary data are very promising and tempts me with a lot of questions. For example, how is 4E2 transported to the SGs, is it via protein-protein interactions or via direct binding to the cap? Both means are possible. Ferrero et al. (2012) has shown that, cap-binding residues of *Dm*4E1 are not important for its localization to SGs and PBs, while Trp residues homologous to h4E1 residue Trp73 responsible for interactions with protein partners such as 4E-T, 4G, 4E-BPs is crucial for its localization to SGs and PBs. These results are somewhat contradictory as SGs are currently understood as a storage sites for the incomplete 48S complexes (Kedersha et al. 2002; Youn et al. 2018). And the only two members of 4F complex that can localize to both SGs and PBs are 4E1 and 4E2 (Frydryskova et al. 2016). Thus I have difficulties to imagine cap-binding residues of 4E1 would be unimportant for its localization to SGs and I think such an assay with human 4E protein family members would worth to be repeted. The ability of 4E2 to bind the cap is discussed in a separated chapter.

Over the last two decades, people interested in RNA granules were trying to show their relation with polysomes via cycloheximide and puromycin experiments.

Their effort of course inspired me, so I performed several attempts myself. The results of previous two attempts have been inconclusive, so I only show here my last trial.

As cycloheximide is a drug known to freeze mRNAs on the polysomes and destabilize pre-formed stress granules that are supposed to be in dynamic equilibrium with polysomes (Kedersha et al. 2000), experiments with cycloheximide have been used to show connection of a protein localizing to stress granules with an active translation (Ferrero et al. 2012). Published reports nevertheless differ in the used methodology, most people treat cells with cycloheximide after the stress, some do so during the stress and strangely, some people add an extra recovery phase after the cycloheximide treatment (Kedersha et al. 2000; Ferrero et al. 2012).

When I was designing cycloheximide experiment, my main goal was to visualize the pure effect of cycloheximide and to distinguish it from the effect of the recovery phase and also to see, if the recovery phase would be necessary.

As you can see from

Fig. **41**, in my hands, most SGs disassemble after 1h with cycloheximide, no additional recovery phase is needed to see decrease in the number of SGs caused by the cycloheximide treatment (compare panel A, B and C in heat and arsenite stressed cells). I have not performed any statistics, yet. Nevertheless, among several imaged foci, I chose the representative image and unintentionally, one fact seems to be obvious. The kinetics of heat stress granules and arsenite stress granules differ compare panel

Fig. **41**B for both the stresses. There are less SGs left after arsenite than heat treatment followed by cycloheximide exposure. Altogether, this experiment provides us a starting point for time-lapse assay of disassembly of the heat and arsenite stress-induced SGs.

Another drug puromycin, which disassembles polysomes, it could unravel potential differences among 4E1/3 and 4E2 SGs in terms of assembly kinetics, when applied and measured *in vivo*, without stress. Providing that 4E2 localizes first to PBs and then travels to SGs via PB-SG fusion, the rise of 4E2 SGs would be delayed in comparison with the rise of 4E1/3 SGs.

7.2.1 Changes in the composition of mammalian stress granules induced by heat and arsenite stresses

There are indeed two types of heat stress-induced SGs in a cell: 4E2 SG, where all the three 4E family member proteins are present and 4E1/3 SGs where 4E2 protein is missing. I was naturally curious about their protein composition. First, I wondered whether there would be stress specific differences in protein compositions between arsenite and heat stressed cells and next, I wanted to find out whether there are some proteins specifically recruited to the 4E1/3 or 4E2 SGs. For example, eIF4G3 is a part of translation initiation 4F complex in hypoxic cells (Ho et al. 2016) and because SGs are considered to be aggregates of aberrant 48S complexes (Kedersha et al. 2002), I expected 4G3 to be enriched in 4E2 SG. Sadly, no differences in protein composition of SGs between 4E1 and 4E2 stable expressing cell lines were found, compare **Fig. 42** with **Fig. 43**.

A dense network of proteins contributes redundantly to SG formation; thus, the compositions of SGs vary under different conditions (Buchan and Parker 2009; Frydryskova et al. 2016; Aulas et al. 2017). This finding was demonstrated by cross-comparison of databases of disease-related SG proteins. Out of 1312 disease-related SG proteins found across 14 databases, almost two-thirds were found exclusively in a single dataset, and as few as 5% of these proteins were found in at least half of the databases (Markmiller et al. 2018).

SG member proteins can be divided into scaffolds and clients. Whereas scaffolds are required for the assembly of the SGs, clients are localized in SGs via their interactions with scaffold components. The distinction between scaffolds and clients could be stress condition-dependent (Ditlev et al. 2018). In line with that, arsenite stress selectively recruits a component of (Baguet et al. 2007; Didiot et al. 2009). Furthermore, fused in sarcoma (FUS), a hallmark of amyotrophic lateral sclerosis, localizes to SGs in HeLa cells treated with 0.5 mM sodium arsenite for 1 h, 0.4 M sorbitol for 1 h, 1.5 mM hydrogen peroxide for 2 h and 50 μM thapsigargin for 30 min but not cells exposed to elevated temperature at 43°C for 30 min (Sama et al. 2013). The group of heat stress-specific SG proteins includes HSP27 (Kedersha et al. 1999); the PB marker DEAD-box helicase 6 (DDX6) (Markmiller et al. 2018); and eukaryotic translation initiation factor (eIF4E2) and eIF4E transporter (4E-T), which are

components of the silencing machinery (Suzuki et al. 2009; Cargnello et al. 2012; Frydryskova et al. 2016).

Similarly, we observe striking differences between SGs produced by heat and arsenite stress compare Fig. 42 and Fig. 43. Heat induced SGs were specifically enriched for silencing complex members eIF4E2, AGO-2 and de-capping enzyme DCP-1. Protein DDX6 however, was enriched in heat stress-induced 4E1 but not so much in 4E2 SGs, compare Fig. 42 and Fig. 43. These figures are collected from several independent heat shock attempts thus, I think this is rather a technical problem than a cell line-specific result. Pavlína might accidently heated 4E2 stable expressing cell lines during detection of DDX6 slightly less than in the case of 4E1 stably expressing cell line.

While the ability of DDX6 to engage in SGs is potentially linked with the severity of the stress treatment, only tagged not the endogenous 4E-T protein is able to localize to SGs, see Fig. 42, Fig. 43 and Fig. 35.

The arsenite stress- specific recruitment of large ribosomal subunit protein L22 to the SGs is supported in the literature by an observation of large ribosomal subunit protein PO, that partially localized to SGs induced by a transfection of COS-7 cells by a pospho-mimetic eIF2α mutant S51D (Kedersha et al. 2002).

In yeast, severe heat shock led to a virtual collapse of PBs and SGs into one particle. In addition to the translation initiation complexes, components of mRNA turnover such as CCR4/Not complex, 5′-3′exonuclase 1 (XRN1) and a classical marker of PBs De-capping enzyme 2 (DCP2) became enriched in SGs (Grousl et al. 2009; Grousl et al. 2015). In severe heat stress conditions, the misfolded proteins could nucleate formation of SGs, unlike normal growth conditions or mild stress (Cherkasov et al. 2013; Kroschwald et al. 2015). Moreover, in both yeast and human cell lines, severe heat stress-induced SGs, rose via eIF2α-phosphorylation- independent pathway and in mammalian cells, G3BP-1 was dispensable for their nucleation (Grousl et al. 2009; Kedersha et al. 2016).

Here, for the first time, such a collapse of SGs and PBs could be observed in mammalian cells. It is evidenced by the re-localization of DDX6 protein to SGs in heat-stress specific manner in U2OS Flip In cell line, Fig. 37 and severely stressed U2OS cells Fig. 38. More evidence for such a fusion can be found on Fig. 42 and Fig. 43, where classical marker of P-bodies de-capping enzyme DCP-1 and a component of

silencing complex AGO-2 localize to heat stressed induced SGs regardless of the 4E1 or 4E2 stably expressing cell lines. In my opinion, such a collapse of SGs with PBs is the underlying reason for the heat-stress specific re-localization of 4E2 to SGs (Frydryskova et al. 2016).

Different temperatures were applied to elucidate what is the triggering temperature of the SG-PB fusion in mammalian cells. Fig. 39 shows that the heat stress must be severe, above 46 °C in order for the fusion to happen. In the figure, 46 °C labelled panel there are separate eIF3B labelled SGs and DDX6 labelled PBs, but in 47 °C and higher temperatures, the DDX6 pattern merges with the eIF3B pattern. This is why we never observe this before in U2OS cell line, see Fig. 16. These cells were heated for half an hour at 49 °C, but with cells stably expressing GFP-4Es, we switched to the 1 hour long heat stress at 47 °C.

In the future, it will be necessary to fine-tune heat stress, so that the temperature will be absolutely reproducible and evaluate the SG/PB fusion event in the connection with apoptosis and translation re-initiation. Next tempting question is, whether the sodium arsenite stress would be able to produce the same PB-SG collapse upon higher concentrations and times.

Last, unlike 4E1, whose depletion resulted in the decreased numbers of SGs (Fournier et al. 2013) and thus 4E1 was found to be functionally important for the SG assembly, the depletion of 4E2 had no effect on the formation of SGs and PBs, see Fig. 40.

7.3 MS analysis of the GFP-4E2 immunoprecipitation

Translation initiation factor eIF4E2 really is a molecule of two faces. An important portion of the literature describes it as an inhibitor of translation in metazoans such as *Drosophila* (Cho et al. 2005; Cho et al. 2006; Yarunin et al. 2011; Valzania et al. 2016), mouse (Villaescusa et al. 2009; Morita et al. 2012) and recently also in humans (Okumura et al. 2007; Tao and Gao 2015; von Stechow et al. 2015; Chapat et al. 2017; Jafarnejad et al. 2018)

On the other hand, 4E2 has been described as a translating protein in *C. elegans* (Dinkova et al. 2005) and by a number of publications, mostly originating from James Uniacke lab and dealing with human hypoxic cells (Uniacke et al. 2012; Ho et al. 2016).

We aimed for a more complex approach and wanted to unravel the complexity of roles, 4E2 may play in the cells in stress-free conditions and therefore we set out to perform MS from 4E2 immunoprecipitation. We most certainly did not count with the possibility of getting back 1466 proteins with approximately half of them being specifically enriched in the 4E2 immunoprecipitation.

First, we wanted to compare our hits with published 4E2 interaction partners. Out of 11 known interaction partners, we were able to detect 7. We did not detect eIF4E-BP1 and of course, mouse Prep-1 (Table 9). Probably because experiments showing they interact with 4E2 were performed using mouse, not human 4E2 (Joshi et al. 2004; Villaescusa et al. 2009). We also failed to detect Hif2α, probably because we did not work with hypoxic cells. Somewhat surprising for us was the detection of 4E-BP2 not 4E-BP1, which was further confirmed by an immunoprecipitation, see Fig. 50.

Next we aimed to summarize the top ten hits. Form the both Table 10, using the service ranking, and the Table 11 using my ranking, that aims to take into account the molecular mass of a particular protein, the connection to the insulin signalling pathway is evident. Upon closer look to the insulin-like growth factor pathway in Table 12, we manage to detect both the receptor IRS4 and three ligands together with some more distantly related proteins to the pathway. Furthermore, insulin-like growth factor binding protein 1 (IGF-BP1) and insulin like growth factor receptor (IGF1R) were detected in a PAR-CLIP experiment by Uniacke et al. (2012) and further characterized as a hits for hypoxic translation.

Another very promising hit was the detection of an entire eIF3 complex Table 13, the most abundant peptides there are parts of the minimal sub complex essential for sustaining the translation initiation in the cells: A, C,B, I (Smith et al. 2016), the subunit C was found among those weakly interacting with recombinant 4E2 in GST pull-down experiment, see Fig. 61

Besides eIF3 complex, we were able to detect two more complexes the FMR complex Table 14 and the RISC complex Table 17. For the FMR complex, we were able to detect all three important components of the complex: Fragile X mental retardation protein 1 (FMRP), Fragile X mental retardation syndrome related protein 1 and 2 (FXR1 and FXR2). This complex is known to interact with miRNA pathway member's AGO-2 and Dicer and display dicing activity on its own (Nakamoto 2005; Maurin et al. 2014). Furthermore, since FMRP-CYFIP-4E1 complex exists and is known to inhibit several FMRP target transcripts (Napoli et al. 2008), one may be tempted to speculate that another pool of transcripts might be inhibited by the complex 4E2-GIGYFs-FMRP, as suggested by the MS results.

Consistent with the localization of 4E2 to the P-bodies, the detection of the RISC complex was not surprising to us. The minimal RISC complex consists of AGO protein, Dicer, dsRNA binding protein such as Mov10 and heat shock protein 70.90 kDa (HSP70-90) system (Meister 2013). All the components of the minimal risk were successfully detected in the MS Table 17. Moreover, according to James et al. (2010), 4E1 and Ago protein interact to stabilize the silenced complexes in the PBs. So one may be tempted to speculate, that 4E2 is another cap-binding protein connecting the cap with the silencing machinery. As evidenced by recent publications, this presumption we had in 2014 was correct (Chapat et al. 2017; Jafarnejad et al. 2018).

Last, we also found in the MS some centromeric proteins, members of the ubiquitin-proteasome pathway, parts of the stress granules and P-bodies, transcription factors, proteins linked to mitochondria and apoptosis and others, see page 119. Recently, Ago-1 and Ago-2 have been shown to interact with splicing factors, directly affecting RNA polymerase II elongation rate and allowing the spliceosome assembly (Ameyar-Zazoua et al. 2012). Consistently a number of proteins belonging to the spliceosome have been found in the analysis, here I refer to Table 15. But since the spliceosome is multi-megadalton - big complex and its proteins are abundant in the cell

and frequently associated also with RNPs dedicated to transport, we do not exaggerate the importance of this finding.

Since we initially thought, 4E2 would be bound on the cap, it was no surprise for us, that we did not found any component of the 5´end processing pathway such as XRN1 or XRN2, instead a number of 3´end processing proteins were found and listed in the Table 16.

7.3.1 Novel interaction partners confirmed using GFP trap

To investigate how efficient and impurities - free is the GFP trap immunoprecipitation, we first performed coomassie blue staining of the gel with the last wash, flow through input and immunoprecipitation samples (Fig. 47), followed by a western blot with β-actin detection. β-actin is an abundant cellular protein and thus it could be and indicator of other unspecifically enriched proteins in the immunoprecipitation. We also run immunoprecipitation in the HEK293 cells that were not transfected (Fig. 48), to prove there was no unspecific binding to the GFP trap resin. Last, we performed immunoprecipitation with pEGFP only to make sure that the interaction partners of 4E1 and 4E3, such as PABP and 4GI are not bound by the GFP itself (Fig. 23)(Frydryskova et al. 2016). The results showed that the GFP trap is a trustworthy approach and thus I began to characterize some of the MS hits.

We showed that, 4E2 is able to immunoprecipitates PABP, eIF3B, both endogenous and overexpressed 4E-T and overexpressed 4E-BP2. Yet, 4E2 is unable to immunoprecipitates 4E-BP1 and 4GI Fig. 50 and Fig. 48. This all is in a good agreement with the literature. Concerning 4E-BP1, Joshi et al. (2004) reported that 4E2 binds 4E-BP2 and 3 more strongly than 4E-BP1. Later on, Tee et al. (2004) and Rosettani et al. (2007) failed to detect 4E-BP1 via classical immunoprecipitation with overexpressed 4E2. On the other hand, in HEK293T cells, 4E2 immunoprecipitated GFP-4EBP1 (Peter et al. 2017). Concerning 4GI, 4E2 has been presumed to be unable to bind 4GI since 2004 (Joshi et al. 2004). We were also naturally curious about the ability of 4E2 to immunoprecipitates 4G3. Ho et al. (2016) reported that 4E2 immunoprecipitates 4G3 in both the normoxic and hypoxic conditions. Yet we have been dealing with an antibody issue for many months and the results are still inconclusive and therefore were not shown.

7.3.2 Is 4E2 able to bind the cap in normoxia?

eIF4E2 has been considered as a cap-binding protein since 2004 (Joshi et al. 2004), Even though it was reported, that 4E2 binds the cap with lower affinity comparing to 4E1 (Rosettani et al. 2007). Other cap-binding assays showed that 4E2 efficiently binds the cap (Morita et al. 2012; Tao and Gao 2015). Except for the latter, everybody has been working with a mouse protein so far.

I decided to perform a cap-binding assay myself and strikingly, I was repeatedly unable to detect 4E2 bound to the cap, see Fig. 53 A. Not even after stimuli, that I hoped might provoked cap-binding, such as the heat stress (due to its localization to SGs exclusively in the heat stress) or the lipopolysaccharide treatment (due to ISG15 addition) that should increase 4E2 affinity for the cap (Okumura et al. 2007), Fig. 53 B. Therefore I had been extremely confused until the Timpano and Uniacke (2016) publication showed 4E2 being completely unable to bind the cap from the cells maintained in 12% oxygen meanwhile with the decreasing concentration of the oxygen, the affinity of 4E2 to the cap increases. Later on, however, two more studies showed efficient cap-binding of human 4E2 irrespective to the oxygen level (Chen and Gao 2017; Jeong et al. 2019).

The underlying reasons of my failure to reproduce binding of 4E2 in normoxic state I can think of is the age of the cap-binding resin, that was about 10 years old at the time of the experiment. I believe that 4E1 cap-binding was preserved due to its 100 times higher affinity for the cap than was reported for 4E2 (Zuberek and Stelmachowska 2017). Same as the authors, I attempted to detect endogenous protein. I also use a similar cell line: Hek T-REX based stable cell lines while HEK293T cells were used in the publication (Jeong et al. 2019).

7.3.3 About the interaction of eIF4E2 with eIF3

Among the large amount of proteins found in the MS analysis, it was of course difficult to set a direction to pursue. But due to the complexity of the hits from the eIF3 complex and our acquaintances with Dr. Valášek, who already did an outstanding piece of research on the eIF3 complex, we set out towards the 4E2-eIF3 path. While a direct interaction between eIF3 and eIF4G is well-established as a bridging point between the cap-binding complex eIF4F and small ribosomal subunit binding eIF3 (Jackson et al.

2010), direct interaction between a cap-binding protein and eIF3 has no known biological sense.

First question that we asked was about the role of mRNA in the interaction. As shown in Fig. 51, the RNAse treatment had no effect on the eIF3-4E2 interaction. Therefore we conclude that the interaction is not mediated via mRNA, but rather it is protein-protein mediated.

Next of course we wondered, whether eIF3 is also able to immunoprecipitates eIF4E2. So called „reverse immunoprecipitation“ shown in Fig. 54 unravelled, that eIF3 is also able to immunoprecipitates 4E2 nevertheless to a much lesser extent than when performed the other way around. In this immunoprecipitation, you may see a β - actin contamination. This contamination is enriched in the immunoprecipitation itself (IP+) in comparison with the empty beads with no antibody (IP-). This observation is in a good agreement with the literature since eIF3 is known to interact with actin (Pincheira et al. 2001) and this might partially account for the specific enrichment.

After understanding, that the interaction is likely protein-protein mediated and to a limited extent reversible, we asked via which eIF3 subunit is the interaction mediated. In the MS analysis, the most abundant subunits in terms of peptide numbers were the members of the minimal sub complex essential for sustaining translation initiation in the cells: eIF3A, C, B, I. We set out to perform a GST pull down experiment with *in vitro* translated individual eIF3 subunits and a recombinant 4E2 cloned into GST fusion Fig. 57, Fig. 60. Unfortunately, we could not see any strong enrichment for a particular eIF3 subunit, nevertheless minor enrichments were repeatedly detected for the subunits C, D, E, H, L Fig. 61. I can think of two possible explanations to this phenomenon.

First, multiple subunits have to be present for the interaction to be formed and the second explanation is somewhat more scary, the interaction is not direct, but mediated by a third partner. Since we know, eIF4E2 does not interact with 4GI, the only third partner I can think of is 4G3. Our attempts to test this are still inconclusive. Nevertheless, another scaffold-like protein Mextli, even though specific for invertebrates, is published in the literature. Mextli, an unusual *Drosophila melanogaster* and *Caenorhabditis elegans* 4E binding partner, promotes the translation via interaction with eIF3 and also interacts with 4E1 when it is bound to the cap structure. Mextli is therefore considered to be an alternative scaffold enabling 4F complex assembly such as 4GI (Hernandez et al. 2013; Peter et al. 2015). Specific to vertebrates is a scaffolding

complex threonyl-tRNA-syntetase (TARS). TARS interacts with PABP, eIF4A, eIF4E2 and also several subunits of eIF3, including eIF3B that gives the strongest signal of all (Jeong et al. 2019). Even though the authors have never tested direct binding of eIF3 to 4E2, it is worth considering that our eIF3 interaction with 4E2 might be mediated via a protein partner such as 4G3 or TARS itself.

At the moment, diploma student Klára Pospíšilová is continuing with the project under the supervision of Dr. Pospíšek, who came up with indeed sophisticated way how to figure out the exact composition of individual 4E2 containing complexes. I keep my fingers crossed for them and I am very much looking forward the results.

Another question to focus on is whether 4E2 in our hands acts as an inhibitor of translation or rather promotes translation. We run polysome profiles Fig. 55, in 5-20% sucrose gradient with subsequent detection of eIF3 and eIF4E2. Even though the two proteins do not co-sediment in the same fractions, eIF4E2 is involved in the heavier fractions than eIF3 itself. This observation is somewhat contradictory to the observation, that 4E2 in our hands does not bind the cap Fig. 53. We have to take into account the fact, that a number of proteins, with no known role in translation initiation are present in the profiles. For example, the helicase DDX6 is enriched in the heavy polysomal fraction (Ayache et al. 2015). The authors reason that it is because of the role of DDX6 in the repression of translation. Upon stalling the polysomes by an addition of the cycloheximide, the association of DDX6 with the polysomes is even magnified.

Resazurin dye is a chemical that allows determination of metabolic activity of living cells. This indicator dye is used to measure oxidation-reduction reactions which occurs in mitochondria. We measured the optical density in time to create the growth curves of individual cell lines expressing GFP-4E2, GFP-4E1 (positive control with pro-growth properties), Hek T-Rex (the background of cells with no overexpression), GFP-4E3_B (negative control, lacking residues essential for the cap-binding and protein-protein interactions). Yet when applying statistics, we were unable to detect any important differences among the cell lines, proving this approach to be inappropriate for measuring impact of 4Es on translation. For the measurements of 4E2 mediated repression of translation, either *in vitro* measurement of an mRNA reporter translation efficiency or *in vivo* addition of puromycin or radiolabelled sulphur to the cell lysate are used (Villaescusa et al. 2009; Morita et al. 2012; Tao and Gao 2015). And as for 4E1 overexpression, it was reported, that it does not accelerate the overall protein synthesis

in mammals (Saghir et al. 2001). Which is consistent with a questioned role of 4E1 as a limiting factor in translation initiation (Hernandez and Vazquez-Pianzola 2005).¨

It is possible though, that the eIF3 in complex with 4E2 is not bound to the mRNA at all or is connected to the mRNA via eIF3 itself. Upon hypoxic conditions, there might be a switch on the cap between eIF3 and 4E2 as described for 4E1 and 4E2 by (Uniacke et al. 2012). Indeed, eIF3 was reported to interact with the cap structure, the interaction was disrupted upon addition of the cap analogue (van Heugten et al. 1992). Moreover, eIF3 subunit D was recently reported to bind the cap and drive translation without the need of any other member of the 4F complex (Lee et al. 2016). To sum it up, one may think of following situations:

I) There is no mRNA in the eIF4E2-eIF3 complex.

II) There is an mRNA in the complex but bound by eIF3 and therefore 4E2 needs eIF3 for the cap-binding, since it is unable to bind the cap in normoxic conditions on its own.

III) No matter if there is an mRNA in the complex or not, 4E2 interacts with eIF3 via third partner, potentially 4G3 or TARS.

IV) The pre-formed complex either waits for hypoxic conditions to translate or have another role unrelated to translation .

V) The pre-formed complex might be having a potential role in the repression of translation in normoxia.

8 CONCLUSIONS

Here, I would like to summarize the major contributions of our work towards the advancement in understanding of the human 4Es. Above all to summarize protein-protein interactions that were confirmed in this work, see Table 19 and to highlight some major findings in the bullet points below the Table 19.

Table 19 Different binding properties of individual human eIF4E family members

	Data supporting interaction			**Data disproving interaction**		
	eIF4E1	**eIF4E2**	**eIF4E3**	**eIF4E1**	**eIF4E2**	**eIF4E3**
M^7GTP	This study; elsewhere	(Joshi et al. 2004; Rosettani et al. 2007; Tao and Gao 2015)	(Osborne et al. 2013)	-	This study; (Ho et al. 2016)	-
eIF4GI	This study; elsewhere	-	(Frydryskova et al. 2016)	-	This study; (Joshi et al. 2004)	-
eIF4G3	-	(Ho et al. 2016)	-	-	-	-
eIF4E-BP1	(Pause et al. 1994; Uniacke et al. 2012)	(Joshi et al. 2004; Tee et al. 2004; Rosettani et al. 2007; Uniacke et al. 2012)	-	-	This study; (Uniacke et al. 2014)	(Joshi et al. 2004)
eIF4E-BP2	(Pause et al. 1994)	This study	-	-	-	-
eIF4E-BP3	(Poulin et al. 1998)	-	-	-	-	-
eIF4E-T	(Dostie et al. 2000)	(Kubacka et al. 2013)	-	-	-	-
eIF3	-	This study	-	-	-	-
PABP	This study elsewhere	This study	(Frydryskova et al. 2016)	-	-	-

Based on the experimental observations, the following conclusions can be drawn:

Aim of the thesis I: To investigate localization of individual human eIF4Es and their variants into P-bodies and stress granules during heat and arsenite stresses.

- Both 4E1_1 and 4E1_3 protein variants localize to SGs and PBs under the condition of heat and arsenite stresses, albeit with different efficiencies. Upon arsenite stress treatment, seventy-five percent of cells transfected by 4E1_1 formed SGs, whereas only fifty-two percent of cells transfected by 4E1_3 formed SGs under the same conditions. Under stress-free conditions, both 4E1 variants localized to PBs.
- All the tested variants of 4E2 localize to PBs in both arsenite and heat stresses as well as in stress-free conditions.
- Heat stress induced two types of SGs in a cell in terms of eIF4Es. Seventy-five percent of SGs contain all three 4Es, while twenty-five percent of them contain only 4E1_1 and 4E3_A.
- Arsenite stress, however, induce only one type of SGs in terms of eIF4Es, those where 4E1 co-localizes with 4E3_A.
- 4E2 is not functionally important for the assembly of SGs and PBs.
- Neither 4E3 protein variant localize to PBs, 4E3_B does not localize to SGs.

Aims of the thesis II: To search for proteins differentially localized into stress granules induced by either heat shock or arsenite stress

- SGs provoked by the heat and arsenite stresses differ in their protein compositions.
- Arsenite induced SGs are enriched for large ribosomal subunit member protein L22.
- SGs provoked by the heat contain some well-established PB markers and proteins active rather in silencing than initiation of translation, such as eIF4E2, DCP-1, AGO-2, depending on the temperature DDX6 and HA tagged but not endogenous 4E-T.
- Upon severe heat stress collapse of SGs and PBs probably takes place such as it is published in yeasts, this might explain why 4E2 localizes to SGs specifically in heat stress

Aims of the thesis III: To search for the eIF4E2 interaction partners

- In the MS analysis of 4E2 immunoprecipitation, components of insulin-like growth factor signalling pathway, all the 13 eIF3 complex subunits, FMR complex, minimal RISC complex, proteins active in splicing, 3´UTR processing and members of SGs and PBs were found.
- In our hands, 4E2 does not bind the cap or eIF4GI, but immunoprecipitates eIF3, 4E-T,PABP, 4E-BP2 but not 4E-BP1.
- eIF3B can also immunoprecipitates 4E2 but to a minor extent in comparison with 4E2 mediated eIF3B immunoprecipitation
- eIF3B-4E2 interaction is not mRNA mediated

9 REFERENCES

1. Abdelfattah, N., S. Rajamanickam, et al. (2018). "MiR-584-5p potentiates vincristine and radiation response by inducing spindle defects and DNA damage in medulloblastoma." Nat Commun **9**(1): 4541.
2. Allen, M. L., A. M. Metz, et al. (1992). "Isolation and sequence of the cDNAs encoding the subunits of the isozyme form of wheat protein synthesis initiation factor 4F." J Biol Chem **267**(32): 23232-23236.
3. Altmann, M., P. P. Muller, et al. (1989). "A mammalian translation initiation factor can substitute for its yeast homologue in vivo." J Biol Chem **264**(21): 12145-12147.
4. Ameyar-Zazoua, M., C. Rachez, et al. (2012). "Argonaute proteins couple chromatin silencing to alternative splicing." Nature Structural & Molecular Biology **19**(10): 998-1004.
5. Amiri, A., B. D. Keiper, et al. (2001). "An isoform of eIF4E is a component of germ granules and is required for spermatogenesis in C. elegans." Development **128**(20): 3899-3912.
6. Anderson, P. and N. Kedersha (2008). "Stress granules: the Tao of RNA triage." Trends Biochem Sci **33**(3): 141-150.
7. Anderson, P. and N. Kedersha (2009). "RNA granules: post-transcriptional and epigenetic modulators of gene expression." Nat Rev Mol Cell Biol **10**(6): 430-436.
8. Anderson, P., N. Kedersha, et al. (2015). "Stress granules, P-bodies and cancer." Biochim Biophys Acta **1849**(7): 861-870.
9. Andrei, M. A., D. Ingelfinger, et al. (2005). "A role for eIF4E and eIF4E-transporter in targeting mRNPs to mammalian processing bodies." RNA **11**(5): 717-727.
10. Apicco, D. J., P. E. A. Ash, et al. (2018). "Reducing the RNA binding protein TIA1 protects against tau-mediated neurodegeneration in vivo." Nat Neurosci **21**(1): 72-80.
11. Aravind, L. and E. V. Koonin (2000). "Eukaryote-specific domains in translation initiation factors: implications for translation regulation and evolution of the translation system." Genome Res **10**(8): 1172-1184.
12. Assouline, S., B. Culjkovic, et al. (2009). "Molecular targeting of the oncogene eIF4E in acute myeloid leukemia (AML): a proof-of-principle clinical trial with ribavirin." Blood **114**(2): 257-260.
13. Aulas, A., M. M. Fay, et al. (2017). "Stress-specific differences in assembly and composition of stress granules and related foci." J Cell Sci **130**(5): 927-937.
14. Aulas, A. and C. Vande Velde (2015). "Alterations in stress granule dynamics driven by TDP-43 and FUS: a link to pathological inclusions in ALS?" Front Cell Neurosci **9**: 423.
15. Ayache, J., M. Benard, et al. (2015). "P-body assembly requires DDX6 repression complexes rather than decay or Ataxin2/2L complexes." Mol Biol Cell **26**(14): 2579-2595.
16. Baguet, A., S. Degot, et al. (2007). "The exon-junction-complex-component metastatic lymph node 51 functions in stress-granule assembly." J Cell Sci **120**(Pt 16): 2774-2784.
17. Banani, S. F., H. O. Lee, et al. (2017). "Biomolecular condensates: organizers of cellular biochemistry." Nat Rev Mol Cell Biol **18**(5): 285-298.

18. Bardoni, B., A. Schenck, et al. (1999). "A novel RNA-binding nuclear protein that interacts with the fragile X mental retardation (FMR1) protein." Hum Mol Genet **8**(13): 2557-2566.
19. Bastet, A., D. Zafirov, et al. (2019). "Mimicking natural polymorphism in eIF4E by CRISPR-Cas9 base editing is associated with resistance to potyviruses." Plant Biotechnol J **17**(9): 1736-1750.
20. Bell, M., S. Schreiner, et al. (2002). "p110, a novel human U6 snRNP protein and U4/U6 snRNP recycling factor." EMBO J **21**(11): 2724-2735.
21. Berlanga, J. J., S. Herrero, et al. (1998). "Characterization of the hemin-sensitive eukaryotic initiation factor 2alpha kinase from mouse nonerythroid cells." J Biol Chem **273**(48): 32340-32346.
22. Bhat, M., N. Robichaud, et al. (2015). "Targeting the translation machinery in cancer." Nat Rev Drug Discov **14**(4): 261-278.
23. Bhattacharyya, S. N., R. Habermacher, et al. (2006). "Stress-induced reversal of microRNA repression and mRNA P-body localization in human cells." Cold Spring Harb Symp Quant Biol **71**: 513-521.
24. Bolger, T. A., A. W. Folkmann, et al. (2008). "The mRNA export factor Gle1 and inositol hexakisphosphate regulate distinct stages of translation." Cell **134**(4): 624-633.
25. Bordeleau, M. E., A. Mori, et al. (2006). "Functional characterization of IRESes by an inhibitor of the RNA helicase eIF4A." Nat Chem Biol **2**(4): 213-220.
26. Bramham, C. R., K. B. Jensen, et al. (2016). "Tuning Specific Translation in Cancer Metastasis and Synaptic Memory: Control at the MNK-eIF4E Axis." Trends in Biochemical Sciences **41**(10): 847-858.
27. Brengues, M., D. Teixeira, et al. (2005). "Movement of eukaryotic mRNAs between polysomes and cytoplasmic processing bodies." Science **310**(5747): 486-489.
28. Brown, J. A., T. L. Roberts, et al. (2011). "A novel role for hSMG-1 in stress granule formation." Molecular and Cellular Biology **31**(22): 4417-4429.
29. Browning, K. S., S. R. Lax, et al. (1987). "Identification of two messenger RNA cap binding proteins in wheat germ. Evidence that the 28-kDa subunit of eIF-4B and the 26-kDa subunit of eIF-4F are antigenically distinct polypeptides." J Biol Chem **262**(23): 11228-11232.
30. Buchan, J. R. (2014). "mRNP granules. Assembly, function, and connections with disease." RNA Biol **11**(8): 1019-1030.
31. Buchan, J. R., R. M. Kolaitis, et al. (2013). "Eukaryotic stress granules are cleared by autophagy and Cdc48/VCP function." Cell **153**(7): 1461-1474.
32. Buchan, J. R., D. Muhlrad, et al. (2008). "P bodies promote stress granule assembly in Saccharomyces cerevisiae." J Cell Biol **183**(3): 441-455.
33. Buchan, J. R. and R. Parker (2009). "Eukaryotic stress granules: the ins and outs of translation." Mol Cell **36**(6): 932-941.
34. Camps, M., A. Nichols, et al. (1998). "Catalytic activation of the phosphatase MKP-3 by ERK2 mitogen-activated protein kinase." Science **280**(5367): 1262-1265.
35. Cargnello, M., J. Tcherkezian, et al. (2012). "Phosphorylation of the Eukaryotic Translation Initiation Factor 4E-Transporter (4E-T) by c-Jun N-Terminal Kinase Promotes Stress-Dependent P-Body Assembly." Mol Cell Biol **32**(22): 4572-4584.
36. Clemens, M. J. (2001). "Initiation factor eIF2 alpha phosphorylation in stress responses and apoptosis." Prog Mol Subcell Biol **27**: 57-89.

37. Cohen, N., M. Sharma, et al. (2001). "PML RING suppresses oncogenic transformation by reducing the affinity of eIF4E for mRNA." EMBO J **20**(16): 4547-4559.
38. Culjkovic, B., I. Topisirovic, et al. (2005). "eIF4E promotes nuclear export of cyclin D1 mRNAs via an element in the 3'UTR." J Cell Biol **169**(2): 245-256.
39. Damgaard, C. K. and J. Lykke-Andersen (2011). "Translational coregulation of 5'TOP mRNAs by TIA-1 and TIAR." Genes Dev **25**(19): 2057-2068.
40. Dang, Y., N. Kedersha, et al. (2006). "Eukaryotic initiation factor 2alpha-independent pathway of stress granule induction by the natural product pateamine A." J Biol Chem **281**(43): 32870-32878.
41. De Benedetti, A. and R. E. Rhoads (1990). "Overexpression of eukaryotic protein synthesis initiation factor 4E in HeLa cells results in aberrant growth and morphology." Proc Natl Acad Sci U S A **87**(21): 8212-8216.
42. De Leeuw, F., T. Zhang, et al. (2007). "The cold-inducible RNA-binding protein migrates from the nucleus to cytoplasmic stress granules by a methylation-dependent mechanism and acts as a translational repressor." Exp Cell Res **313**(20): 4130-4144.
43. De Rubeis, S. and C. Bagni (2010). "Fragile X mental retardation protein control of neuronal mRNA metabolism: Insights into mRNA stability." Mol Cell Neurosci **43**(1): 43-50.
44. Dhalia, R., C. R. S. Reis, et al. (2005). "Translation initiation in Leishmania major: characterisation of multiple eIF4F subunit homologues." Mol Biochem Parasitol **140**(1): 23-41.
45. Didiot, M. C., M. Subramanian, et al. (2009). "Cells lacking the fragile X mental retardation protein (FMRP) have normal RISC activity but exhibit altered stress granule assembly." Mol Biol Cell **20**(1): 428-437.
46. Dinkova, T. D., B. D. Keiper, et al. (2005). "Translation of a small subset of Caenorhabditis elegans mRNAs is dependent on a specific eukaryotic translation initiation factor 4E isoform." Molecular and Cellular Biology **25**(1): 100-113.
47. Ditlev, J. A., L. B. Case, et al. (2018). "Who's In and Who's Out-Compositional Control of Biomolecular Condensates." J Mol Biol **430**(23): 4666-4684.
48. Dong, S., Y. Wang, et al. (2011). "Specific and modular binding code for cytosine recognition in Pumilio/FBF (PUF) RNA-binding domains." J Biol Chem **286**(30): 26732-26742.
49. Dostie, J., M. Ferraiuolo, et al. (2000). "A novel shuttling protein, 4E-T, mediates the nuclear import of the mRNA 5' cap-binding protein, eIF4E." EMBO J **19**(12): 3142-3156.
50. Duffy, A. G., O. V. Makarova-Rusher, et al. (2016). "Modulation of tumor eIF4E by antisense inhibition: A phase I/II translational clinical trial of ISIS 183750-an antisense oligonucleotide against eIF4E-in combination with irinotecan in solid tumors and irinotecan-refractory colorectal cancer." Int J Cancer **139**(7): 1648-1657.
51. Duprat, A., C. Caranta, et al. (2002). "The Arabidopsis eukaryotic initiation factor (iso)4E is dispensable for plant growth but required for susceptibility to potyviruses." Plant J **32**(6): 927-934.
52. Emara, M. M., K. Fujimura, et al. (2012). "Hydrogen peroxide induces stress granule formation independent of eIF2alpha phosphorylation." Biochem Biophys Res Commun **423**(4): 763-769.
53. Evsikov, A. V. and C. Marin de Evsikova (2009). "Evolutionary origin and phylogenetic analysis of the novel oocyte-specific eukaryotic translation initiation factor 4E in Tetrapoda." Dev Genes Evol **219**(2): 111-118.

54. Fabian, M. R., M. K. Cieplak, et al. (2011). "miRNA-mediated deadenylation is orchestrated by GW182 through two conserved motifs that interact with CCR4-NOT." Nat Struct Mol Biol **18**(11): 1211-1217.
55. Ferraiuolo, M. A., S. Basak, et al. (2005). "A role for the eIF4E-binding protein 4E-T in P-body formation and mRNA decay." J Cell Biol **170**(6): 913-924.
56. Ferrero, P. V., C. Layana, et al. (2012). "Cap binding-independent recruitment of eIF4E to cytoplasmic foci." Biochim Biophys Acta **1823**(7): 1217-1224.
57. Ferretti, E., J. C. Villaescusa, et al. (2006). "Hypomorphic mutation of the TALE gene Prep1 (pKnox1) causes a major reduction of Pbx and Meis proteins and a pleiotropic embryonic phenotype." Molecular and Cellular Biology **26**(15): 5650-5662.
58. Fournier, M. J., L. Coudert, et al. (2013). "Inactivation of the mTORC1-eukaryotic translation initiation factor 4E pathway alters stress granule formation." Mol Cell Biol **33**(11): 2285-2301.
59. Franovic, A., C. E. Holterman, et al. (2009). "Human cancers converge at the HIF-2alpha oncogenic axis." Proc Natl Acad Sci U S A **106**(50): 21306-21311.
60. Freire E.R, M. M., Vashisht A.A., Zuberek J.,Saada E.A., Langousis G., Nascimento J.D.F., Moura D., Darzynkiewicz E., Hill K., de Melo Neto O.P., Wohlschlegel J.A., Sturm N.R., Campbell D.A. (2014). "*Trypanosoma brucei* Translation Initiaition Factor Homolog EIF4E6 Forms a Tripartite Cytosolic Complex with EIF4G5 and a capping Enzyme Homolog." Eukaryot Cell **13**(7): 896-908.
61. Freire, E. R., R. Dhalia, et al. (2011). "The four trypanosomatid eIF4E homologues fall into two separate groups, with distinct features in primary sequence and biological properties." Mol Biochem Parasitol **176**(1): 25-36.
62. Freire, E. R., D. M. N. Moura, et al. (2017). "Trypanosoma brucei EIF4E2 cap-binding protein binds a homolog of the histone-mRNA stem-loop-binding protein." Current Genetics **64**(4): 821-839.
63. Freire, E. R., A. A. Vashisht, et al. (2014). "eIF4F-like complexes formed by cap-binding homolog TbEIF4E5 with TbEIF4G1 or TbEIF4G2 are implicated in post-transcriptional regulation inTrypanosoma brucei." RNA **20**(8): 1272-1286.
64. Frydryskova, K., T. Masek, et al. (2016). "Distinct recruitment of human eIF4E isoforms to processing bodies and stress granules." BMC Mol Biol **17**(1): 21.
65. Fu, R., M. T. Olsen, et al. (2016). "Recruitment of the 4EHP-GYF2 cap-binding complex to tetraproline motifs of tristetraprolin promotes repression and degradation of mRNAs with AU-rich elements." RNA **22**(3): 373-382.
66. Fujimura, K., A. T. Sasaki, et al. (2012). "Selenite targets eIF4E-binding protein-1 to inhibit translation initiation and induce the assembly of non-canonical stress granules." Nucleic Acids Res **40**(16): 8099-8110.
67. Fukuyo, A., Y. In, et al. (2011). "Structural scaffold for eIF4E binding selectivity of 4E-BP isoforms: crystal structure of eIF4E binding region of 4E-BP2 and its comparison with that of 4E-BP1." J Pept Sci **17**(9): 650-657.
68. Gessert, S., V. Bugner, et al. (2010). "FMR1/FXR1 and the miRNA pathway are required for eye and neural crest development." Dev Biol **341**(1): 222-235.
69. Gilks, N., N. Kedersha, et al. (2004). "Stress granule assembly is mediated by prion-like aggregation of TIA-1." Mol Biol Cell **15**(12): 5383-5398.
70. Gingras, A. C., S. P. Gygi, et al. (1999). "Regulation of 4E-BP1 phosphorylation: a novel two-step mechanism." Genes Dev **13**(11): 1422-1437.

71. Gingras, A. C., S. G. Kennedy, et al. (1998). "4E-BP1, a repressor of mRNA translation, is phosphorylated and inactivated by the Akt(PKB) signaling pathway." Genes Dev **12**(4): 502-513.
72. Gingras, A. C., B. Raught, et al. (2001). "Hierarchical phosphorylation of the translation inhibitor 4E-BP1." Genes Dev **15**(21): 2852-2864.
73. Gingras, A. C., B. Raught, et al. (1999). "eIF4 initiation factors: effectors of mRNA recruitment to ribosomes and regulators of translation." Annu Rev Biochem **68**: 913-963.
74. Giovannone, B., E. Lee, et al. (2003). "Two novel proteins that are linked to insulin-like growth factor (IGF-I) receptors by the Grb10 adapter and modulate IGF-I signaling." J Biol Chem **278**(34): 31564-31573.
75. Giovannone, B., W. G. Tsiaras, et al. (2009). "GIGYF2 gene disruption in mice results in neurodegeneration and altered insulin-like growth factor signaling." Hum Mol Genet **18**(23): 4629-4639.
76. Green, K. M., A. E. Linsalata, et al. (2016). "RAN translation-What makes it run?" Brain Res **1647**: 30-42.
77. Grousl, T., P. Ivanov, et al. (2009). "Robust heat shock induces eIF2alpha-phosphorylation-independent assembly of stress granules containing eIF3 and 40S ribosomal subunits in budding yeast, Saccharomyces cerevisiae." J Cell Sci **122**(Pt 12): 2078-2088.
78. Grousl, T., M. Opekarova, et al. (2015). "Evolutionarily conserved 5'-3' exoribonuclease Xrn1 accumulates at plasma membrane-associated eisosomes in post-diauxic yeast." PLoS One **10**(3): e0122770.
79. Guzikowski, A. R., Y. S. Chen, et al. (2019). "Stress-induced mRNP granules: Form and function of processing bodies and stress granules." Wiley Interdiscip Rev RNA **10**(3): e1524.
80. Haimov, O., H. Sinvani, et al. (2015). "Cap-dependent, scanning-free translation initiation mechanisms." Biochim Biophys Acta **1849**(11): 1313-1318.
81. Hamada, T., M. Yako, et al. (2018). "Stress granule formation is induced by a threshold temperature rather than a temperature difference inArabidopsis." Journal of Cell Science **131**(16): jcs216051.
82. Harel-Sharvit, L., N. Eldad, et al. (2010). "RNA polymerase II subunits link transcription and mRNA decay to translation." Cell **143**(4): 552-563.
83. He, Y. and R. Smith (2009). "Nuclear functions of heterogeneous nuclear ribonucleoproteins A/B." Cell Mol Life Sci **66**(7): 1239-1256.
84. Hernandez, G., M. Altmann, et al. (2005). "Functional analysis of seven genes encoding eight translation initiation factor 4E (eIF4E) isoforms in Drosophila." Mech Dev **122**(4): 529-543.
85. Hernandez, G., H. Han, et al. (2012). "Eukaryotic initiation factor 4E-3 is essential for meiotic chromosome segregation, cytokinesis and male fertility in Drosophila." Development **139**(17): 3211-3220.
86. Hernandez, G., M. Miron, et al. (2013). "Mextli is a novel eukaryotic translation initiation factor 4E-binding protein that promotes translation in Drosophila melanogaster." Molecular and Cellular Biology **33**(15): 2854-2864.
87. Hernandez, G. and P. Vazquez-Pianzola (2005). "Functional diversity of the eukaryotic translation initiation factors belonging to eIF4 families." Mech Dev **122**(7-8): 865-876.
88. Hinnebusch, A. G. (2006). "eIF3: a versatile scaffold for translation initiation complexes." Trends Biochem Sci **31**(10): 553-562.

89. Ho, J. J., M. Wang, et al. (2016). "Systemic Reprogramming of Translation Efficiencies on Oxygen Stimulus." Cell Rep **14**(6): 1293-1300.
90. Houseley, J., J. LaCava, et al. (2006). "RNA-quality control by the exosome." Nat Rev Mol Cell Biol **7**(7): 529-539.
91. Hu, W., Y. Liu, et al. (2014). "Microarray meta-analysis of RNA-binding protein functions in alternative polyadenylation." PLoS One **9**(3): e90774.
92. Hubstenberger, A., M. Courel, et al. (2017). "P-Body Purification Reveals the Condensation of Repressed mRNA Regulons." Mol Cell **68**(1): 144-157 e145.
93. Humphreys, D. T., B. J. Westman, et al. (2005). "MicroRNAs control translation initiation by inhibiting eukaryotic initiation factor 4E/cap and poly(A) tail function." Proc Natl Acad Sci U S A **102**(47): 16961-16966.
94. Cha, J. D., H. J. Kim, et al. (2011). "Genetic alterations in oral squamous cell carcinoma progression detected by combining array-based comparative genomic hybridization and multiplex ligation-dependent probe amplification." Oral Surg Oral Med Oral Pathol Oral Radiol Endod **111**(5): 594-607.
95. Chalupnikova, K., P. Solc, et al. (2014). "An oocyte-specific ELAVL2 isoform is a translational repressor ablated from meiotically competent antral oocytes." Cell Cycle **13**(7): 1187-1200.
96. Chapat, C., S. M. Jafarnejad, et al. (2017). "Cap-binding protein 4EHP effects translation silencing by microRNAs." Proc Natl Acad Sci U S A **114**(21): 5425-5430.
97. Chasse, H., S. Boulben, et al. (2019). "Translational Control of Canonical and Non-Canonical Translation Initiation Factors at the Sea Urchin Egg to Embryo Transition." Int J Mol Sci **20**(3).
98. Chen, S. and G. Gao (2017). "MicroRNAs recruit eIF4E2 to repress translation of target mRNAs." Protein Cell **8**(10): 750-761.
99. Cherkasov, V., S. Hofmann, et al. (2013). "Coordination of translational control and protein homeostasis during severe heat stress." Curr Biol **23**(24): 2452-2462.
100. Chichester, L., A. T. Wylie, et al. (2015). "Muscle heat shock protein 70 predicts insulin resistance with aging." J Gerontol A Biol Sci Med Sci **70**(2): 155-162.
101. Cho, P. F., C. Gamberi, et al. (2006). "Cap-dependent translational inhibition establishes two opposing morphogen gradients in Drosophila embryos." Curr Biol **16**(20): 2035-2041.
102. Cho, P. F., F. Poulin, et al. (2005). "A new paradigm for translational control: inhibition via 5'-3' mRNA tethering by Bicoid and the eIF4E cognate 4EHP." Cell **121**(3): 411-423.
103. Isken, O., Y. K. Kim, et al. (2008). "Upf1 phosphorylation triggers translational repression during nonsense-mediated mRNA decay." Cell **133**(2): 314-327.
104. Jackson, R. J., C. U. Hellen, et al. (2010). "The mechanism of eukaryotic translation initiation and principles of its regulation." Nat Rev Mol Cell Biol **11**(2): 113-127.
105. Jafarnejad, S. M., C. Chapat, et al. (2018). "Translational control of ERK signaling through miRNA/4EHP-directed silencing." Elife **7**.
106. Jain, S., J. R. Wheeler, et al. (2016). "ATPase-Modulated Stress Granules Contain a Diverse Proteome and Substructure." Cell **164**(3): 487-498.
107. James, V., Y. Zhang, et al. (2010). "LIM-domain proteins, LIMD1, Ajuba, and WTIP are required for microRNA-mediated gene silencing." Proc Natl Acad Sci U S A **107**(28): 12499-12504.
108. Jayabalan, A. K., A. Sanchez, et al. (2016). "NEDDylation promotes stress granule assembly." Nat Commun **7**: 12125.

109. Jeong, S. J., S. Park, et al. (2019). "A threonyl-tRNA synthetase-mediated translation initiation machinery." Nat Commun **10**(1): 1357.
110. Jin, H., M. R. Suh, et al. (2009). "Human UPF1 participates in small RNA-induced mRNA downregulation." Molecular and Cellular Biology **29**(21): 5789-5799.
111. Joshi, B., A. Cameron, et al. (2004). "Characterization of mammalian eIF4E-family members." Eur J Biochem **271**(11): 2189-2203.
112. Joshi, B., K. Lee, et al. (2005). "Phylogenetic analysis of eIF4E-family members." BMC Evol Biol **5**: 48.
113. Joshi, B., J. Robalino, et al. (2002). "Yeast "knockout-and-rescue" system for identification of eIF4E-family members possessing eIF4E-activity." Biotechniques **33**(2): 392-393, 395-396, 398 passim.
114. Jung, M. Y., L. Lorenz, et al. (2006). "Translational control by neuroguidin, a eukaryotic initiation factor 4E and CPEB binding protein." Molecular and Cellular Biology **26**(11): 4277-4287.
115. Kanhoush, R., B. Beenders, et al. (2010). "Novel domains in the hnRNP G/RBMX protein with distinct roles in RNA binding and targeting nascent transcripts." Nucleus **1**(1): 109-122.
116. Kedersha, M. D. Panas, et al. (2016). "G3BP-Caprin1-USP10 complexes mediate stress granule condensation and associate with 40S subunits." J Cell Biol **212**(7): 845-860.
117. Kedersha, N., S. Chen, et al. (2002). "Evidence that ternary complex (eIF2-GTP-tRNA(i)(Met))-deficient preinitiation complexes are core constituents of mammalian stress granules." Mol Biol Cell **13**(1): 195-210.
118. Kedersha, N., M. R. Cho, et al. (2000). "Dynamic shuttling of TIA-1 accompanies the recruitment of mRNA to mammalian stress granules." J Cell Biol **151**(6): 1257-1268.
119. Kedersha, N., P. Ivanov, et al. (2013). "Stress granules and cell signaling: more than just a passing phase?" Trends Biochem Sci **38**(10): 494-506.
120. Kedersha, N., G. Stoecklin, et al. (2005). "Stress granules and processing bodies are dynamically linked sites of mRNP remodeling." J Cell Biol **169**(6): 871-884.
121. Kedersha, N. L., M. Gupta, et al. (1999). "RNA-binding proteins TIA-1 and TIAR link the phosphorylation of eIF-2 alpha to the assembly of mammalian stress granules." J Cell Biol **147**(7): 1431-1442.
122. Keiper, B. D., B. J. Lamphear, et al. (2000). "Functional characterization of five eIF4E isoforms in Caenorhabditis elegans." J Biol Chem **275**(14): 10590-10596.
123. Kelly, N. J., J. F. A. Varga, et al. (2018). "Hypoxia activates cadherin-22 synthesis via eIF4E2 to drive cancer cell migration, invasion and adhesion." Oncogene **37**(5): 651-662.
124. Kim, W. J., J. H. Kim, et al. (2007). "Anti-inflammatory lipid mediator 15d-PGJ2 inhibits translation through inactivation of eIF4A." EMBO J **26**(24): 5020-5032.
125. Klein, C., M. Terrao, et al. (2015). "Polysomes of Trypanosoma brucei: Association with Initiation Factors and RNA-Binding Proteins." PLoS One **10**(8): e0135973.
126. Kobayashi, T., S. Winslow, et al. (2012). "PKCalpha binds G3BP2 and regulates stress granule formation following cellular stress." PLoS One **7**(4): e35820.
127. Kong, J. and P. Lasko (2012). "Translational control in cellular and developmental processes." Nat Rev Genet **13**(6): 383-394.

128. Kramer, S., R. Queiroz, et al. (2008). "Heat shock causes a decrease in polysomes and the appearance of stress granules in trypanosomes independently of eIF2 phosphorylation at Thr169." Journal of Cell Science **121**(18): 3002-3014.
129. Kroschwald, S., S. Maharana, et al. (2015). "Promiscuous interactions and protein disaggregases determine the material state of stress-inducible RNP granules." Elife **4**: e06807.
130. Kubacka, D., A. Kamenska, et al. (2013). "Investigating the Consequences of eIF4E2 (4EHP) Interaction with 4E-Transporter on Its Cellular Distribution in HeLa Cells." PLoS One **8**(8): e72761.
131. Kwon, S., Y. Zhang, et al. (2007). "The deacetylase HDAC6 is a novel critical component of stress granules involved in the stress response." Genes Dev **21**(24): 3381-3394.
132. Lai, M. C., H. W. Kuo, et al. (2003). "A novel splicing regulator shares a nuclear import pathway with SR proteins." EMBO J **22**(6): 1359-1369.
133. Landon, A. L., P. A. Muniandy, et al. (2014). "MNKs act as a regulatory switch for eIF4E1 and eIF4E3 driven mRNA translation in DLBCL." Nat Commun **5**: 5413.
134. Landthaler, M., D. Gaidatzis, et al. (2008). "Molecular characterization of human Argonaute-containing ribonucleoprotein complexes and their bound target mRNAs." Rna **14**(12): 2580-2596.
135. Lavoie, C. A., P. E. Lachance, et al. (1996). "Alternatively spliced transcripts from the Drosophila eIF4E gene produce two different Cap-binding proteins." J Biol Chem **271**(27): 16393-16398.
136. Lee, A. S., P. J. Kranzusch, et al. (2016). "eIF3d is an mRNA cap-binding protein that is required for specialized translation initiation." Nature **536**(7614): 96-99.
137. Lee, H. C., H. Cho, et al. (2008). "Ectopic expression of eIF4E-transporter triggers the movement of eIF4E into P-bodies, inhibiting steady-state translation but not the pioneer round of translation." Biochem Biophys Res Commun **369**(4): 1160-1165.
138. Lejbkowicz, F., C. Goyer, et al. (1992). "A fraction of the mRNA 5' cap-binding protein, eukaryotic initiation factor 4E, localizes to the nucleus." Proc Natl Acad Sci U S A **89**(20): 9612-9616.
139. Lellis, A. D., K. D. Kasschau, et al. (2002). "Loss-of-susceptibility mutants of Arabidopsis thaliana reveal an essential role for eIF(iso)4E during potyvirus infection." Curr Biol **12**(12): 1046-1051.
140. Leppek, K., J. Schott, et al. (2013). "Roquin promotes constitutive mRNA decay via a conserved class of stem-loop recognition motifs." Cell **153**(4): 869-881.
141. Li, C. H., T. Ohn, et al. (2010). "eIF5A promotes translation elongation, polysome disassembly and stress granule assembly." PLoS One **5**(4): e9942.
142. Li, L. and C. C. Wang (2005). "Identification in the ancient protist Giardia lamblia of two eukaryotic translation initiation factor 4E homologues with distinctive functions." Eukaryot Cell **4**(5): 948-959.
143. Li, Y. R., O. D. King, et al. (2013). "Stress granules as crucibles of ALS pathogenesis." J Cell Biol **201**(3): 361-372.
144. Lin, J. C. and W. Y. Tarn (2009). "RNA-binding motif protein 4 translocates to cytoplasmic granules and suppresses translation via argonaute2 during muscle cell differentiation." J Biol Chem **284**(50): 34658-34665.
145. Lopez de Silanes, I., S. Galban, et al. (2005). "Identification and functional outcome of mRNAs associated with RNA-binding protein TIA-1." Molecular and Cellular Biology **25**(21): 9520-9531.

146. Loschi, M., C. C. Leishman, et al. (2009). "Dynein and kinesin regulate stress-granule and P-body dynamics." J Cell Sci **122**(Pt 21): 3973-3982.
147. Lu, L., A. P. Han, et al. (2001). "Translation initiation control by heme-regulated eukaryotic initiation factor 2alpha kinase in erythroid cells under cytoplasmic stresses." Mol Cell Biol **21**(23): 7971-7980.
148. Luo, Y., Z. Na, et al. (2018). "P-Bodies: Composition, Properties, and Functions." Biochemistry **57**(17): 2424-2431.
149. Mahboubi, H. and U. Stochaj (2017). "Cytoplasmic stress granules: Dynamic modulators of cell signaling and disease." Biochim Biophys Acta Mol Basis Dis **1863**(4): 884-895.
150. Marcotrigiano, J., A. C. Gingras, et al. (1999). "Cap-dependent translation initiation in eukaryotes is regulated by a molecular mimic of eIF4G." Mol Cell **3**(6): 707-716.
151. Markmiller, S., A. Fulzele, et al. (2019). "Active Protein Neddylation or Ubiquitylation Is Dispensable for Stress Granule Dynamics." Cell Rep **27**(5): 1356-1363 e1353.
152. Markmiller, S., S. Soltanieh, et al. (2018). "Context-Dependent and Disease-Specific Diversity in Protein Interactions within Stress Granules." Cell **172**(3): 590-604 e513.
153. Martin, K. C. and A. Ephrussi (2009). "mRNA localization: gene expression in the spatial dimension." Cell **136**(4): 719-730.
154. Masutani, M., N. Sonenberg, et al. (2007). "Reconstitution reveals the functional core of mammalian eIF3." EMBO J **26**(14): 3373-3383.
155. Mateju, D., T. M. Franzmann, et al. (2017). "An aberrant phase transition of stress granules triggered by misfolded protein and prevented by chaperone function." EMBO J **36**(12): 1669-1687.
156. Mathonnet, G., M. R. Fabian, et al. (2007). "MicroRNA inhibition of translation initiation in vitro by targeting the cap-binding complex eIF4F." Science **317**(5845): 1764-1767.
157. Matsuo, H., H. Li, et al. (1997). "Structure of translation factor eIF4E bound to m7GDP and interaction with 4E-binding protein." Nat Struct Biol **4**(9): 717-724.
158. Maurin, T., S. Zongaro, et al. (2014). "Fragile X Syndrome: from molecular pathology to therapy." Neurosci Biobehav Rev **46 Pt 2**: 242-255.
159. Mazier, M., F. Flamain, et al. (2011). "Knock-Down of Both eIF4E1 and eIF4E2 Genes Confers Broad-Spectrum Resistance against Potyviruses in Tomato." PLoS One **6**(12).
160. Meister, G. (2013). "Argonaute proteins: functional insights and emerging roles." Nat Rev Genet **14**(7): 447-459.
161. Melanson, G., S. Timpano, et al. (2017). "The eIF4E2-Directed Hypoxic Cap-Dependent Translation Machinery Reveals Novel Therapeutic Potential for Cancer Treatment." Oxidative Medicine and Cellular Longevity.
162. Menon, R. P., T. J. Gibson, et al. (2004). "The C terminus of fragile X mental retardation protein interacts with the multi-domain Ran-binding protein in the microtubule-organising centre." J Mol Biol **343**(1): 43-53.
163. Metz, A. M., R. T. Timmer, et al. (1992). "Isolation and sequence of a cDNA encoding the cap binding protein of wheat eukaryotic protein synthesis initiation factor 4F." Nucleic Acids Res **20**(15): 4096.
164. Mientjes, E. J., R. Willemsen, et al. (2004). "Fxr1 knockout mice show a striated muscle phenotype: implications for Fxr1p function in vivo." Hum Mol Genet **13**(13): 1291-1302.

165. Mieulet, V. and R. F. Lamb (2008). "Shooting the messenger: CULLIN' insulin signaling with Fbw8." Dev Cell **14**(6): 816-817.
166. Miles, W. O., K. Tschop, et al. (2012). "Pumilio facilitates miRNA regulation of the E2F3 oncogene." Genes Dev **26**(4): 356-368.
167. Minshall, N., M. H. Reiter, et al. (2007). "CPEB interacts with an ovary-specific eIF4E and 4E-T in early Xenopus oocytes." J Biol Chem **282**(52): 37389-37401.
168. Moens, C. B. and L. Selleri (2006). "Hox cofactors in vertebrate development." Dev Biol **291**(2): 193-206.
169. Mokas, S., J. R. Mills, et al. (2009). "Uncoupling stress granule assembly and translation initiation inhibition." Mol Biol Cell **20**(11): 2673-2683.
170. Mollet, S., N. Cougot, et al. (2008). "Translationally repressed mRNA transiently cycles through stress granules during stress." Mol Biol Cell **19**(10): 4469-4479.
171. Morales, J., O. Mulner-Lorillon, et al. (2006). "Translational control genes in the sea urchin genome." Dev Biol **300**(1): 293-307.
172. Morita, M., L. W. Ler, et al. (2012). "A Novel 4EHP-GIGYF2 Translational Repressor Complex Is Essential for Mammalian Development." Molecular and Cellular Biology **32**(17): 3585-3593.
173. Mrvova, S., K. Frydryskova, et al. (2018). "Major splice variants and multiple polyadenylation site utilization in mRNAs encoding human translation initiation factors eIF4E1 and eIF4E3 regulate the translational regulators?" Mol Genet Genomics **293**(1): 167-186.
174. Nakamoto, M. (2005). "Physiological identification of human transcripts translationally regulated by a specific microRNA." Hum Mol Genet **14**(24): 3813-3821.
175. Nakamura, A., K. Sato, et al. (2004). "Drosophila cup is an eIF4E binding protein that associates with Bruno and regulates oskar mRNA translation in oogenesis." Dev Cell **6**(1): 69-78.
176. Napoli, I., V. Mercaldo, et al. (2008). "The fragile X syndrome protein represses activity-dependent translation through CYFIP1, a new 4E-BP." Cell **134**(6): 1042-1054.
177. Nelson, M. R., A. M. Leidal, et al. (2004). "Drosophila Cup is an eIF4E-binding protein that functions in Smaug-mediated translational repression." EMBO J **23**(1): 150-159.
178. Nicaise, V., S. German-Retana, et al. (2003). "The Eukaryotic Translation Initiation Factor 4E Controls Lettuce Susceptibility to the Potyvirus Lettuce mosaic virus1." Plant Physiol **132**(3): 1272-1282.
179. Niessing, D., S. Blanke, et al. (2002). "Bicoid associates with the 5'-cap-bound complex of caudal mRNA and represses translation." Genes Dev **16**(19): 2576-2582.
180. Nikolakaki, E., R. Kohen, et al. (2001). "Cloning and characterization of an alternatively spliced form of SR protein kinase 1 that interacts specifically with scaffold attachment factor-B." J Biol Chem **276**(43): 40175-40182.
181. Nishimura, T., Z. Padamsi, et al. (2015). "The eIF4E-Binding Protein 4E-T Is a Component of the mRNA Decay Machinery that Bridges the 5' and 3' Termini of Target mRNAs." Cell Rep **11**(9): 1425-1436.
182. Nover, L., K. D. Scharf, et al. (1983). "Formation of cytoplasmic heat shock granules in tomato cell cultures and leaves." Molecular and Cellular Biology **3**(9): 1648-1655.

183. Ohn, T., N. Kedersha, et al. (2008). "A functional RNAi screen links O-GlcNAc modification of ribosomal proteins to stress granule and processing body assembly." Nat Cell Biol **10**(10): 1224-1231.
184. Okumura, F., W. Zou, et al. (2007). "ISG15 modification of the eIF4E cognate 4EHP enhances cap structure-binding activity of 4EHP." Genes Dev **21**(3): 255-260.
185. Olsen, D. S., B. Jordan, et al. (1998). "Isolation of the gene encoding the Drosophila melanogaster homolog of the Saccharomyces cerevisiae GCN2 eIF-2alpha kinase." Genetics **149**(3): 1495-1509.
186. Osborne, M. J., L. Volpon, et al. (2013). "eIF4E3 acts as a tumor suppressor by utilizing an atypical mode of methyl-7-guanosine cap recognition." Proc Natl Acad Sci U S A **110**(10): 3877-3882.
187. Ou, H. L., C. S. Kim, et al. (2019). "Somatic Niche Cells Regulate the CEP-1/p53-Mediated DNA Damage Response in Primordial Germ Cells." Dev Cell **50**(2): 167-183 e168.
188. Ozgur, S., J. Basquin, et al. (2015). "Structure of a Human 4E-T/DDX6/CNOT1 Complex Reveals the Different Interplay of DDX6-Binding Proteins with the CCR4-NOT Complex." Cell Rep **13**(4): 703-711.
189. Pan, Q., O. Shai, et al. (2008). "Deep surveying of alternative splicing complexity in the human transcriptome by high-throughput sequencing." Nat Genet **40**(12): 1413-1415.
190. Pariani, M. J., A. Spencer, et al. (2009). "A 785kb deletion of 3p14.1p13, including the FOXP1 gene, associated with speech delay, contractures, hypertonia and blepharophimosis." Eur J Med Genet **52**(2-3): 123-127.
191. Pause, A., G. J. Belsham, et al. (1994). "Insulin-dependent stimulation of protein synthesis by phosphorylation of a regulator of 5'-cap function." Nature **371**(6500): 762-767.
192. Pereira, M. M., A. M. Malvezzi, et al. (2013). "The eIF4E subunits of two distinct trypanosomatid eIF4F complexes are subjected to differential post-translational modifications associated to distinct growth phases in culture." Mol Biochem Parasitol **190**(2): 82-86.
193. Peter, D., V. Ruscica, et al. (2019). "Molecular basis for GIGYF-Me31B complex assembly in 4EHP-mediated translational repression." Genes Dev.
194. Peter, D., R. Weber, et al. (2015). "Mextli proteins use both canonical bipartite and novel tripartite binding modes to form eIF4E complexes that display differential sensitivity to 4E-BP regulation." Genes Dev **29**(17): 1835-1849.
195. Peter, D., R. Weber, et al. (2017). "GIGYF1/2 proteins use auxiliary sequences to selectively bind to 4EHP and repress target mRNA expression." Genes Dev **31**(11): 1147-1161.
196. Pillai, R. S., S. N. Bhattacharyya, et al. (2005). "Inhibition of translational initiation by Let-7 MicroRNA in human cells." Science **309**(5740): 1573-1576.
197. Pincheira, R., Q. Chen, et al. (2001). "Two subcellular localizations of eIF3 p170 and its interaction with membrane-bound microfilaments: implications for alternative functions of p170." Eur J Cell Biol **80**(6): 410-418.
198. Pisarev, A. V., C. U. Hellen, et al. (2007). "Recycling of eukaryotic posttermination ribosomal complexes." Cell **131**(2): 286-299.
199. Poulin, F., A. C. Gingras, et al. (1998). "4E-BP3, a new member of the eukaryotic initiation factor 4E-binding protein family." J Biol Chem **273**(22): 14002-14007.
200. Pratt, A. J. and I. J. MacRae (2009). "The RNA-induced silencing complex: a versatile gene-silencing machine." J Biol Chem **284**(27): 17897-17901.

201. Protter, D. S. and R. Parker (2016). "Principles and Properties of Stress Granules." Trends Cell Biol **26**(9): 668-679.
202. Ptushkina, M., K. Berthelot, et al. (2001). "A second eIF4E protein in Schizosaccharomyces pombe has distinct eIF4G-binding properties." Nucleic Acids Res **29**(22): 4561-4569.
203. Ptushkina, M., N. Malys, et al. (2004). "eIF4E isoform 2 in Schizosaccharomyces pombe is a novel stress-response factor." EMBO Rep **5**(3): 311-316.
204. Ptushkina, M., T. von der Haar, et al. (1999). "Repressor binding to a dorsal regulatory site traps human eIF4E in a high cap-affinity state." EMBO J **18**(14): 4068-4075.
205. Ptushkina, M., T. von der Haar, et al. (1998). "Cooperative modulation by eIF4G of eIF4E-binding to the mRNA 5' cap in yeast involves a site partially shared by p20." EMBO J **17**(16): 4798-4808.
206. Pyronnet, S., H. Imataka, et al. (1999). "Human eukaryotic translation initiation factor 4G (eIF4G) recruits mnk1 to phosphorylate eIF4E." EMBO J **18**(1): 270-279.
207. Qi, N. N., S. Tian, et al. (2019). "Up-regulation of microRNA-496 suppresses proliferation, invasion, migration and in vivo tumorigenicity of human osteosarcoma cells by targeting eIF4E." Biochimie.
208. Querol-Audi, J., C. Sun, et al. (2013). "Architecture of human translation initiation factor 3." Structure **21**(6): 920-928.
209. Ramaswami, M., J. P. Taylor, et al. (2013). "Altered ribostasis: RNA-protein granules in degenerative disorders." Cell **154**(4): 727-736.
210. Ramaswamy, S., K. N. Ross, et al. (2003). "A molecular signature of metastasis in primary solid tumors." Nat Genet **33**(1): 49-54.
211. Raoult, D., S. Audic, et al. (2004). "The 1.2-megabase genome sequence of Mimivirus." Science **306**(5700): 1344-1350.
212. Reyes, R. and J. M. Izquierdo (2008). "Half pint couples transcription and splicing of eIF4E-1,2 gene during fly development." Biochem Biophys Res Commun **374**(4): 758-762.
213. Richter, J. D. and N. Sonenberg (2005). "Regulation of cap-dependent translation by eIF4E inhibitory proteins." Nature **433**(7025): 477-480.
214. Riz, I., T. S. Hawley, et al. (2016). "Noncanonical SQSTM1/p62-Nrf2 pathway activation mediates proteasome inhibitor resistance in multiple myeloma cells via redox, metabolic and translational reprogramming." Oncotarget.
215. Robalino, J., B. Joshi, et al. (2004). "Two zebrafish eIF4E family members are differentially expressed and functionally divergent." J Biol Chem **279**(11): 10532-10541.
216. Rodriguez, C. M., M. A. Freire, et al. (1998). "The Arabidopsis thaliana cDNAs coding for eIF4E and eIF(iso)4E are not functionally equivalent for yeast complementation and are differentially expressed during plant development." Plant J **13**(4): 465-473.
217. Rom, E., H. C. Kim, et al. (1998). "Cloning and characterization of 4EHP, a novel mammalian eIF4E-related cap-binding protein." J Biol Chem **273**(21): 13104-13109.
218. Rosettani, P., S. Knapp, et al. (2007). "Structures of the human eIF4E homologous protein, h4EHP, in its m7GTP-bound and unliganded forms." J Mol Biol **368**(3): 691-705.
219. Rousseau, D., R. Kaspar, et al. (1996). "Translation initiation of ornithine decarboxylase and nucleocytoplasmic transport of cyclin D1 mRNA are increased in

cells overexpressing eukaryotic initiation factor 4E." Proc Natl Acad Sci U S A **93**(3): 1065-1070.
220. Rouya, C., N. Siddiqui, et al. (2014). "Human DDX6 effects miRNA-mediated gene silencing via direct binding to CNOT1." RNA **20**(9): 1398-1409.
221. Ruud, K. A., C. Kuhlow, et al. (1998). "Identification and characterization of a novel cap-binding protein from Arabidopsis thaliana." J Biol Chem **273**(17): 10325-10330.
222. Ryan, P. D. and P. E. Goss (2008). "The emerging role of the insulin-like growth factor pathway as a therapeutic target in cancer." Oncologist **13**(1): 16-24.
223. Saghir, A. N., W. J. Tuxworth, Jr., et al. (2001). "Modifications of eukaryotic initiation factor 4F (eIF4F) in adult cardiocytes by adenoviral gene transfer: differential effects on eIF4F activity and total protein synthesis rates." Biochem J **356**(Pt 2): 557-566.
224. Sama, R. R., C. L. Ward, et al. (2013). "FUS/TLS assembles into stress granules and is a prosurvival factor during hyperosmolar stress." J Cell Physiol **228**(11): 2222-2231.
225. Sgorbissa, A. and C. Brancolini (2012). "IFNs, ISGylation and cancer: Cui prodest?" Cytokine Growth Factor Rev **23**(6): 307-314.
226. Shaner, N. C., P. A. Steinbach, et al. (2005). "A guide to choosing fluorescent proteins." Nat Methods **2**(12): 905-909.
227. Shi, Y., K. M. Vattem, et al. (1998). "Identification and characterization of pancreatic eukaryotic initiation factor 2 alpha-subunit kinase, PEK, involved in translational control." Molecular and Cellular Biology **18**(12): 7499-7509.
228. Shirokikh, N. E. and T. Preiss (2018). "Translation initiation by cap-dependent ribosome recruitment: Recent insights and open questions." Wiley Interdisciplinary Reviews: RNA **9**(4): e1473.
229. Scheper, G. C., J. L. Parra, et al. (2003). "The N and C termini of the splice variants of the human mitogen-activated protein kinase-interacting kinase Mnk2 determine activity and localization." Molecular and Cellular Biology **23**(16): 5692-5705.
230. Schwanhausser, B., D. Busse, et al. (2011). "Global quantification of mammalian gene expression control." Nature **473**(7347): 337-342.
231. Smith, M. D., L. Arake-Tacca, et al. (2016). "Assembly of eIF3 Mediated by Mutually Dependent Subunit Insertion." Structure **24**(6): 886-896.
232. Soares, R. J., S. Cagnin, et al. (2014). "Involvement of microRNAs in the regulation of muscle wasting during catabolic conditions." J Biol Chem **289**(32): 21909-21925.
233. Sonenberg, N. and A. C. Gingras (1998). "The mRNA 5' cap-binding protein eIF4E and control of cell growth." Curr Opin Cell Biol **10**(2): 268-275.
234. Song, A., S. Labella, et al. (2010). "A C. elegans eIF4E-family member upregulates translation at elevated temperatures of mRNAs encoding MSH-5 and other meiotic crossover proteins." J Cell Sci **123**(Pt 13): 2228-2237.
235. Souquere, S., S. Mollet, et al. (2009). "Unravelling the ultrastructure of stress granules and associated P-bodies in human cells." J Cell Sci **122**(Pt 20): 3619-3626.
236. Spilka, R., C. Ernst, et al. (2013). "Eukaryotic translation initiation factors in cancer development and progression." Cancer Lett **340**(1): 9-21.
237. Standart, N. and D. Weil (2018). "P-Bodies: Cytosolic Droplets for Coordinated mRNA Storage." Trends Genet **34**(8): 612-626.
238. Stoecklin, G. and N. Kedersha (2013). "Relationship of GW/P-bodies with stress granules." Adv Exp Med Biol **768**: 197-211.

239. Sudhakaran, I. P., J. Hillebrand, et al. (2014). "FMRP and Ataxin-2 function together in long-term olfactory habituation and neuronal translational control." Proc Natl Acad Sci U S A **111**(1): E99-E108.
240. Sukarieh, R., N. Sonenberg, et al. (2009). "The eIF4E-binding proteins are modifiers of cytoplasmic eIF4E relocalization during the heat shock response." Am J Physiol Cell Physiol **296**(5): C1207-1217.
241. Suzuki, Y., M. Minami, et al. (2009). "The Hsp90 inhibitor geldanamycin abrogates colocalization of eIF4E and eIF4E-transporter into stress granules and association of eIF4E with eIF4G." J Biol Chem **284**(51): 35597-35604.
242. Syntichaki, P., K. Troulinaki, et al. (2007). "eIF4E function in somatic cells modulates ageing in Caenorhabditis elegans." Nature **445**(7130): 922-926.
243. Takata, M., W. Ogawa, et al. (1999). "Requirement for Akt (protein kinase B) in insulin-induced activation of glycogen synthase and phosphorylation of 4E-BP1 (PHAS-1)." J Biol Chem **274**(29): 20611-20618.
244. Talior-Volodarsky, I., V. K. Randhawa, et al. (2008). "Alpha-actinin-4 is selectively required for insulin-induced GLUT4 translocation." J Biol Chem **283**(37): 25115-25123.
245. Tamanini, F., C. Bontekoe, et al. (1999). "Different targets for the fragile X-related proteins revealed by their distinct nuclear localizations." Hum Mol Genet **8**(5): 863-869.
246. Tamanini, F., R. Willemsen, et al. (1997). "Differential expression of FMR1, FXR1 and FXR2 proteins in human brain and testis." Hum Mol Genet **6**(8): 1315-1322.
247. Tan, N. G. S., H. C. Ardley, et al. (2003). "Human homologue of ariadne promotes the ubiquitylation of translation initiation factor 4E homologous protein, 4EHP." FEBS Letters **554**(3): 501-504.
248. Taniuchi, S., M. Miyake, et al. (2016). "Integrated stress response of vertebrates is regulated by four eIF2alpha kinases." Sci Rep **6**: 32886.
249. Tao, X. and G. Gao (2015). "Tristetraprolin Recruits Eukaryotic Initiation Factor 4E2 To Repress Translation of AU-Rich Element-Containing mRNAs." Molecular and Cellular Biology **35**(22): 3921-3932.
250. Tee, A. R., J. A. Tee, et al. (2004). "Characterizing the interaction of the mammalian eIF4E-related protein 4EHP with 4E-BP1." FEBS Lett **564**(1-2): 58-62.
251. Thevenon, J., N. Monnier, et al. (2014). "Delineation of the 3p14.1p13 microdeletion associated with syndromic distal limb contractures." Am J Med Genet A **164A**(12): 3027-3034.
252. Tcherkezian, J., P. A. Brittis, et al. (2010). "Transmembrane receptor DCC associates with protein synthesis machinery and regulates translation." Cell **141**(4): 632-644.
253. Timpano, S. and J. Uniacke (2016). "Human Cells Cultured under Physiological Oxygen Utilize Two Cap-binding Proteins to recruit Distinct mRNAs for Translation." J Biol Chem **291**(20): 10772-10782.
254. Tomecki, R., M. S. Kristiansen, et al. (2010). "The human core exosome interacts with differentially localized processive RNases: hDIS3 and hDIS3L." EMBO J **29**(14): 2342-2357.
255. Topisirovic, I. and K. L. Borden (2005). "Homeodomain proteins and eukaryotic translation initiation factor 4E (eIF4E): an unexpected relationship." Histol Histopathol **20**(4): 1275-1284.

256. Topisirovic, I., B. Culjkovic, et al. (2003). "The proline-rich homeodomain protein, PRH, is a tissue-specific inhibitor of eIF4E-dependent cyclin D1 mRNA transport and growth." EMBO J **22**(3): 689-703.
257. Tourriere, H., K. Chebli, et al. (2003). "The RasGAP-associated endoribonuclease G3BP assembles stress granules." J Cell Biol **160**(6): 823-831.
258. Truitt, M. L., C. S. Conn, et al. (2015). "Differential Requirements for eIF4E Dose in Normal Development and Cancer." Cell **162**(1): 59-71.
259. Uhlen, M., L. Fagerberg, et al. (2015). "Proteomics. Tissue-based map of the human proteome." Science **347**(6220): 1260419.
260. Uniacke, J., C. E. Holterman, et al. (2012). "An oxygen-regulated switch in the protein synthesis machinery." Nature **486**(7401): 126-129.
261. Uniacke, J., J. K. Perera, et al. (2014). "Cancer cells exploit eIF4E2-directed synthesis of hypoxia response proteins to drive tumor progression." Cancer Research **74**(5): 1379-1389.
262. Valasek, L. S. (2012). "'Ribozoomin'--translation initiation from the perspective of the ribosome-bound eukaryotic initiation factors (eIFs)." Curr Protein Pept Sci **13**(4): 305-330.
263. Valzania, L., H. Ono, et al. (2016). "Drosophila 4EHP is essential for the larval-pupal transition and required in the prothoracic gland for ecdysone biosynthesis." Dev Biol **410**(1): 14-23.
264. Van Etten, J., T. L. Schagat, et al. (2012). "Human Pumilio proteins recruit multiple deadenylases to efficiently repress messenger RNAs." J Biol Chem **287**(43): 36370-36383.
265. van Heugten, H. A., A. A. Thomas, et al. (1992). "Interaction of protein synthesis initiation factors with the mRNA cap structure." Biochimie **74**(5): 463-475.
266. Vasilescu, S., M. Ptushkina, et al. (1996). "Mutants of eukaryotic initiation factor eIF-4E with altered mRNA cap binding specificity reprogram mRNA selection by ribosomes in Saccharomyces cerevisiae." J Biol Chem **271**(12): 7030-7037.
267. Vasudevan, S., Y. Tong, et al. (2007). "Switching from repression to activation: microRNAs can up-regulate translation." Science **318**(5858): 1931-1934.
268. Villa, N., A. Do, et al. (2013). "Human eukaryotic initiation factor 4G (eIF4G) protein binds to eIF3c, -d, and -e to promote mRNA recruitment to the ribosome." J Biol Chem **288**(46): 32932-32940.
269. Villaescusa, J. C., C. Buratti, et al. (2009). "Cytoplasmic Prep1 interacts with 4EHP inhibiting Hoxb4 translation." PLoS One **4**(4): e5213.
270. Volpon, L., M. J. Osborne, et al. (2013). "eIF4E3, a new actor in mRNA metabolism and tumor suppression." Cell Cycle **12**(8): 1159-1160.
271. von Stechow, L., D. Typas, et al. (2015). "The E3 ubiquitin ligase ARIH1 protects against genotoxic stress by initiating a 4EHP-mediated mRNA translation arrest." Molecular and Cellular Biology **35**(7): 1254-1268.
272. Wagner, S., A. Herrmannova, et al. (2014). "Functional and biochemical characterization of human eukaryotic translation initiation factor 3 in living cells." Molecular and Cellular Biology **34**(16): 3041-3052.
273. Wakiyama, M., M. Saigoh, et al. (1995). "mRNA encoding the translation initiation factor eIF-4E is expressed early in Xenopus embryogenesis." FEBS Lett **360**(2): 191-193.
274. Wang, E. T., R. Sandberg, et al. (2008). "Alternative isoform regulation in human tissue transcriptomes." Nature **456**(7221): 470-476.

275. Wang, X., W. Li, et al. (2003). "The C terminus of initiation factor 4E-binding protein 1 contains multiple regulatory features that influence its function and phosphorylation." Mol Cell Biol **23**(5): 1546-1557.
276. Waris, S., M. C. Wilce, et al. (2014). "RNA recognition and stress granule formation by TIA proteins." Int J Mol Sci **15**(12): 23377-23388.
277. Weidmann, C. A. and A. C. Goldstrohm (2012). "Drosophila Pumilio protein contains multiple autonomous repression domains that regulate mRNAs independently of Nanos and brain tumor." Molecular and Cellular Biology **32**(2): 527-540.
278. Wheeler, J. R., T. Matheny, et al. (2016). "Distinct stages in stress granule assembly and disassembly." Elife **5**.
279. Widberg, C. H., N. J. Bryant, et al. (2003). "Tomosyn interacts with the t-SNAREs syntaxin4 and SNAP23 and plays a role in insulin-stimulated GLUT4 translocation." J Biol Chem **278**(37): 35093-35101.
280. Will, C. L. and R. Luhrmann (2011). "Spliceosome structure and function." Cold Spring Harb Perspect Biol **3**(7).
281. Williams, B. R. (1997). "Role of the double-stranded RNA-activated protein kinase (PKR) in cell regulation." Biochem Soc Trans **25**(2): 509-513.
282. Wu, L., J. Fan, et al. (2008). "Importance of translation and nonnucleolytic ago proteins for on-target RNA interference." Curr Biol **18**(17): 1327-1332.
283. Wu, R., X. Zheng, et al. (2018). "Micro RNA-1298 opposes the effects of chronic oxidative stress on human trabecular meshwork cells via targeting on EIF4E3." Biomed Pharmacother **100**: 349-357.
284. Xie, X., S. Matsumoto, et al. (2018). "Deubiquitylases USP5 and USP13 are recruited to and regulate heat-induced stress granules through their deubiquitylating activities." J Cell Sci **131**(8).
285. Yang, R., D. J. Weber, et al. (2006). "Post-transcriptional regulation of thioredoxin by the stress inducible heterogenous ribonucleoprotein A18." Nucleic Acids Res **34**(4): 1224-1236.
286. Yarunin, A., R. E. Harris, et al. (2011). "Patterning of the Drosophila oocyte by a sequential translation repression program involving the d4EHP and Belle translational repressors." RNA Biol **8**(5): 904-912.
287. Yi, T., E. Papadopoulos, et al. (2013). "Hypoxia-inducible factor-1alpha (HIF-1alpha) promotes cap-dependent translation of selective mRNAs through up-regulating initiation factor eIF4E1 in breast cancer cells under hypoxia conditions." J Biol Chem **288**(26): 18732-18742.
288. Youn, J. Y., W. H. Dunham, et al. (2018). "High-Density Proximity Mapping Reveals the Subcellular Organization of mRNA-Associated Granules and Bodies." Mol Cell **69**(3): 517-532 e511.
289. Zappavigna, V., F. Piccioni, et al. (2004). "Cup is a nucleocytoplasmic shuttling protein that interacts with the eukaryotic translation initiation factor 4E to modulate Drosophila ovary development." Proc Natl Acad Sci U S A **101**(41): 14800-14805.
290. Zhang, P., B. Fan, et al. (2019). "Chronic optogenetic induction of stress granules is cytotoxic and reveals the evolution of ALS-FTD pathology." Elife **8**.
291. Zhang, Y., J. P. O'Connor, et al. (1995). "The fragile X mental retardation syndrome protein interacts with novel homologs FXR1 and FXR2." EMBO J **14**(21): 5358-5366.
292. Zhou, M., A. M. Sandercock, et al. (2008). "Mass spectrometry reveals modularity and a complete subunit interaction map of the eukaryotic translation factor eIF3." Proc Natl Acad Sci U S A **105**(47): 18139-18144.

293. Zhu, X., C. Buhrer, et al. (2016). "Cold-inducible proteins CIRP and RBM3, a unique couple with activities far beyond the cold." Cell Mol Life Sci **73**(20): 3839-3859.
294. Zonta, E., D. Bittencourt, et al. (2013). "The RNA helicase DDX5/p68 is a key factor promoting c-fos expression at different levels from transcription to mRNA export." Nucleic Acids Res **41**(1): 554-564.
295. Zuberek, J., D. Kubacka, et al. (2007). "Weak binding affinity of human 4EHP for mRNA cap analogs." RNA **13**(5): 691-697.
296. Zuberek, J., K. Kuchta, et al. (2016). "Diverse cap-binding properties of Drosophila eIF4E isoforms." Biochim Biophys Acta **1864**(10): 1292-1303.
297. Zuberek, J. and A. Stelmachowska (2017). "Tryptophan Residues from Cap Binding Slot in eIF4E Family Members: Their Contributions to Near-UV Circular Dichroism Spectra." Journal of Physical Chemistry & Biophysics **07**(02).

10 APPENDIX

10.1 Mass spectrometry analysis

Table 20 Original MS results from the EMBL service

Gene name	Accession Number	Molecular Weight	Ctrl	GFP4E2_IP
EIF4E2	EMBOSS001	57 kDa	10	288
GIGYF1	***PERQ1_HUMAN***	***115 kDa***		***62***
EIF4ENIF1	***sp|Q9NRA8|4E-T_HUMAN***	***108 kDa***		***52***
IRS4	IRS4_HUMAN	134 kDa		51
HSPA2	HSP72_HUMAN	70 kDa		21
TARS	B4DEG8_HUMAN	87 kDa		19
PRRC2B	sp|Q5JSZ5|PRC2B_HUMAN	243 kDa		18
CUL7	F5H0L1_HUMAN	200 kDa		17
ACTN4	ACTN4_HUMAN	105 kDa		15
PATL1	sp|Q86TB9|PATL1_HUMAN	87 kDa		15
ELAVL2	sp|Q12926-2|ELAV2_HUMAN	38 kDa		9
EIF3G	EIF3G_HUMAN	36 kDa		7
SNAP23	H3BM38_HUMAN	14 kDa		4
SSBP1	C9K0U8_HUMAN	14 kDa		4
EIF4EBP2	***4EBP2_HUMAN***	***13 kDa***		***4***
GLIPR2	GAPR1_HUMAN	17 kDa		4
GIGYF2	***sp|Q6Y7W6|PERQ2_HUMAN***	***150 kDa***	***3***	***152***
ZNF598	**sp|Q86UK7-2|ZN598_HUMAN**	**98 kDa**	**2**	**44**
EIF3A	EIF3A_HUMAN	167 kDa	6	51
RBM14	sp|Q96PK6|RBM14_HUMAN	69 kDa	2	15
PRRC2C	E7EPN9_HUMAN	309 kDa	4	29
FXR2	FXR2_HUMAN	74 kDa	2	13
PRRC2A	sp|P48634|PRC2A_HUMAN	229 kDa	2	13
PUM1	E9PCJ0_HUMAN	127 kDa	2	13
RBMX	sp|P38159|RBMX_HUMAN	42 kDa	3	17
EIF3B	B4DV79_HUMAN	85 kDa	6	33
EIF3EIP	B0QY89_HUMAN	71 kDa	4	20
UPF1	sp|Q92900-2|RENT1_HUMAN	123 kDa	3	15
EIF3C	B4DDN4_HUMAN	92 kDa	9	42
EIF3I	EIF3I_HUMAN	37 kDa	7	28
EIF3E	EIF3E_HUMAN	52 kDa	5	20
EIF3D	A8MWD3_HUMAN	62 kDa	4	16
HNRNPA2B1	sp|P22626|ROA2_HUMAN	37 kDa	10	36
IGF2BP3	sp|O00425|IF2B3_HUMAN	64 kDa	9	31
PABPC4	B1ANR0_HUMAN	68 kDa	10	27

GLB1	E7EQ29_HUMAN	60 kDa	14
KRT19	K1C19_HUMAN	44 kDa	13
KRT8	F8VXB4_HUMAN	57 kDa	10
HELZ	HELZ_HUMAN	219 kDa	10
EIF3H	EIF3H_HUMAN	40 kDa	10
LIMA1	sp|Q9UHB6-4|LIMA1_HUMAN	85 kDa	9
KRT18	K1C18_HUMAN	48 kDa	9
FXR1	B4DXZ6_HUMAN	68 kDa	9
EIF4G3	H7BYW0_HUMAN	196 kDa	9
HECTD3	sp|Q5T447|HECD3_HUMAN	97 kDa	8
SAMD4B	SMAG2_HUMAN	75 kDa	8
EIF2C2	sp|Q9UKV8-2|AGO2_HUMAN	94 kDa	7
DSG2	DSG2_HUMAN	122 kDa	7
DBN1	A8MV58_HUMAN	76 kDa	7
MATR3	A8MXP9_HUMAN	100 kDa	7
EIF3M	B4E2Q4_HUMAN	28 kDa	7
SCRIB	sp|Q14160-2|SCRIB_HUMAN	165 kDa	7
NKRF	G3V1N1_HUMAN	79 kDa	7
KRT13	sp|P13646|K1C13_HUMAN	50 kDa	7
ATXN2	F8VQP2_HUMAN	117 kDa	6
DICER1	sp|Q9UPY3-2|DICER_HUMAN	208 kDa	6
CTNNB1	B4DGU4_HUMAN	85 kDa	6
NNT	NNTM_HUMAN	114 kDa	6
TNRC6B	A8MYY3_HUMAN	183 kDa	6
UQCRC2	QCR2_HUMAN	48 kDa	6
FBXW8	sp|Q8N3Y1-2|FBXW8_HUMAN	61 kDa	6
SART3	B7ZKM0_HUMAN	106 kDa	5
DIS3L	***sp|Q8TF46-2|DI3L1_HUMAN***	***105 kDa***	***5***
PCM1	E7ETA6_HUMAN	228 kDa	5
ARIH1	***ARI1_HUMAN***	***64 kDa***	***5***
PHF8	H0Y3N9_HUMAN	106 kDa	5
CASC3	B4DKR6_HUMAN	70 kDa	5
LARP4B	LAR4B_HUMAN	81 kDa	5
LSM14B	sp|Q9BX40|LS14B_HUMAN	42 kDa	5
UTRN	UTRO_HUMAN	394 kDa	5
SAPCD2	SAPC2_HUMAN	43 kDa	5
PUM2	B4E2B6_HUMAN	108 kDa	5
NDUFS1	B4DJ81_HUMAN	67 kDa	4
STAU2	E5RJN7_HUMAN	35 kDa	4
EPB41L2	sp|O43491|E41L2_HUMAN	113 kDa	4
SFXN1	SFXN1_HUMAN	36 kDa	4
TNRC6A	H7C269_HUMAN	99 kDa	4
HLA-C	1C06_HUMAN	41 kDa	4
EPB41L3	sp|Q9Y2J2-2|E41L3_HUMAN	97 kDa	4
SRSF7	C9JAB2_HUMAN	27 kDa	4
CTNNA1	B4E2G8_HUMAN	98 kDa	4

HERC2	HERC2_HUMAN	527 kDa	4
PKP2	sp|Q99959-2|PKP2_HUMAN	93 kDa	4
GTF2F1	E7EUG6_HUMAN	48 kDa	4
KIAA1671	sp|Q9BY89|K1671_HUMAN	197 kDa	4
TP53	sp|P04637-4|P53_HUMAN	39 kDa	4
APC	sp|P25054-2|APC_HUMAN	300 kDa	4
BYSL	BYST_HUMAN	50 kDa	4
PCNT	sp|O95613-2|PCNT_HUMAN	356 kDa	4
HNRNPH3	sp|P31942-2|HNRH3_HUMAN	35 kDa	4
CENPV	sp|Q7Z7K6|CENPV_HUMAN	30 kDa	4
NUFIP2	NUFP2_HUMAN	76 kDa	4
RRP1B	sp|Q14684-2|RRP1B_HUMAN	82 kDa	4
AP2B1	F5GYG9_HUMAN	76 kDa	4
PHKA2	KPB2_HUMAN	138 kDa	4
PHKA1	A6NIT2_HUMAN	133 kDa	4
ANAPC1	APC1_HUMAN	217 kDa	4
TRAFD1	TRAD1_HUMAN	65 kDa	3
EFNB1	EFNB1_HUMAN	38 kDa	3
MYO1B	E9PDF6_HUMAN	128 kDa	3
CTSA	PPGB_HUMAN	54 kDa	3
RACGAP1	RGAP1_HUMAN	71 kDa	3
LTBP4	E7ENG9_HUMAN	169 kDa	3
WDR26	sp|Q9H7D7-2|WDR26_HUMAN	70 kDa	3
ATAD3A	G3V1I6_HUMAN	58 kDa	3
FMR1	A8MQB8_HUMAN	66 kDa	3
RANBP10	B4DQH9_HUMAN	65 kDa	3
FARP1	C9JME2_HUMAN	122 kDa	3
SVIL	sp|O95425-2|SVIL_HUMAN	201 kDa	3
EIF3K	B7ZAM9_HUMAN	24 kDa	3
LSM14A	sp|Q8ND56-2|LS14A_HUMAN	51 kDa	3
TMOD3	H0YKU1_HUMAN	21 kDa	3
DNMT1	F5GX68_HUMAN	183 kDa	3
GTPBP4	B7Z7A3_HUMAN	68 kDa	3
EFHD2	EFHD2_HUMAN	27 kDa	3
DDRGK1	sp|Q96HY6-2|DDRGK_HUMAN	35 kDa	3
DHX37	DHX37_HUMAN	130 kDa	3
MRPS28	RT28_HUMAN	21 kDa	3
FAM120C	F8W881_HUMAN	99 kDa	3
EIF2C3	sp|Q9H9G7-2|AGO3_HUMAN	71 kDa	3
SFPQ	sp|P23246|SFPQ_HUMAN	76 kDa	3
TTC28	TTC28_HUMAN	271 kDa	3
TSR1	TSR1_HUMAN	92 kDa	3
LARP4	G5E976_HUMAN	72 kDa	3
PKN3	PKN3_HUMAN	99 kDa	3
CIRBP	CIRBP_HUMAN	19 kDa	3
TTC3	sp|P53804-2|TTC3_HUMAN	203 kDa	3

MCCC1	E7ETG7_HUMAN	64 kDa	3
CORO1C	A7MAP0_HUMAN	54 kDa	3
STX4	A8MXY0_HUMAN	34 kDa	3
UBR5	E7EMW7_HUMAN	309 kDa	3
PHLDB2	E9PFQ4_HUMAN	125 kDa	3
YTHDF1	F8W840_HUMAN	55 kDa	3
PTPRU	E9PH42_HUMAN	162 kDa	3
CNOT3	H7C148_HUMAN	39 kDa	3
FAM175B	F175B_HUMAN	47 kDa	3
SLC1A5	AAAT_HUMAN	57 kDa	3
HSPH1	B4DYH1_HUMAN	97 kDa	3
MYO6	E7EW20_HUMAN	149 kDa	2
FAM29A	Q5VY60_HUMAN	91 kDa	2
RANBP9	sp|Q96S59|RANB9_HUMAN	78 kDa	2
ANKRD27	ANR27_HUMAN	117 kDa	2
FLOT1	B0V109_HUMAN	40 kDa	2
VDAC2	B4DKM5_HUMAN	27 kDa	2
IMMT	B9A067_HUMAN	79 kDa	2
CCDC8	CCDC8_HUMAN	59 kDa	2
CSDE1	E9PGZ0_HUMAN	91 kDa	2
GRAMD1A	F5GZ02_HUMAN	90 kDa	2
PKP4	F8W7E2_HUMAN	68 kDa	2
SLC12A2	G3XAL9_HUMAN	125 kDa	2
PRPF8	PRP8_HUMAN	274 kDa	2
NOP2	Q3KQS4_HUMAN	93 kDa	2
ATP1B3	AT1B3_HUMAN	32 kDa	2
HMOX2	HMOX2_HUMAN	36 kDa	2
PIKFYVE	E9PDH4_HUMAN	157 kDa	2
MYO1D	MYO1D_HUMAN	116 kDa	2
EXOSC2	A3KFL2_HUMAN	32 kDa	2
AFG3L2	AFG32_HUMAN	89 kDa	2
LRCH1	F8W6F0_HUMAN	85 kDa	2
DTNA	B4DIR0_HUMAN	50 kDa	2
SHKBP1	B4DUV2_HUMAN	52 kDa	2
FMNL2	Q6ZN96_HUMAN	64 kDa	2
EIF3J	B4DUI3_HUMAN	23 kDa	2
GNAQ	GNAQ_HUMAN	42 kDa	2
EPHA2	EPHA2_HUMAN	108 kDa	2
DOCK6	DOCK6_HUMAN	230 kDa	2
SOGA1	sp|O94964-2|SOGA1_HUMAN	184 kDa	2
UTP18	B2RAX6_HUMAN	58 kDa	2
SUGP2	sp|Q8IX01-3|SUGP2_HUMAN	116 kDa	2
SRPK2	H7C5L6_HUMAN	33 kDa	2
AKAP8	AKAP8_HUMAN	76 kDa	2
PEX5	sp|P50542-3|PEX5_HUMAN	70 kDa	2
CPSF3	CPSF3_HUMAN	77 kDa	2

DDX54	sp|Q8TDD1-2|DDX54_HUMAN	99 kDa		2
CPSF1	CPSF1_HUMAN	161 kDa		2
FAM83H	FA83H_HUMAN	127 kDa		2
RBM10	sp|P98175-2|RBM10_HUMAN	103 kDa		2
CPSF6	F8WJN3_HUMAN	52 kDa		2
CACNA2D1	E7ERK3_HUMAN	35 kDa		2
PNO1	F8WBJ6_HUMAN	15 kDa		2
UBE2S	UBE2S_HUMAN	24 kDa		2
ABHD12	sp|Q8N2K0-2|ABD12_HUMAN	46 kDa		2
GNB1	GBB1_HUMAN	37 kDa		2
HCG2044799	H3BQZ7_HUMAN	85 kDa		2
DHX36	E7EWK3_HUMAN	91 kDa		2
RPTOR	F5H7J5_HUMAN	132 kDa		2
CDC20	B4E1H5_HUMAN	52 kDa		2
MYO1C	F5H3W9_HUMAN	120 kDa		2
CAT	CATA_HUMAN	60 kDa		2
LMNB1	E9PBF6_HUMAN	45 kDa		2
THRAP3	TR150_HUMAN	109 kDa		2
TUBGCP6	E7EQL8_HUMAN	164 kDa		2
UCC1	A4D1W8_HUMAN	38 kDa		2
RC3H1	sp|Q5TC82-2|RC3H1_HUMAN	125 kDa		2
NDUFS2	B7Z9L2_HUMAN	27 kDa		2
ADD1	A2A3N8_HUMAN	73 kDa		2
TRIO	sp|O75962-4|TRIO_HUMAN	342 kDa		2
TRIM56	TRI56_HUMAN	81 kDa		2
NYNRIN	sp|Q9P2P1|NYNRI_HUMAN	208 kDa		2
SRSF9	SRSF9_HUMAN	26 kDa		2
MRE11A	B3KTC7_HUMAN	81 kDa		2
ASCC2	ASCC2_HUMAN	86 kDa		2
EPB41	E9PEX0_HUMAN	78 kDa		2
LSM3	LSM3_HUMAN	12 kDa		2
ITPR3	ITPR3_HUMAN	304 kDa		2
ASCC3	sp|Q8N3C0|ASCC3_HUMAN	251 kDa	2	10
AIFM1	sp|O95831-3|AIFM1_HUMAN	66 kDa	2	9
SPTAN1	A6NG51_HUMAN	285 kDa	4	17
YTHDC2	YTDC2_HUMAN	160 kDa	2	8
ZZEF1	sp|O43149|ZZEF1_HUMAN	331 kDa	2	8
MTDH	LYRIC_HUMAN	64 kDa	3	11
AKAP8L	AKP8L_HUMAN	72 kDa	2	7
KIAA1967	sp|Q8N163-2|K1967_HUMAN	103 kDa	5	17
HNRNPUL1	sp|Q9BUJ2-2|HNRL1_HUMAN	90 kDa	3	10
LARP1	sp|Q6PKG0|LARP1_HUMAN	124 kDa	3	10
DDX6	DDX6_HUMAN	54 kDa	3	10
SPTBN1	sp|Q01082|SPTB2_HUMAN	275 kDa	4	13
VIM	VIME_HUMAN	54 kDa	3	9
PHB2	F5GY37_HUMAN	30 kDa	3	9

EMD	EMD_HUMAN	29 kDa	2	6
GNAS	A6NI00_HUMAN	46 kDa	2	6
ATP2B1	sp|P20020-3|AT2B1_HUMAN	135 kDa	2	6
POLR2A	RPB1_HUMAN	217 kDa	2	6
PURB	PURB_HUMAN	33 kDa	2	6
EDC4	sp|Q6P2E9-2|EDC4_HUMAN	110 kDa	3	8
RBM4	**sp|Q9BWF3|RBM4_HUMAN**	**40 kDa**	**2**	**5**
HNRNPA0	ROA0_HUMAN	31 kDa	2	5
DCAF7	DCAF7_HUMAN	39 kDa	2	5
SEC16A	sp|O15027-2|SC16A_HUMAN	229 kDa	9	21
PSMD11	PSD11_HUMAN	47 kDa	3	7
POLD1	DPOD1_HUMAN	124 kDa	3	7
SCAMP3	sp|O14828-2|SCAM3_HUMAN	35 kDa	3	7
PDIA4	PDIA4_HUMAN	73 kDa	12	27
DDX5	DDX5_HUMAN	69 kDa	8	18
EIF3F	*B3KSH1_HUMAN*	*39 kDa*	*4*	*9*
DHX30	H7BXY3_HUMAN	131 kDa	6	13
ATP1A1	B7Z3U6_HUMAN	110 kDa	9	19
IGF2BP1	IF2B1_HUMAN	63 kDa	17	35
IGF2BP2	F8W930_HUMAN	67 kDa	12	24
MOV10	Q5JR04_HUMAN	107 kDa	7	14
SMC1A	SMC1A_HUMAN	143 kDa	4	8
PHB	C9JW96_HUMAN	27 kDa	3	6
SDHA	DHSA_HUMAN	73 kDa	3	6
PSMC6	PRS10_HUMAN	44 kDa	3	6
FAM120A	sp|Q9NZB2-4|F120A_HUMAN	117 kDa	3	6
PSMD1	sp|Q99460-2|PSMD1_HUMAN	102 kDa	2	4
CTNND1	C9JZR2_HUMAN	105 kDa	2	4
SRPK1	H3BLV9_HUMAN	76 kDa	2	4
EIF4G1	E7EUU4_HUMAN	172 kDa	10	18
FUBP3	sp|Q96I24|FUBP3_HUMAN	62 kDa	5	9
PSMC5	A8K3Z3_HUMAN	45 kDa	5	9
PABPC1	sp|P11940|PABP1_HUMAN	71 kDa	24	42
TARDBP	sp|Q13148-2|TADBP_HUMAN	45 kDa	4	7
HNRNPH1	E9PCY7_HUMAN	47 kDa	7	12
ATP5A1	ATPA_HUMAN	60 kDa	16	27
HADHB	B4E2W0_HUMAN	49 kDa	3	5
SRSF6	sp|Q13247-3|SRSF6_HUMAN	38 kDa	3	5
TRIM25	TRI25_HUMAN	71 kDa	3	5
STAU1	Q5JW30_HUMAN	55 kDa	3	5
HNRNPM	sp|P52272-2|HNRPM_HUMAN	74 kDa	47	76
ARG1	sp|P05089-2|ARGI1_HUMAN	36 kDa	7	11
PSMA1	sp|P25786-2|PSA1_HUMAN	30 kDa	9	14
FLG2	FILA2_HUMAN	248 kDa	10	15
CEP170	H0Y2V6_HUMAN	172 kDa	4	6
ARHGEF2	Q5VY93_HUMAN	111 kDa	4	6

PSMB4	PSB4_HUMAN	29 kDa	4	6
ELAVL1	ELAV1_HUMAN	36 kDa	4	6
ITGB1	sp|P05556|ITB1_HUMAN	88 kDa	2	3
SLC25A3	F8VVM2_HUMAN	36 kDa	2	3
PDXP	PLPP_HUMAN	32 kDa	2	3
XRN2	B4DZC3_HUMAN	102 kDa	2	3
RNF31	sp|Q96EP0|RNF31_HUMAN	120 kDa	2	3
DDX17	H3BLZ8_HUMAN	80 kDa	20	29
PSMA5	PSA5_HUMAN	26 kDa	7	10
UBB	B4DV12_HUMAN	17 kDa	39	52
TIMM50	sp|Q3ZCQ8-2|TIM50_HUMAN	50 kDa	9	12
HNRNPA1	F8VRQ1_HUMAN	33 kDa	9	12
PSMC2	PRS7_HUMAN	49 kDa	6	8
EPPK1	EPIPL_HUMAN	556 kDa	3	4
HIST3H3	H31T_HUMAN	16 kDa	3	4
PSMC3	E9PM69_HUMAN	44 kDa	3	4
ADSS	F8W9D6_HUMAN	48 kDa	3	4
PDE12	F6T1Q0_HUMAN	52 kDa	3	4
AGPS	ADAS_HUMAN	73 kDa	3	4
PSMD2	E7EW34_HUMAN	86 kDa	7	9
ACTG1	ACTG_HUMAN	42 kDa	46	59
HSPA1B	H0YG33_HUMAN	77 kDa	72	91
HSPA5	GRP78_HUMAN	72 kDa	27	34
HSPD1	CH60_HUMAN	61 kDa	24	30
IRS2	IRS2_HUMAN	137 kDa	4	5
KHDRBS1	E7ET98_HUMAN	46 kDa	4	5
PDCD2L	PDD2L_HUMAN	39 kDa	4	5
HNRNPA3	sp|P51991|ROA3_HUMAN	40 kDa	4	5
RPL12	sp|P30050|RL12_HUMAN	18 kDa	4	5
ATP5B	ATPB_HUMAN	57 kDa	22	27
UBR4	sp|Q5T4S7-2|UBR4_HUMAN	576 kDa	5	6
HNRNPF	HNRPF_HUMAN	46 kDa	5	6
PDLIM5	sp|Q96HC4|PDLI5_HUMAN	64 kDa	5	6
HNRNPK	Q5T6W5_HUMAN	48 kDa	18	21
HADHA	ECHA_HUMAN	83 kDa	6	7
HSPA9	B7Z4V2_HUMAN	72 kDa	26	30
IRAK1	D3YTB5_HUMAN	76 kDa	7	8
HSPA8	sp|P11142|HSP7C_HUMAN	71 kDa	66	73
KRT10	K1C10_HUMAN	59 kDa	129	131
TUBB6	B4DP54_HUMAN	47 kDa	32	32
CNOT1	sp|A5YKK6|CNOT1_HUMAN	267 kDa	16	16
DCD	sp|P81605|DCD_HUMAN	11 kDa	13	13
PFKP	K6PP_HUMAN	86 kDa	12	12
XRCC6	B1AHC7_HUMAN	64 kDa	11	11
HUWE1	sp|Q7Z6Z7-2|HUWE1_HUMAN	480 kDa	10	10
USP9X	sp|Q93008-1|USP9X_HUMAN	290 kDa	10	10

ATP2A2	sp|P16615-2|AT2A2_HUMAN	110 kDa	8	8
PLEC	sp|Q15149-2|PLEC_HUMAN	518 kDa	6	6
RNH1	RINI_HUMAN	50 kDa	5	5
RPN1	B7Z4L4_HUMAN	50 kDa	5	5
CNOT2	F8VV52_HUMAN	59 kDa	5	5
NSUN2	sp|Q08J23-2|NSUN2_HUMAN	82 kDa	4	4
RPS21	RS21_HUMAN	9 kDa	4	4
TOP2A	C9J5P2_HUMAN	179 kDa	4	4
PHKB	sp|Q93100-2|KPBB_HUMAN	124 kDa	4	4
TTC37	TTC37_HUMAN	175 kDa	4	4
RPL27A	RL27A_HUMAN	17 kDa	4	4
TRIP6	TRIP6_HUMAN	50 kDa	4	4
G3BP1	G3BP1_HUMAN	52 kDa	4	4
FBXO21	H0YHF6_HUMAN	26 kDa	4	4
DNAJA3	sp|Q96EY1|DNJA3_HUMAN	52 kDa	4	4
OSGEP	OSGEP_HUMAN	36 kDa	4	4
HNRNPAB	D6R9P3_HUMAN	30 kDa	3	3
UCHL5	B4DW59_HUMAN	22 kDa	3	3
GPHN	H0YJ30_HUMAN	30 kDa	3	3
LMAN1	LMAN1_HUMAN	58 kDa	3	3
RPL31	sp|P62899|RL31_HUMAN	14 kDa	3	3
SRPRB	SRPRB_HUMAN	30 kDa	3	3
LMAN2	B4DWN1_HUMAN	33 kDa	3	3
PSMD6	C9IZE4_HUMAN	52 kDa	3	3
ATXN2L	sp|Q8WWM7|ATX2L_HUMAN	113 kDa	3	3
POLR2B	C9J2Y9_HUMAN	133 kDa	3	3
RPL32	D3YTB1_HUMAN	16 kDa	3	3
BOLA2	sp|Q9H3K6|BOLA2_HUMAN	10 kDa	3	3
RPS28	RS28_HUMAN	8 kDa	3	3
STOML2	B4E1K7_HUMAN	33 kDa	2	2
NMT1	B7Z8J4_HUMAN	15 kDa	2	2
PSMA3	sp|P25788-2|PSA3_HUMAN	28 kDa	2	2
TMEM109	TM109_HUMAN	26 kDa	2	2
SRPR	E9PJS4_HUMAN	67 kDa	2	2
PDHX	E9PB14_HUMAN	51 kDa	2	2
HIST1H2AD	H2A1D_HUMAN	14 kDa	2	2
SCAMP2	SCAM2_HUMAN	37 kDa	2	2
SRSF3	B4E241_HUMAN	14 kDa	2	2
NCAPH2	sp|Q6IBW4-2|CNDH2_HUMAN	66 kDa	2	2
TMEM48	B4DZG6_HUMAN	38 kDa	2	2
EXOSC6	EXOS6_HUMAN	28 kDa	2	2
RNF214	B4DTD1_HUMAN	61 kDa	2	2
BAG3	BAG3_HUMAN	62 kDa	2	2
EDC3	EDC3_HUMAN	56 kDa	2	2
PTK7	E9PFZ5_HUMAN	119 kDa	2	2
DDX47	DDX47_HUMAN	51 kDa	2	2

EEA1	EEA1_HUMAN	162 kDa	2	2
IGF2R	MPRI_HUMAN	274 kDa	2	2
KIAA0564	E2QRD0_HUMAN	204 kDa	2	2
KRT9	K1C9_HUMAN	62 kDa	160	151
SNRPA1	RU2A_HUMAN	28 kDa	17	16
CCT3	B4DUR8_HUMAN	56 kDa	16	15
YBX1	YBOX1_HUMAN	36 kDa	14	13
ZC3HAV1	sp|Q7Z2W4-2|ZCCHV_HUMAN	78 kDa	12	11
KRT2	K22E_HUMAN	65 kDa	153	140
PPP2R1A	2AAA_HUMAN	65 kDa	11	10
SRRM2	F5GWZ7_HUMAN	215 kDa	10	9
PCBP2	B4DXP5_HUMAN	34 kDa	10	9
HNRNPU	sp|Q00839-2|HNRPU_HUMAN	89 kDa	16	14
CKAP4	CKAP4_HUMAN	66 kDa	8	7
RPS14	RS14_HUMAN	16 kDa	8	7
CSDA	sp|P16989-2|DBPA_HUMAN	32 kDa	8	7
SYNCRIP	sp|O60506-3|HNRPQ_HUMAN	63 kDa	15	13
DHX9	sp|Q08211|DHX9_HUMAN	141 kDa	21	18
LASP1	sp|Q14847|LASP1_HUMAN	30 kDa	13	11
DDX3X	sp|O00571-2|DDX3X_HUMAN	71 kDa	19	16
LRPPRC	LPPRC_HUMAN	158 kDa	12	10
VARS	B0V043_HUMAN	140 kDa	10	8
PSMD4	sp|P55036|PSMD4_HUMAN	41 kDa	5	4
GEMIN4	GEMI4_HUMAN	120 kDa	5	4
NSF	B4DFA2_HUMAN	72 kDa	5	4
TUBGCP3	sp|Q96CW5-2|GCP3_HUMAN	94 kDa	5	4
SH3GLB2	B7ZC38_HUMAN	44 kDa	5	4
RBM39	E1P5S2_HUMAN	41 kDa	5	4
CAPRIN1	G3V153_HUMAN	70 kDa	5	4
DLST	ODO2_HUMAN	49 kDa	5	4
NDUFAF3	sp|Q9BU61|NDUF3_HUMAN	20 kDa	5	4
RPLP0	RLA0_HUMAN	34 kDa	9	7
RPL24	RL24_HUMAN	18 kDa	9	7
GAPDH	E7EUT4_HUMAN	32 kDa	8	6
HNRNPR	sp|O43390-2|HNRPR_HUMAN	71 kDa	8	6
SMN1	E7EQZ4_HUMAN	32 kDa	4	3
SLC25A5	ADT2_HUMAN	33 kDa	4	3
MDN1	MDN1_HUMAN	633 kDa	4	3
DDX39B	B4DP52_HUMAN	41 kDa	4	3
SLC3A2	F5GZS6_HUMAN	65 kDa	4	3
UBAP2L	F8W726_HUMAN	113 kDa	4	3
EFTUD2	B4DK30_HUMAN	105 kDa	4	3
YTHDF2	F5H8I7_HUMAN	61 kDa	4	3
COASY	sp|Q13057-2|COASY_HUMAN	65 kDa	4	3
USP10	sp|Q14694-2|UBP10_HUMAN	93 kDa	4	3
HRNR	HORN_HUMAN	282 kDa	35	26

TUFM	EFTU_HUMAN	50 kDa	19	14
MIF	MIF_HUMAN	12 kDa	66	48
EIF2S3	IF2G_HUMAN	51 kDa	7	5
KRT6A	K2C6A_HUMAN	60 kDa	96	68
TUBB4B	TBB4B_HUMAN	50 kDa	109	77
KRT5	K2C5_HUMAN	62 kDa	101	71
KRT1	K2C1_HUMAN	66 kDa	206	143
TUBB2A	TBB2A_HUMAN	50 kDa	91	61
DSG1	DSG1_HUMAN	114 kDa	24	16
HIST1H1C	H12_HUMAN	21 kDa	15	10
RPSAP58	A6NE09_HUMAN	33 kDa	12	8
YWHAG	1433G_HUMAN	28 kDa	9	6
CLASP2	E3W994_HUMAN	139 kDa	6	4
PELO	PELO_HUMAN	43 kDa	6	4
DOCK7	sp|Q96N67-2|DOCK7_HUMAN	241 kDa	6	4
ATP5O	ATPO_HUMAN	23 kDa	6	4
RPS20	sp|P60866-2|RS20_HUMAN	16 kDa	6	4
PKP1	sp|Q13835-2|PKP1_HUMAN	80 kDa	3	2
TMX1	TMX1_HUMAN	32 kDa	3	2
DBNL	B4DDD6_HUMAN	46 kDa	3	2
SMC3	SMC3_HUMAN	142 kDa	3	2
SEC61B	SC61B_HUMAN	10 kDa	3	2
TBK1	TBK1_HUMAN	84 kDa	3	2
NDUFS7	B3KRI2_HUMAN	22 kDa	3	2
TFRC	TFR1_HUMAN	85 kDa	3	2
GTPBP2	sp|Q9BX10-2|GTPB2_HUMAN	57 kDa	3	2
DNAJA1	DNJA1_HUMAN	45 kDa	3	2
SERBP1	sp|Q8NC51-2|PAIRB_HUMAN	44 kDa	3	2
CD2AP	CD2AP_HUMAN	71 kDa	3	2
KCTD12	KCD12_HUMAN	36 kDa	3	2
RPL28	E9PB24_HUMAN	19 kDa	3	2
LSM12	sp|Q3MHD2-2|LSM12_HUMAN	22 kDa	3	2
PDLIM7	sp|Q9NR12-2|PDLI7_HUMAN	47 kDa	3	2
SHMT2	B4DLV4_HUMAN	45 kDa	3	2
RFC2	sp|P35250-2|RFC2_HUMAN	35 kDa	3	2
ARAF	ARAF_HUMAN	68 kDa	3	2
RPS27	RS27_HUMAN	9 kDa	3	2
VPS35	F5GYF5_HUMAN	76 kDa	3	2
KRT14	K1C14_HUMAN	52 kDa	94	62
TRIM28	sp|Q13263|TIF1B_HUMAN	89 kDa	23	15
CCT2	sp|P78371-2|TCPB_HUMAN	53 kDa	20	13
COPA	sp|P53621-2|COPA_HUMAN	139 kDa	16	10
DDX21	sp|Q9NR30-2|DDX21_HUMAN	80 kDa	8	5
RPL22	RL22_HUMAN	15 kDa	8	5
PSMD3	F5H8K4_HUMAN	60 kDa	13	8
CAD	F8VPD4_HUMAN	236 kDa	41	25

ILF3	G5E9M5_HUMAN	96 kDa	23	14
FASN	FAS_HUMAN	273 kDa	50	30
RPS19	RS19_HUMAN	16 kDa	10	6
GMPS	B4DUT7_HUMAN	71 kDa	10	6
PSMB6	PSB6_HUMAN	25 kDa	5	3
PRDX3	E9PH29_HUMAN	26 kDa	5	3
ATP6V1A	B7Z1R5_HUMAN	65 kDa	5	3
SND1	E7ESM6_HUMAN	101 kDa	5	3
RPL18	F8VWC5_HUMAN	18 kDa	12	7
MCM7	sp|P33993|MCM7_HUMAN	81 kDa	19	11
TUBB	F8VW92_HUMAN	49 kDa	119	68
TCOF1	E9PHK9_HUMAN	156 kDa	7	4
RBBP7	E9PC52_HUMAN	47 kDa	7	4
NEDD1	G3V3F1_HUMAN	73 kDa	7	4
RPL5	B3KTM6_HUMAN	28 kDa	18	10
WRNIP1	sp|Q96S55-2|WRIP1_HUMAN	69 kDa	9	5
TES	H0Y2M4_HUMAN	48 kDa	9	5
TXNDC5	B2RDM2_HUMAN	36 kDa	9	5
TUBA1B	TBA1B_HUMAN	50 kDa	56	31
RUVBL1	sp|Q9Y265|RUVB1_HUMAN	50 kDa	15	8
HSP90AA1	sp|P07900-2|HS90A_HUMAN	98 kDa	23	12
HSP90AB1	HS90B_HUMAN	83 kDa	32	16
ENO1	sp|P06733|ENOA_HUMAN	47 kDa	18	9
HSPA4	HSP74_HUMAN	94 kDa	12	6
RPL6	F8W181_HUMAN	26 kDa	12	6
GSR	sp|P00390-2|GSHR_HUMAN	52 kDa	12	6
SAE1	B3KNJ4_HUMAN	33 kDa	10	5
BAX	sp|Q07812-2|BAX_HUMAN	24 kDa	10	5
TARS2	SYTM_HUMAN	81 kDa	8	4
EIF2S1	IF2A_HUMAN	36 kDa	8	4
EEF1D	E9PK01_HUMAN	29 kDa	8	4
GLUD1	DHE3_HUMAN	61 kDa	6	3
CNP	sp|P09543-2|CN37_HUMAN	45 kDa	6	3
VCP	TERA_HUMAN	89 kDa	6	3
CAPZA1	CAZA1_HUMAN	33 kDa	6	3
RPL29	RL29_HUMAN	18 kDa	6	3
LETM1	LETM1_HUMAN	83 kDa	6	3
PSMC1	B4DR63_HUMAN	41 kDa	4	2
POLDIP3	F8WCX5_HUMAN	31 kDa	4	2
RAB5C	F8W1H5_HUMAN	27 kDa	4	2
PSMD12	sp|O00232|PSD12_HUMAN	53 kDa	4	2
RPS29	sp|P62273|RS29_HUMAN	7 kDa	4	2
ABCE1	ABCE1_HUMAN	67 kDa	4	2
RPS10P5	RS10L_HUMAN	20 kDa	4	2
MDH2	G3XAL0_HUMAN	25 kDa	4	2
RCCD1	RCCD1_HUMAN	40 kDa	4	2

KPNA2	IMA2_HUMAN	58 kDa	4	2
SACM1L	B4DK71_HUMAN	61 kDa	4	2
GPSM1	sp|Q86YR5-4|GPSM1_HUMAN	72 kDa	4	2
ZCCHC11	sp|Q5TAX3|TUT4_HUMAN	185 kDa	4	2
SLFN11	SLN11_HUMAN	103 kDa	4	2
TGM3	TGM3_HUMAN	77 kDa	4	2
PRKDC	sp|P78527|PRKDC_HUMAN	469 kDa	79	38
DSP	sp|P15924|DESP_HUMAN	332 kDa	75	35
RPS18	RS18_HUMAN	18 kDa	15	7
CCT6A	B4DPJ8_HUMAN	55 kDa	15	7
KRT16	K1C16_HUMAN	51 kDa	106	49
NCL	NUCL_HUMAN	77 kDa	36	16
CHD4	F5GWX5_HUMAN	217 kDa	9	4
HSPA4L	E7ES43_HUMAN	98 kDa	9	4
RPL4	E7EWF1_HUMAN	46 kDa	23	10
HSP90B1	ENPL_HUMAN	92 kDa	7	3
SMC2	sp|O95347|SMC2_HUMAN	136 kDa	7	3
HNRNPD	D6RAF8_HUMAN	23 kDa	7	3
RPS13	RS13_HUMAN	17 kDa	7	3
PROSC	PROSC_HUMAN	30 kDa	7	3
PRKAR2A	KAP2_HUMAN	46 kDa	7	3
AHCY	SAHH_HUMAN	48 kDa	19	8
YWHAB	*sp|P31946-2|1433B_HUMAN*	*28 kDa*	*12*	*5*
JUP	F5GWP8_HUMAN	66 kDa	68	28
ERP44	ERP44_HUMAN	47 kDa	22	9
PARP1	PARP1_HUMAN	113 kDa	27	11
ALB	E7ESU5_HUMAN	70 kDa	27	11
AARS2	SYAM_HUMAN	107 kDa	10	4
CANX	CALX_HUMAN	68 kDa	10	4
EIF2B3	sp|Q9NR50|EI2BG_HUMAN	50 kDa	10	4
DDX1	B4DME8_HUMAN	69 kDa	10	4
ABCF1	sp|Q8NE71-2|ABCF1_HUMAN	92 kDa	10	4
SEC22B	SC22B_HUMAN	25 kDa	10	4
NACA	E9PAV3_HUMAN	205 kDa	5	2
HIST1H4A	H4_HUMAN	11 kDa	5	2
GALK1	GALK1_HUMAN	42 kDa	5	2
CDC5L	CDC5L_HUMAN	92 kDa	5	2
PSMA7	sp|O14818|PSA7_HUMAN	28 kDa	5	2
ALDH16A1	F5H4B6_HUMAN	67 kDa	5	2
DIS3	G3V1J5_HUMAN	91 kDa	5	2
PA2G4	F8VTY8_HUMAN	42 kDa	5	2
ESYT1	sp|Q9BSJ8-2|ESYT1_HUMAN	124 kDa	5	2
PTER	sp|Q96BW5-2|PTER_HUMAN	33 kDa	5	2
PTBP1	sp|P26599-2|PTBP1_HUMAN	59 kDa	5	2
SMG9	sp|Q9H0W8|SMG9_HUMAN	58 kDa	5	2
MYH10	F8VTL3_HUMAN	233 kDa	5	2

UMPS	sp|P11172|UMPS_HUMAN	52 kDa	5	2
BSG	I3L4S8_HUMAN	33 kDa	5	2
RUVBL2	RUVB2_HUMAN	51 kDa	28	11
KIF5B	KINH_HUMAN	110 kDa	18	7
RPS3	RS3_HUMAN	27 kDa	26	10
TPM3	Q5VU66_HUMAN	29 kDa	13	5
PTPN11	sp|Q06124|PTN11_HUMAN	68 kDa	13	5
HSD17B10	sp|Q99714-2|HCD2_HUMAN	26 kDa	13	5
HAGH	H3BPK3_HUMAN	26 kDa	16	6
EIF2B4	E7ERK9_HUMAN	60 kDa	8	3
AIP	AIP_HUMAN	38 kDa	8	3
KRT33B	KT33B_HUMAN	46 kDa	8	3
XRCC5	XRCC5_HUMAN	83 kDa	8	3
ISYNA1	G3V1R9_HUMAN	45 kDa	8	3
RCC2	RCC2_HUMAN	56 kDa	19	7
GART	sp|P22102|PUR2_HUMAN	108 kDa	30	11
FARSB	SYFB_HUMAN	66 kDa	22	8
PSMB5	sp|P28074|PSB5_HUMAN	28 kDa	11	4
RAB14	RAB14_HUMAN	24 kDa	11	4
CLTC	sp|Q00610-2|CLH1_HUMAN	188 kDa	25	9
KHSRP	sp|Q92945-2|FUBP2_HUMAN	73 kDa	42	15
RPS4X	RS4X_HUMAN	30 kDa	14	5
DHX15	DHX15_HUMAN	91 kDa	17	6
RPS3A	RS3A_HUMAN	30 kDa	17	6
KRT6B	K2C6B_HUMAN	60 kDa	72	25
JUP	PLAK_HUMAN	82 kDa	26	9
PARK7	PARK7_HUMAN	20 kDa	48	16
PDIA3	B3KQT9_HUMAN	54 kDa	33	11
PDIA6	B5MCQ5_HUMAN	53 kDa	30	10
TAGLN2	TAGL2_HUMAN	22 kDa	15	5
RPL8	RL8_HUMAN	28 kDa	12	4
PFAS	PUR4_HUMAN	145 kDa	9	3
RPL23A	A8MUS3_HUMAN	22 kDa	9	3
LDHB	LDHB_HUMAN	37 kDa	9	3
PGAM5	sp|Q96HS1|PGAM5_HUMAN	32 kDa	6	2
KRT86	KRT86_HUMAN	53 kDa	6	2
RFC3	C9JU95_HUMAN	35 kDa	6	2
AP2A1	sp|O95782-2|AP2A1_HUMAN	105 kDa	6	2
MACF1	F5GZL7_HUMAN	606 kDa	6	2
MARCKS	MARCS_HUMAN	32 kDa	6	2
RAB11A	B4DT13_HUMAN	18 kDa	6	2
PPP2R2A	sp|P63151-2|2ABA_HUMAN	53 kDa	6	2
RPS5	RS5_HUMAN	23 kDa	6	2
MTOR	MTOR_HUMAN	289 kDa	6	2
RPS25	RS25_HUMAN	14 kDa	6	2
MAP1B	MAP1B_HUMAN	271 kDa	38	12

IARS	SYIC_HUMAN	145 kDa	16	5
EPRS	SYEP_HUMAN	171 kDa	29	9
NUP155	B4DLT2_HUMAN	151 kDa	13	4
KRT77	K2C1B_HUMAN	62 kDa	30	9
TNKS1BP1	sp|Q9C0C2|TB182_HUMAN	182 kDa	10	3
KPNB1	IMB1_HUMAN	97 kDa	10	3
DRG1	DRG1_HUMAN	41 kDa	10	3
GNB2L1	GBLP_HUMAN	35 kDa	10	3
KRT17	K1C17_HUMAN	48 kDa	68	20
DDB1	DDB1_HUMAN	127 kDa	17	5
QARS	B4DWJ2_HUMAN	87 kDa	17	5
CBR1	CBR1_HUMAN	30 kDa	35	10
SUPT16H	SP16H_HUMAN	120 kDa	14	4
NUMA1	sp|Q14980-2|NUMA1_HUMAN	237 kDa	7	2
EIF4A2	E7EQG2_HUMAN	41 kDa	7	2
SEC24C	E7EP00_HUMAN	107 kDa	7	2
COPB2	B4DZI8_HUMAN	99 kDa	7	2
RPS15A	I3L3P7_HUMAN	11 kDa	7	2
HDAC6	HDAC6_HUMAN	131 kDa	50	14
FLNB	sp|O75369-2|FLNB_HUMAN	276 kDa	18	5
RPL7	A8MUD9_HUMAN	24 kDa	15	4
RPS8	Q5JR95_HUMAN	22 kDa	15	4
MARS	SYMC_HUMAN	101 kDa	15	4
ACADVL	F5H2A9_HUMAN	73 kDa	15	4
IGHA1	IGHA1_HUMAN	38 kDa	15	4
ACLY	E7ENH9_HUMAN	126 kDa	19	5
GCN1L1	GCN1L_HUMAN	293 kDa	47	12
FLNA	Q5HY54_HUMAN	277 kDa	60	15
CRKL	CRKL_HUMAN	34 kDa	28	7
PCBP1	PCBP1_HUMAN	37 kDa	24	6
SNX2	SNX2_HUMAN	58 kDa	20	5
RPS2	RS2_HUMAN	31 kDa	12	3
ALKBH4	ALKB4_HUMAN	34 kDa	8	2
STRAP	B4DNJ6_HUMAN	40 kDa	8	2
PRDX4	PRDX4_HUMAN	31 kDa	8	2
SH3GLB1	sp|Q9Y371-2|SHLB1_HUMAN	43 kDa	8	2
NARFL	sp|Q9H6Q4-3|NARFL_HUMAN	42 kDa	8	2
PCNA	PCNA_HUMAN	29 kDa	8	2
CTPS1	PYRG1_HUMAN	67 kDa	25	6
RPL7A	RL7A_HUMAN	30 kDa	21	5
UBA1	UBA1_HUMAN	118 kDa	17	4
RARS	sp|P54136|SYRC_HUMAN	75 kDa	17	4
CSE1L	F8W904_HUMAN	104 kDa	26	6
CAPZB	B1AK87_HUMAN	29 kDa	13	3
KARS	sp|Q15046-2|SYK_HUMAN	71 kDa	13	3
MTHFD1	C1TC_HUMAN	102 kDa	36	8

SF3B3	sp|Q15393|SF3B3_HUMAN	136 kDa	9	2
ALDOA	ALDOA_HUMAN	39 kDa	9	2
PFN2	C9J0J7_HUMAN	10 kDa	9	2
EEF1G	B4DTG2_HUMAN	56 kDa	9	2
SERPINB3	sp|P29508-2|SPB3_HUMAN	39 kDa	9	2
CYFIP1	sp|Q7L576|CYFP1_HUMAN	145 kDa	14	3
RPL13	RL13_HUMAN	24 kDa	19	4
EEF1A1	EF1A1_HUMAN	50 kDa	19	4
DNPEP	DNPEP_HUMAN	52 kDa	20	4
CASP14	CASPE_HUMAN	28 kDa	16	3
TIMM44	TIM44_HUMAN	51 kDa	16	3
PLS3	B7Z6M1_HUMAN	66 kDa	16	3
MCM3	MCM3_HUMAN	91 kDa	22	4
EEF2	EF2_HUMAN	95 kDa	22	4
SMC4	E9PD53_HUMAN	144 kDa	11	2
YWHAE	sp|P62258-2|1433E_HUMAN	27 kDa	11	2
ACACA	sp|Q13085-2|ACACA_HUMAN	260 kDa	17	3
CCT5	B7ZAR1_HUMAN	55 kDa	17	3
DYNC1H1	DYHC1_HUMAN	532 kDa	47	8
PPIA	PPIA_HUMAN	18 kDa	30	5
BCAP31	sp|P51572-2|BAP31_HUMAN	35 kDa	12	2
MCMBP	sp|Q9BTE3-2|MCMBP_HUMAN	73 kDa	12	2
RPL3	RL3_HUMAN	46 kDa	12	2
MAP4	E7EVA0_HUMAN	245 kDa	25	4
SNX1	sp|Q13596|SNX1_HUMAN	59 kDa	32	5
PRDX1	PRDX1_HUMAN	22 kDa	32	5
SBSN	E9PBV3_HUMAN	61 kDa	13	2
PCMT1	H7BY58_HUMAN	30 kDa	13	2
PKM2	sp|P14618-2|KPYM_HUMAN	58 kDa	14	2
C22orf28	RTCB_HUMAN	55 kDa	14	2
MYH9	sp|P35579|MYH9_HUMAN	227 kDa	14	2
OPA1	E5KLJ5_HUMAN	118 kDa	31	4
PHGDH	SERA_HUMAN	57 kDa	16	2
LANCL1	LANC1_HUMAN	45 kDa	59	7
CCT8	G5E9B2_HUMAN	59 kDa	28	3
GOLGA4	F8W8Q7_HUMAN	262 kDa	32	3
IPO5	sp|O00410-3|IPO5_HUMAN	126 kDa	24	2
KRT78	sp|Q8N1N4|K2C78_HUMAN	57 kDa	28	
FBXO22	sp|Q8NEZ5|FBX22_HUMAN	45 kDa	25	
FBXO3	E9PJM3_HUMAN	49 kDa	22	
CCT4	TCPD_HUMAN	58 kDa	18	
DARS	SYDC_HUMAN	57 kDa	18	
FARSA	SYFA_HUMAN	58 kDa	18	
TCP1	TCPA_HUMAN	60 kDa	18	
ANXA2	sp|P07355-2|ANXA2_HUMAN	40 kDa	17	
AGL	sp|P35573|GDE_HUMAN	175 kDa	20	

RAB7A	RAB7A_HUMAN	23 kDa	17
DNAJC7	DNJC7_HUMAN	56 kDa	15
PRMT1	E9PKG1_HUMAN	38 kDa	17
CCT7	B8ZZC9_HUMAN	55 kDa	18
CSTA	CYTA_HUMAN	11 kDa	12
HPRT1	HPRT_HUMAN	25 kDa	16
LARS	B4DER1_HUMAN	131 kDa	14
AHNAK	AHNK_HUMAN	629 kDa	17
MCM5	B1AHB1_HUMAN	78 kDa	13
HCFC1	A6NEM2_HUMAN	213 kDa	13
LTF	B7Z4X2_HUMAN	73 kDa	13
ZC3HAV1L	sp|Q96H79|ZCCHL_HUMAN	33 kDa	15
DPYSL3	sp|Q14195-2|DPYL3_HUMAN	74 kDa	12
PDCD6	PDCD6_HUMAN	22 kDa	11
RPS16	RS16_HUMAN	16 kDa	15
S100A8	S10A8_HUMAN	11 kDa	10
TMPO	LAP2A_HUMAN	75 kDa	11
RPL15	E7EQV9_HUMAN	21 kDa	11
FN3KRP	F5H4E4_HUMAN	29 kDa	12
CKAP5	sp|Q14008-2|CKAP5_HUMAN	219 kDa	12
RPL10	F8W7C6_HUMAN	19 kDa	13
CUL1	CUL1_HUMAN	90 kDa	13
C21orf33	sp|P30042|ES1_HUMAN	28 kDa	9
NME1	sp|P15531-2|NDKA_HUMAN	20 kDa	12
IKBKAP	ELP1_HUMAN	150 kDa	11
LCN1	LCN1_HUMAN	19 kDa	9
KRT84	KRT84_HUMAN	65 kDa	12
CNN3	CNN3_HUMAN	36 kDa	10
IMPDH2	H0Y4R1_HUMAN	51 kDa	12
RFC4	RFC4_HUMAN	40 kDa	11
CBS	B7Z2D6_HUMAN	56 kDa	11
RPL23	RL23_HUMAN	15 kDa	9
SRP54	sp|P61011-2|SRP54_HUMAN	50 kDa	10
RPL10A	RL10A_HUMAN	25 kDa	8
FUS	B4DR70_HUMAN	45 kDa	7
RPL14	B7Z6S8_HUMAN	15 kDa	9
NPM1	sp|P06748-2|NPM_HUMAN	29 kDa	9
RPL21	RL21_HUMAN	19 kDa	6
EWSR1	B0QYK0_HUMAN	65 kDa	9
USP5	sp|P45974-2|UBP5_HUMAN	93 kDa	7
RPS6	RS6_HUMAN	29 kDa	11
RPL19	RL19_HUMAN	23 kDa	9
AZGP1	ZA2G_HUMAN	34 kDa	5
SNX5	SNX5_HUMAN	47 kDa	10
ILF2	ILF2_HUMAN	43 kDa	9
P4HB	E7EPA8_HUMAN	55 kDa	9

BUB3	sp|O43684-2|BUB3_HUMAN	37 kDa	10
SEC23A	F5H365_HUMAN	83 kDa	9
TRIM65	TRI65_HUMAN	57 kDa	10
KRT80	sp|Q6KB66-2|K2C80_HUMAN	47 kDa	8
H1FX	H1X_HUMAN	22 kDa	6
HBB	HBB_HUMAN	16 kDa	8
DSC1	sp|Q08554-2|DSC1_HUMAN	94 kDa	5
ECM29	ECM29_HUMAN	204 kDa	10
RPL26	RL26_HUMAN	17 kDa	8
CTSD	CATD_HUMAN	45 kDa	9
EIF5B	IF2P_HUMAN	139 kDa	7
PSMD9	F5GX23_HUMAN	20 kDa	9
RPLP2	RLA2_HUMAN	12 kDa	8
ATXN10	sp|Q9UBB4-2|ATX10_HUMAN	46 kDa	9
MAT2A	METK2_HUMAN	44 kDa	8
PAICS	E9PBS1_HUMAN	46 kDa	6
NEK9	NEK9_HUMAN	107 kDa	9
PRDX2	sp|P32119|PRDX2_HUMAN	22 kDa	9
GANAB	F5H6X6_HUMAN	96 kDa	9
USP24	B7WPF4_HUMAN	277 kDa	10
ALDH7A1	E7EPT3_HUMAN	54 kDa	10
SNX6	SNX6_HUMAN	47 kDa	9
RPL17	RL17_HUMAN	21 kDa	9
HBA1	HBA_HUMAN	15 kDa	6
RPS9	B5MCT8_HUMAN	17 kDa	7
GATAD2B	P66B_HUMAN	65 kDa	6
PPA1	IPYR_HUMAN	33 kDa	7
INPPL1	sp|O15357|SHIP2_HUMAN	139 kDa	7
XPO1	XPO1_HUMAN	123 kDa	9
RPS11	RS11_HUMAN	18 kDa	6
POLR2E	RPAB1_HUMAN	25 kDa	7
PLIN3	sp|O60664-3|PLIN3_HUMAN	47 kDa	6
EIF2S2	IF2B_HUMAN	38 kDa	7
KNTC1	KNTC1_HUMAN	251 kDa	7
PRMT5	sp|O14744-2|ANM5_HUMAN	71 kDa	7
TRIP13	sp|Q15645|PCH2_HUMAN	49 kDa	7
SSRP1	SSRP1_HUMAN	81 kDa	8
PSMA4	H0YL69_HUMAN	26 kDa	8
IPO7	IPO7_HUMAN	120 kDa	8
NT5DC2	E9PAL9_HUMAN	64 kDa	9
LSS	E9PEI9_HUMAN	82 kDa	8
GFPT1	sp|Q06210-2|GFPT1_HUMAN	77 kDa	9
KRT36	sp|O76013|KRT36_HUMAN	52 kDa	11
TBC1D15	sp|Q8TC07-2|TBC15_HUMAN	77 kDa	8
SRP68	F5H5Y3_HUMAN	60 kDa	9
PITHD1	sp|Q9GZP4|PITH1_HUMAN	24 kDa	9

RPL38	RL38_HUMAN	8 kDa	10
HSPB1	HSPB1_HUMAN	23 kDa	6
CDK1	sp|P06493|CDK1_HUMAN	34 kDa	5
KIF2C	B7Z6Q6_HUMAN	77 kDa	8
AMPD2	E9PNG0_HUMAN	88 kDa	5
C9orf142	CI142_HUMAN	22 kDa	5
RPL11	sp|P62913-2|RL11_HUMAN	20 kDa	5
FKBP1A	FKB1A_HUMAN	12 kDa	4
CTPS2	PYRG2_HUMAN	66 kDa	7
TFAM	TFAM_HUMAN	29 kDa	5
ARFIP1	sp|P53367|ARFP1_HUMAN	42 kDa	7
CIAPIN1	H3BV90_HUMAN	26 kDa	6
UGGT1	sp|Q9NYU2-2|UGGG1_HUMAN	175 kDa	7
XPOT	XPOT_HUMAN	110 kDa	7
S100A7	S10A7_HUMAN	11 kDa	5
MCCC2	sp|Q9HCC0-2|MCCB_HUMAN	58 kDa	7
MSH2	B4E2Z2_HUMAN	97 kDa	7
RAD50	sp|Q92878-2|RAD50_HUMAN	155 kDa	7
TNC	E9PC84_HUMAN	211 kDa	8
RPL13A	RL13A_HUMAN	24 kDa	7
TXNDC12	TXD12_HUMAN	19 kDa	8
ARF1	ARF1_HUMAN	21 kDa	8
CUL5	CUL5_HUMAN	91 kDa	7
CPT2	CPT2_HUMAN	74 kDa	8
TGM1	TGM1_HUMAN	90 kDa	3
CCDC124	CC124_HUMAN	26 kDa	5
MMS19	F8W9Y2_HUMAN	108 kDa	4
IBA57	CAF17_HUMAN	38 kDa	5
THOP1	THOP1_HUMAN	79 kDa	5
DPYSL2	B4DR31_HUMAN	58 kDa	4
TRAF2	B1AMX9_HUMAN	47 kDa	3
S100A9	S10A9_HUMAN	13 kDa	4
RPL27	RL27_HUMAN	16 kDa	4
TPD52L2	Q5JWU6_HUMAN	25 kDa	4
PSMA6	G3V295_HUMAN	23 kDa	5
CSRP2	CSRP2_HUMAN	21 kDa	5
VAPB	sp|O95292|VAPB_HUMAN	27 kDa	5
ISOC2	sp|Q96AB3-2|ISOC2_HUMAN	24 kDa	5
DUT	H0YKC5_HUMAN	24 kDa	4
VAMP3	VAMP3_HUMAN	11 kDa	4
TRMT112	F5GYQ2_HUMAN	9 kDa	4
POLDIP2	PDIP2_HUMAN	42 kDa	6
POLD2	DPOD2_HUMAN	51 kDa	6
DNAJC10	F8W884_HUMAN	86 kDa	5
HDAC1	HDAC1_HUMAN	55 kDa	6
CSK	CSK_HUMAN	51 kDa	5

GTF2I	B4DH52_HUMAN	112 kDa	4
PFKM	sp|P08237|K6PF_HUMAN	85 kDa	6
ALDH18A1	sp|P54886-2|P5CS_HUMAN	87 kDa	4
DYNC1I2	B7ZA04_HUMAN	70 kDa	4
SRP72	G5E9Z8_HUMAN	68 kDa	6
RPS12	RS12_HUMAN	15 kDa	5
CARM1	sp|Q86X55-1|CARM1_HUMAN	63 kDa	6
GGCT	sp|O75223|GGCT_HUMAN	21 kDa	6
SNRNP200	sp|O75643|U520_HUMAN	245 kDa	5
YWHAH	1433F_HUMAN	28 kDa	8
CARS	A8MVQ3_HUMAN	84 kDa	4
GMDS	E9PI88_HUMAN	39 kDa	8
RPL18A	B4DM74_HUMAN	18 kDa	5
TXLNG	sp|Q9NUQ3|TXLNG_HUMAN	61 kDa	7
NCKAP1	sp|Q9Y2A7-2|NCKP1_HUMAN	130 kDa	7
NADKD1	sp|Q4G0N4|NAKD1_HUMAN	49 kDa	7
SNX4	SNX4_HUMAN	52 kDa	5
ATP6V1B2	VATB2_HUMAN	57 kDa	7
GLRX3	GLRX3_HUMAN	37 kDa	6
TMED10	TMEDA_HUMAN	25 kDa	6
PRPF19	PRP19_HUMAN	55 kDa	7
WDHD1	WDHD1_HUMAN	126 kDa	8
UBA6	sp|A0AVT1|UBA6_HUMAN	118 kDa	7
RPL30	E5RI99_HUMAN	13 kDa	8
NAP1L4	A8MZ22_HUMAN	44 kDa	7
PSMD13	B4DJ66_HUMAN	35 kDa	7
PEF1	PEF1_HUMAN	30 kDa	7
GBAS	H7C333_HUMAN	14 kDa	7
UBE3A	F8W9C2_HUMAN	100 kDa	4
RPL9	H0Y9V9_HUMAN	22 kDa	4
KLC2	sp|Q9H0B6-2|KLC2_HUMAN	60 kDa	4
DCP1A	DCP1A_HUMAN	63 kDa	2
NBN	F5H3R2_HUMAN	53 kDa	6
PPT1	sp|P50897|PPT1_HUMAN	34 kDa	5
NASP	B4DS57_HUMAN	75 kDa	6
CPVL	CPVL_HUMAN	54 kDa	2
HIST2H2BF	B4DR52_HUMAN	18 kDa	3
NTPCR	NTPCR_HUMAN	21 kDa	5
MAD2L1	MD2L1_HUMAN	24 kDa	4
RPS17	H0YK46_HUMAN	22 kDa	5
HSD17B12	DHB12_HUMAN	34 kDa	4
ETHE1	ETHE1_HUMAN	28 kDa	5
TRIM33	sp|Q9UPN9-2|TRI33_HUMAN	121 kDa	4
APMAP	sp|Q9HDC9-2|APMAP_HUMAN	32 kDa	5
ACAT1	THIL_HUMAN	45 kDa	6
FAM98B	A8MUW5_HUMAN	46 kDa	4

TPP1	B4DSE2_HUMAN	42 kDa	4
XIAP	XIAP_HUMAN	57 kDa	5
HSD17B4	DHB4_HUMAN	80 kDa	5
EGLN1	sp|Q9GZT9|EGLN1_HUMAN	46 kDa	5
TBC1D4	sp|O60343-2|TBCD4_HUMAN	140 kDa	5
EXOSC10	sp|Q01780-2|EXOSX_HUMAN	98 kDa	4
KIAA0664	C9J6D7_HUMAN	147 kDa	4
BAT3	B0UX83_HUMAN	119 kDa	4
GEMIN5	GEMI5_HUMAN	169 kDa	5
NOMO1	NOMO1_HUMAN	134 kDa	4
RRM2	RIR2_HUMAN	45 kDa	4
MTA2	MTA2_HUMAN	75 kDa	5
GRB2	sp|P62993|GRB2_HUMAN	25 kDa	5
CAND1	sp|Q86VP6|CAND1_HUMAN	136 kDa	5
HNRNPC	B2R603_HUMAN	33 kDa	5
PDCD4	B5ME91_HUMAN	51 kDa	5
TRMT1	sp|Q9NXH9-2|TRM1_HUMAN	69 kDa	5
FLNC	sp|Q14315-2|FLNC_HUMAN	287 kDa	8
AKAP12	sp|Q02952-2|AKA12_HUMAN	182 kDa	6
SMAP1	sp|Q8IYB5-2|SMAP1_HUMAN	48 kDa	6
RAB6A	sp|P20340-2|RAB6A_HUMAN	24 kDa	7
HSD17B8	DHB8_HUMAN	27 kDa	6
CAMK2D	D6R938_HUMAN	56 kDa	6
CTH	E9PDV0_HUMAN	41 kDa	6
RECQL	RECQ1_HUMAN	73 kDa	5
TXLNA	TXLNA_HUMAN	62 kDa	6
PYGL	E9PK47_HUMAN	94 kDa	6
SKP1	E5RJR5_HUMAN	19 kDa	5
VAT1	B0AZP7_HUMAN	28 kDa	6
RAB2A	sp|P61019|RAB2A_HUMAN	24 kDa	6
LRRC40	LRC40_HUMAN	68 kDa	6
PSMB1	PSB1_HUMAN	26 kDa	6
TXN	THIO_HUMAN	12 kDa	5
PRDX6	PRDX6_HUMAN	25 kDa	5
IPO9	IPO9_HUMAN	116 kDa	6
TSG101	F5H442_HUMAN	41 kDa	4
LIMD1	C9JRJ5_HUMAN	66 kDa	2
EXOSC9	D6RIY6_HUMAN	47 kDa	2
LDHA	E9PH51_HUMAN	34 kDa	5
PALLD	sp|Q8WX93-3|PALLD_HUMAN	109 kDa	3
SERPINB12	Q3SYB4_HUMAN	48 kDa	2
MAT2B	sp|Q9NZL9-2|MAT2B_HUMAN	36 kDa	3
PITPNB	B7Z7Q0_HUMAN	32 kDa	3
GCLM	GSH0_HUMAN	31 kDa	4
LIN7A	LIN7A_HUMAN	26 kDa	3
CDK4	CDK4_HUMAN	34 kDa	4

YWHAQ	1433T_HUMAN	28 kDa	6
RALA	H7C3P7_HUMAN	18 kDa	4
RAB18	sp|Q9NP72|RAB18_HUMAN	23 kDa	3
HSPE1	B8ZZL8_HUMAN	11 kDa	4
PSMA2	PSA2_HUMAN	26 kDa	4
PSMB2	PSB2_HUMAN	23 kDa	4
CHTOP	sp|Q9Y3Y2-3|CHTOP_HUMAN	27 kDa	3
RAB13	RAB13_HUMAN	23 kDa	6
RNF114	C9JU49_HUMAN	21 kDa	3
EIF4EBP1	***4EBP1_HUMAN***	***13 kDa***	***3***
NUDC	NUDC_HUMAN	38 kDa	3
ALG1	ALG1_HUMAN	53 kDa	3
AP2M1	E9PFW3_HUMAN	52 kDa	4
ALDH3A2	sp|P51648-2|AL3A2_HUMAN	58 kDa	4
WDR45	C9J471_HUMAN	29 kDa	3
ANAPC7	F8VZ62_HUMAN	23 kDa	3
GNB1L	sp|Q9BYB4-2|GNB1L_HUMAN	23 kDa	4
RBM22	F5GWK3_HUMAN	41 kDa	3
PCYT1A	C9J050_HUMAN	34 kDa	2
PDHB	sp|P11177-2|ODPB_HUMAN	37 kDa	3
SERPINH1	B4DN87_HUMAN	44 kDa	4
ELMOD2	D6RBS5_HUMAN	20 kDa	4
MIA3	sp|Q5JRA6-2|MIA3_HUMAN	207 kDa	4
LRBA	E9PEM5_HUMAN	287 kDa	4
SMEK1	G3V5Z3_HUMAN	82 kDa	4
POP1	POP1_HUMAN	115 kDa	4
TNPO1	sp|Q92973-2|TNPO1_HUMAN	101 kDa	4
GYS1	sp|P13807-2|GYS1_HUMAN	76 kDa	3
RAB3GAP2	RBGPR_HUMAN	156 kDa	4
USP7	B7Z815_HUMAN	126 kDa	4
ATP6V1H	G3V126_HUMAN	52 kDa	4
HDLBP	VIGLN_HUMAN	141 kDa	4
TOMM34	TOM34_HUMAN	35 kDa	3
RPS26	RS26_HUMAN	13 kDa	4
POLR1C	sp|O15160-2|RPAC1_HUMAN	39 kDa	5
GPD2	sp|P43304|GPDM_HUMAN	81 kDa	3
ACP1	sp|P24666|PPAC_HUMAN	18 kDa	5
NME3	NDK3_HUMAN	19 kDa	5
SAR1A	SAR1A_HUMAN	22 kDa	5
PFN1	PROF1_HUMAN	15 kDa	6
AIMP1	sp|Q12904-2|AIMP1_HUMAN	37 kDa	5
MTHFD1L	sp|Q6UB35|C1TM_HUMAN	106 kDa	6
PFKFB3	B7Z955_HUMAN	61 kDa	5
ARFGAP1	E7EV62_HUMAN	40 kDa	5
DNAJB11	DJB11_HUMAN	41 kDa	5
NMD3	C9JA08_HUMAN	60 kDa	6

NCLN	sp|Q969V3-2|NCLN_HUMAN	63 kDa	6
C11orf67	E9PNP3_HUMAN	16 kDa	5
GCLC	GSH1_HUMAN	73 kDa	5
TRIM32	TRI32_HUMAN	72 kDa	4
CLTB	sp|P09497-2|CLCB_HUMAN	23 kDa	5
ASNS	ASNS_HUMAN	64 kDa	5
POLR2H	C9JBJ6_HUMAN	13 kDa	4
MCM6	MCM6_HUMAN	93 kDa	5
SF3B1	SF3B1_HUMAN	146 kDa	5
SEPT7	B4DNE4_HUMAN	45 kDa	5
DEK	D6RDA2_HUMAN	14 kDa	5
RIPK2	sp|O43353-2|RIPK2_HUMAN	46 kDa	5
RANBP1	RANG_HUMAN	23 kDa	5
HK1	B4DG62_HUMAN	102 kDa	5
SMARCA4	F5H0X5_HUMAN	189 kDa	5
PDCD6IP	E9PFU1_HUMAN	97 kDa	5
SPTLC1	sp|O15269|SPTC1_HUMAN	53 kDa	5
YEATS4	YETS4_HUMAN	27 kDa	6
BCAT1	F5H5E4_HUMAN	44 kDa	6
RTN3	F5H774_HUMAN	101 kDa	4
RPS24	E7EPK6_HUMAN	32 kDa	4
DCTPP1	DCTP1_HUMAN	19 kDa	5
MSH6	sp|P52701|MSH6_HUMAN	153 kDa	5
MTPN	MTPN_HUMAN	13 kDa	4
GPX1	GPX1_HUMAN	22 kDa	5
PPIL4	PPIL4_HUMAN	57 kDa	2
TTC1	TTC1_HUMAN	34 kDa	2
LACRT	LACRT_HUMAN	14 kDa	2
SIRT5	sp|Q9NXA8-2|SIR5_HUMAN	33 kDa	4
RPA1	RFA1_HUMAN	68 kDa	5
ASRGL1	sp|Q7L266|ASGL1_HUMAN	32 kDa	2
CORO7	I3L416_HUMAN	114 kDa	2
BAG2	B4DXE2_HUMAN	20 kDa	2
PML	E9PBR7_HUMAN	49 kDa	2
NCAPD3	CNDD3_HUMAN	169 kDa	2
CHAF1B	CAF1B_HUMAN	61 kDa	2
PYCRL	H0Y6C3_HUMAN	27 kDa	3
FLYWCH2	FWCH2_HUMAN	15 kDa	3
YRDC	YRDC_HUMAN	29 kDa	3
PSMC3IP	sp|Q9P2W1-2|HOP2_HUMAN	24 kDa	3
TPD52	F5H0B0_HUMAN	31 kDa	3
COPS4	CSN4_HUMAN	46 kDa	3
TTC4	Q5TA95_HUMAN	46 kDa	3
CDK9	sp|P50750-2|CDK9_HUMAN	53 kDa	3
EPHX1	HYEP_HUMAN	53 kDa	3
TRIM4	B4DEC5_HUMAN	38 kDa	2

TUBB3	TBB3_HUMAN	50 kDa	51
PSMD7	PSD7_HUMAN	37 kDa	2
SSB	E9PFH8_HUMAN	42 kDa	2
PTPN1	B4DSN5_HUMAN	41 kDa	3
THUMPD3	THUM3_HUMAN	57 kDa	3
MRPL11	sp|Q9Y3B7-2|RM11_HUMAN	18 kDa	3
SEC31A	B7ZL00_HUMAN	128 kDa	2
PLCG1	sp|P19174-2|PLCG1_HUMAN	149 kDa	3
SKIV2L2	SK2L2_HUMAN	118 kDa	3
EIF4G2	D3DQV9_HUMAN	102 kDa	3
KIF2A	E9PB70_HUMAN	78 kDa	4
KLC4	B4DME9_HUMAN	60 kDa	2
UFC1	UFC1_HUMAN	19 kDa	2
COPB1	COPB_HUMAN	107 kDa	2
SF3B2	E9PJ04_HUMAN	39 kDa	3
MLH1	MLH1_HUMAN	85 kDa	2
RBM26	sp|Q5T8P6-2|RBM26_HUMAN	111 kDa	3
PSMC4	sp|P43686|PRS6B_HUMAN	47 kDa	2
GATAD2A	B5MC40_HUMAN	70 kDa	3
OGFR	E7ESW4_HUMAN	54 kDa	4
ALG5	B4DR67_HUMAN	25 kDa	2
GTF3C5	H7BY84_HUMAN	58 kDa	3
UBAP2	UBAP2_HUMAN	117 kDa	2
NARS	SYNC_HUMAN	63 kDa	2
TBCA	E5RIW3_HUMAN	10 kDa	3
FBXO17	E7EX87_HUMAN	58 kDa	3
MSN	MOES_HUMAN	68 kDa	3
TRAP1	F5H897_HUMAN	74 kDa	4
IGHG2	IGHG2_HUMAN	36 kDa	2
EIF4A3	IF4A3_HUMAN	47 kDa	4
SAMHD1	sp|Q9Y3Z3-2|SAMH1_HUMAN	69 kDa	3
NEDD4L	sp|Q96PU5-2|NED4L_HUMAN	105 kDa	3
MRPS23	RT23_HUMAN	22 kDa	3
CFL1	COF1_HUMAN	19 kDa	3
GLOD4	B7Z403_HUMAN	32 kDa	3
KIF4A	sp|O95239-2|KIF4A_HUMAN	128 kDa	3
COQ6	B7Z3K8_HUMAN	49 kDa	3
PPOX	B4DY76_HUMAN	47 kDa	3
MPO	sp|P05164-2|PERM_HUMAN	74 kDa	3
CKB	E7EUJ8_HUMAN	39 kDa	3
KIF11	KIF11_HUMAN	119 kDa	3
GAK	E9PGR2_HUMAN	134 kDa	3
TAB1	sp|Q15750-2|TAB1_HUMAN	50 kDa	4
AAAS	F8VZ44_HUMAN	46 kDa	4
PPAT	PUR1_HUMAN	57 kDa	4
GAPVD1	sp|Q14C86-2|GAPD1_HUMAN	163 kDa	4

AARS	SYAC_HUMAN	107 kDa	4
VPS13C	sp|Q709C8-2|VP13C_HUMAN	408 kDa	4
PM20D2	P20D2_HUMAN	48 kDa	4
CMBL	CMBL_HUMAN	28 kDa	4
GOPC	F5H1Y4_HUMAN	51 kDa	4
UCHL1	D6R956_HUMAN	27 kDa	4
HDHD3	HDHD3_HUMAN	28 kDa	4
ISCA2	ISCA2_HUMAN	16 kDa	4
DYNC1LI2	B4DZP4_HUMAN	45 kDa	4
PPP5C	H0YDU8_HUMAN	55 kDa	4
SUCLG2	sp|Q96I99|SUCB2_HUMAN	47 kDa	4
SMARCA5	F5GZI1_HUMAN	117 kDa	4
CTTN	sp|Q14247-2|SRC8_HUMAN	71 kDa	4
PITRM1	C9JSL2_HUMAN	118 kDa	4
UBL4A	Q5HY81_HUMAN	21 kDa	4
MPP6	B8ZZG1_HUMAN	49 kDa	3
C14orf166	CN166_HUMAN	28 kDa	4
EIF4E	D6RBW1_HUMAN	29 kDa	4
MYL12A	ML12A_HUMAN	20 kDa	4
YWHAZ	1433Z_HUMAN	28 kDa	5
HN1L	A6NGP5_HUMAN	19 kDa	4
VPS28	E9PM90_HUMAN	21 kDa	4
LENG9	LENG9_HUMAN	53 kDa	4
MMAB	MMAB_HUMAN	27 kDa	3
ALDH1L2	sp|Q3SY69|AL1L2_HUMAN	102 kDa	4
ARMC6	sp|Q6NXE6-2|ARMC6_HUMAN	52 kDa	4
PHKG2	sp|P15735-2|PHKG2_HUMAN	43 kDa	4
DLD	B4DHG0_HUMAN	44 kDa	4
CBX3	CBX3_HUMAN	21 kDa	3
ACP6	sp|Q9NPH0|PPA6_HUMAN	49 kDa	4
DUS3L	sp|Q96G46|DUS3L_HUMAN	73 kDa	4
LRRC47	LRC47_HUMAN	63 kDa	5
CSTB	CYTB_HUMAN	11 kDa	5
NFU1	sp|Q9UMS0-3|NFU1_HUMAN	26 kDa	4
UBA2	SAE2_HUMAN	71 kDa	4
ACTR3	ARP3_HUMAN	47 kDa	4
RFC1	sp|P35251-2|RFC1_HUMAN	128 kDa	3
STT3A	E9PNQ1_HUMAN	70 kDa	4
SNRPD2	SMD2_HUMAN	14 kDa	4
C7orf50	C9JQV0_HUMAN	22 kDa	4
CAPN2	H0Y323_HUMAN	83 kDa	4
VAPA	sp|Q9P0L0-2|VAPA_HUMAN	33 kDa	3
FECH	sp|P22830-2|HEMH_HUMAN	49 kDa	4
DYNC1LI1	DC1L1_HUMAN	57 kDa	4
SUB1	TCP4_HUMAN	14 kDa	4
ELP2	E7EP23_HUMAN	100 kDa	4

RDH11	sp|Q8TC12-2|RDH11_HUMAN	34 kDa	4
ILKAP	ILKAP_HUMAN	43 kDa	4
COPG1	COPG1_HUMAN	98 kDa	4
SEC23B	SC23B_HUMAN	86 kDa	3
PRPF6	sp|O94906-2|PRP6_HUMAN	102 kDa	4
C1orf55	C9JIQ2_HUMAN	49 kDa	4
ARL8A	ARL8A_HUMAN	21 kDa	4
RPL35A	RL35A_HUMAN	13 kDa	4
COBRA1	NELFB_HUMAN	66 kDa	3
RPL36	RL36_HUMAN	12 kDa	5
CAPNS1	CPNS1_HUMAN	28 kDa	5
PPIB	PPIB_HUMAN	24 kDa	3
GRWD1	GRWD1_HUMAN	49 kDa	4
SEC61A1	B4DR61_HUMAN	53 kDa	4
PPIH	A6NNE7_HUMAN	14 kDa	3
MPP1	G3XAI1_HUMAN	50 kDa	4
DPH1	I3L1H5_HUMAN	47 kDa	4
CGGBP1	C9JUJ0_HUMAN	12 kDa	4
WDR6	E9PDU5_HUMAN	116 kDa	3
AAMP	AAMP_HUMAN	47 kDa	4
L2HGDH	C9JVN9_HUMAN	48 kDa	4
MTAP	MTAP_HUMAN	31 kDa	5
CDK5	sp|Q00535-2|CDK5_HUMAN	30 kDa	4
PCYOX1	B7Z3Y2_HUMAN	48 kDa	4
XPO5	XPO5_HUMAN	136 kDa	4
FHL1	B7Z6U8_HUMAN	29 kDa	3
HDGF	HDGF_HUMAN	27 kDa	4
SDR39U1	sp|Q9NRG7-2|D39U1_HUMAN	31 kDa	3
WARS	sp|P23381-2|SYWC_HUMAN	48 kDa	4
CALM1	CALM_HUMAN	17 kDa	2
CDIPT	B3KY94_HUMAN	26 kDa	4
PGK1	B4E1H9_HUMAN	35 kDa	4
LANCL2	LANC2_HUMAN	51 kDa	2
AP3S1	AP3S1_HUMAN	22 kDa	2
ATP5D	ATPD_HUMAN	17 kDa	2
ISOC1	ISOC1_HUMAN	32 kDa	2
BID	sp|P55957-2|BID_HUMAN	27 kDa	2
MYL6	B7Z6Z4_HUMAN	27 kDa	3
EXOSC4	EXOS4_HUMAN	26 kDa	2
GLRX	GLRX1_HUMAN	12 kDa	2
MRPS26	RT26_HUMAN	24 kDa	2
SLIRP	G3V2S9_HUMAN	14 kDa	2
LRRC59	LRC59_HUMAN	35 kDa	2
PNKD	PNKD_HUMAN	15 kDa	2
GCDH	B4DK85_HUMAN	42 kDa	2
FAR1	E7ETC1_HUMAN	38 kDa	2

LPCAT4	LPCT4_HUMAN	57 kDa	2
PIH1D1	PIHD1_HUMAN	32 kDa	2
TDP2	sp|O95551-2|TYDP2_HUMAN	44 kDa	2
PDK1	B7Z7N6_HUMAN	41 kDa	2
PGRMC1	PGRC1_HUMAN	22 kDa	2
PPM1G	F5H7G7_HUMAN	57 kDa	2
OTUB1	F5GYJ8_HUMAN	32 kDa	2
SET	sp|Q01105-2|SET_HUMAN	32 kDa	2
ACAD9	ACAD9_HUMAN	69 kDa	3
KIFC1	KIFC1_HUMAN	74 kDa	2
NUP93	H3BVG0_HUMAN	100 kDa	2
PPP6R1	PP6R1_HUMAN	97 kDa	2
TRIP12	Q14CA3_HUMAN	226 kDa	2
ATG2A	sp|Q2TAZ0-3|ATG2A_HUMAN	213 kDa	2
TARBP1	TARB1_HUMAN	182 kDa	3
ALDH2	ALDH2_HUMAN	56 kDa	2
ERO1L	ERO1A_HUMAN	54 kDa	2
CABC1	Q5T7A4_HUMAN	64 kDa	2
ZC3H14	F8W848_HUMAN	66 kDa	2
NAMPT	NAMPT_HUMAN	56 kDa	2
UCK2	sp|Q9BZX2-2|UCK2_HUMAN	13 kDa	2
SEC23IP	F5H0L8_HUMAN	90 kDa	2
DDOST	E7EWT1_HUMAN	47 kDa	2
ACSL1	B7Z3Z9_HUMAN	59 kDa	2
NIPSNAP1	C9JDV8_HUMAN	9 kDa	2
KPRP	KPRP_HUMAN	64 kDa	2
SRM	SPEE_HUMAN	34 kDa	2
EXOC8	EXOC8_HUMAN	82 kDa	2
ADSL	B4DUM2_HUMAN	35 kDa	2
VPS16	Q5JUA8_HUMAN	59 kDa	2
MAPRE1	MARE1_HUMAN	30 kDa	2
CDC45	E9PDH7_HUMAN	69 kDa	2
PDCD2	F5H4V9_HUMAN	34 kDa	2
PRMT3	F5GXU2_HUMAN	58 kDa	2
ZFR	B5MEH6_HUMAN	115 kDa	2
EIF2B5	E9PC74_HUMAN	78 kDa	2
HAUS5	HAUS5_HUMAN	72 kDa	2
PFKL	sp|P17858|K6PL_HUMAN	85 kDa	6
POLR2C	H3BRR2_HUMAN	5 kDa	2
SRSF1	sp|Q07955-2|SRSF1_HUMAN	32 kDa	2
RIOK1	RIOK1_HUMAN	66 kDa	2
GSPT1	sp|P15170-2|ERF3A_HUMAN	69 kDa	2
SRR	SRR_HUMAN	37 kDa	2
APOD	APOD_HUMAN	21 kDa	2
DDX50	DDX50_HUMAN	83 kDa	4
XRCC1	B4DEB2_HUMAN	43 kDa	2

STK3	B3KYA7_HUMAN	59 kDa	2
CHD1L	sp|Q86WJ1-2|CHD1L_HUMAN	90 kDa	2
EIF5	IF5_HUMAN	49 kDa	2
PTPRF	sp|P10586-2|PTPRF_HUMAN	212 kDa	2
NCAPH	C9J470_HUMAN	68 kDa	2
GARS	SYG_HUMAN	83 kDa	2
OSBPL9	B1AKJ6_HUMAN	84 kDa	3
CHP	CHP1_HUMAN	22 kDa	3
GSTM2	E9PEM9_HUMAN	23 kDa	3
COPS8	E9PGT6_HUMAN	19 kDa	3
SRP14	SRP14_HUMAN	15 kDa	3
RIF1	sp|Q5UIP0-2|RIF1_HUMAN	272 kDa	3
LAP3	sp|P28838-2|AMPL_HUMAN	53 kDa	3
DCUN1D5	DCNL5_HUMAN	28 kDa	3
CDC37	CDC37_HUMAN	44 kDa	4
GMPPA	sp|Q96IJ6-2|GMPPA_HUMAN	52 kDa	3
C4orf27	CD027_HUMAN	39 kDa	3
SMARCC2	F8VTJ5_HUMAN	127 kDa	3
ACTL6A	sp|O96019-2|ACL6A_HUMAN	43 kDa	3
NUDT10	NUD10_HUMAN	18 kDa	3
RAB8A	RAB8A_HUMAN	24 kDa	5
CXorf26	A6NDF3_HUMAN	27 kDa	3
ERAL1	sp|O75616|ERAL1_HUMAN	48 kDa	3
PRIM2	sp|P49643|PRI2_HUMAN	59 kDa	2
SMARCE1	B4DFR4_HUMAN	39 kDa	3
SELENBP1	sp|Q13228|SBP1_HUMAN	52 kDa	3
TOP1	TOP1_HUMAN	91 kDa	3
NAA15	sp|Q9BXJ9-4|NAA15_HUMAN	62 kDa	3
PUS1	F5H1S9_HUMAN	42 kDa	3
HSDL2	sp|Q6YN16-2|HSDL2_HUMAN	37 kDa	3
NPEPL1	E9PN47_HUMAN	53 kDa	3
PRKAG1	AAKG1_HUMAN	38 kDa	3
HMGB2	HMGB2_HUMAN	24 kDa	3
CACYBP	B3KSF1_HUMAN	23 kDa	3
TBRG4	sp|Q969Z0|TBRG4_HUMAN	71 kDa	3
CUL3	sp|Q13618-2|CUL3_HUMAN	86 kDa	3
CPNE7	sp|Q9UBL6-2|CPNE7_HUMAN	62 kDa	3
SF3A1	F5H048_HUMAN	77 kDa	3
PDK3	sp|Q15120-2|PDK3_HUMAN	48 kDa	3
CLIC4	CLIC4_HUMAN	29 kDa	3
DNAJA2	DNJA2_HUMAN	46 kDa	2
LYPLAL1	sp|Q5VWZ2|LYPL1_HUMAN	26 kDa	3
SPG20	SPG20_HUMAN	73 kDa	3
VPS29	F8VXU5_HUMAN	24 kDa	3
SEPT9	sp|Q9UHD8-2|SEPT9_HUMAN	64 kDa	3
PAPSS1	PAPS1_HUMAN	71 kDa	3

LRRFIP1	sp|Q32MZ4-2|LRRF1_HUMAN	86 kDa	3
UGDH	sp|O60701-2|UGDH_HUMAN	48 kDa	3
RRBP1	F8W7S5_HUMAN	84 kDa	3
RRM1	E9PD78_HUMAN	79 kDa	3
OGT	sp|O15294-2|OGT1_HUMAN	103 kDa	3
LIG3	sp|P49916-2|DNLI3_HUMAN	106 kDa	3
PANK4	PANK4_HUMAN	86 kDa	3
MCM2	F5H1E9_HUMAN	107 kDa	3
ELP3	sp|Q9H9T3-2|ELP3_HUMAN	61 kDa	3
USP11	G5E9A6_HUMAN	105 kDa	2
DCAKD	sp|Q8WVC6|DCAKD_HUMAN	27 kDa	3
RUFY3	B4DKC2_HUMAN	51 kDa	3
TCEB2	B7WPD3_HUMAN	18 kDa	3
NEFM	E7EMV2_HUMAN	79 kDa	3
PPP6R3	E9PKF6_HUMAN	94 kDa	3
PCID2	F8W955_HUMAN	46 kDa	3
GLRX5	GLRX5_HUMAN	17 kDa	3
NOP56	H0Y653_HUMAN	24 kDa	3
APIP	MTNB_HUMAN	27 kDa	3
NDUFS3	NDUS3_HUMAN	30 kDa	2
PGAM1	PGAM1_HUMAN	29 kDa	3
STRN	Q3B874_HUMAN	84 kDa	3
MRPL14	RM14_HUMAN	16 kDa	3
RPS23	RS23_HUMAN	16 kDa	2
ARFIP2	sp|P53365|ARFP2_HUMAN	38 kDa	3
DAD1	DAD1_HUMAN	12 kDa	3
GPS1	sp|Q13098-5|CSN1_HUMAN	55 kDa	3
PTPMT1	sp|Q8WUK0|PTPM1_HUMAN	23 kDa	3
VPS37A	sp|Q8NEZ2-2|VP37A_HUMAN	41 kDa	3
CHMP1A	CHM1A_HUMAN	22 kDa	3
KDM1A	F6S0T5_HUMAN	95 kDa	3
RAB3GAP1	A6H8Z3_HUMAN	105 kDa	2
PRKAA1	sp|Q13131-2|AAPK1_HUMAN	66 kDa	3
RAN	B5MDF5_HUMAN	26 kDa	3
DDX59	B7Z5N6_HUMAN	63 kDa	3
STAT5A	Q1KLZ6_HUMAN	87 kDa	2
PFDN2	PFD2_HUMAN	17 kDa	2
EXOC4	B7Z321_HUMAN	99 kDa	3
STMN1	sp|P16949-2|STMN1_HUMAN	20 kDa	3
CST4	CYTS_HUMAN	16 kDa	2
NDUFAF2	MIMIT_HUMAN	20 kDa	3
SEC24B	B7ZKM8_HUMAN	140 kDa	3
MTA1	E7EN71_HUMAN	71 kDa	4
SACS	sp|Q9NZJ4-2|SACS_HUMAN	437 kDa	3
NUDT5	A6NCQ0_HUMAN	20 kDa	3
UNK	UNK_HUMAN	88 kDa	3

IKBKB	E5RGW5_HUMAN	43 kDa	3
EPS15	B1AUU8_HUMAN	84 kDa	3
ATP5F1	AT5F1_HUMAN	29 kDa	2
PRUNE	H7BXM2_HUMAN	43 kDa	3
SLK	sp|Q9H2G2-2|SLK_HUMAN	139 kDa	3
RPS15	RS15_HUMAN	17 kDa	3
PLRG1	A8MW61_HUMAN	57 kDa	2
FNTA	E9PQP6_HUMAN	30 kDa	3
FEN1	F5H1Y3_HUMAN	18 kDa	4
GPT2	sp|Q8TD30|ALAT2_HUMAN	58 kDa	2
C20orf43	A8MSH5_HUMAN	38 kDa	3
ARPC2	ARPC2_HUMAN	34 kDa	2
EPM2A	sp|O95278-3|EPM2A_HUMAN	37 kDa	4
ECI1	H3BP91_HUMAN	32 kDa	3
CAMK1	H7C071_HUMAN	29 kDa	3
ACTR2	ARP2_HUMAN	45 kDa	3
PPP4C	H3BTA2_HUMAN	31 kDa	3
VPS11	VPS11_HUMAN	108 kDa	3
WDR61	H0YMF9_HUMAN	21 kDa	3
RPL35	F2Z388_HUMAN	11 kDa	3
TSN	E9PGT1_HUMAN	26 kDa	2
SCGB1D1	SG1D1_HUMAN	10 kDa	3
DCTD	sp|P32321-2|DCTD_HUMAN	21 kDa	3
TUBG1	TBG1_HUMAN	51 kDa	3
UNC45A	sp|Q9H3U1-2|UN45A_HUMAN	102 kDa	3
SCO1	SCO1_HUMAN	34 kDa	3
PGP	PGP_HUMAN	34 kDa	2
RHOG	RHOG_HUMAN	21 kDa	3
HSPBP1	sp|Q9NZL4|HPBP1_HUMAN	39 kDa	3
TTLL12	B1AH89_HUMAN	74 kDa	2
CYP51A1	F5H3N4_HUMAN	51 kDa	3
BPNT1	A6NF51_HUMAN	32 kDa	4
TRAPPC3	A6NDN0_HUMAN	15 kDa	2
GSTP1	A8MX94_HUMAN	19 kDa	2
SLC25A6	ADT3_HUMAN	33 kDa	4
ARPC5L	ARP5L_HUMAN	17 kDa	2
AS3MT	AS3MT_HUMAN	42 kDa	2
LOC84661	B4DIS3_HUMAN	14 kDa	2
RNF220	B4DLZ9_HUMAN	40 kDa	2
TRMT6	B4DUV6_HUMAN	36 kDa	2
HARS	B4DY73_HUMAN	53 kDa	2
BIRC6	BIRC6_HUMAN	530 kDa	2
ZC3HC1	C9J0I9_HUMAN	51 kDa	2
CLIC1	CLIC1_HUMAN	27 kDa	2
C19orf43	CS043_HUMAN	18 kDa	2
TCEB1	E5RGD9_HUMAN	11 kDa	2

CYFIP2	E7EVF4_HUMAN	146 kDa	10
TOR1AIP1	E9PKD1_HUMAN	47 kDa	2
UBQLN2	F5H2G2_HUMAN	53 kDa	2
FHL2	FHL2_HUMAN	32 kDa	2
IDH3A	H0YKD0_HUMAN	12 kDa	2
NSDHL	NSDHL_HUMAN	42 kDa	2
PDS5A	PDS5A_HUMAN	151 kDa	2
PPP2CA	PP2AA_HUMAN	36 kDa	2
RRAGC	RRAGC_HUMAN	44 kDa	2
SSR4	SSRD_HUMAN	19 kDa	2
TTC27	TTC27_HUMAN	97 kDa	2
UBE2M	UBC12_HUMAN	21 kDa	2
WASF1	WASF1_HUMAN	62 kDa	2
DFFA	sp|O00273|DFFA_HUMAN	37 kDa	2
IPO8	sp|O15397|IPO8_HUMAN	120 kDa	2
CDC42EP1	sp|Q00587-2|BORG5_HUMAN	40 kDa	2
LARP7	sp|Q4G0J3|LARP7_HUMAN	67 kDa	2
SMARCD1	sp|Q96GM5-2|SMRD1_HUMAN	53 kDa	2
KLHL13	sp|Q9P2N7-2|KLH13_HUMAN	69 kDa	3
STUB1	sp|Q9UNE7|CHIP_HUMAN	35 kDa	2
ACTA2	ACTA_HUMAN	42 kDa	20
HNRPLL	B7WPG3_HUMAN	56 kDa	2
NHLRC2	sp|Q8NBF2|NHLC2_HUMAN	79 kDa	2
PNPO	B4E152_HUMAN	25 kDa	2
UCKL1	F8WAC3_HUMAN	61 kDa	2
SUGT1	F5H5A9_HUMAN	32 kDa	2
CEP44	sp|Q9C0F1-2|CEP44_HUMAN	45 kDa	2
PDHA1	sp|P08559-2|ODPA_HUMAN	44 kDa	2
SOLH	sp|O75808|CAN15_HUMAN	117 kDa	2
UBE2L3	B4DDG1_HUMAN	14 kDa	2
CHEK1	E7EPP6_HUMAN	56 kDa	2
PYCR2	P5CR2_HUMAN	34 kDa	2
ZYX	B4DQR8_HUMAN	52 kDa	3
TP53BP1	A6NNK5_HUMAN	209 kDa	2
COQ5	F8VVX6_HUMAN	25 kDa	2
SCCPDH	E9PEA8_HUMAN	26 kDa	2
SYNGR1	B5MCD7_HUMAN	18 kDa	2
CWF19L1	sp|Q69YN2-3|C19L1_HUMAN	46 kDa	2
ILK	B7Z1I0_HUMAN	36 kDa	2
MARS2	B4DVV7_HUMAN	58 kDa	2
ARL1	ARL1_HUMAN	20 kDa	2
SNX9	SNX9_HUMAN	67 kDa	2
EIF2B2	EI2BB_HUMAN	39 kDa	2
PGRMC2	PGRC2_HUMAN	24 kDa	2
PMPCB	MPPB_HUMAN	54 kDa	2
DENND4A	E7EPL3_HUMAN	214 kDa	2

EML4	B5MBZ0_HUMAN	110 kDa	2
AHCYL2	D7UEQ7_HUMAN	57 kDa	2
ACBD3	GCP60_HUMAN	61 kDa	2
PSMB3	PSB3_HUMAN	23 kDa	2
ACAD11	sp|Q709F0|ACD11_HUMAN	87 kDa	2
MDH1	F5H098_HUMAN	39 kDa	2
UPF3B	Q0VAK7_HUMAN	25 kDa	2
KIAA0930	B0AZU2_HUMAN	44 kDa	2
CLCC1	sp|Q96S66-2|CLCC1_HUMAN	56 kDa	2
USO1	F5GYR8_HUMAN	109 kDa	2
ARPC3	ARPC3_HUMAN	21 kDa	2
HK2	E9PB90_HUMAN	99 kDa	4
LYPLA1	E5RGR0_HUMAN	21 kDa	2
ADA	ADA_HUMAN	41 kDa	2
PRPF4	sp|O43172-2|PRP4_HUMAN	58 kDa	2
USP19	B5MEG5_HUMAN	150 kDa	2
CPOX	HEM6_HUMAN	50 kDa	2
CEP97	E9PG22_HUMAN	90 kDa	2
C15orf38	CO038_HUMAN	25 kDa	2
WDR45L	B4DMI6_HUMAN	35 kDa	2
RBM28	E9PDD9_HUMAN	70 kDa	2
SMARCC1	SMRC1_HUMAN	123 kDa	3
XPO7	E7ESC6_HUMAN	124 kDa	2
FKBP4	FKBP4_HUMAN	52 kDa	2
EIF2B1	B4DGX0_HUMAN	25 kDa	2
SNRPD3	B4DJP7_HUMAN	13 kDa	2
ACOT9	sp|Q9Y305-2|ACOT9_HUMAN	46 kDa	2
GNL3	sp|Q9BVP2-2|GNL3_HUMAN	61 kDa	2
SYNGR2	SNG2_HUMAN	25 kDa	2
C19orf54	sp|Q5BKX5|CS054_HUMAN	38 kDa	2
SNX30	SNX30_HUMAN	50 kDa	2
RCC1	C9JW69_HUMAN	40 kDa	2
KIAA1033	sp|Q2M389|WASH7_HUMAN	136 kDa	2
TARSL2	sp|A2RTX5-2|SYTC2_HUMAN	82 kDa	2
ADAT3	ADAT3_HUMAN	38 kDa	2
ARPC4	ARPC4_HUMAN	20 kDa	2
NFKB2	sp|Q00653-4|NFKB2_HUMAN	97 kDa	2
RPL34	RL34_HUMAN	13 kDa	2
MYD88	H0Y4G9_HUMAN	35 kDa	2
SEPT2	B5MCX3_HUMAN	37 kDa	2
CRYZ	A6NN60_HUMAN	32 kDa	2
SNRPE	RUXE_HUMAN	11 kDa	2
APRT	APT_HUMAN	20 kDa	2
WASF2	sp|Q9Y6W5|WASF2_HUMAN	54 kDa	2
SGPL1	SGPL1_HUMAN	64 kDa	2
FAM203A	F203A_HUMAN	42 kDa	2

SUGP1	sp|Q8IWZ8|SUGP1_HUMAN	72 kDa	2
ALOX12B	LX12B_HUMAN	80 kDa	2
PIK3C3	A8MYT4_HUMAN	94 kDa	2
RABEPK	Q5T1S4_HUMAN	17 kDa	2
NDUFA5	C9IZN5_HUMAN	11 kDa	2
LAMP1	LAMP1_HUMAN	45 kDa	2
RRAGA	RRAGA_HUMAN	37 kDa	2
ABHD14B	ABHEB_HUMAN	22 kDa	2
TPR	TPR_HUMAN	267 kDa	2
SERPINB6	SPB6_HUMAN	43 kDa	2
PAPSS2	E7ER89_HUMAN	70 kDa	2
UBE2O	UBE2O_HUMAN	141 kDa	2
MSANTD2	B4E1M0_HUMAN	18 kDa	2
TMED8	TMED8_HUMAN	36 kDa	2
PRPS1	PRPS1_HUMAN	35 kDa	2
ZW10	A1A528_HUMAN	77 kDa	2
PRPF31	E7ESA8_HUMAN	50 kDa	2
BAG5	sp|Q9UL15-2|BAG5_HUMAN	56 kDa	2
ACAT2	B7Z233_HUMAN	45 kDa	2
TALDO1	F2Z393_HUMAN	35 kDa	2
MAPK9	sp|P45984-2|MK09_HUMAN	44 kDa	2
CCRN4L	NOCT_HUMAN	48 kDa	2
FANCI	sp|Q9NVI1|FANCI_HUMAN	149 kDa	2
IAH1	H7C5G1_HUMAN	25 kDa	2
NT5DC1	NT5D1_HUMAN	52 kDa	2
PTGES2	H7C5L1_HUMAN	34 kDa	2
KEAP1	KEAP1_HUMAN	70 kDa	2
METTL2B	sp|Q6P1Q9-2|MET2B_HUMAN	36 kDa	2
LPCAT1	PCAT1_HUMAN	59 kDa	2
DNM2	A8K1B6_HUMAN	98 kDa	2
PPA2	E2QRM6_HUMAN	36 kDa	4
LAGE3	LAGE3_HUMAN	15 kDa	2
COPG2	COPG2_HUMAN	98 kDa	2
TECR	B3KSQ1_HUMAN	37 kDa	2
ARRB2	H0Y688_HUMAN	48 kDa	2
D2HGDH	sp|Q8N465|D2HDH_HUMAN	56 kDa	2
PPCDC	H3BQB0_HUMAN	18 kDa	2
UBTF	E9PKP7_HUMAN	87 kDa	2
AK2	E7EWH4_HUMAN	22 kDa	2
SELRC1	SELR1_HUMAN	26 kDa	2
CUL2	CUL2_HUMAN	87 kDa	2
CRYGD	CRGD_HUMAN	21 kDa	2
KCTD6	F5H7I0_HUMAN	8 kDa	2
SPAG9	H7BY21_HUMAN	117 kDa	2
RPP30	C9JJX7_HUMAN	28 kDa	2
FABP5	FABP5_HUMAN	15 kDa	2

SRI	A8MTH6_HUMAN	20 kDa	2
WDR41	B4DHS8_HUMAN	20 kDa	2
ZNF768	H3BS42_HUMAN	57 kDa	2
BZW2	BZW2_HUMAN	48 kDa	2
ATM	ATM_HUMAN	351 kDa	2

Table lists all the proteins, that were successfully detected by MS analysis in the GFP-4E2 immunoprecipitation. Ctr stands for number of peptides in the control immunoprecipitation from empty HEK cells and GFP-4E2 IP stands for number of peptides indetified in the GFP-4E2 immunoprecipitation. Highlighted proteins are trustworthy hits.

10.2 Data for quantification of stress granules formed by individual eIF4E isoforms

Table 21 Percentage of cells that form SGs under arsenite stress, related to Fig. 19

	BR1	BR2	BR3	Average (%)	SD
4E1_1	85.06	68.37	71.3	74.91	7.28
4E1_3	54.35	53.4	48.5	52.08	2.56
4E3_A	52.32	53.9	40.85	49.02	5.82
pEGFP	20.55	11.96	20.75	17.75	4.10

BR1,2,3 stands for independent biological replications. Average stands for percentage of cells, that formed SGs where individual GFP tagged 4E variant localized. SD stands for standard deviation. eIF4E1_1, eIF4E1_3, and eIF4E3_A proteins were ectopically produced in fusion with GFP from the same vector in U2OS cells. Nineteen hours post-transfection, the cells were treated with 1 mM sodium arsenite for 40 min, and those forming SGs were counted and plotted as a fraction of all transfected cells. Error bars indicate differences among three independent experiments in which approximately 100 of the transfected cells were assessed.

10.3 List of supplementary material located on the enclosed CD

1) Primary data for quantification of arsenite stress-induced cells transfected by eIF4E1_1, eIF4E1_3, and eIF4E3_A and their ability for form SGs, related to Table 21 and Fig. 19
2) Primary data for quantification of SGs formed by individual eIF4Es , related to Fig. 32 and Fig. 33
3) Full-resolution microscopy figures
4) Primary MS analysis

10.4 List of publications

10.4.1 Distinct recruitment of human eIF4E isoforms to P-bodies and stress granules

FRYDRÝŠKOVÁ K., MAŠEK T., BORČIN K., MRVOVÁ S., VENTURI V., POSPÍŠEK M.

BMC Mol. Biol., Aug 2016, vo 17, no 1. (cited 19x)

10.4.2 Major splice variants and multiple polyadenylation site utilization in mRNAs encoding human translation initiation factors eIF4E1 and eIF4E3 regulate the translational regulators?

MRVOVÁ S., FRYDRÝŠKOVÁ K., POSPÍŠEK M., VOPÁLENSKÝ V., MAŠEK T.

Mol. Genet. Genomics, Sep 2017, vo 293, no 1. (cited 2x)

10.4.3 Changing faces of stress: Impact of heat and arsenite treatment on the composition of stress granules

FRYDRÝŠKOVÁ K., MAŠEK T., POSPÍŠEK M.

This manuscript has been sent in September 2019 to Wiley Interdisciplinary Reviews: RNA for review.